2013

Effect of nonlinear friction on the motion of an object on solid surface induced by external vibration

Partho Sarathi Goohpattader
Lehigh University

Effect of nonlinear friction on the motion of an object on solid surface induced by external vibration

By

Partho Sarathi Gooh Pattader

A Dissertation

Presented to the Graduate and Research Committee

of Lehigh University

in Candidacy of the Degree of

Doctor of Philosophy

in

Chemical Engineering

Lehigh University

May 2013

Approved and recommended for acceptance as a dissertation in partial fulfillment of the

requirements for the degree of Doctor of Philosophy.

_____

Date

                                                _____

Dr. Manoj K. Chaudhury, Dissertation

Advisor

_____

Accepted Date

Committee Members:

_____

Dr. Mayuresh V. Kothare

_____

Dr. Cesar A. Silebi

_____

Dr. Mark A. Snyder

_____

Dr. Jeffrey M. Rickman

ii

Acknowledgement

This dissertation would not have been completed without the contribution of many individuals, to whom I am deeply indebted. First of all, I would like to thank my advisor, Professor Manoj K. Chaudhury, for his priceless guidance, encouragement and support throughout this work. Without his constant motivation, innovative ideas and contagious enthusiasm this work would not have been possible. I would also like to express my gratitude to my thesis committee members Professor Cesar A. Silebi, Professor Mayuresh V. Kothare, Dr. Mark A. Snyder and Professor Jeffrey M. Rickman for serving on my dissertation committee and for their valuable suggestions in the progress of this work.

I take this opportunity to thank all my colleagues - Jon Longly, Chih Hsiu Lin, Kim, Srinivas Mettu, Aditi Chakrabarti, Rushikesh Matkar and Darius who were being supportive and helpful throughout the course of my thesis work. I specially thank Jon for his help in surface characterization using AFM, Ellipsometry and Chih Hsiu Lin, Srinivas and Richard Bai for teaching me SAM coating technique and fibrillar rubber surface preparation. I would also like to thank Joseph A. Zelinski for letting me use the grit blasting unit to prepare my samples.

I also thank Professor Cesar A. Silebi and Professor Kemal Tuzla for giving me opportunity to serve as a teaching assistant in several courses. This work would not have been possible without the help of many individuals, specifically Paul N. Bader and John

To my family

Contents

List of Figures

reciprocal noise strength for various compostions of glycerin-water solutions (0% corresponds to water and 100 % corresponds to glycerin). (b) The results of the subcritical drift dynamics (upper curve) are compared with those of the barrier crossing experiments (lower curve) by plotting $ln(v_d \rho KV^{7/3}/v^2)$ versus $(v/\rho KV^{5/3})$ in both cases.

Figure 8.10: Fluctuation of the air-water interface of a 20μl water drop when it was deposited on a horizontal flat PDMS surface of 95μm fibrillar spacing (upper panel), 50μm fibrillar spacing (middle panel) and smooth hydrocarbon treated Si wafer respectively. As soon as a drop of water is released on a surface via retraction of a needle, it starts to oscillate, the amplitude of which decays with time. The amplitude of this oscillation after 1s of disposal of the drop on a PDMS surface (50μm fibrillar spacing) is comparable to that observed with the drop undergoing critical speeding (Figure 8.2c, main text) on a similar surface (1s after the release of the drop). However, under a comparable condition, the amplitude of this oscillation on a PDMS surface with larger fibrillar spacing (95 μm) is significantly smaller than that observed with a drop undergoing a critical dynamics on a similar surface. As the measurements of the interface fluctuation shown in Figure 8.2c were performed after 1s of the drop disposal, we can safely say that the oscillation due to syringe retraction did not contribute significantly on a surface with a 95 μm fibrillar spacing. Although the argument is weaker for a 50 μm spaced fibrillar surface, we note that the amplitude of oscillation did not decay as the drop sprinted over such a surface, i.e. the initial oscillation is, at least, sustained. The amplitude of the interface oscillation decays much faster (within 1.5s) for a drop released on a smooth hydrophobic Si wafer. The air-water interface fluctuation of a water drop moving steadily on such a surface (Figure 8.2c) was recorded long time (~ 40s) after the deposition of the drop as it moved rather slowly (~ 0.06 cm/sec).

Figure 8.11: Power spectra of the interface fluctuation of a water drop and a solid glass sphere on a fibrillar surface. The upper blue curve depicts the power spectrum of a 10 μl drop of water trapped before a barrier (see Figure 8.4a) by subjecting it to an external noise of strength $0.17m^2/s^3$. This spectrum is similar to that of Figure 8.6a except that the background noise of the spectrum was reduced by adding and averaging the spectra obtained from ten different experiments. The red curve represents the power spectrum of the self-excited noise a 10 μl water drop undergoing a critical speeding dynamics on an inclined (10°) fibrillar surface (see Figure 8.2b). The lower black curve represents the power spectrum of a rigid glass sphere (2.4mm diameter) as it drifted on a fibrillar surface that was inclined by 5^0 without any external noise. These control experiments were performed to show that the resonance modes of a drop excited by a self-generated noise is similar to that obtained with an external noise, whereas no such resonance modes are observed with a rigid sphere that cannot undergo a shape fluctuation.

Abstract

There are enumerable examples of natural processes which fall in the class of non-equilibrium stochastic dynamics. In the literature it is prescribed that such a process can be described completely using transition probability that satisfy the Fokker Planck equation. The analytical solutions of transition probability density function are difficult to obtain and are available for linear systems along with few first order nonlinear systems. We studied such nonlinear stochastic systems and tried to identify the important parameters associated with the dynamics and energy dissipative mechanism using statistical tools.

We present experimental study of macroscopic systems driven away far from equilibrium with an applied bias and external mechanical noise. This includes sliding of small solid object, gliding of a liquid drop or a rolling of a rigid sphere. We demonstrated that the displacement statistics are non-Gaussian at short observation time, but they tend towards a Gaussian behavior at long time scale. We also found that, the drift velocity increases sub-linearly, but the diffusivity increases super-linearly with the strength of the noise. These observations reflect that the underlying non-linear friction controls the stochastic dynamics in each of these cases. We established a new statistical approach to determine the underlying friction law and identified the operating range of linear and nonlinear friction regime.

1

In all these experiments source of the noise and the origin of the energy dissipation mechanism (i.e. friction) are decoupled. Naturaly question arises whether the stochastic dynamics of these athermal systems are amenable to Einstein's Fluctuation dissipation theorem which is valid strictly for a closed thermodynamic system. We addressed these issues by comparing Einstein's ratio of Diffusivity and mobility which are measurable quantities in our experimental systems.

As all our experimental systems exhibit substantial negative fluctuations of displacement that diminishes with observation time scale, we used another approach of integrated fluctuation theorem to identify athermal temperature of the system by characterizing a persistence time of negative fluctuations in terms of the measurable quantity.

Specific experiments have also been designed to study the crossing of a small object over a physical barrier assisted by an external noise and a bias force. These results mimic the classical Arrhenius behavior from which another effective temperature may be deduced. All these studies confer that the nonlinear system does not possess any unique temperature.

Detachment of a solid sphere as well as a liquid drop from a structured rubber surface during subcritical motion in presence of external noise was examined in the light of Arrhenius' activated rate equation. Drift velocity of small drops of water-glycerin solution behaves nonlinearly with viscosity which is reminiscence of Kramers' turn over

theory of activated rate. In a designed experiment of barrier crossing of liquid drops we satisfactorily verified the Kramers' formalism of activated rate at the low friction limit.

1. CHAPTER ONE: Introduction

1.1 Introduction

The prime theme of this dissertation is to study friction or hysteresis at the interface of two moving bodies which are in a noisy environment. The motivation for this work is to understand seemingly mundane but profoundly interesting rich phenomena like flowing of cereals from a packet to the milk bowl, trickling down of raindrops on window pane, sorting of fruits in packaging industries, rolling of tiers on a rough street etc. Not only these macroscopic phenomena but also microscopic realm of colloidal particles or molecular transport within cells etc. has enough ingredients to kindle this work.

Recently there is a boom in development of microfluidic devices and MEMs in context of the need of the fast world. These two generic areas find its application in various different fields such as medical science, reaction engineering, computational and information technologies, robotic engineering and so on. Study of the interaction at the interface of the two bodies become essential in controlling the motion of micro droplets in a microfluidic devise or particle manipulation on a surface. This interaction is nothing but friction (or hysteresis in the context of liquid –solid interface) which is the reason of energy loss for a thermodynamically open system, and at the same time is an indispensable component of the motion of an object [1]. One way to manipulate the friction is modification of the interacting surfaces. As it is associated with the change in properties of the mother surfaces, this path may not be suitable for some specific

requirements where surface properties are of prime interest. Hence we seek a path to overcome or attenuate the effect of friction. Imposing an external noise to the system allows one to control the effect of friction. In this thesis we will study this effect and address some critical questions such as - How an external noise affects the dynamics of an object while friction is operating at the interface of the moving bodies? What will happen if the underlying friction is linear or nonlinear in nature?

Friction at static or dynamic solid-solid interface is one of the oldest but still fuzzy areas of physical science. One of the main reasons of this obscurity of friction is its nonlinear nature with various parameters like velocity, stochastic and/or deterministic applied force etc. In this work we tried to analyze friction and its nonlinear behavior from a different angle using statistical tools and set a unique approach to study non-linear systems. Most of the practical scenario associated with motion of particles or liquid drops are non-equilibrium systems which are driven away far from equilibrium by an applied biased force. Hence it is of utmost importance to understand the difference between equilibrium and non-equilibrium systems.

Equilibrium thermodynamics is a well-investigated and firmly established subject, at least in the context of a system which is in thermal equilibrium with its surroundings [2]. The equilibrium systems possess certain characteristics, which are not pertinent to non-equilibrium systems. Most stable and preferred state of an equilibrium system is governed by the global minimization of free energy. Irrespective of the initial state of the system, it eventually reaches this state. System driven away far from

equilibrium with an external force field cannot be described by this kind of simple energy minimization principle. Understanding of non-equilibrium system is of considerable interest in recent years although not fully perceived yet. In this line some important work is done by Evan, Cohen and Morriss [3]. They pointed out the apparent violation of second law of thermodynamics in non-equilibrium steady state systems and came up with a relation between the probability of entropy production and entropy consumption known as fluctuation theorem.

Although there exists a plethora of experimental studies [4–7] in the literature related to above mentioned non equilibrium dynamics, some areas call for more exploration specifically the athermal stochastic system where the source of the random noise and the origin of the energy dissipation mechanism are decoupled. In this dissertation, we study some simple experimental athermal systems, which fall in the realm of the non-equilibrium thermodynamics.

Let's first describe two situations which reveal the main contrasts between equilibrium and non-equilibrium systems. Consider a system, boundary of which encompasses a beaker filled with water having constant temperature T, same as the surrounding. Now if we put an ink drop in the water, the ink particles due to random collisions with the surrounding water molecules will exhibit Brownian motion and diffuse in the water. After some time the ink particles will be uniformly distributed throughout the water bath. The system is now in dynamic equilibrium state. During the random motion of the ink particles, they experience viscous drag force which reflects in

their mobility. Einstein in his classical paper on Brownian motion [8] derived the connection among the diffusivity (D), mobility (μ) and temperature (T) of the bath which is known as famous fluctuation dissipation relation (Eq. 1.1):

$$\frac{D}{\mu} = k_B T \qquad\qquad 1.1$$

Where k_B is the Boltzmann constant. This relation is proposed for a thermodynamically closed system which is in thermal equilibrium. The kinetic energy of the ink particles dissipates, due to viscous friction at the particle water interface, as a form of thermal energy inside the water bath itself. This thermal energy in turn drives the water molecules which bombards on the ink particles to set them in Brownian motion.
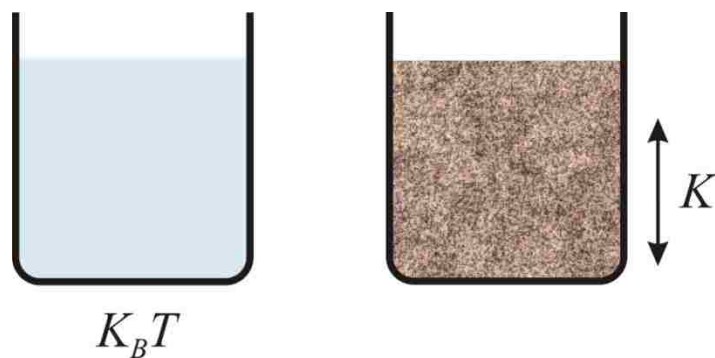
Figure 1.1: (left) Equilibrium thermal system – ink drop in water after a long time and (right) non-equilibrium athermal system – vertically vibrated sand filled beaker .

As a second situation let's consider an athermal system: a beaker, full of sand particles or tiny hard spheres, placed on a platform which is vibrated vertically up and down. This set up is similar in spirit of that reported in reference [9]. The system is in

non-equilibrium state in a sense that there is wide distribution of measurable variables such as local velocities of the particles, packing density etc. In this case energy dissipates, due to Coulombic friction at solid–solid interface. This dissipated energy is irrecoverable. Unlike the thermal system described above, here kinetic energy associated with each sand particle is too small to keep it in agitated form, hence continuous supply of energy as external vibration is mandatory. The analysis of such a system becomes more challenging because of two reasons. First, the nonlinear nature of the Coulombic friction in comparison to linear viscous friction makes the situation complex. Secondly, presence of too many particles makes it difficult to characterize the system precisely unless some sophisticated approach is adopted and that yet to be developed. Such a system which is far from equilibrium does not obey the conventional fluctuation dissipation theorem described in Eq.1.1.

Now question arises can we characterize stochastic dynamics of non-equilibrium, athermal system with some intensive parameters (like temperature) which relates fluctuations and response function similar to the fluctuation dissipation relation for equilibrium thermal systems? Some studies pointed out that from the relation between diffusivity and the response to an external force one can define 'effective temperature' in some cases of non-equilibrium dissipative system. This effective temperature can be used to characterize various properties of the systems [10–16]. But what will happen if the underlying energy dissipative mechanism (friction) is linear or nonlinear? Exploring different frictional regime can anyone control the dynamics of such a system?

We introduced simple model experimental systems to address these issues and which at the same time allow us to study the energy dissipative phenomena at solid-solid interface (i.e. friction) as well as at solid-liquid interface (i.e. hysteresis), which is of immense practical interest.

1.2 Objective

There are enumerable straight forward examples in our everyday life which deserves a close attention to feel nonlinear dynamic systems. Sticking and running of a water drop on a window pane or on a wind shield of a car is governed by nonlinear dynamics. Flow of particle through open channels or pipes, sorting of particle based on its specific surface and body properties, separation of a particle from adhered surface, steer an object in specific direction etc. can be manipulated with better knowledge of the underlying nonlinear dynamics. Study of tribology is very important in various engineering applications such as high precision servo control, robotics, pneumatic devices, breaks for cars, traction of tier etc. to name a few.

The frictional study might be relevant to understand many biological transport processes that occur within the cell. A recent experiment [17] shows when a colloid particle diffuse along a linear phospholipid bilayer microtubule, the diffusion process is very fast but the distribution of the displacement is exponential rather than Gaussian. In general the Gaussian distribution is expected for a random walker. Authors attributed this transport process as an activated diffusion similar to that observed in glassy systems. In this thesis we addressed the origin of such exponential distribution of displacement,

which is frequently encountered in many natural dynamic processes, as a result of the nonlinear frictional dissipation at the interface of the two moving bodies.

The objective of this research is to explore the realm of nonlinear dynamics and friction, specifically to:

a. Introduce a simple model system and develop a new approach to study non-equilibrium steady state processes.

b. Study the effect of Coulombic friction and nonlinear kinematic friction on the dynamics of an object that is excited externally.

c. Identify a fluctuation dissipation like relationship for an athermal system.

d. Establish new approach to identify the underlying friction law.

e. Whether the dynamic behavior of a solid object or a liquid drop can be described by a class of activated rate process.

A brief introduction on the notion of some statistical tools used in this research is described in chapter 2. We introduced a simple phenomenological model to describe the main features of the friction in chapter 3. In chapter 4 we addressed the characteristics of the nonlinear friction and effect of external bias force on diffusivity. In this chapter we also pointed out the effect of the surface characteristics on the dynamic response. A new experimental methodology is described in chapter 5 to identify the underlying nonlinear friction. In chapter 6 we discussed the mechanical activation of a rolling rigid sphere in adhesive contact with a fibrillar PDMS in presence of external perturbation. Theoretical exploration of this process is described in chapter 7. The noise activated dynamics of a

liquid droplet on the fibrillar rubber surface and effect of viscosity on this process along with the report of some interesting findings about critical and subcritical dynamics were discussed in chapter 8. We summarized in chapter 9 with suggestions for future works.

References:

[1]   S. Mettu and M. K. Chaudhury, Langmuir : the ACS Journal of Surfaces and Colloids **27**, 10327–10333 (2011).

[2]   J. W. Gibbs, *Elementary Principles in Statistical Mechanics: Developed with Especial Reference to the Rational Foundation of Thermodynamics* (Charles Scribner's Sons, 1902).

[3]   D. J. Evans, E. G. D. Cohen, and G. P. Morriss, Physical Review Letters **71**, 2401–2404 (1993).

[4]   G. M. Wang, E. M. Sevick, E. Mittag, D. J. Searles, and D. J. Evans, Physical Rev. Lett. **89**, 050601 (2002).

[5]   V. Blickle, T. Speck, L. Helden, U. Seifert, and C. Bechinger, Rev. Lett. **96**, 070603 (2006).

[6]   F. Douarche, S. Joubaud, N. B. Garnier, A. Petrosyan, and S. Ciliberto, Rev. Lett. **97**, 140603 (2006).

[7]   N. Garnier and S. Ciliberto, Rev. E **71**, 060101 (2005).

[8]   A. Einstein, Annalen Der Physik **7**, 549–560 (1905).

[9]   G. D. Anna, P. Mayor, A. Barrat, V. Loreto, and F. Nori, Nature 909–912 (2003).

[10]   L. F. Cugliandolo, **55**, 3898–3914 (1997).

[11]   H. a Makse and J. Kurchan, Nature **415**, 614–7 (2002).

[12]   I. Ono, C. O'Hern, D. Durian, S. Langer, A. Liu, and S. Nagel, Physical Review Letters **89**, 4–7 (2002).

[13] B. Abou and F. Gallet, Physical Review Letters **93**, 160603 (2004).

[14] K. Feitosa and N. Menon, Phys. Rev. Lett. **92**, 164301 (2004).

[15] R. P. Ojha, P. Lemieux, P. K. Dixon, a J. Liu, and D. J. Durian, Nature **427**, 521–3 (2004).

[16] T. Haxton and A. Liu, Physical Review Letters **99**, 7–10 (2007).

[17] B. Wang, S. M. Anthony, S. C. Bae, and S. Granick, Proceedings of the National Academy of Sciences of the United States of America **106**, 15160–4 (2009).

2. CHAPTER TWO: Background

2.1 Introduction

Classical thermodynamics deals with the macroscopic properties (temperature, pressure, volume, energy, entropy etc.) of an equilibrium system and their relationship. These macroscopic properties are determined by the behavior of the ensemble of large number of microscopic particles. Advancement of the molecular theory of matter calls for a new approach to study the nature of these microscopic particles. At this microscopic level the fluctuations of the dynamic properties of molecules become essential to explain various macroscopic properties. Statistical mechanics is the theory with which one can study the behavior of the natural and spontaneous fluctuations [1]. Fluctuations of the molecules of matter encode the energetic states of the system and statistical mechanics is the deciphering tool. In this thesis we will use this tool to study the dynamic behavior of a macroscopic object and in this journey, we will try to extract the information about the nature of dissipative mechanism, i.e. friction. Response of a system to random input variables is a stochastic process. Specifically we will consider few mechanical systems where the input will be a bias force along with a random forcing function and the output will be either velocity or displacement which are stochastic in nature. The fluctuation of displacement or velocity encodes the dissipative nature of the dynamic system, whether it is linear or nonlinear. We will systematically address these issues in this thesis. In this chapter we will discuss some definitions of the statistical terms and their characteristics which will be useful to understand the discussions in subsequent chapters.

The study of random process is started mainly in the field of Brownian motion. Before that, in 1738 Swiss physicist Bernoulli first pointed out that thermodynamic parameters like pressure, temperature etc. is the result of stochastic motion of gas molecules and the collisions among themselves or with the enclosing walls. Later in 1958 Maxwell first gave the mathematical description of the molecular velocities through a distribution called Maxwell distribution. Boltzmann enriched this field of study and proposed the fundamental relationship between the entropy and the number of microstates of a system.

2.2 Markov Process

A Markov process is defined as a stochastic process which is 'memory-less' in nature, i.e. the next state of the system depends only on the present state, and independent of all the previous states it experienced before the current state. Ships in a turbulent sea, erratic motion of kite in the sky, moving vehicle, motion of colloidal particle in thermal fluid etc. are the example of a Markov process. Let us focus our discussion on the motion of colloid particles in the fluid.

The Brownian motion of a colloid particle in a fluid inseminate from the random bombardments of the surrounding fluid molecules on the colloid particle. Hence the velocity of the colloid particle randomly varies in magnitude and directions. At a certain instance t if the particle has velocity V, the particle will collide with more fluid molecules in the front than in the rear. Any change in the velocity at the next small time window dt will solely depend on the velocity V and will be independent of any earlier history of the

particle. Thus the velocity of the colloid particle is an example of the Markov process. Not only the velocity the position of the particle also a Markov process, as the probability distribution of the next displacement jump does not depends on the earlier history. But there is a caveat in the above description of the Brownian motion. The Brownian motion is a Markov process if the observation time scale is larger than the velocity autocorrelation time. As by the definition, the Markov process should have zero autocorrelation time. In reality the Brownian particle possess finite autocorrelation time. A large instantaneous velocity does not damp out in zero time, hence its effect still persists in the next few observations unless the observation time scale is large enough so that it appears that there is no correlation between two observations. Such a process is called approximate Markov process.

Before going to deeper in the Markov process, its attributes and application we first need to have some essence of probability theory.

2.3 Probability theory

Probability is the chance of occurrence of an event in repeated trial experiments in identical condition. The definition of probability is empirical in a sense that it is based upon the observations. Let's assume in an experiment we are interested to have a specific outcome $X=x_i$ and N_i number of times it happened among the total N number of trials, where N is very large. Hence the probability of having $X=x_i$ is defined as: $P(X=x_i) = N_i/N$ or shortly $P(x_i) = N_i/N$. Probability has no unit. By definition the probability has following basic properties:

$$P(x_i) \geq 0$$

$$\sum_i P(x_i) = 1 \qquad \text{2.1}$$

Here x_i is a discrete stochastic variable. For a continuous stochastic variable x_i we estimate the chance of its occurrence within a small window dx and the probability is defined as:

$P(x_o < x_i < x_o + dx) = P(x_i)dx$

Here $P(x_i)$ is the probability density function having unit of (dx^{-1}).

The notion of probability is closely resemble to the ensemble rather than a single entity. The ensemble is the consolidation of stochastic variables from different samples having different time histories. For example colloidal particles in a Newtonian fluid will serve as an ensemble representing the Gaussian probability distribution of velocity. Average behavior of the ensemble of the colloidal particles can be described by the probability distribution. Complete description of a stochastic process involves characterizing the distribution of the stochastic variables associated with the process. For this purpose it is essential to identify the characteristic function or moment generating function.

2.3.1 Characteristic function

The characteristic function of a stochastic variable X is defined as:

$$G(k) = \langle e^{ikX} \rangle = \int_I e^{ikx} P(x)\, dx \qquad \text{2.2}$$

Here I is the range of the variable X consisting of real numbers.

Conversely, if the characteristic function G(k) of a distribution is known, the distribution $P(x)$ can be obtained by taking the Fourier transform of the characteristic function G(k).

i.e.

$$P(x) = \frac{1}{2\pi} \int_{-\infty}^{\infty} G(k)e^{-ikx}dk \qquad\qquad 2.3$$

Important properties of characteristic function are:

$$G(0) = 1; \quad |G(k)| \leq 1 \qquad\qquad 2.4$$

The Taylor expansion in k of this characteristic function gives the moments of the distribution function $P(x)$. i.e. if μ_j is the jth moment of $P(x)$, then the relation between the characteristic function and μ_j is:

$$G(k) = \sum_{j=0}^{\infty} \frac{(ik)^j}{j!} \mu_j \qquad\qquad 2.5$$

Note that these moments are 'moments about zero', not the central moment (or moment about mean). There is difference between these two, for example '1st moment about zero' gives the mean, but 1st central moment (or 1st moment about mean) is always zero. Unless otherwise stated we use the term 'moment' to refer 'moment about zero' in this section of the thesis. Another quantity cumulants (m_j, j^{th} cumulant) can be generated from the characteristic function. These cumulants can be used to calculate the central moments of a distribution. The relationship between cumulants and the moments are as follows:

$$m_1 = \mu_1$$

$$m_2 = \mu_2 - \mu_1^2 = \sigma^2$$

$$m_3 = \mu_3 - 3\mu_2\mu_1 + 2\mu_1^3$$

$$m_4 = \mu_4 - 4\mu_3\mu_1 - 3\mu_2^2 + 12\mu_2\mu_1^2 - 6\mu_1^4$$

2.6

We will show later that why these cumulants are essential to analyze the shape and characteristics of a probability density function of stochastic variables. For example let us consider Gaussian distribution, which is very important in the context of this thesis.

$$P(x) = \frac{1}{\sigma\sqrt{2\pi}} e^{-\frac{(x-\mu)^2}{2\sigma^2}}$$

2.7

The characteristic function of the Gaussian distribution according to Eq. 2.2 will be:

$$G(k) = \frac{1}{\sigma\sqrt{2\pi}} \int_{-\infty}^{\infty} e^{ikx}\; e^{-\frac{(x-\mu)^2}{2\sigma^2}} dx$$

$$G(k) = e^{ik\mu - \frac{k^2\sigma^2}{2}}$$

$$G(k) = 1 + ik\mu - \frac{k^2}{2}(\sigma^2 + \mu^2) - \cdots$$

2.8

Comparing this result with Eq. 2.5 reveals that

$$\mu_1 = \mu$$

$$\mu_2 = \sigma^2 + \mu^2$$

2.9

This states that first moment of the Gaussian distribution is the mean μ and second cumulant is the variance σ^2 of the distribution. First and second cumulants give the rough idea about the peak position and the width of a distribution. Indication about the shape of a distribution is given by 'skewness' and 'kurtosis' which are associated with higher order cumulants.

2.3.2 Skewness (S)

Skewness (*S*) is the measure of asymmetry of a distribution. A distribution is said to be symmetrical if the frequencies are symmetrically distributed about the mean, i.e. when the values of the random variables equidistance from the mean have same frequencies. Skewness of the distribution is given by :

$$S = \frac{m_3}{m_2^{3/2}}$$
2.10

Here m_3 and m_2 are the 3rd and 2nd cumulants.
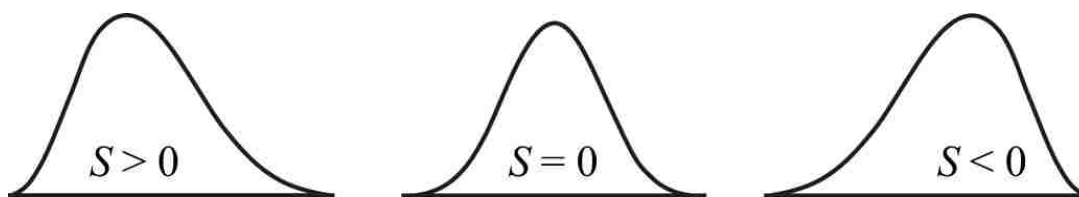
Figure 2.1: Schematic depicting Skewness (*S*) of a distribution.

For a symmetric distribution, *S*=0, otherwise it is positive or negative value depending on whether it is skewed towards the values larger or smaller than the mean respectively.

2.3.3 Kurtosis (β)

Kurtosis (β) is the measure of 'peakedness' of the distribution. A distribution having sharper peak is called 'Leptokurtic' and that having relatively flat top is called 'Platykurtic'. A normal distribution is called 'Mesokurtic'. For Mesokurtic distribution the kurtosis β =3, for Leptokurtic and Platykurtic distribution the values of β is greater and smaller than 3 respectively.
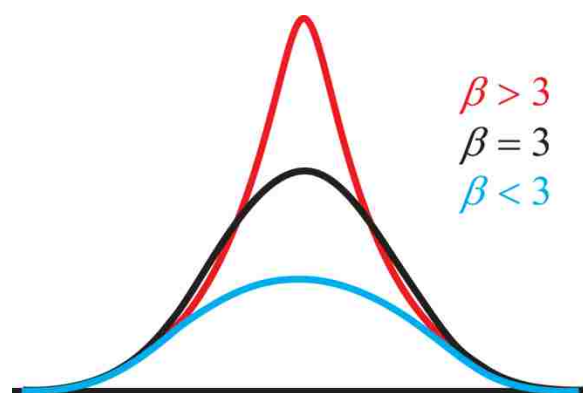
Figure 2.2: Schematic depicting Kurtosis (β) of Leptokurtic (β >3), Mesokurtic (β =3) and Platykurtic (β <3) distribution.

The value of β is estimated as:

$$\beta = \frac{m_4}{m_2^2} \qquad\qquad 2.11$$

Here m_4 and m_2 are the 4th and 2nd cumulants respectively. Sometimes the peakedness is reported as excess kurtosis, which is defined as $\gamma_3 = (\beta - 3)$.

2.4 Gaussian noise

Gaussian noise is ubiquitous in many natural sources. Brownian motion of the colloid particle, thermal fluctuation of atoms in a conductor can be described by the Gaussian distribution. Gaussian distribution has finite mean and variance. In this thesis we will mainly focus on the dynamics of an object influenced by a bias force and external white noise. Unless otherwise stated, in most of the part we are going to use Gaussian noise as an external white noise. In our experiments external Gaussian noise is fed to the system as time dependent random acceleration pulse ($\gamma(t)$) having constant temporal pulse width (τ_c) of 40μs. The acceleration is measured with accelerometer (PCB Peizotronics, Model No: 353B17) and the information is analyzed using an oscilloscope (Tektronix, Model No. TDS 3012B) after passing through a signal conditioner (PCB Peizotronics, Model No: 482). A typical distribution of the acceleration is shown in Figure 2.3.
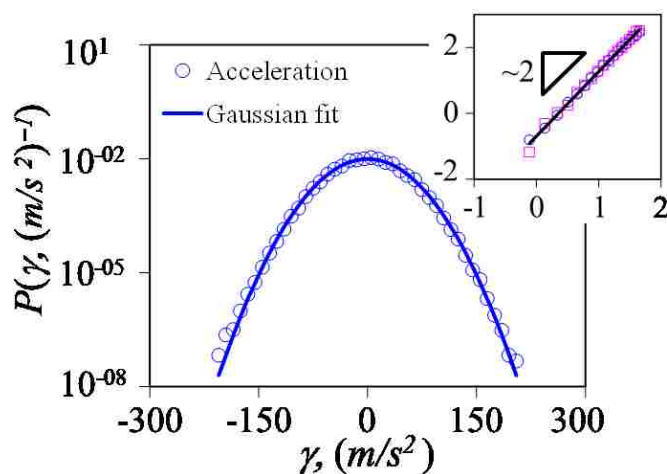
Figure 2.3:Input noise $\gamma(t)$ (acceleration, m/s^2) distribution, fitted with Gaussian distribution. Inset shows the plot of $ln[-ln(P/P_o)]$ vs $ln|\gamma|$ with slope 2.

Gaussian distribution of the input acceleration is given by

$$P(\gamma) = P_0 e^{-\frac{\gamma^2}{\sigma^2}}$$ 2.12

Here P_o is the normalization constant. As the input noise is unbiased, the mean of the distribution is zero but having a finite standard deviation σ. Eq. 2.12 can be rearranged as:

$$ln\left[-ln\left(\frac{P}{P_0}\right)\right] = 2ln\left|\frac{\gamma}{\sigma}\right|$$ 2.13

When $ln[-ln(P/P_o)]$ is plotted against $ln|\gamma|$, the slope of the line should be 2 for a Gaussian distribution. This is shown in the inset of the Figure 2.3.

A true white noise should have pulses which are delta correlated. Hence the autocorrelation time should tend to zero and the noise will have flat power spectra over the entire range of the frequency. In reality the scenario is quite different due to experimental limitations, for example algorithm used to generate the random numbers, the recoiling effect of the oscillator etc. Hence our experimental input noise has following properties:

$$\langle \gamma(t_1)\gamma(t_2)\rangle = \Gamma^2 \qquad for\ |t_1-t_2| < \tau_c$$
$$\langle \gamma(t_1)\gamma(t_2)\rangle = 0 \qquad for\ |t_1-t_2| > \tau_c$$ 2.14

22

Here Γ be the root mean square acceleration. For convenience, we introduce a symbol K, which is the power of noise and is defined as $\Gamma^2\tau_c$ (m^2/s^3).

A sample Gaussian noise trace and its power spectra are shown in Figure 2.4. With a total bandwidth (-f_{max} to + f_{max}, f_{max} being the maximum frequency) of 25 *kHz*, the spectrum is quite flat up to ~10 *kHz*, after which it tends to fall.
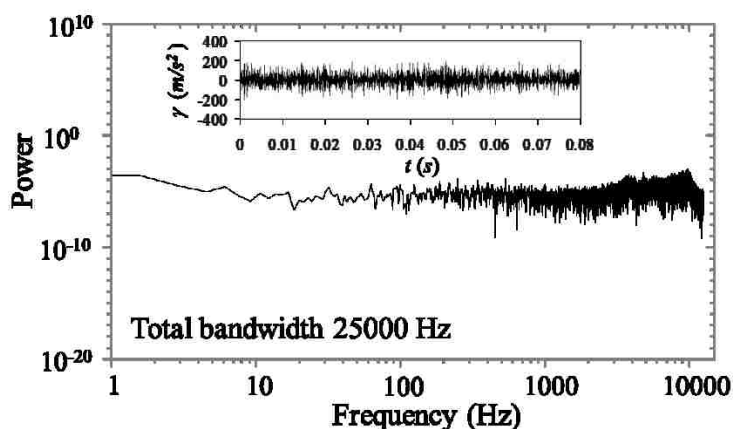
Figure 2.4: A typical trace of the acceleration pulses (inset) corresponding to strength K =0.16 m^2/s^3. Corresponding power spectrum taken at a bandwidth of 25*kHz*.

Using 10 *kHz* as the corner frequency 'f ' (Figure 2.4), a time constant τ_c, as estimated from 1/(2πf), is about 16 μs. However this time scale corresponds to a slightly tainted white noise. More correct time constant should be about 30 μs (assuming corner frequency of ~5*kHz*) as the spectrum corresponding to this time scale represents almost perfectly flat spectrum.

2.5 Fokker Planck Equation

When a particle is immersed in a Newtonian fluid the particle will experience a friction force given by Stokes law: $= -6\pi\eta av$, where η is the viscosity of the fluid, a is the radius of the particle and v is the velocity. Hence equation of motion for the particle is given by

$$\frac{dv}{dt} + \frac{v}{\tau_L} = 0 \qquad\qquad 2.15$$

Where τ_L is the relaxation time (=$1/6\pi\eta a$). The above description is valid when the particle is large enough so that the random bombardment by the surrounding fluid molecules on the particle average out and hence the thermal fluctuation of the particle is negligible compare to the viscous friction force. For a small particle, P. Langevin [2] suggested an additional term that accounts for stochastic thermal fluctuations.

$$\frac{dv}{dt} + \frac{v}{\tau_L} = \gamma(t) \qquad\qquad 2.16$$

This stochastic description cannot give the estimation of some useful parameters like drift or diffusion analytically. These parameters can be obtained from Fokker Planck equation, which is the equation of motion of the distribution function of a stochastic variable. In presence of an additional bias force $\bar{\gamma}$ the Fokker Planck equation corresponding to Eq. 2.16 is given by:

$$\frac{\partial P(x,V,t)}{\partial t} = -\frac{\partial (VP)}{\partial x} + \frac{\partial \left(-\bar{\gamma}P + \frac{VP}{\tau_L}\right)}{\partial V} + \frac{K}{2}\frac{\partial^2 P}{\partial V^2} \qquad \text{2.17}$$

The derivation of Eq. 2.17 is well explained in the literature [3,4]. For spatially homogenous system, the steady state solution of Eq. 2.17 is given by

$$P(V) = P_o e^{\left(-\frac{V^2}{K\tau_L} + \frac{2V\bar{\gamma}}{K}\right)} \qquad \text{2.18}$$

Once this distribution is obtained one can estimate the drift velocity using the following equation:

$$V_{drift} = \frac{\int_{-\infty}^{\infty} VP(V)dV}{\int_{-\infty}^{\infty} P(V)dV} \qquad \text{2.19}$$

Eq. 2.16, 2.17 and 2.18 corresponds to a system having linear energy dissipation. Now let us discuss a generalized version where a nonlinear system is considered.

$$\frac{dv}{dt} + f(V) = \gamma(t) \qquad \text{2.20}$$

Here $f(V)$ is a nonlinear function of velocity. The corresponding Fokker Planck equation is given by

$$\frac{\partial P(V)}{\partial t} = \frac{\partial [f(V)P(V)]}{\partial V} + \frac{K}{2}\frac{\partial^2 P(V)}{\partial V^2} \qquad \text{2.21}$$

For the stationary distribution (i.e. at long time limit, $t \rightarrow \infty$) above Eq. reduced to

$$\frac{\partial [f(V)P(V)]}{\partial V} + \frac{K}{2}\frac{\partial^2 P(V)}{\partial V^2} = 0 \qquad \text{2.22}$$

The only solution that satisfies Eq. 2.22 reads as [5],

$$P(V) = P_o \exp[-\frac{2F(V)}{K}] \qquad \text{2.23}$$

Here P_o is the normalization constant and $F(V) = \int f(V)dV$.

Dynamics of a solid particle moving on a solid surface can be described by the equation 2.20 [6–8], where $f(V)$ will represent frictional dissipative term which may be a linear combination of viscous (V/τ_L) and Coulombic friction ($\Delta\sigma(V)$) which make the overall system nonlinear. Here Δ represents the magnitude of the Coulombic friction and $\sigma(V)$ is the signum function of V with $\sigma(0) = 0$. Hence $f(V)$ will read as:

$$f(V) = \frac{V}{\tau_L} + \Delta\sigma(V) \qquad \text{2.24}$$

Then according to Eq. 2.23 the steady state velocity distribution will be given by,

26

$$P(V) = P_o exp \left[-\frac{V^2}{K\tau_L} - \frac{2\Delta|V|}{K} \right] \qquad 2.25$$

Using this distribution and Eq. 2.19 one can calculate the drift velocity of the particle.

The above example of solid motion on a solid surface is well discussed by de Gennes [8]. According to him in presence of a bias force $\bar{\gamma}$, drift velocity can be estimated as,

$$V_{drift} = \int_{-\infty}^{t} \{\langle \gamma(t') \rangle + \bar{\gamma} - \Delta \langle \sigma(V(t')) \rangle\} \, exp \left\{ -\frac{t-t'}{\tau_L} \right\} dt'$$

$$V_{drift} = \tau_L [\bar{\gamma} - \Delta \langle \sigma \rangle] \qquad 2.26$$

$$for \; small \; bias, \;\; \langle \sigma \rangle \sim \frac{\Delta V_{drift}}{K}$$

Using these scaling laws, drift velocity is given by [9],

$$V_{drift} = \frac{\bar{\gamma}\tau_L}{1 + \frac{\Delta^2 \tau_L}{K}} \qquad 2.27$$

If $\Delta=0$, i.e. in the absence of Coulombic friction the drift velocity is given by $\bar{\gamma}\tau_L$ which depends on viscous relaxation time τ_L and independent of the strength of external noise. This derivation of drift velocity is approximate one and based on the scaling laws proposed by de Gennes.

Another elegantly simple alternate route to obtain the physical parameters associated to the nonlinear stochastic system is suggested by Caughey [5], in which he

prescribed a method called effective linearization of the nonlinear system. This method [10] later adopted by Crandall *et al* [11] and others [12] to model the sliding of building foundation in response to earthquake. Let's first extensively describe the dynamics of non-linear system using modified Langevin equation:

$$\frac{dv}{dt} + \frac{V}{\tau_L} + \Delta\sigma(V) = \gamma(t) \qquad 2.28$$

The corresponding linear system will be given in terms of an effective relaxation time τ^* and an additional reminder term $\varphi(V)$.

$$\frac{dv}{dt} + \frac{V}{\tau^*} + \varphi(V) = \gamma(t) \qquad 2.29$$

Here the root mean square deficiency $\varphi(V)$ is given by:

$$\varphi = \frac{V}{\tau^*} - \frac{V}{\tau_L} - \sigma(V)\Delta \qquad 2.30$$

The success of equivalent linearization technique lies on the minimization of the average value of φ^2 with respect to effective relaxation time τ_L^*, which leads to the following equation:

$$\frac{1}{\tau^*} = \frac{1}{\tau_L} + \frac{2\Delta\langle\sigma(V)V\rangle}{\langle V^2\rangle} \qquad\qquad 2.31$$

The average quantities $\langle...\rangle$ in Eq. 2.31 can be obtained from the stationary velocity distribution described by Eq. 2.25. For a dry friction dominated situation Eq. 2.31 reads as

$$\frac{1}{\tau^*} = \frac{1}{\tau_L} + \frac{\Delta^2}{K} \qquad\qquad 2.32$$

We have already seen for a linear system under the influence of a small bias force $\bar{\gamma}$, drift velocity is given by $\bar{\gamma}\tau_L$. Now for a system with combination of Coulombic friction and the linear viscous friction the drift velocity will be read as $\bar{\gamma}\tau^*$. Where τ^* is given by Eq. 2.32. which gives the identical relationship (Eq. 2.27) as obtained from the approximate scaling analysis of de Gennes.

In a similar way, analogy to the case of linear kinematic friction, the diffusivity reads as:

$$D = \frac{K\tau^{*2}}{2} = \frac{K^3\tau_L^2}{2(K + \Delta^2\tau_L)^2} \qquad\qquad 2.33$$

At low power, when $K << \Delta^2\tau_L$, diffusivity is dominated by Coulombic friction and D $\rightarrow$ K^3/Δ^4, which is predicted by de Gennes [8].

2.6 Conclusion

The subject of nonlinear stochastic dynamics intrigued physicists for long time. MacDonald [13] was first to study the Brownian movement with nonlinear relaxation and later Caughey and Dienes [5] used Fokker Planck equation corresponding to Eq. 2.28 to obtain the transition probability density. From the velocity correlations, obtained from the solution of Fokker Planck equation, they estimated diffusivity of the object when the motion is dictated by the dry friction and found that the diffusivity$(D \sim K^3/\Delta^4)$ is stronger function of the strength of the noise than the situation which is governed by the linear friction $(D \sim K)$. Later de Gennes, without knowing the work of Caughey and Dienes, reached the identical results through an approximate scaling analysis.

While studying the nonlinear friction in granular gas, Kawarada and Hayakawa [6] identified the exponential velocity distribution. This observation also made by Caughey and Dienes earlier [5]. Recently another approach of path integral route is taken by Baule et. al [14,15] to obtain the analytical expression of transition probability where nonlinear friction is dominating. While others mostly considered the velocity as the stochastic variable, Menzel and Goldenfeld [16] dealt with the distribution of displacement fluctuation. In this line a recent experimental investigation is also performed by Wang *et al.* [17] where the displacement of a colloid particle along a bilayer membrane tube is studied.

Our experimental studies with a small solid sliding block on a glass surface or a rolling rigid sphere on a rubber surface in presence of external vibration or bias force

relates many of these theoretical and experimental studies. We also addressed the characteristics of pinning depinning transition of a rigid sphere as well as liquid droplet on a structured rubber surface vibrated with external noise of low power.

References

[1]   D. G. Chandler, *Introduction to Modern Statistical Mechanics* (Oxford University Press,, 1987).

[2]   D. S. Lemons, A. Gythiel, and M. P. Langevin, Am J Phys. **65**, 1079–1081 (1997).

[3]   S. Chandrasekhar, Rev. Mod. Phys. **15**, 1 (1943).

[4]   M. C. Wang and G. E. Uhlenbeck, Rev. Mod. Phys. **17**, 323 (1945).

[5]   T. K. Caughey and J. K. Dienes, Journal of Applied Physics **32**, 2476–2479 (1961).

[6]   A. Kawarada and H. Hayakawa, Journal of the Physical Society of Japan **73**, 2037 (2004).

[7]   H. Hayakawa, Physica D **205**, 48–56 (2005).

[8]   P.-G. De Gennes, Journal of Statistical Physics **119**, 953–962 (2005).

[9]   M. K. Chaudhury and S. Mettu, Langmuir **24**, 6128–32 (2008).

[10]   S. H. Crandall, Structural Control and Health Monitoring **13**, 27–40 (2006).

[11]   S. H. Crandall, S. S. Lee, and J. H. Williams, Journal of Applied Mechanics **42**, 1094–1098 (1974).

[12]   G. Ahmadi, Int. J. Engng. Sci. **21**, 93 (1983).

[13]   D. K. C. MacDonald, Physical Review **108**, 541 (1957).

[14]   A. Baule, E. G. D. Cohen, and H. Touchette, Journal of Physics A: Mathematical and Theoretical **43**, 025003 (2010).

[15]   A. Baule, H. Touchette, and G. D. Cohen, Nonlinearity **24**, 351 (2011).

[16]   A. Menzel and N. Goldenfeld, Physical Review E **84**, 1–9 (2011).

[17]   B. Wang, S. M. Anthony, S. C. Bae, and S. Granick, Proceedings of the National Academy of Sciences of the United States of America **106**, 15160–4 (2009).

3. CHAPTER THREE: Role of Coulombic Friction on the Dynamics of Solid Object[1]

3.1 Introduction

Friction is inevitable part of our life. Sometimes it makes nuisance (as a reason of wear, heat up the parts and failure of machines, inefficient energy utilization in unit operations etc.), sometimes it is essentially useful (for example in walking or driving a car, to hold an object with hands etc). Till date the friction is not fully understood. Different models of friction mechanism are offered depending on the velocity dependency. Friction at near zero velocity is recognized by the name of Coulomb/dry friction. First atomistic and simple view on this matter was proposed by Prandtl and Tomlinson, where the stick-slip instability was responsible for Coulomb friction [1,2]. For the last few decades the effect of Coulombic friction was studied on the damping of harmonic oscillator [3–6]. Recently in an experimental study Simbach and Priest identified the difference between Columbic dry friction and kinematic friction [7]. In their study they observed the nature of dampening of the amplitude of a swinging pendulum. Usually if such a system is controlled by linear kinetic friction, the amplitude of oscillation should decay exponentially with time. What they found is that the

---

amplitude decays much faster and linearly with time as Coulombs friction dampens the oscillation.

The problem of Coulomb dampening of the motion of an object in presence of white noise was theoretically analyzed by Caughey and Dienes [8]. They dealt with the Fokker Planck equation involving Coulombic friction and Caughey [9] proposed the method of equivalent linearization technique to estimate certain useful parameters of the stochastic system. In the last decade Kawarada, Hayakawa and de Gennes studied Coulombic friction as the energy dissipation mechanism at the interface of two relatively moving solids [10–12]. When a solid prism is placed on another solid support, vibrated with external white noise, the prism undergoes a stochastic motion with a net drift and specific diffusivity. This mean drift velocity and diffusivity is different than that expected from a liner kinematic friction case. Such a nonlinear system was extensively studied by de Gennes [12],who proposed certain scaling laws of the diffusivity in terms of the magnitude of the Columbic friction and the strength of the imposed external noise.

According to de Gennes (see also Hayakawa [10] as well as Kawarada and Hayakawa [11]), the dynamics of the object on a surface subjected to an external vibration ($\gamma(t)$) and a bias ($\bar{\gamma}$) is described by the modified Langevin equation [12,13]:

$$\frac{dV}{dt} + \frac{V}{\tau_L} = \bar{\gamma} + \gamma(t) - \sigma(V)\Delta \qquad\qquad 3.1$$

Here, V is the velocity of the particle, τ_L ($=m/\zeta$) is the Langevin relaxation time, where m is the mass of the particle and ζ is the kinematic friction coefficient, $\bar{\gamma}$ is the applied

acceleration (external force divided by the mass of the particle). $\gamma(t)$ is the time dependent acceleration that the object experiences from the white noise source. Ideally, this acceleration is delta correlated and has a zero mean value. If the magnitude of the static friction force is smaller than $(\bar{\gamma} + \gamma(t))$, the object moves, otherwise it remains stuck to the surface. $\sigma(V)$ is the signum function of velocity with $\sigma(0) = 0$, Δ is a measure of the Columbic friction (force/mass). The noise $\gamma(t)$ that has the following properties:

$$\langle \gamma(t_1)\gamma(t_2)\rangle = \Gamma^2 \qquad for \; |t_1 - t_2| < \tau_c$$

$$\langle \gamma(t_1)\gamma(t_2)\rangle = 0 \qquad for \; |t_1 - t_2| > \tau_c$$

3.2

where Γ be the root mean square acceleration and τ_c be the duration of the pulse. For convenience we introduce a symbol K, which is the power of noise and is equal to $\Gamma^2\tau_c$; $K/2$ is also the diffusivity in the velocity space.

The solution of the corresponding Klein-Kramers [14] form of the spatially homogeneous Fokker-Planck equation of the Langevin equation 3.1 is given by

$$-\frac{K}{2}\frac{\partial P(V)}{\partial V} - \Delta\frac{|V|}{V}P(V) - \frac{VP(V)}{\tau_L} = -\bar{\gamma}P(V) \qquad\qquad 3.3$$

Here, $P(V)$ is the steady state probability density function [10,11,13,15] of the velocity which can be obtained by integrating equation 3.3.

$$P(V) = P_o exp\left(-\frac{V^2}{K\tau_L} - \frac{2|V|\Delta}{K} + \frac{2V\bar{\gamma}}{K}\right) \qquad\qquad 3.4$$

Where, P_o is normalization constant. According to equation 3.4, when $\Delta = 0$, the velocity distribution is Gaussian about the mean $\bar{\gamma}\tau_L$, i.e. it resembles the situation of a simple dragged Brownian particle with a diffusivity of $K\tau_L^2/2$. However, when $\Delta \neq 0$, the velocity pdf has also an exponential component. Similar prediction was made by Mauger [13] where he pointed out the non-Lipschitz continuous nature at velocity V=0. Let us consider the case for $\Delta \neq 0$ and $\bar{\gamma} < \Delta$ and set the kinematic friction to zero. In this case, De Gennes showed that the object exhibits a diffusive motion with a value of diffusivity as $\sim K^3/\Delta^4$, which is strongly sensitive to the power of the noise in contrast to the simple kinematic situation, where diffusivity is $K\tau_L^2/2$. Furthermore, when the object is agitated with a white noise vibration, it drifts with a velocity $\sim K\bar{\gamma}/\Delta^2$, which is also uniquely different from the case of pure kinematic friction for which the drift velocity at any value of K is just $\bar{\gamma}\tau_L$. Thus, while the ratio of diffusivity and mobility is $K\tau_L/2$ for the case with kinematic friction that for the dry friction is $\sim (K/\Delta)^2$. As in this case, the energy is being delivered by external work, which is different from a typical thermal system, no fluctuation dissipation relation is expected. An effective temperature can still be defined as *D/μ.*

3.2 Experiment

Our experimental set up is based on the inertial tribometer demonstrated by Baumberger et. al. [16,17]. They placed a solid object as a slider on a track, which is subjected to an external periodic oscillation and the response of the slider was recorded using a displacement gauge. This set up enabled them to study the micro-slip and corresponding dissipation at the solid solid interface. We adopted the similar set-up with little modification.

We place a solid glass block (~2g) with dimension of ~ 12mm x 12mm x 6mm on a grit blasted glass slide (Fisherbrand) as a support. Grit blasting of the glass support using alumina particle was needed to incorporate micron level roughening on the glass surface which was necessary for the uniform sliding of the glass block over it. Otherwise the block adheres to the glass support so strongly that very high excitation is needed to dislodge it from the surface. The glass block and the rough support was pre cleaned by sequential sonication in acetone and water for half an hour each and was dried with blowing dry Nitrogen gas.

Experimental set up is illustrated in Figure 3.1. The roughened glass substrate was firmly attached to an aluminum platform and fixed on the stem of a mechanical oscillator (Pasco Scientific, Model No: SF-9324). The angle of inclination of the glass support was controlled by a precise Goniometer (CVI Melles Griot, Model No: 07 GON 006).White noise that was generated using Matlab® program was fed through the sound card of the computer to the oscillator via a power amplifier (Sherwood, Model No: RX-

4105). The whole set-up was placed on a vibration isolation table (Micro-g, TMC) to eliminate the effect of ground vibration. The acceleration of the supporting aluminum plate was estimated with a calibrated accelerometer (PCB Peizotronics, Model No: 353B17) driven by Signal Conditioner (PCB Peizotronics, Model No: 482) and connected to an oscilloscope (Tektronix, Model No. TDS 3012B). The drift velocities of the glass prism were measured on the inclined plate with a low speed (30fps) normal Sony camera (DCR-HC85 NTSC) and the stochastic motion of the prisms were monitored with a high speed (1000fps) Redlake Motion-Pro video camera at different powers of noise. The data obtained with the high speed camera were subjected to an analysis using 'Midas2.0 Xcitex' software to obtain the instantaneous position as a function of time by tracking the edge of the prism. When the position of the prism is plotted against time with the data obtained from a low speed camera, excellent straight line is obtained over a distance of 40 mm with good reproducibility, which signifies that the property of the surface is somewhat uniform over a significant length for meaningful measurements of velocity and other properties.
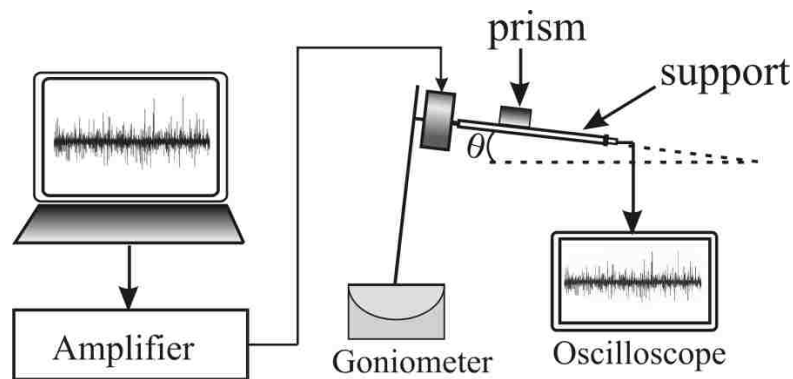
Figure 3.1: Schematic of the experimental set up.

There are few limitations in this experimental technique. First of all, we restricted our high speed video recording to the 1000fps to obtain a longer record length. This temporal resolution is not sufficient to capture finer details of the object motion. Spatial resolution is also restricted to the 0.1μm with a tracking error of ±5μm. Another experimental limitation is random rotation of the glass prism about its vertical axis while it drifted down over the inclined support in presence of the external noise. We discarded the tracks having significant amount of this types of rotational motion for the simplicity of the analysis.
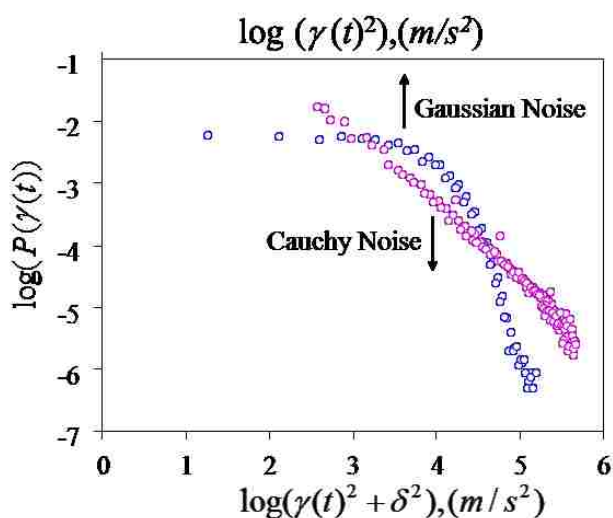
Figure 3.2: A solid object or a liquid drop drifts downward on a vibrating inclined substrate by overcoming the forces of Columbic friction or hysteresis. The probability distribution functions $P(\gamma(t))$ of the Gaussian and a truncated Cauchy noises that were used to vibrate the substrate are also shown. δ represents the width of the truncated Cauchy distribution, $\gamma(t)$ are the random acceleration pulses.

One advantage of this experimental set up is choice of the noise. Being an external white noise, it could be Gaussian or Levy noise with specific α index. The true Levy noise has infinite energy that is not realistic in nature. Hence we experimented with both Gaussian and truncated Levy noise. Truncated Levy noise has finite power with fat tails and observed in many natural phenomena [18–20] and is applied in directed transport processes [21–24] or as an optimal search engine [25,26].We use a truncated Levy noise with $\alpha=1$(Cauchy) of finite power as an external energy input to the glass slider that experiences Columbic static friction in addition to the kinematic friction during motion. With a truncated Levy noise, finite variance exists in both velocity and real spaces. Thus it appears that we may be able to use the same probability conservation equations 3.3 and 3.4 as is the case with the Gaussian noise. We expect that all the transport properties measured in terms of drift and diffusion would be identical to those obtained with a Gaussian noise, which we indeed find experimentally. In view of the above mentioned indistinguishabilities of the Gaussian and the truncated Levy noises, it may be asked why should we consider using the Levy noise in the first place. We will show later that the truncated Levy noise, although behaving like a Gaussian noise, offers certain advantages by improving the statistics in the low probability regions of the distributions due to its fat tails.

3.3 Results and discussion

3.3.1 Drift and diffusivity of solid object

At a small inclination of the support, glass prism does not slide spontaneously. A static Columbic friction of the magnitude $\mu_s mg \cos\theta$ operates at the interface of the prism and the glass support. Here μ_s is the static friction coefficient, *m* is the mass of the prism, *g* is the gravitational acceleration and θ is the angle of inclination of the plate. The glass prism will slide over the support if the applied gravitational pulling force $mg\sin\theta$ exceeds the static friction force $\mu_s mg \cos\theta_c$. Here θ_c is the critical angle above which this criterion is met. At a smaller angle, i.e. $\theta < \tan^{-1}\mu_s$, the prism can be considered to be at a stuck state. If there was no static friction and the object would experience only linear kinematic friction, just like a colloidal particle in a fluid, the glass prism would always be in moving state and its drift velocity could have been estimated as $\bar{\gamma}\tau_L$, where $\bar{\gamma} = g\sin\theta$ and $\tau_L = m/\zeta$ with ζ being the kinematic friction coefficient. However, with the application of a white noise, the prism exhibits stochastic forward and backward motion along with the net drift toward the applied bias even at an angle much smaller than the critical angle. Still there is intermittent sticking and running phases with the time window of sticking phase decreases with increasing noise strength, hence net drift velocity increases with noise. A point to be noted that if the imposed noise was truly white noise, there would always be a powerful impulse within any short duration of time that would dislodge the object. In a real situation, there is no external noise which can be perfectly white, and thus within a short duration of time, the object may not be dislodged.

The object remains in stuck state on the surface, till an impulse of sufficient strength arrives to rescue it from that state [12].
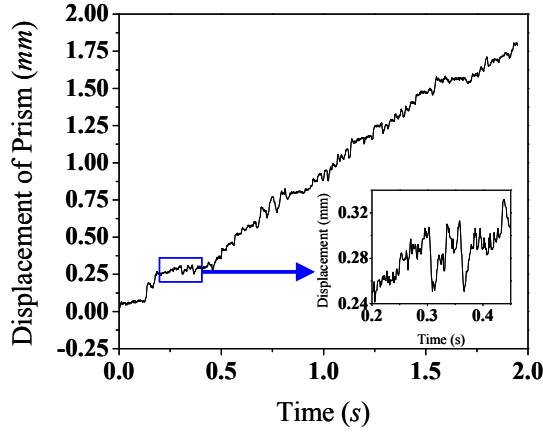
Figure 3.3: Stochastic motion of prism on solid substrate subjected to truncated Cauchy noise of power 0.053 m^2/s^3.

The solid prism moves stochastically with an average downward drift is shown in Figure 3.3. Both the drift velocities and diffusivities were measured by varying the power of the noise. With the definition of the velocity probability distribution described by equation 3.4, the average drift velocity of the prism can be obtained from the following equation:

$$V_{drift} = \frac{\int_{-\infty}^{+\infty} VP(V)dV}{\int_{-\infty}^{+\infty} P(V)dV} \qquad 3.5$$
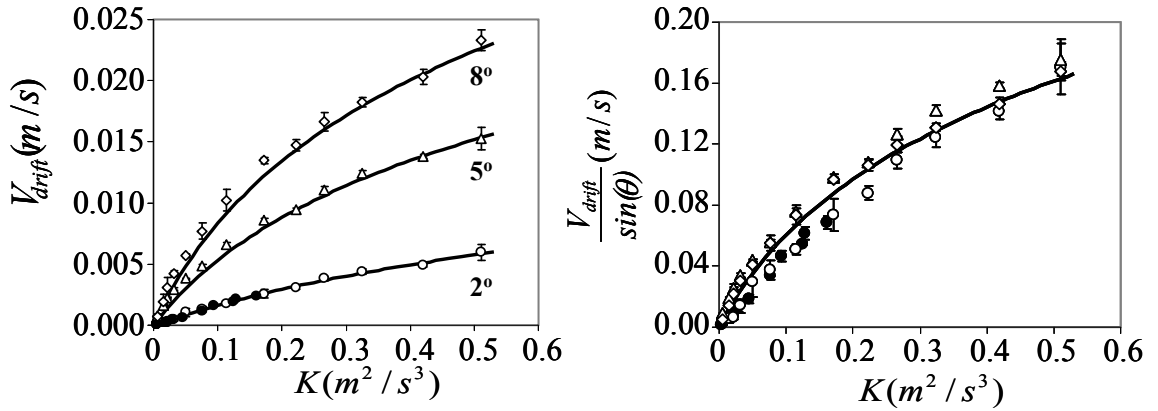
Figure 3.4: (Left) Drift velocities (V_{drift}) of a glass prism on a slightly roughened glass support at three different inclinations (angles are shown in the figure) and various powers (K) of the noise. (Right) Drift velocities (V_{drift}) are divided by $\sin\theta$ where θ is angle of inclination. Open symbols correspond to Gaussian noise and closed symbols correspond to truncated Cauchy noise. All the data roughly fall close to a single master curve.

Figure 3.4 summarizes the drift velocities of the solid prism as a function of the power of Gaussian white noise K at three different angles of the inclination of the plate. As expected, V_{drift} increases both with K and θ. These data could be analyzed with equations 3.4 and 3.5, with $\bar{\gamma} = g\sin\theta$. From this analysis, the average values of Δ and τ_L are estimated to be 3.84 m/s^2 and 0.067 s respectively. These values of Δ and τ_L were used for the numerical simulations of the drift velocity and diffusivity to be discussed below. The velocities obtained with truncated Cauchy noises of various powers are also given in these figures for comparison. Indeed the velocities obtained with both types of white noises are indistinguishable.

43

An approximate equation that can describe the drift velocity as a function of $\bar{\gamma}, \Delta, K$ and τ_L, has been reported in reference [15] :

$$V_{drift} = \frac{\bar{\gamma}\tau_L}{1 + \frac{\Delta^2 \tau_L}{K}}$$

3.6

All the drift velocity data can also be fitted with equation 3.6 quite well with slightly different numerical values of Δ (3.6 m/s^2) and τ_L (0.03s).

The diffusivities were estimated from the stochastic motion of the prism on the 2$^\text{o}$ inclined surface subjected to Cauchy noise of different powers as well as to Gaussian noise at power 0.09m^2/s^3. Displacement fluctuation or jump length (x_τ) data for a various time segments (τ) as obtained from several tracks were combined from which a probability distribution for displacement was constructed. The mean $\langle x_\tau \rangle$ and variance $\sigma^2 = \langle x_\tau^2 \rangle - \langle x_\tau \rangle^2$ was estimated from the probability distribution of the displacement fluctuation. The variance increases linearly with τ as expected of a simple diffusive process (Figure 3.5), the slope of which gives the estimation of the diffusivity according to the following relation: $\sigma^2 = 2D\tau$. For this analysis to be valid, τ needs to be sufficiently large in order to ensure that a steady state is reached. In the steady state regime, the variance of the displacement is linear with time.
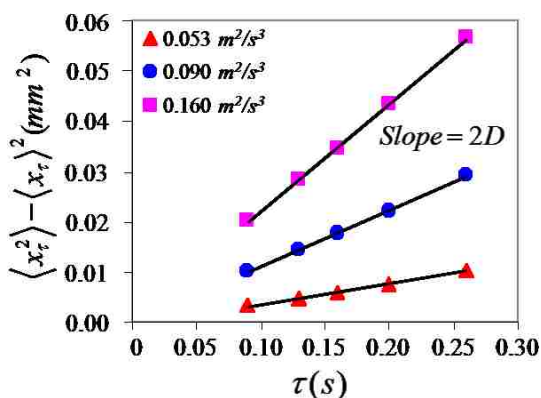
Figure 3.5: Plot of the variance $\langle x_\tau^2 \rangle - \langle x_\tau \rangle^2$ of the displacement of the prism subjected to truncated Cauchy noise of different powers. The diffusivity, which is calculated from the slope of linear plots, increases with the power of the noise. Here data are shown for three powers only. We have performed these measurements for a total of five different powers.

At this point, we would like to justify the use of truncated Cauchy noise over Gaussian noise in our statistical experiments involving the estimation of diffusivity, and displacement fluctuation analysis. As illustrated in Figure 3.6, the experimentally observed pdf's of the displacement for both the Gaussian and truncated Cauchy noises almost super-impose onto each other except for the low $P(x_\tau)$ region where the statistics become somewhat poorer for the Gaussian distribution compared to the truncated Cauchy distribution.
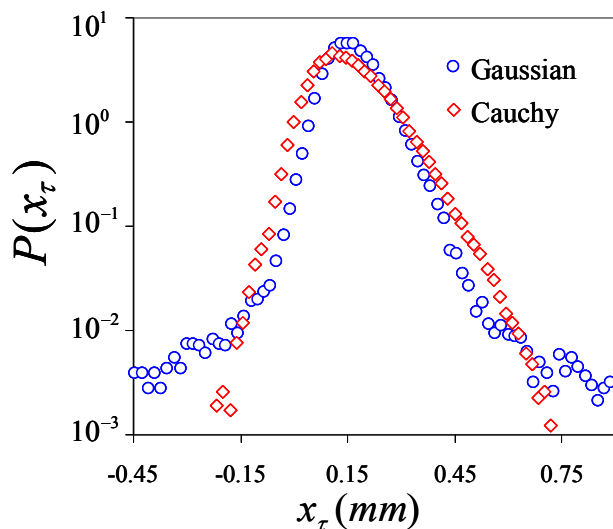
Figure 3.6: Log-Linear plot of the probability distributions of the displacement (x_τ) of the prism subjected to Gaussian and truncated Cauchy noises. The data for each noise was obtained from about 132 steady state tracks, each lasting for about 2.5 seconds. In the lower part of the distributions, the statistics for the Cauchy noise is much better than that of a Gaussian noise, where considerable scatter is observed. The experiment is carried out at a power (K) of $0.09\, m^2 / s^3$. The displacement distributions are for $\tau = 0.09\sec$.

This difference may inseminate from the heavy tail distribution of the Cauchy noise, which is especially useful for the analysis of the displacement fluctuation to be discussed later. Thus these two properties of a truncated Cauchy noise that produce drift and diffusion exactly same as that of a Gaussian noise, and that it improves the statistics in the region of low probability region are quite ideal for us. The features resulting from a real Levy distribution cannot be reproduced in our system, as its power diverges.

3.3.2 Numerical simulation

We numerically integrated the Langevin equation 3.1 using the generalized integration method for stochastic differential equation as prescribed by Gillespie [27]. Displacement (x) of prism as a function of time (t) was obtained from the instantaneous velocity given by the solution of equation3.1. We used $\bar{\gamma} = g\sin\theta$ which is the bias force acting on the prism, with θ set to 2° as in the experiments. We used the acceleration data, $\gamma(t)$, obtained directly from the accelerometer as input acceleration for the numerical analysis. The external acceleration $\gamma(t)$ acting on the prism has either Gaussian or truncated Cauchy probability distributions with a mean that almost approaches zero (~0.4% of the rms value). The non-exact zero mean results from the fact that very large numbers of acceleration are averaged coupled with the fact that the numbers are rounded off during the digitizing process. However, this small numerical error does not contribute appreciably in estimating the values of diffusivities, although it can lead to some error in estimating the drift velocities at very low bias. Here we focus our attention on the estimation of diffusivity. As the high-speed video recording in experiments is done at an interval (*dt*) of 1ms, data from the accelerometer is obtained at the same interval. These acceleration data are then scaled in order to match the power of noise (0.004 to 0.16 $m^2/\sec^3$) used in the experiments with two additional values estimated at powers of 0.3 and 0.5 $m^2/\sec^3$. The Langevin equation is then integrated with an integration time step of *dt* =1ms, which is equal to the video recording interval in experiments. The simulations are carried out for 50 tracks with an integration time of 10sec for each track.

The values of Δ and τ used in the simulation are 3.84 m/s^2 and 0.067 s respectively, which were obtained from the analysis of the data shown in Figure 3.4. Since the Columbic friction $\sigma(V)\Delta$ always acts in the direction opposite to the motion of the prism, it is set as $\sigma(V)=V/|V|$ in the simulations. When the net acceleration ($|\bar{\gamma}+\gamma(t)|$) acting on the prism is less than the threshold acceleration (Δ) required to set the prism into motion, the prism gets stuck to the plate, hence the velocity of prism is set to zero. The displacement data for a given time interval τ obtained from several tracks are combined to obtain a probability distribution for displacement as is done for the experimental analysis of the displacement data. The diffusivity was estimated from the slope of the plot σ^2 versus τ.

Analytical theory and stochastic Langevin simulations for a prism on a solid substrate both show that the diffusivity varies linearly with K in the absence of dry friction (Figure 3.7). Nature of the noise, whether it is Gaussian or the truncated Cauchy noise do not make any significant difference to the results of the simulation. However, when $\Delta \neq 0$, the simulated diffusivity is much lower than that for $\Delta = 0$ and it varies as $K^{1.74}$ (Figure 3.7). The observed exponent of K is certainly larger than 1 which is for purely kinematic friction case, but it is smaller than the value of 3 as expected for a pure dry friction [12]. This disagreement is expected as we have the situation which is governed by combination of both dry friction and kinematic friction.

Numerical solution also predicts that the diffusivities vary by four orders of magnitude (10^{-9}m^2/s to 10^{-5} m^2/s) with the variation of the power from 0.004 m^2/s^3 to 0.5

m^2/s^3 which is slightly higher than that obtained from the experimental results (Figure 3.7). These values are much lower than the values obtained with $\Delta = 0$. Except for the datum obtained with the lowest power (0.004 m^2/s^3), the experimental diffusivity increases with *K* with an exponent of 1.61. This exponent is also close to that (1.74) obtained from the simulations with the Columbic friction. When the power reaches to a value as low as 0.004 m^2/s^3, the dynamics of the prism slows down dramatically. It is possible that at such low power, other effects such as heterogeneities, both static and dynamic, may start to play additional roles over that of the average effect of Columbic and kinematic friction. Another possibility of this suppressed diffusivity at low noise strength may be due to the domination of the Coulombic friction over the kinematic friction at this low noise regime.

The prime finding of this work is that the external noise induced diffusivity of one solid on another is significantly dominated by Columbic friction. This diffusivity is at least couple of orders of magnitude lower than that controlled by kinematic friction. A Langevin equation with an additional Columbic dry friction term enables us to analyze the situation of both the diffusivity and the drift velocity rather satisfactorily. The drift velocity is predicted to increase sub-linearly with the power of the noise, which is in agreement with the experimental observations. The experimental diffusivity values are also close to the simulated values with dry friction. While the experimental diffusivity increases with the power of the noise as $K^{1.61}$, the simulations predict $K^{1.74}$.
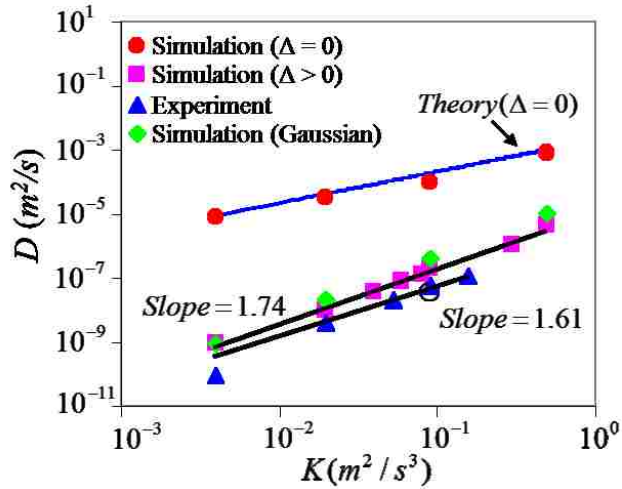
Figure 3.7: Log-Log plot of diffusivity as a function of power of noise. The scaling law established from experiments (blue triangles) is $D \sim K^{1.61}$ whereas the numerical simulation (pink squares) predicts $D \sim K^{1.74}$. Diffusivity values obtained by numerical simulation in the absence of dry friction ($\Delta = 0$) are also shown (red filled circles) which agree well with theoretically predicted values (blue solid line) for kinematic friction only. The experimental diffusivity (open circle) of prism subjected to Gaussian noise of power 0.09 m²/s³ is close to the value obtained using Cauchy noise at the same power.

Although these exponents do not represent a large discrepancy, there are differences in the numerical values of the simulated and measured diffusivities. We should be aware of some potential pitfalls related to the simulations and experiments.

1.   The simulations are coarse-grained, in which the data collection and the video recordings were done at the interval of 1 ms. Some of the finer details of the stochastic dynamics may be lost in these simulations.

2. Equation 3.1 may be an oversimplification to account for the Columbic friction because heterogeneity and metastable states may be involved in real situation.

3. Heslot *et al* [28] studied the effect of Columbic friction on the dynamics of an object in which they have taken into account the state and rate dependent Columbic friction laws. Our current friction law is, on the other hand, is extremely simple. Columbic friction signifies elastic energy dissipation during the contact and breaking of junctions. When the slider receives an external impulse of a short duration, it should accelerate or decelerate with concomitant energy dissipation in bursts. At high speeds, turbulent micro-slip may occur at the interface leading to high energy dissipation. These details are not taken into account in our studies as we employ only a constant value of the Columbic friction, Δ.

3.3.3 Displacement PDF in presence of Coulombic friction

Mauger already pointed out theoretically that the non-Lipschitz continuity of the Coulombic friction results the non-Gaussian distribution of the velocity distribution [13]. For a process governed by kinematic friction, the distribution function is itself Gaussian. However, in the granular media, a non-Gaussian distribution [29–36] of the velocity pdf has been linked to the energy loss due to inelastic collisions. There are other cases to consider in which a threshold force of a different nature may act on a particle. An example of which involves biological cells partially adhering to a solid surface, in which case the random motion [37] of the cells exhibits a stick-slip process. Another example is the condensation and growth of liquid drops on a surface that may be prone to a random motion due to various fluctuations, but its motion is inhibited by wetting hysteresis [38]. In another study of the random motion of liquid droplet [15] revealed that the critical force due to hysteresis significantly reduces the mobility of the drops.
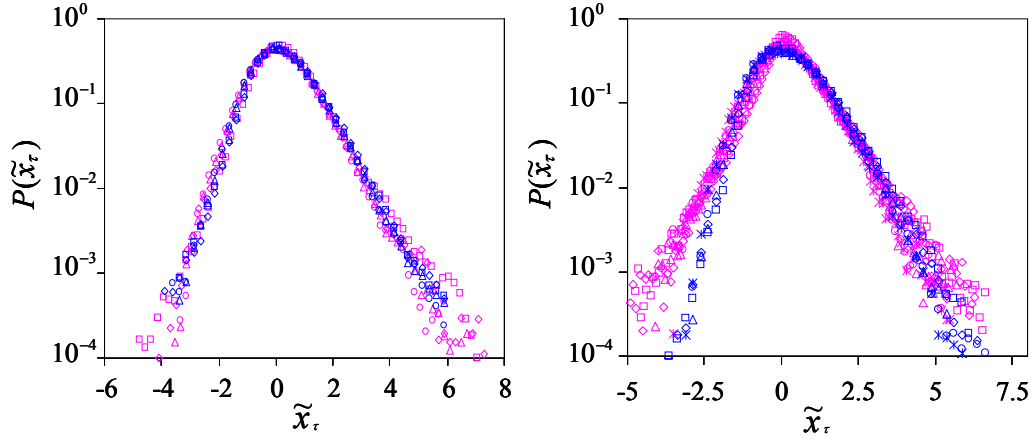
Figure 3.8: (Left) Probability distribution of normalized displacement $\left(\tilde{x}_\tau = \left(x_\tau - x_p \right) / \sigma_{x_\tau} \right)$ of prism at time intervals: 0.05s (□), 0.09s (◊), 0.13s (Δ) and 0.16s (o) with a Gaussian noise (power 0.09 m^2/s^3), but in presence of a Columbic friction. The blue and pink colors indicate experimental data and simulation results respectively. (Right) Normalized displacement distribution with a Cauchy noise (power 0.09 m^2/s^3) for time intervals: 0.07s (□), 0.09s (◊), 0.16s (Δ) and 0.20s (o). The blue and pink colors indicate experimental data and simulation results respectively. In order to generate such fluctuation plots data obtained from about 132 steady state tracks, each lasting for about 2.5 seconds, were combined.

The pdf of the displacement fluctuation of the solid prism is predominantly exponential except being Gaussian towards the central region for both the Gaussian and truncated Cauchy noise. The normalized plots of experimental and simulated displacement pdfs are shown in Figure 3.8. Irrespective of the previously mentioned limitations of the simulations, the predictions of equation 3.1 are reasonably good, at least to a first order of approximation. The general shapes of the displacement distributions, and its asymmetry in some cases, are reproduced rather well. Simulations also show that the distribution is mainly exponential for $\Delta \neq 0$, but it becomes Gaussian when $\Delta = 0$ (Figure 3.9). Thus the phenomenon resulting from Columbic friction ($\Delta \neq 0$) is clearly encoded in the

experimental displacement distribution function as expected according to theoretical prediction of the velocity distribution function (Eq.3.4), as velocity *V=dx/dt*. In a recent paper Jarzynski [39] already mentioned that the distribution functions encode various types of physical processes. For example, it could encode the free energy changes in a dynamic process. Several recent experiments [40,41] used this idea to estimate equilibrium free energy change of biological processes from the dissipative work measurements.
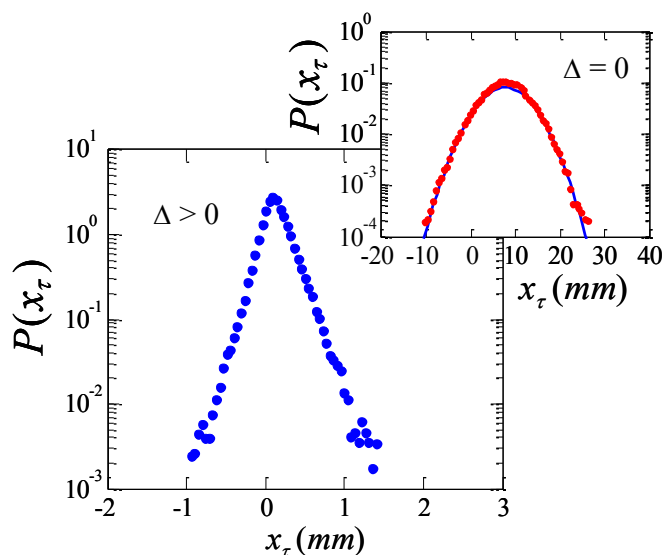
Figure 3.9: Log-Linear plot of the probability distribution of displacement (x_τ) obtained using numerical simulation of modified Langevin equation (Eq. 1). The simulation is carried out at a power (*K*) of 0.09 m^2/s^3 with parameters $\Delta = 3.84\,m/s^2$ and $\tau_L = 0.067\,\sec$ which are obtained by fitting drift velocities data to equation 3.5. The distribution is clearly exponential. The inset shows the simulated probability distribution of displacement obtained by setting $\Delta = 0$. The displacement distribution fits well with Gaussian distribution as shown by blue thick solid line. The displacement distribution shown here for $\tau = 0.09\,\sec$.

Since the displacement distribution is found to have a finite variance that is linear with time, we expect that the displacement pdf to be Gaussian for the case with pure kinematic friction:

$$P(x_\tau) = P_o e^{-\frac{(x_\tau - x_m)^2}{(4D\tau)}} \qquad\qquad 3.7$$

where all the terms have their usual meanings. A work fluctuation like equation [42–46] is easily anticipated from equation 3.7 if we define the work as $W_\tau = \bar{\gamma} x_\tau$. However, this could be a bit misleading in our case since work is being performed by both noise and gravity. The above Gaussian distribution is valid for $\Delta = 0$ when the relaxation time is the characteristic Langevin relaxation time and the ratio of the diffusivity to mobility $\left(\mu = \frac{V_{drift}}{m\bar{\gamma}} \right)$ is:

$$\frac{D}{\mu} = \frac{mK\tau_L}{2} \qquad\qquad 3.8$$

Experimental (Figure 3.10) ratio of D/μ is found to increase slightly sub-linearly with K as $K^{0.8}$ with relaxation time scales (0.0002s to 0.0004s) that is much smaller than any of the relaxation times of the system, either of the dry friction ($\tau_\Delta = K/2\Delta^2 \sim 0.003$ s) or of the kinematic friction ~ 0.067 s. It is not surprising in the first place as Eq. 3.8 is applicable for a system controlled by purely kinematic friction. We expect that distribution function as shown in equation 3.7 needs to be multiplied by an appropriate exponential function in order to obtain a result as close as possible to the real

(experimental) distributions. However, a proper theoretical treatment must also take into account the asymmetric distribution that is observed experimentally. Some of this asymmetry definitely arises from the biased step length towards the applied force, although a significant source of the asymmetry may also come from the fact that the noise is not a true white noise, but colored with appreciable correlation that couples non-linearly with the dry friction. We have some numerical results to support the above points, which we will address in detail in next chapters.
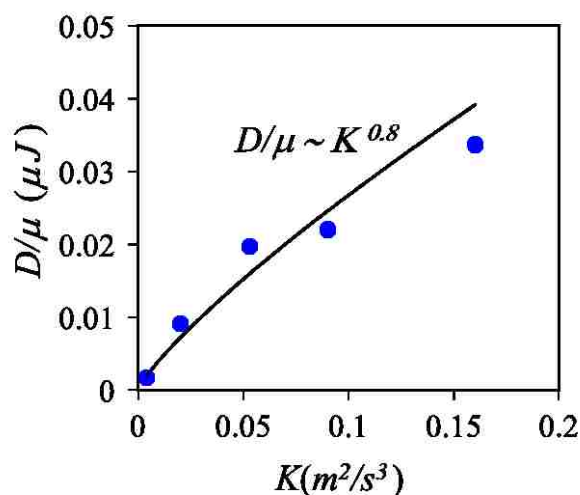
Figure 3.10: D/μ obtained for a prism subjected to truncated Cauchy noise as a function of power of noise (K).

With increasing τ , the exponential displacement distribution, which is the signature of a dry friction, eventually evolves into a Gaussian distribution, prominently in the central region. The degree of "peakedness" of a distribution is generally measured by Kurtosis (β), which is defined by the ratio of the fourth central moment of a distribution

and fourth power of standard deviation. For highly peaked distribution (e.g. exponential distribution), β is greater than 3(Leptokurtic distribution) and equals to 3 for Gaussian distribution. Estimation of β for different time intervals reveals that with time it approaches towards 3 starting from a high value (Figure 3.11). In the present situation, although the distribution is more like Gaussian at large time scale, the underlying effect of the dry friction is still there which is evident from the asymmetric exponential nature of the tail region of the distribution. Similar observation is reported recently which is related to the study of the displacement distribution of a colloidal bead adhered and diffusing on lipid tubes [47]. The exponential displacement distribution at the short time limit is observed in their system due to the presence of Coulomb like friction as a disguise of adhesion force between the colloidal particle and the lipid microtubule.
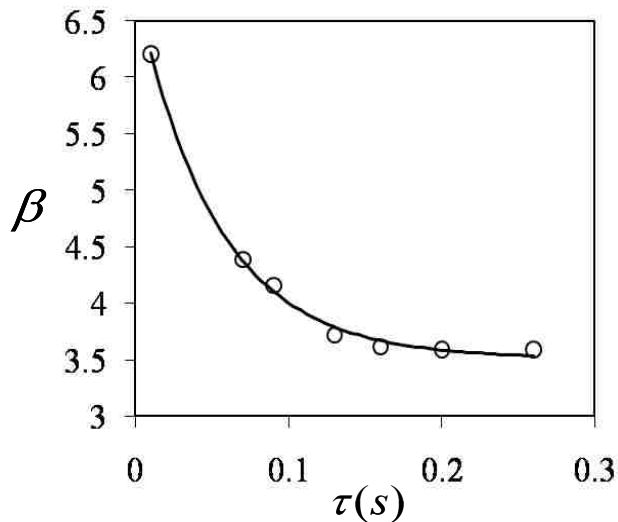
Figure 3.11: Kurtosis (β) of displacement distribution as a function of time for the prism subjected to a truncated Cauchy noise of power 0.09 m^2/s^3.

3.3.4 Displacement fluctuation theorem

Although we considered that the experimental distribution function is represented approximately with a Gaussian function but with the values of the diffusivities and mobilities resulting from such do not satisfy the fluctuation relation $D/\mu = mK\tau_L/2$ (Figure 3.10). We calculate the probabilities of observing positive and negative displacement fluctuations from equation 3.7 and rearrange the results as follows:

$$\frac{P(+x_\tau)}{P(-x_\tau)} = e^{\left(\frac{\bar{\gamma}x_\tau}{(D/\mu)}\right)} \tag{3.9}$$

For the dry friction, as the value of D/μ is much smaller than that expected of a kinematic friction, the probability of a negative displacement fluctuation is more strongly suppressed than the case with the pure kinematic friction. We study the displacement fluctuation in terms of a scaled variable $\bar{x}_\tau = x_\tau / x_p$. As defined above, x_p is the displacement value at the peak of the distribution function, whereas the mean displacement is x_m. Equation 3.9 can be rearranged as

$$\left(\frac{D\tau}{x_m x_p}\right) ln\frac{P(+\bar{x}_\tau)}{P(-\bar{x}_\tau)} = \bar{x}_\tau \tag{3.10}$$

Figure 13 shows that the fluctuation pdf of the scaled displacement obtained for the solid prism becomes stiffer either with the increase of time or with the increase of the power as expected from equation 3.10. All the probability data can be normalized by multiplying the function $ln\frac{P(+\bar{x}_\tau)}{P(-\bar{x}_\tau)}$ with $D\tau/x_m x_p$. We plot this normalized function (

$\pi(\bar{x}_\tau)$), i.e. the left side of equation 3.10 as a function $\bar{x}_\tau$ either taking the data from the measurements done at various time segments for a constant power or at different powers corresponding to a fixed time segment. In both cases, we obtain results that superficially agree with the conventional fluctuation theorems of different varieties (Figure 3.13) [42–46].
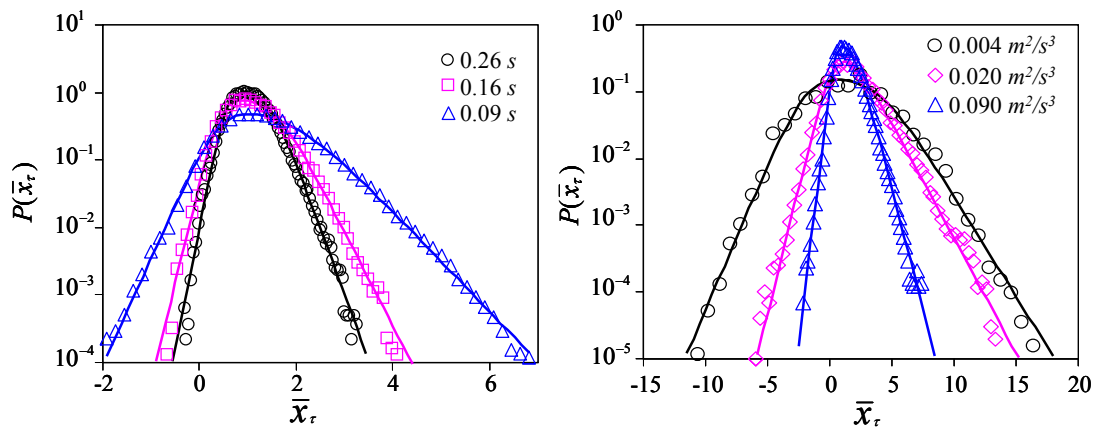
Figure 3.12: (Left) Some representative probability distributions of the normalized displacement $\left(\bar{x}_\tau = x_\tau / x_p\right)$ of solid prism subjected to Cauchy noise (power 0.09 m²/s³), at different time intervals. (Right) Some representative probability distribution of normalized displacement of prism at different powers of Cauchy noise for a particular time interval ($\tau = 0.09s$). In order to obtain these distributions, data obtained from about 50 to 130 tracks were combined in order to generate good statistics. The total number of tracks is based upon the duration of each track so that a total of about 300 seconds of data are obtained.
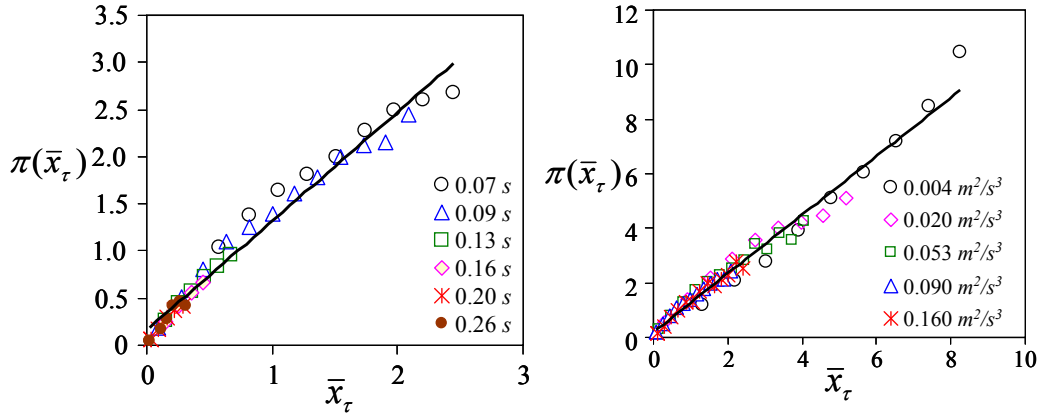
Figure 3.13: (Left) Fluctuation plot of normalized displacement $\left(\bar{x}_\tau = x_\tau / x_p\right)$ of the solid prism subjected to Cauchy noise (power 0.09 m²/s³) at different time intervals. (Right) Fluctuation plot of normalized displacement of prism at different powers of Cauchy noise for a particular time interval $(\tau = 0.09s)$. Here $\pi(\bar{x}_\tau)$ is defined as $\left(D\tau / x_m x_p\right)\ln\left(P(+\bar{x}_\tau) / P(-\bar{x}_\tau)\right)$.

3.3.5 Energy dissipation rate

In order to seek a relationship between D/μ and the rate of energy dissipation ($\dot{q}$), which directly measures the power experienced by the slider we attempted to make a rough estimate of the power dissipation. Let's examine the integrated form of the Langevin equation:

$$\frac{1}{2}[V^2(t+\tau) - V^2(t)] = gsin\theta \int_t^{t+\tau} V(t)dt + \int_t^{t+\tau} \gamma(t)V(t)dt - \int_t^{t+\tau} \left(\frac{V^2(t)}{t} + \Delta|V(t)|\right)dt \qquad 3.11$$

Kinetic energy   Gravitational work   Vibrational work   Heat

The term on the left side of equation 3.11 is the change of the kinetic energy in going from one state to another, the average value of which is zero. The first term on the right

side of the equation is the work done by the external force, the second term is the work done by the external noise, whereas the third term in the above equation is the net energy dissipation. This term has two components: its first component is the heat generated (and dissipated) by the kinematic friction, whereas its second component is the energy dissipation due to Columbic friction. In order to make an approximate estimate of the total energy dissipation, we consider their averages values as :

$$\dot{q} \approx \left\langle \left(\frac{V^2(t)}{\tau} + \Delta|V(t)| \right) \right\rangle \qquad \qquad 3.12$$

It is easy to show that $\dot{q}$ is related to the power of noise as *K/2*. This can be demonstrated by neglecting the kinematic friction term of equation 3.12 and calculating $\left\langle |V(t)| \right\rangle$ using equation 3.5. One thus finds, $\left\langle |V(t)| \right\rangle = K/2\Delta$, from which we get $\dot{q} = K/2$. Equation 3.12 then becomes:

$$\frac{D}{\mu} = \dot{q}\tau_d \qquad \qquad 3.13$$

where τ_d is a characteristic time for energy dissipation.

As mentioned earlier that we lost some of the finer details of the displacement fluctuations and hence the estimation of velocities is coarse grained due to the limitation of the temporal resolution of the video camera (1000fps). Some of the stochastic processes occur at a faster rate than what our experimental set-up can capture. Thus, this does not allow us to get an handle on the transients, or the fast acceleration/deceleration phases, which could be behind some of the interesting physics of fluctuations. In any

event, the ratio D/μ is found to increase with $\dot{q}$ (Figure 3.14) roughly linearly. The positive intercept of the regression line on the $\dot{q}$ axis suggests that a minimum power is needed before the prism starts sliding on the surface. At a power lower than the threshold, there is, of course, neither any energy dissipation nor any mobility of the slider. In this low power region, there may underlie additional interesting physics akin to jamming or glassy dynamics that may be worth pursuing in future.
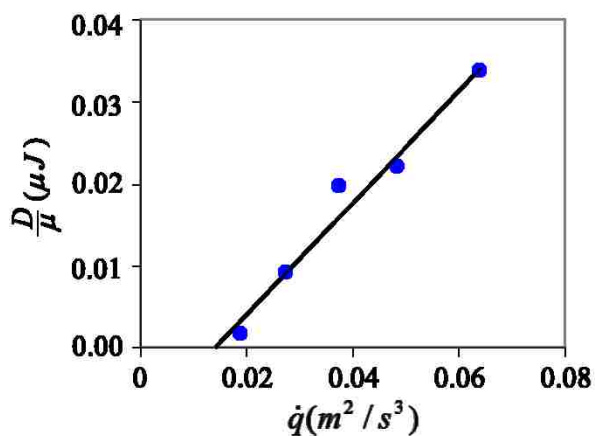
Figure 3.14: D/μ varies approximately linearly with the rate of energy dissipation ($\dot{q}$).

Characterization of systems that is driven away from equilibrium by an external force is traditionally done in the contexts of the fluctuations theorems [48–53], which deal with the entropy production in time reversible systems. These theorems consider a finite probability of the decrease of entropy in certain trajectories of a dynamic process and states that the ratio of the probabilities of positive and negative entropy production rates varies exponentially with the rate of positive entropy generation. Various attempts

have been made to examine the validity of non-equilibrium fluctuation theorems experimentally and via numerical simulations. At the microscopic level, an elegant and popular experiment [54–56] is to trap a colloid particle in an optical tweezers and move it with pre-determined controls of parameters. What is observed is that the colloid particle moves along the direction of motion of the trap most of the time: these are the entropy generating trajectories. Occasionally the particle exhibits reverse trajectories signifying entropy consumption. The probability distributions of these entropy generating and entropy consuming events have been found to exhibit a fluctuation type relationship. Other experiments that successfully verified GC theorem involve mechanical oscillators [57], stochastic motion of a pendulum [57] immersed in a liquid resulting from the thermal noise and measurements of the energy fluctuation [58] due to flow of current in electric circuits.

Aumatre *et al* [59,60] verified the GC like fluctuation theorem numerically by studying the power injection in a shell model of turbulence, granular gas and a Burridge-Knopo spring-block model. More recently, Majumdar and Sood [61] observed that the non-equilibrium fluctuation relation holds for sheared micellar gel in a jammed state. Feitosa and Menon [62] found experimentally that the power flux fluctuation in a granular gas is generally in accord with the GC theorem as well. The energetic scaling needed to fit the power fluctuation data with the GC theorem prompted these authors to define an effective temperature of the system. Several authors [59,61–68] however cautioned about the applicability of the conventional fluctuation relations to macroscopic systems in strict thermodynamic sense as these systems do not exhibit micro-reversibility.

However, a fluctuation like relation may still work [60,63,64] in certain cases in the probabilistic sense of a "large deviation theorem".

As with the granular gases, there is no microscopic reversibility in our case either. Secondly, the energy is delivered to the slider in terms of work and not in terms of a thermal energy. Hence, we cannot strictly analyze any of our results with the conventional entropy fluctuations theorems in any straight-forward way. We feel that even converting the displacement to work is problematic as work is being done by both the noise and gravity. Even if the displacement is negative (i.e. slider moves upward), it is not convincing that a negative work is performed in the process --powerful fluctuations push the object upward once in a while. This point can be clarified further by taking into consideration an experiment published [68] a few years ago by our group in collaboration with L. Mahadevan. A hydrogel rod was placed perpendicularly to an asymmetric cut of a support and the latter was vibrated with a periodic vibration. The asymmetry in the friction rectified the vibration induced force and led to the motion of the hydrogel. More recently, Buguin *et al* [69] performed an experiment (similar to that reported in ref [70]), in which a coin moved on a substrate vibrated with an asymmetric waveform. In both the above experiments, where work is being done by the external vibration, velocity increased linearly with the amplitude of vibration. However, in both the experiments (Figures 4 and 2 in references [68] and [69] respectively), a threshold amplitude is observed below which no motion takes place. This threshold force is indicative of the presence of a Columbic friction at the interface. Now, it should also be possible to induce the motion of the hydrogel on the surface having asymmetric friction

with a white noise vibration with a zero mean. As there is no bias, the only work done on

the hydrogel rod would be of the form: $m\int\limits_{t}^{t+\tau}\gamma(t)V(t)dt$, where $V(t)$ is the fluctuating

velocity. If the acceleration pulse and the velocity response are highly correlated, then the

above work is mostly positive, as found by Farago [63], even though the velocity and

displacement fluctuate between the negative and positive values. On the other hand, there

will be negative fluctuation of the above work if the acceleration pulse and velocity are

somewhat uncorrelated. In any event, in the context of the current experiment, the work

done by vibration, $m\int\limits_{t}^{t+\tau}\gamma(t)V(t)dt$ has to be added to that done by the gravity,

$mg\sin\theta\int\limits_{t}^{t+\tau}V(t)dt$ in order obtain the total work done on the slider. This total work may

turn out to be mainly a positive quantity with very few negative fluctuations.

Gaussian distribution would always follow the fluctuation relation of the type

shown in equation 3.9. For example, Seitaridou *et al* [71] recently found that the

diffusion flux of colloids in small systems exhibit a Gaussian fluctuation, which is

consistent with a conventional fluctuation theorem. Whether or not such a compliance

with the conventional fluctuation theorems has a deeper physical significance for systems

driven out of equilibrium with external noise needs further studies. At present, we

hesitate to attaching specific thermodynamic significance to the measured displacement

fluctuations other than recognizing that it is a kind of measure of the gravitational

potential energy fluctuation. However, all the terms pertaining to works performed by

the noise as well as the gravitational field and the energy dissipations by all the frictional terms need to be sorted out more clearly experimentally as well as theoretically.

3.4 Conclusion

1. A solid block stick to a surface and would not move till the external force is larger than the Columbic friction. The objects would, however, move on the substrate if they are vibrated with a white noise. The drift velocity can be accounted for with a Langevin equation with Columbic friction within the framework of Klein-Kramers equation.

2. In addition to studying the drift velocity, we can also study the fluctuations of the displacements related to these systems. It has been found that the probability distributions of displacements in all cases are non-Gaussian, which is adequately supported by the numerical simulation of the Langevin equation including Columbic friction. The simulations also confirm that the exponential distribution of the displacement arises due to the presence of a threshold force (Columbic friction) that needs to be overcome to initiate motion.

3. The ratio of the diffusivity to mobility varies sub-linearly with the power of noise. However, the characteristic time scale observed from this analysis is much smaller than any of the characteristic time scales of the system.

4. A final and important comment is about the asymmetry of the displacement distributions of either the block or the drop in the presence of a Columbic friction or hysteresis. When the object is vibrated with a white noise with $\Delta = 0$, the probability

distribution is symmetrical. However, the distribution becomes asymmetric when $\Delta > 0$ and this asymmetry increases with $\bar{\gamma}$ as well as with the power of the noise. Thus, the asymmetric distribution could be another signature (in addition to the predominance of the exponential distributions) of a non-equilibrium system where a threshold force such as a Columbic friction (for solids) or a hysteresis (for drop) is operative at the interface.

References

[1]   L. Z. Prandtl, Angew Math. Mech. **8**, 85 (1928).

[2]   G. A. Tomlinson, Philosophical Magazine **7**, 905 (1929).

[3]   I. R. Lapidus, American Journal of Physics **38**, 1360 (1970).

[4]   C. Barrat and G. L. Strobel, American Journal of Physics **49**, 500 (1981).

[5]   C. B. Clark and C. E. Swartz, The Physics Teacher **34**, 550–554 (1996).

[6]   R. D. Peters and T. Pritchett, American Journal of Physics **65**, 1067 (1997).

[7]   J. C. Simbach and J. Priest, Notes 2004–2006 (2005).

[8]   T. K. Caughey and J. K. Dienes, J Applied Physics **32**, 2476 (1961).

[9]   T. K. Caughey, J Acoust. Soc. Am. **35**, 1706 (1963).

[10]   H. Hayakawa, Physica D **205**, 48–56 (2005).

[11]   A. Kawarada and H. Hayakawa, Journal of the Physical Society of Japan **73**, 2037 (2004).

[12]   P.-G. De Gennes, Journal of Statistical Physics **119**, 953–962 (2005).

[13]   A. Mauger, Physica A: Statistical Mechanics and Its Applications **367**, 129–135 (2006).

[14]   H. Risken, *Risken, H., The Fokker-Planck-Equation. Methods of Solution and Applications. ISBN3-540-50498-2 (Springer Series in Synergetics 18)*, Second ed (Springer-Verlag, 1991).

[15]   M. K. Chaudhury and S. Mettu, Langmuir : the ACS Journal of Surfaces and Colloids **24**, 6128–32 (2008).

[16]   T. Baumberger, L. Bureau, M. Busson, E. Falcon, and B. Perrin, Review of Scientific Instruments **69**, 2416–2420 (1998).

[17]   L. Bureau, C. Caroli, and T. Baumberger, Proceedings of the Royal Society A: Mathematical, Physical and Engineering Sciences **459**, 2787–2805 (2003).

[18]   A. Chechkin, V. Gonchar, J. Klafter, and R. Metzler, Physical Review E **72**, 28–30 (2005).

[19]   R. N. Mantegna and H. E. Stanley, in *The Physics of Complex Systems [Proceedings of the International School of Physics "Enrico Fermi" Course CXXXIV]*, edited by F. Mallamace and H. E. Stanley (IOS Press, Amsterdam, 1997), p. 473.

[20]   R. N. Mantegna and H. E. Stanley, Phys. Rev. Lett. **73**, 2946 (1994).

[21]   J.-D. Bao, Physica A: Statistical Mechanics and Its Applications **346**, 261–270 (2005).

[22]   B. Dybiec, E. Gudowska-Nowak, and I. Sokolov, Physical Review E **78**, 1–9 (2008).

[23]   H. Touchette and E. Cohen, Physical Review E **76**, 2–5 (2007).

[24]   D. del-Castillo-Negrete, V. Y. Gonchar, and a. V. Chechkin, Physica A: Statistical Mechanics and Its Applications **387**, 6693–6704 (2008).

[25]   O. Bénichou, C. Loverdo, M. Moreau, and R. Voituriez, Physical Review E **74**, 1–4 (2006).

[26]   M. A. Lomholt, T. Koren, R. Metzler, and J. Klafter, PNAS **105**, 11055–11059 (2008).

[27] D. T. Gillespie, Am J Phys **64**, 225 (1996).

[28] F. Heslot, T. Baumberger, B. Caroli, and B. Perrin, **49**, (1994).

[29] W. Losert, D. G. W. Cooper, J. Delour, a. Kudrolli, and J. P. Gollub, Chaos (Woodbury, N.Y.) **9**, 682–690 (1999).

[30] J. Olafsen and J. Urbach, Physical Review Letters **81**, 4369–4372 (1998).

[31] J. S. Olafsen and J. S. Urbach, Physical Review E **60**, 2468–2471 (1999).

[32] F. Rouyer and N. Menon, Physical Review Letters **85**, 3676–9 (2000).

[33] T. P. C. Van Noije and M. H. Ernst, Granular Matter **1**, 57–64 (1998).

[34] C. Bizon, M. D. Shattuck, J. B. Swift, and H. L. Swinney, Physical Review. E, Statistical Physics, Plasmas, Fluids, and Related Interdisciplinary Topics **60**, 4340–51 (1999).

[35] X. Nie, E. Ben-Naim, and S. Y. Chen, Europhysics Letters **51**, 679 (2000).

[36] A. Prevost, D. Egolf, and J. Urbach, Physical Review Letters **89**, 1–4 (2002).

[37] D. Selmeczi, L. Li, L. I. I. Pedersen, S. F. Nrrelykke, P. H. Hagedorn, S. Mosler, N. B. Larsen, E. C. Cox, and H. Flyvbjerg, The European Physical Journal Special Topics **157**, 1–15 (2008).

[38] S. Daniel, M. K. Chaudhury, and J. C. Chen, Science (New York, N.Y.) **291**, 633–6 (2001).

[39] C. Jarzynski, Phys. Rev. Lett. **78**, 2690 (1997).

[40] F. Ritort, Poincare Seminar **2**, 193 (2003).

[41] C. Bustamante, Z. Bryant, and S. B. Smith, Nature **421**, 423 (2003).

[42] G. N. Bochkov and Y. E. Kuzovlev, Physica A **106**, 443–479 (1981).

[43] G. N. Bochkov and Y. E. Kuzovlev, Physica A **106**, 480–520 (1981).

[44] O. Mazonka and C. Jarzynski, arXiv:cond-mat/9912121 1–15 (1999).

[45] A. Imparato, L. Peliti, G. Pesce, G. Rusciano, and A. Sasso, Phys. Rev. E **76**, 1–4 (2007).

[46] R. Van Zon and E. G. D. Cohen, Physical Review E (2003).

[47] B. Wang, S. M. Anthony, S. C. Bae, and S. Granick, Proceedings of the National Academy of Sciences of the United States of America **106**, 15160–4 (2009).

[48] G. Gallavotti and E. G. D. Cohen, Physical Review Letters **74**, 2694–2697 (1995).

[49] G. Gallavotti and E. G. D. Cohen, Stat. Phys **80**, 931–970 (1995).

[50] D. J. Evans, E. G. D. Cohen, and G. P. Morriss, Physical Review Letters **71**, 2401–2404 (1993).

[51] G. Gallavotti, J Stat. Phys. **84**, 37 (1996).

[52] D. J. Evans and D. J. Searles, Phys. Rev. E **50**, 1645 (1994).

[53] J. Kurchan, J Phys. A **31**, 3719 (1998).

[54] G. M. Wang, E. M. Sevick, E. Mittag, D. J. Searles, and D. J. Evans, Rev. Lett. **89**, 050601 (2002).

[55] D. Carberry, J. Reid, G. Wang, E. Sevick, D. Searles, and D. Evans, Physical Review Letters **92**, 1–4 (2004).

[56] V. Blickle, T. Speck, L. Helden, U. Seifert, and C. Bechinger, Rev. Lett. **96**, 070603 (2006).

[57] F. Douarche, S. Joubaud, N. B. Garnier, A. Petrosyan, and S. Ciliberto, Rev. Lett. **97**, 140603 (2006).

[58] N. Garnier and S. Ciliberto, Rev. E **71**, 060101 (2005).

[59] S. Aumaitre, S. Fauve, S. McNamara, and P. Poggi, European Physical Journal B **460**, 449–460 (2001).

[60] S. Aumaitre, J. Farago, S. Fauve, and S. M. Namara, The European Physical Journal B **42**, 255–261 (2004).

[61] S. Majumdar and A. K. Sood, Phys. Rev. Lett. **101**, 078301 (2008).

[62] K. Feitosa and N. Menon, Phys. Rev. Lett. **92**, 164301 (2004).

[63] J. Farago, J Stat. Phys. **107**, 781–803 (2002).

[64] J. Farago, Physica A: Statistical Mechanics and Its Applications **331**, 69–89 (2004).

[65] P. Visco, a Puglisi, a Barrat, E. Trizac, and F. Van Wijland, Europhysics Letters (EPL) **72**, 55–61 (2005).

[66] A. Puglisi, P. Visco, A. Barrat, E. Trizac, and F. van Wijland, Physical Review Letters **95**, 1–4 (2005).

[67] P. Visco, A. Puglisi, A. Barrat, E. Trizac, and F. Wijland, Journal of Statistical Physics **125**, 533–568 (2006).

[68] L. Mahadevan, S. Daniel, and M. K. Chaudhury, Proceedings of the National Academy of Sciences **101**, 23 (2004).

[69]   a Buguin, F. Brochard, and P.-G. de Gennes, The European Physical Journal. E, Soft Matter **19**, 31–6 (2006).

[70] S. Daniel, M. K. Chaudhury, and P.-G. de Gennes, Langmuir : the ACS Journal of Surfaces and Colloids **21**, 4240–8 (2005).

[71] E. Seitaridou, M. M. Inamdar, R. Phillips, K. Ghosh, and K. Dill, The Journal of Physical Chemistry. B **111**, 2288–92 (2007).

4. CHAPTER FOUR: Diffusive Motion with Non-linear Friction[2]

4.1 Introduction

An unperturbed sand pile that can withstand the shear force to some extent can be identified as property of a solid. However when tapped, the pile flows and forms a layer of sands to minimize the gravitational potential energy. When the sands were buried under the pile the bulk sand particles deformed slightly and can withstand the shear force and behave like solids but when tapped the particle vibrates and loosen up the confined state and starts flowing like liquid. Many experimental and numerical studies on the rheology of granular media is well known in literature [1–4]. These studies reveal similarity with the phase transition behavior of a matter with temperature, although the temperature in the above mentioned systems is identified as the athermal noise. In the present work we are going to investigate the dynamics of an energy dissipative athermal system where white noise is injected externally in presence of bias force. We have identified a phase transition like behavior for such a system and studied the nonlinear nature of the system specific energy dissipation. There are plenty of examples of nonlinear dissipative systems such as DNA electrophoresis [5] in a gel, the diffusion of a colloidal particle in contact with a soft microtubule [6] etc. In the first case, the mobility

of the DNA is significantly reduced. In the latter case, role of non-linearity is apparent in the non-Gaussian distribution of displacements having exponential tails. Non-Gaussian displacements have also been reported for the case of palladium adatoms diffusing on tungsten. [7,8]. All these studies are in the class of thermal system.

The signature of non-linearity and thus the non-Gaussian distributions of displacement or energy fluctuations are also evident in various athermal systems that include granular flow, [9–14] hydrodynamic turbulence [15–19], evolution of climate [20], dusty plasma [21], and the driven motion of a liquid drop or a solid object on a surface [22–27]. While, some of the results can be explained on the basis of a joint probability distribution function (PDF) of the forcing and response functions [19,28] as in the power input distribution, or within the framework of superstatistics [29,30] as in the velocity distribution in turbulence, there are also perceived physical mechanisms behind some of these non-Gaussian PDFs. Examples of latter cases include the inelastic collision [31] and the Coulombic slip [32] between particles in granular gases.

Based on the previous works of de Gennes [33] as well as that of Kawarada and Hayakawa [32], it has been shown recently that a non-Gaussian PDF ensues naturally when the resistance to motion of an object is non-linear. The non-linearity may arise from a Coulombic dry friction [27] for the solid-solid case, from wetting hysteresis [22,23,27] for a liquid-solid case or (possibly) from an adhesion hysteresis related to the rolling motion of a particle on a soft substrate [6]. These non-linear resistances have one common unique feature that no motion may occur when the noise pulse is smaller than

the threshold resistance, while motion occurs when a large pulse rescues the object from the stuck state at a later stage. Mauger [34] specifically argued that it is the non-Lipschitz continuity of a resistive term in the Langevin equation that gives rise to an exponential distribution of velocity of a particle.

In this work we modified the surface chemically as well as physically to control friction and studied its effect systematically to see how it modifies a stochastic dynamics. By extending some of our previous studies [27], here we investigate how the stochastic behavior of a small solid object on a solid support is influenced by a non-linear friction when it is subjected to a Gaussian white noise and an external bias. The long term objective of this research is to implement such surface modification technologies as self-assembled monolayers, and chemi-adsorbed polymers in order to control the specific and non-specific interactions at surfaces and study their effects on friction and diffusive dynamics. The objective of the current study is to establish the methodology as well as the phenomenology underlying this approach primarily with the contact of two solid surfaces. In one case, a smooth glass prism slides against a roughened glass support. In another case, a thin (~3.7 *nm*) polydimethyl siloxane (PDMS) grafted smooth glass prism slides against a PDMS grafted silicon wafer. In the first case, the non-linearity comes from dry friction, whereas in the latter case it comes from the non-linear kinematic friction. In order to focus our discussion, let us consider a modified version of the Langevin equation as discussed by de Gennes [33] as well as by Kawarada and Hayakawa [32].

$$\frac{dV}{dt} + \frac{V}{\tau_L} + \sigma(V)\Delta = \bar{\gamma} + \gamma(t) \qquad\qquad 4.1$$

Here, V is the velocity and $\bar{\gamma}$ is the external force per unit mass, τ_L is the Langevin relaxation time (mass (m) /kinematic friction coefficient (ξ)), Δ is a non-linear resistive force divided by the mass of the object and $\gamma(t)$ is the time dependent acceleration that the object experiences from external vibration. It should be mentioned here that Daniel *et al.* [24] proposed a coupled set of equations similar to Eq. 4.1 in order to formulate the motion of a liquid drop on a surface by vibration, in which wetting hysteresis provides the non-linear resistance. When the kinetic friction itself is non-linear [21], the Langevin equation assumes the following form:

$$\frac{dV}{dt} + \frac{A|V|^n}{m}\sigma(V) = \bar{\gamma} + \gamma(t) \qquad\qquad 4.2$$

Here $A|V|^n$ is the nonlinear friction force, with the exponent n being less than unity. In general, $\gamma(t)$ can be periodic (symmetric or asymmetric) or stochastic. Let us consider the stochastic case here, for which the power (also called noise strength) associated with the noise is K. In Eq. 4.1 if the magnitude of Δ is smaller than $(\bar{\gamma} + \gamma(t))$, the object moves, otherwise it remains stuck to the surface. For this reason, it is suitable to multiply Δ with a signum function $\sigma(V)$ which is positive when $V > 0$ and negative when $V < 0$ with $\sigma(0) = 0$. In Eq. 4.2 we do not have to consider a specific value of friction to make a demarcation between locked and running phase of the object motion. In the stochastic setting, the non-linear friction makes the dynamics of an object governed

by Eq. 4.1 or Eq. 4.2 quite different from that of a conventional Brownian particle. For the dry friction case, according to de Gennes [33], the object exhibits a diffusive motion even in the absence of the kinematic friction, where the variance of the displacement increases linearly with time, but with a diffusivity ($\sim K^3/\Delta^4$) that depends more strongly on the power of the noise than that ($\sim K$) of a normal Brownian particle. Furthermore, the object drifts with a velocity $\sim K\bar{\gamma}/\Delta^2$ that is uniquely different from that of a free Brownian particle, where the drift velocity is simply a product of the bias $\bar{\gamma}$ and the Langevin relaxation time τ_L. We will show later that the non-linear kinematic friction, as shown in Eq. 4.2, also leads to some unusual behavior that are similar to the case of dry friction. This nonlinear kinematic friction also produce exponential velocity distribution similar to that observed in granular gases due to dry friction [32].

There are certain dissimilarities between this athermal system with those of a thermal system [35]. In a thermal system, the noise and the friction are coupled to each other, unlike the case of an external noise. However, the provision of delivering the noise externally in our mechanical system allows us to decouple the origin of the noise (external) and the resistance to motion (*i.e.* dry and/or kinematic friction) at the solid–solid interface. The basic notion of FDR (Fluctuation Dissipation Relation) is that the frictional constant obtained from the ratio of the available vibration energy to the resulting diffusivity is same as that obtained from the ratio of the applied force to the resulting drift velocity and is valid strictly for a closed thermal system. As we inject the noise externally, this is an open thermodynamic system, which should not follow FDR.

Nevertheless, we seek for such a relationship to define temperature of an athermal system.

We used an inertial tribometer, which was first used to investigate the nature of dry friction by Baumberger *et al*. [36] They placed a small solid object on a solid support, which was subjected to a biased oscillatory force of varying amplitude. The similar idea of inertial tribometer was also used by Sanchez *et al*. [3], to study the spreading dynamics of a cylindrical granular drop on a surface, excited by a periodic vibration. Our approach to study the motion of the solid object on a solid support is similar to those of the above authors, except that the excitation is done with a white noise rather than a periodic vibration.

We study two model systems. In one case, a smooth glass prism slides against a rough glass support. In the second case, a polymer (polydimethylsiloxane or PDMS) grafted smooth glass prism slides against a PDMS grafted silicon wafer. In the first system, which has been studied more extensively, we are able to identify three distinct interfacial regimes: a solid like, a fluid like and a transition region characterized by a stick-slip motion of the object. Although Eq. 4.1 describes the behavior of this system in a general way, a potentially important new finding about this kind of motion is that the stochastic velocities are poorly correlated thus leading to a much lower diffusivity than that predicted by de Gennes [33] for a similar system. The second system is studied here for the main purpose of showing that the non-Gaussian displacement fluctuation can also arise when the kinematic friction itself is non-linear.

4.2 Background

When a prism is placed on a tilted support, it experiences two types of external forces: one is the driving force ($mg \sin \theta$) for motion and another is the static friction force ($\mu_s mg \cos \theta$) acting parallel to the surface but opposite to the direction of motion. Here m is the mass of the prism, μ_s is the static friction co-efficient, g is the gravitational acceleration, and θ is the angle of inclination of the support. The glass prism slides on the inclined surface when the gravitational force is larger than the static friction force, otherwise it remains stuck. In presence of the external noise the scenario changes. The prism is rescued from this stuck state when the strength of a noise pulse is high enough that the noise and bias force together ($m\gamma(t) + mg \sin \theta$) is larger than the static friction force $\mu_s mg \cos \theta$. We use Eq. 4.1 in which $\bar{\gamma}$ is to be identified with $g \sin \theta$ and $\Delta = \mu_s g \cos \theta$. For a spatially homogeneous and steady state system the Klein-Kramers' [22,37,38] form of the Fokker-Planck equation corresponding to equation 4.1and 4.2 can be written as:

$$\frac{K}{2} \frac{\partial P}{\partial V} + \Delta \frac{|V|}{V} P + \frac{VP}{\tau_L} = \bar{\gamma} P, (dry\ friction) \qquad 4.3$$

$$\frac{K}{2} \frac{\partial P}{\partial V} + \frac{AV^n}{m} \frac{|V|}{V} P = \bar{\gamma} P, (non-linear\ kinematic\ friction) \qquad 4.4$$

The solutions of the equations 4.3 and 4.4 yield the PDF of velocity fluctuation ($P(V)$) as follows:

$$P(V) = P_o exp\left(-\frac{V^2}{K\tau_L} - \frac{2|V|\Delta}{K} + \frac{2V\bar{\gamma}}{K}\right) \qquad 4.5$$

$$P(V) = P_o'' exp\left(-\frac{2A|V|^{1+n}}{m(1+n)K} + \frac{2V\bar{\gamma}}{K}\right) \qquad 4.6$$

Here, P_o' and P_o'' are normalization constants. From equation 4.5, it is evident that the velocity distribution has a Gaussian component due to kinematic friction term $\frac{V^2}{K\tau_L}$ and an exponential component due to Coulombic dry friction term $\frac{2|V|\Delta}{K}$, whereas from equation 4.6 we expect a stretched Gaussian distribution. Equations 4.5 and 4.6 are useful in the sense that both the drift velocity and the variance of velocity distribution can be estimated by calculating the first and second moments of velocity distribution provided that the values of τ_L and Δ (for Eq. 4.5) as well as n and A (for Eq. 4.6) are at our disposal. Conversely, the experimental drift velocities obtained at different values of $\bar{\gamma}$ and the power of the noise K can be used to estimate these parameters. We used the second method to estimate τ_L and Δ as well as n and A, which were then used for further analysis and simulations.

4.3 Experiment

A solid glass prism (~1.67 *g*), having dimension of ~11 *mm* × 11 *mm* × 6 *mm*, was placed on a glass plate. The experimental set up is illustrated in Figure 4.1. As with our previous studies [27], some roughening of the support was necessary to induce easy and uniform sliding of the glass prism over it. Very smooth surfaces adhere to each other so strongly that a very high level of vibration is needed to dislodge it. We avoided such high adhesion situations by roughening the surface, as our objective is to study the stochastic dynamics of the motion from a very low to a high power. While the main work of this paper focuses on the above described system, we also present some results of a study where a polydimethyl siloxane (PDMS) grafted smooth glass prism slides against a PDMS grafted polished silicon wafer (Figure 4.2). In the latter case, as the PDMS reduces the surface energy of the smooth surfaces considerably, the surfaces do not stick to each other strongly. Thus diffusive experiments could be performed without roughening the surfaces.

4.3.1 Preparation of glass surfaces

A glass slide (Fisherbrand)(~ 9 *g*) having dimension of 75 *mm* × 50 *mm* × 1 *mm* was grit blasted with alumina particles (~45 *μm*) at a pressure of 90 *psi* for 45 *s* in an air fluidized bed. The grit blasted glass surface was blown with a jet of dry nitrogen gas followed by washing with copious amount of Millipore water.
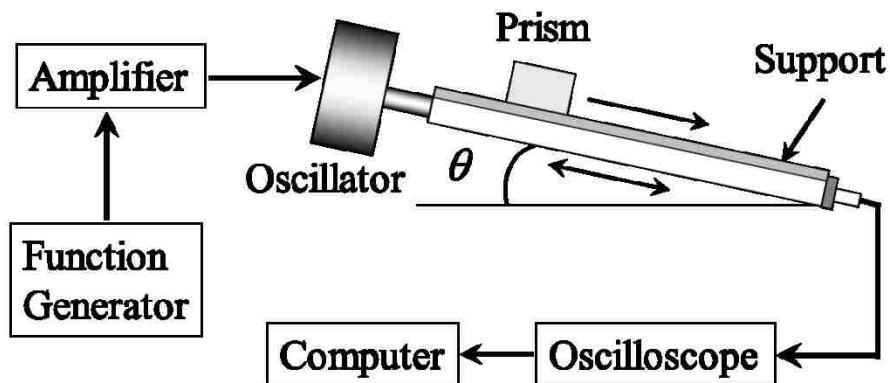
Figure 4.1: Schematic of the experimental set up.

The roughened glass plate and a glass prism were sonicated first in de-ionized water and then in acetone for 30 min each. They were sonicated again in de-ionized water for 30min. After rinsing the plate and the prism with de-ionized water, they were dried with nitrogen gas. Both the glass surfaces were completely wettable by de-ionized water in the contact angle measurements, which ensures that they are free of gross organic contaminations. No debris was also evident in optical microscopic examinations. The roughened glass surface was examined using a laser optical profilometer (STIL micromeasure, CHR 150-N) at different spots on the surface, each having a scanning area of 500 μm × 500 μm, with a scanning step size of 2.5 μm. The root mean square value of the surface height fluctuation was about ~16 μm, which varied slightly (within 1 μm) from spot to spot. The rectangular glass prism was prepared by cutting a borosilicate glass plate (ACE Glass, USA) using a fine glass grinder. The root mean square roughness

of the glass prism was about 4 *nm* over an area of 100 μm^2 measured using an atomic force microscope (AFM, Digital Instruments, USA).

4.3.2 Preparation of polymer grafted Si wafer and glass prism

We used a method similar to that published in reference [39] with a slight modification in order to graft PDMS chains on the glass prism and the silicon wafer. Pieces (75 *mm* × 30 *mm* × 0.6 *mm*) of silicon wafer (Silicon Quest International) and a glass prism of weight 1.7 *g* and dimensions of 11 *mm* × 11 *mm* × 6 *mm* were first cleaned in piranha solution (a mixture of concentrated Sulfuric acid and 30% Hydrogen peroxide in 4:1 volume ratio) for 30 *min*. After rinsing the samples with copious amounts of deionized water (Millipore) and drying with nitrogen gas, they were further cleaned with oxygen plasma. The roughness of the silicon and the glass prism were 0.4 *nm* and 4 *nm* respectively as evidenced from the AFM measurements. The samples were immersed in trimethylsiloxy-terminated poly-dimethylsiloxane (PDMS) (Gelest Inc., product code: DMS-T22, MW ~ 9430) in a cleaned glass petri dish. The petri dish was covered and kept in an oven at 100° C for 24 *hrs*. The samples were then cooled to room temperature and dipped in 99.9% pure toluene (ACS grade) for 10 *min*. Both the samples were rinsed with copious amounts of flowing toluene, after which they were dried with nitrogen gas. Using spectroscopic ellipsometry (J. A. Woollan Co., Inc. VB-400 Vase Ellipsometer) the thickness of the PDMS grafted onto silicon wafer was estimated to be ~3.7 *nm*. Because of the poor contrast of the reflectivity of the glass prism and the PDMS, it was not possible to make reliable estimate of the thickness of the grafted PDMS layer on this surface. However, as the methodologies used to graft PDMS were identical in both cases,

the thickness of PDMS on the glass surface should be similar to that on the silicon wafer. The advancing and the receding contact angles of water on both the surfaces were ~ 110° and 103° respectively, suggesting that their surface energetic properties were the same.
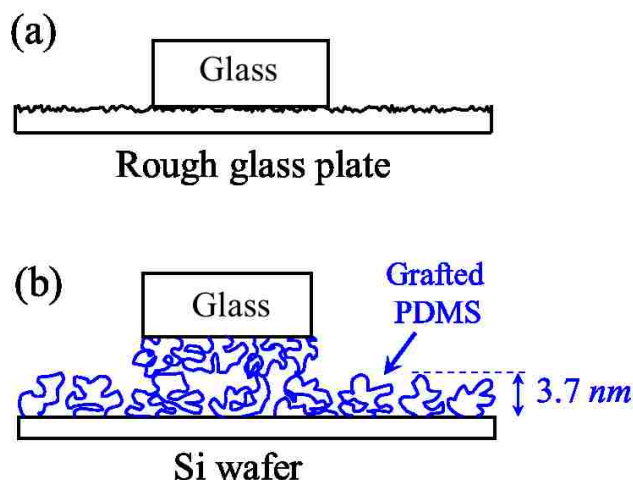
Figure 4.2: Two test systems are shown: (a) a smooth glass prism on a rough glass support and (b) a PDMS grafted smooth glass prism on a PDMS grafted silicon wafer.

In a previous paper [40] we reported the thickness of the grafted PDMS chains on surfaces where one end of polymer reacted with the surface. With the data presented in that report, the thickness of the grafted layer of PDMS on silicon was about 8.7 *nm* for a PDMS of molecular weight comparable to that studied here. Here, both end of the chain can react with the surface; consequently, the thickness of the grafted layer is close to half of that found previously.

The roughened glass plate or the PDMS grafted silicon wafer were firmly attached to a metal (aluminum) platform that was mounted on a mechanical oscillator

(Pasco Scientific, Model No: SF-9324) (Figure 4.1and Figure 4.2). Gaussian white noise was generated with a waveform generator (Agilent, model 33120A) and fed to the oscillator via a power amplifier (Sherwood, Model No: RX-4105). By controlling the amplification of the power amplifier, noises of different powers were generated while keeping the pulse width constant at ~ 40 μs. The acceleration of the supporting aluminum plate was estimated with a calibrated accelerometer (PCB Peizotronics, Model No: 353B17) driven by a Signal Conditioner (PCB Peizotronics, Model No: 482) and connected to an oscilloscope (Tektronix, Model No. TDS 3012B). The PDFs of these accelerations are Gaussian (Figure 4.3) and their power spectrums are flat up to a total bandwidth of 10 kHz.
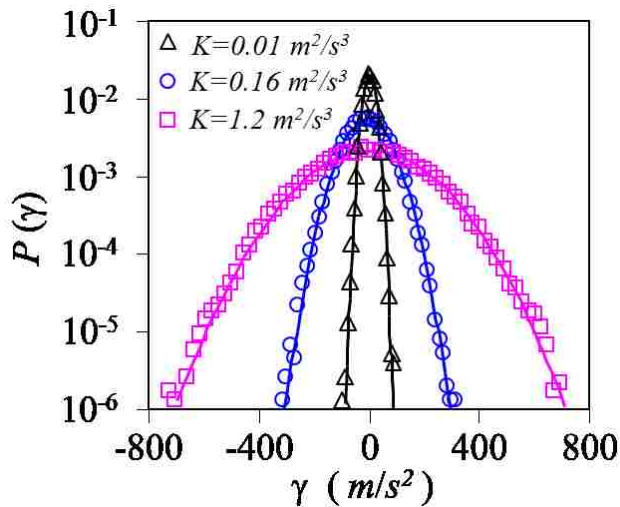
Figure 4.3: Probability distribution functions of Gaussian white noise obtained from accelerometer at three different powers (K) as indicated inside the figure. The solid lines represent Gaussian fit through the data.

The entire set-up was placed on a vibration isolation table in order to eliminate the effect of ground vibration. The drifted and the stochastic motion of the glass prism were captured with a high speed (1000 fps) Redlake Motion-Pro video camera, which was later analyzed using 'Midas 2.0 Xcitex' software to obtain the position of the prism relative to a fixed reference on the vibrating plate as a function of time. All measurements were done under ambient conditions, at a temperature of 23° C and relative humidity of 40%.

The sliding experiments with the prism on the roughened glass were carried out at eleven different powers of the noise ranging from 0.0003 m^2/s^3 to 1.83 m^2/s^3 and five different biases by varying the angle of inclinations with a sensitive goniometer (CVI Melles Griot, Model No: 07 GON 006) from 1° to 10° that correspond to forces ranging from 0.29 mN to 2.8 mN. For the case with PDMS grafted glass on a PDMS grafted silicon wafer, the drift velocities were measured at eight different powers. However, the detailed examination of the displacement fluctuations were carried out at one power (K=0.1 m^2/s^3) and one bias (0.29 mN).

We estimated the experimental error induced background noise in order to ensure that our data are far above it. In order to accomplish this task, the prism was fastened to the supporting plate with an adhesive tape, and then the plate was subjected to white noise vibrations of different powers. The position of the fixed prism with respect to a fixed reference point was again analyzed using the software mentioned above. This tracking allowed us to estimate the background noise that arose due to the errors of the measurement. We will show later (Fig. 13) that this background noise leads to a false

diffusivity, which is nonetheless much smaller than the lowest diffusivity used in our analysis.

4.4 Results and discussion

4.4.1 Stochastic motion of the prism on a rough surface

The stochastic motions of the prism on the solid support at two different powers of the noise are shown in Figure 4.4, where it is evident that the prism exhibits a stick-slip like motion at a very low power, but a dispersive fluid-like motion at a high power.
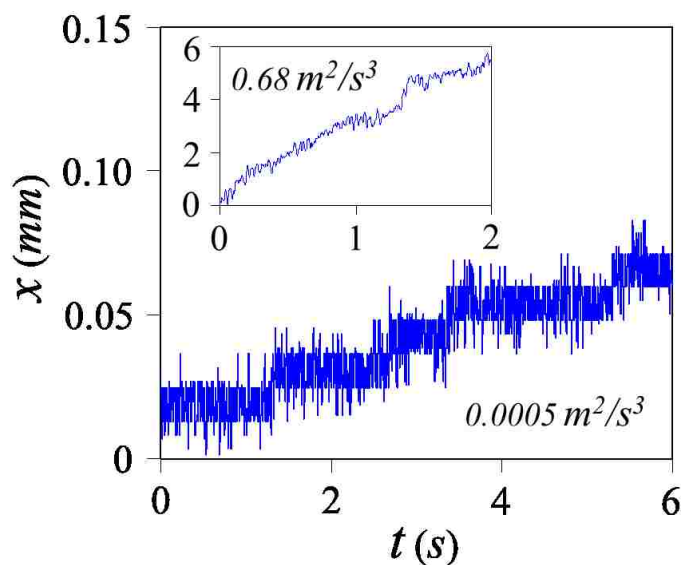
Figure 4.4: The trajectory of the stochastic motion of a glass prism on a glass substrate under the influence of applied bias (0.29 *mN*) and Gaussian white noise of power 0.0005 m^2/s^3 is shown. A typical trajectory at same bias but at a high power (0.68 m^2/s^3) is presented in the inset. Stick-slip motion at the low power and smooth motion at the high power are evident.

Two types of analyses have been performed with these data. First is the estimation of the drift velocity from the net displacement as a function of time, and second is the estimation of the diffusivity from the stochastic fluctuations of the displacement.

4.4.2 Drift velocity and the mobility

On the roughened glass substrate, the displacement data were taken over several tracks on different parts of the surface, each for certain duration of time. The prism showed an occasional tendency to rotate as it drifted on the surface, especially at higher powers and biases. Those tracks that did not exhibit any rotation were used for data analysis
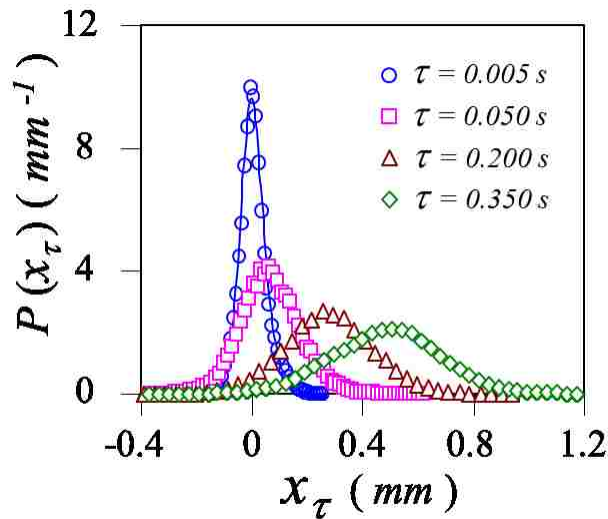
Figure 4.5: Probability distribution functions of the displacement of a glass prism on a rough glass support for $K= 0.16$ m^2/s^3 and $m\bar{\gamma} = 0.29\,mN$ at different time intervals τ shown inside figure.

. At lower powers, although about 10 to 12 tracks were sufficient for the estimation of the drift velocity and the diffusivity, 25 tracks were used for the data analysis. However, for the higher powers, larger numbers of tracks (~50) were used owing to shorter duration of time (~2 *s*) for each track.

A typical evolution of a displacement distribution function is shown in Figure 4.5 in linear scales. The general pattern here is much like the case of the propagation of a Gaussian distribution as shown in Eq.4.7.

$$P(x_\tau) = P_o e^{-\frac{(x_\tau - V_{drift}\tau)^2}{4D\tau}} \qquad\qquad 4.7$$

When plotted in the log-linear scales, as we will see later, these PDFs exhibit non-Gaussian (exponential or stretched Gaussian) tails in many situations, although the central part of the distribution is nearly Gaussian at longer time scales. Equation 4.7 suggests that the peak of the PDF moves with a velocity V_{drift}, and its variance broadens with τ, both of which apply in our case. We estimate the drift velocity and the diffusivity from the gradients of the displacement and variance with respect to time respectively. With appropriate substitutions, Eq. 4.7 can also be converted to Eq. 4.8, which represents the fluctuation of gravitational work (gravitational potential energy).

$$\frac{P(+W_\tau)}{P(-W_\tau)} = exp\left[\frac{W_\tau}{(D/\mu)}\right] \qquad\qquad 4.8$$

Here $W_\tau = m\bar\gamma\, x_\tau$ is the work performed by gravity, which fluctuates with x_τ and

$\mu = V_{drift}/m\bar\gamma$ is the mobility. According to Eq. 4.8, if W_τ is non-dimensionalized by

dividing it with D/μ, we obtain a work fluctuation relation for this system driven with an

external force and excited by an external noise. This equation states that the ratio of the

probabilities of finding the positive and negative values of a particular value of work is

equal to the exponential of the positive value. As D/μ is equal to k_BT in a thermal system

according to Einstein equation, it is interesting to check if a similar equation can be

obtained by replacing k_BT with an equivalent energy scale $mK\tau$ */2* in the current

athermal system.
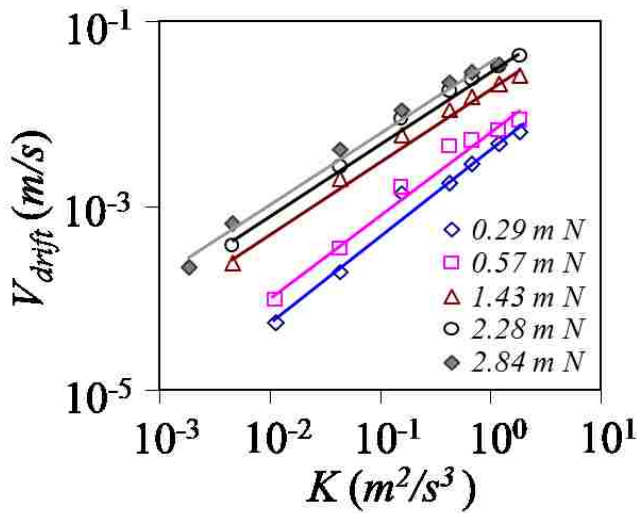
Figure 4.6: Log-log plot of the drift velocities (V_{drift}) of a glass prism on a glass plate as a function of the power (K) of the Gaussian noise and different applied biases indicated inside figure.

For the prism on the roughened glass support, V_{drift} increases sub- linearly with K (Figure 4.6), while at a given value of K, the velocity increases linearly with the bias. When the drift velocities are normalized by dividing it with $m\bar{\gamma}$ to obtain a generalized mobility as a function of K, all the mobilities do indeed cluster nicely around a single master curve (Fig. 7). These data are consistent with our previous report [27], although the previous studies were conducted with a smaller variation of bias and smaller range of K.
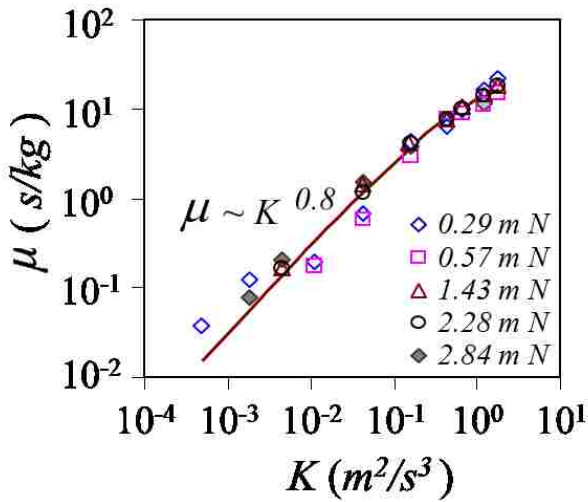
Figure 4.7: Log-log plot of the mobility as a function of power of the noise (K) at different biases. The solid line represents the mobility that is estimated by calculating V_{drift} from the first moment of PDF given by Eq. 4.5 and dividing it by the bias. For the bias 0.29 *mN*, the data corresponding to the stick slip motion of the prism are also included in this plot.

The master curve of the generalized mobility can be analyzed in conjunction with the drift velocity estimated from the first moment of the PDFs shown in equations 4.5and 4.6 as a function of $\bar{\gamma}$ and K and subsequently normalizing it by dividing it with applied bias

$m\bar{\gamma}$ (Figure 4.7). For the prism on the roughened glass the values of Δ and τ_L needed to obtain the best agreement between the experimental data and the theoretical estimates are 4.5 m/s^2 and 0.06 s respectively.

4.4.3 Numerical simulations of the motion of the prism

Having established the values of Δ and τ_L in the previous section, we simulated the stochastic motion of the prism at two different powers using the modified Langevin Eq. 4.1. $\gamma(t)$ values as obtained from the accelerometer were used as input acceleration for the numerical simulations. Since the dry friction force $\sigma(V)\Delta$ always acts in the direction opposite to the motion of the prism, it is set as $\Delta V/|V|$ in the simulations. When the net acceleration $|\bar{\gamma} + \gamma(t)|$ acting on the prism is less than Δ, the velocity of the prism is set to zero. Equation 4.1 is integrated with an integration time step of $\Delta t = 0.001$ s, which is same as the resolution time of the high speed camera used to track the stochastic motion.
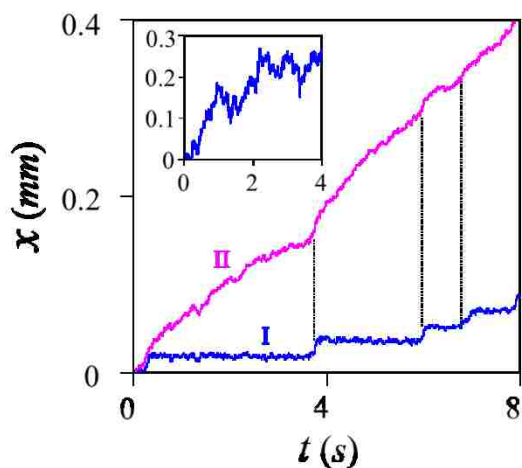
Figure 4.8: Line I, representing the stick-slip motion, is the simulated trajectory of a glass prism on a glass support vibrated with the Gaussian noise of power 0.0005 m^2/s^3 and applied bias 0.29 mN when a periodic pinning potential is considered. Line II depicts the simulation without the sinusoidal potential at same condition. The line in the inset is the simulated trajectory with the sinusoidal potential at a higher power (0.01 m^2/s^3) but at same applied bias (0.29 mN).

Line II in Fig. 8 shows the trajectory of the prism that is obtained from the numerical solution of Eq. 4.1 at a low power (0.0005 m^2/s^3), in which no stick slip motion is predicted. Stick-slip motion usually is an indicator of the existence of metastable energy states on a surface, which is not explicit in a uniform dry friction used in our simulation. We thus carried out a simulation of Eq. 4.1 by incorporating an additional sinusoidal term [38] $H\sin(2\pi x/L)$ that represents a pinning potential. Here L represents the length scale and H denotes the amplitude of perturbation. We surmise that Δ represents a background value of the static friction, whereas the perturbation term represents defects distributed at a larger length scale. Although the above description of friction is somewhat speculative, it provides an approximate way of describing the effect

91

of pinning defects on the motion of the prism. While the simulation is carried out with somewhat arbitrary values of *H* and *L* as 0.3 m/s^2 and 17 μm respectively, we note that the chosen value of *L* is close to the lowest jump length of the stepwise motion of the prism as reported in Figure 4.8. Simulations do indeed predict a stick-slip motion of the solid for the low power (0.0005 m^2/s^3) when the pinning potential is considered (line I in Figure 4.8). But at a high power, a fluid like motion is observed even in presence of the same sinusoidal potential (inset of Figure 4.8). Here, one important point should be noticed. As we have used the same noise input file for both the trajectories, with or without the pinning potential, we can keep record of the nature of the impulses. From Fig. 8, it is evident that whenever a pulse of large acceleration arrives from the noise field, the solid exhibits a big jump. The solid does not remain trapped on the surface unless there is a pinning potential.

4.4.4 Displacement fluctuation

Figure 4.9 summarizes the fluctuations of the displacements of the prism on the solid surface corresponding to a low bias (0.29 *mN*) and a low power (0.04 m^2/s^3) but at different time intervals τ; and corresponding to the same power as above and a fixed value of τ (0.08 *s*) but for three biases: 0.29 *mN* , 1.43 *mN* and 2.84 *mN*. Evidently, all these probability distributions are non-Gaussian and distinctly asymmetric with the degree of asymmetry increasing with τ as well as with the bias. In order to estimate the degree of asymmetry, we estimated the 'skewness' (S) of the displacement PDFs, which is defined as the ratio of the third central moment of a distribution to the cube of the standard deviation of that distribution. For symmetric distribution, skewness is close to

zero, whereas positive and negative skewness portray right sided or left sided asymmetry respectively.
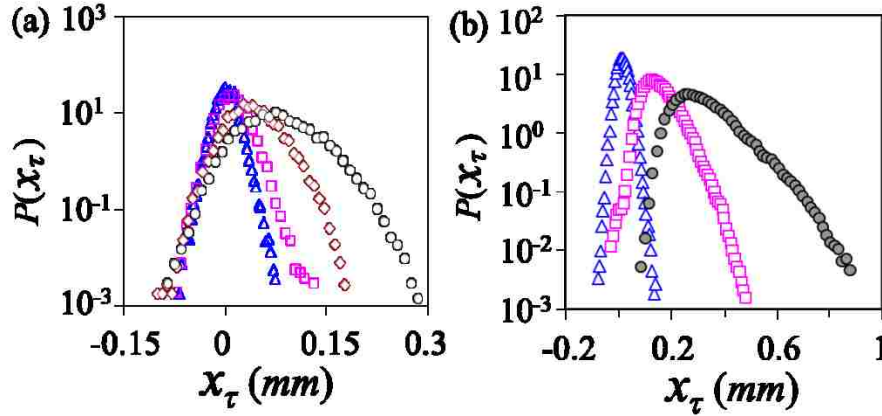
Figure 4.9: Probability distribution function of displacement fluctuation of the glass prism on a glass substrate subjected to Gaussian white noise of power 0.04 m^2/s^3: Fig. (a) corresponds to a bias of 0.29 mN and different time intervals τ: 0.005 s (Δ), 0.05 s ($\square$), 0.20 s ($\lozenge$), 0.40 s ($\circ$) ; Fig. (b) corresponds to $\tau = 0.08$ s but for different biases: 0.29 mN(Δ), 1.43 mN ($\square$), 2.84 mN ($\bullet$). In Fig. (a), skewness value increases with τ from 0.001 (for τ=0.005 s) to 0.33(for τ=0.40 s) and the kurtosis decreases from 3.5 (τ =0.005 s) to 3.1 (τ=0.40 s). In Fig. (b) skewness increases with bias from 0.23 (0.29 mN) to 1.12 (2.84 mN). The kurtosis also increases with bias from 3.4 (0.29 mN) to 4.5 (2.84 mN).

In order to quantify the 'peakedness' of a distribution, we estimated its kurtosis (β), which is defined as the ratio of the fourth central moment of a distribution to the square of the variance. For Gaussian distribution, β is close to 3 whereas this value increases with the peakedness of a distribution reaching a value of 6 for an exponential PDF.
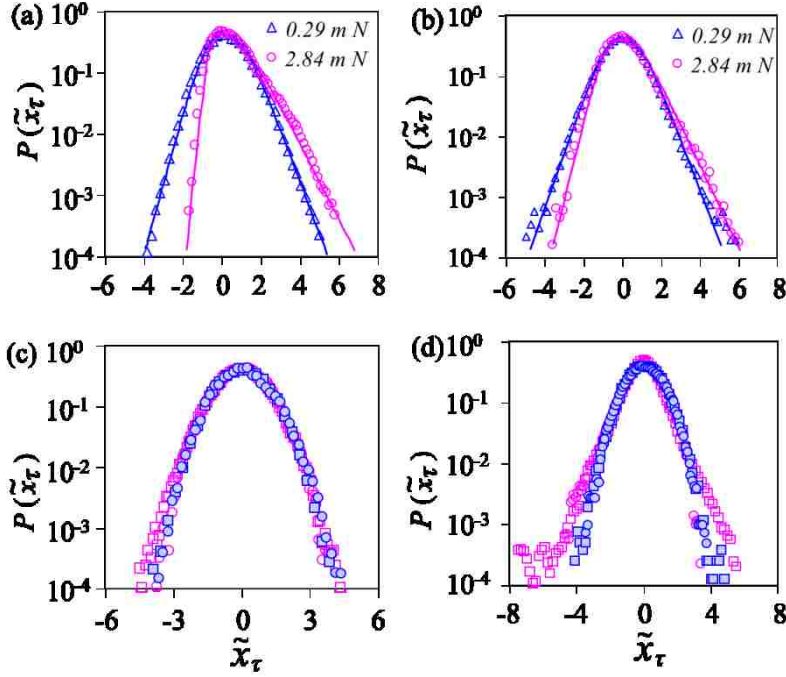
Figure 4.10: Experimental (a) and simulated (b) probability distributions of dimensionless displacement fluctuations $\left(\widetilde{x}_\tau = \left(x_\tau - x_p\right)/\sigma_{x\tau}\right)$ of a glass prism moving on a glass plate under the influence of Gaussian noise of power 0.04 m^2/s^3 at different applied biases as indicated at top right corner. Here x_p corresponds to the displacement with peak probability density and $\sigma_{x\tau}$ is the standard deviation of the displacement distribution. The time interval τ used for this plot is 0.08 s. The solid lines are obtained by fitting the experimental data with asymmetric double sigmoidal functions, the centers of which are bell-shaped, but have exponential tails. (c) and (d) represent PDFs of dimensionless displacement at the time intervals of 0.08 s (□) and 0.35 s (○)at different powers: 0.01 m^2/s^3 (c) and 1.21 m^2/s^3 (d). The filled and open symbols indicate the experimental and simulation results respectively. The applied bias in all cases is 0.29 mN. It should be emphasized here that these simulated PDFs are not in exact numerical agreements with the experimental results when plotted in terms of the absolute values of x_τ. The variance of the simulated PDF is considerably higher than that obtained experimentally. However, when plotted in the dimensionless form, it reproduces the general features of the experimental distributions.

In Figure 4.10, we re-plot two representative PDFs with the data taken from

Figure 4.9 in non-dimensional forms, which are compared with those obtained from the

94

numerical integration of Eq. 4.1. The simulations do indeed reproduce the non-Gaussian features of the displacement distributions along with the asymmetry, although the degrees of asymmetry observed in the experiments (S = 0.23 for $m\bar{\gamma}$ = 0.29 mN; S = 1.12 for $m\bar{\gamma}$ = 2.84 mN) are somewhat larger than those found in the simulations (S = 0.10 for $m\bar{\gamma}$ = 0.29 mN; S = 0.68 for $m\bar{\gamma}$ = 2.84 mN).

By contrast, the non-Gaussian nature of the displacement PDFs observed in experiments (β = 3.4 for $m\bar{\gamma}$ = 0.29 mN; β = 4.5 for $m\bar{\gamma}$ = 2.84 mN) compare well with those obtained from simulations (β = 4.0 for $m\bar{\gamma}$ = 0.29 mN; β = 4.6 for $m\bar{\gamma}$ = 2.84 mN). The displacement PDFs (Figure 4.10) obtained at a lower power (K=0.01 m^2/s^3) as well as at a higher power (K=1.21 m^2/s^3), however, paint a somewhat different story. Here, the PDFs obtained from the experimental data show that they are quite symmetric (S ~ 0) and Gaussian (β ~ 3.0). The simulations suggest that the PDF should be Gaussian at the low power (K = 0.01 m^2/s^3, β = 3.1) as found in the experiments; but it has strong exponential tails at a higher power (K = 1.21 m^2/s^3, β = 5.3), which disagrees with the experimental observations. On the other hand, negligible values of the skewness (S ~ 0) obtained from simulations at both low and high powers suggest that the displacement distributions should be quite symmetric, which is consistent with the experimental observations. Figure 4.11 summarizes the experimentally obtained PDFs of the displacement fluctuation as a function of the power of the noise, along with the value of the kurtosis stamped inside each figure. The distribution is clearly Gaussian at a low power (as discussed above), but becomes non-Gaussian and asymmetric as the power increases. It

becomes Gaussian and symmetric again at a very high power. It seems that the effect of static friction is overcome at a very high power of the noise, which may indicate a subtle level of continuous transition occurring at the interface with increasing K. The Gaussian distribution at the very low power results from the insufficiency of the number of high acceleration pulses, *i.e.* the statistics is poor. This subject will be taken up again in the discussion section.
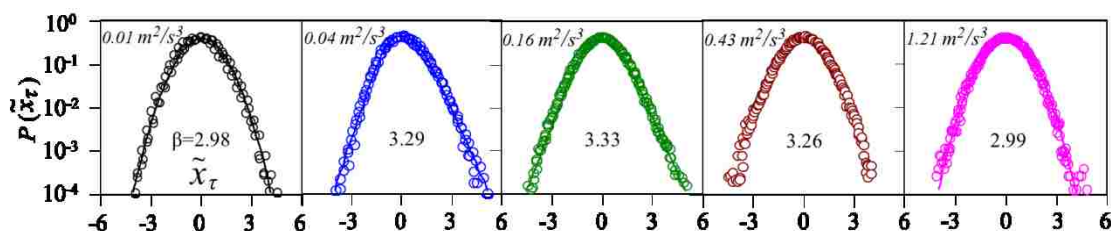
Figure 4.11: PDFs of the dimensionless displacement $\left(\widetilde{x}_\tau = \left(x_\tau - x_p\right)/\sigma_{x\tau}\right)$ of a solid prism on a solid surface subjected to Gaussian noise of different powers (indicated in the top left corner). The applied bias is 0.29 *mN*. The value of the kurtosis (β) is stamped inside each PDF. Skewness values of the PDFs are 0.07, 0.27, 0.05, 0 and 0 for the powers 0.01 m^2/s^3, 0.04 m^2/s^3, 0.16 m^2/s^3, 0.43 m^2/s^3 and 1.21 m^2/s^3 respectively.

At this juncture we would like to mention that a recent model on the slip avalanches [41] shows that local failure stress ('pinning stress') has to be overcome for a slip to occur. Depending on the weakening of the threshold failure stress, a continuous phase transition from brittle to ductile and hardening can occur. This may be somewhat related to our observations here.

4.4.5 Diffusivity: the effect of the noise strength and bias

The experimental data of the stochastic displacement (x_τ) of the prism as a function of time, as obtained from several tracks were combined in order to obtain the PDF of x_τ for *K* ranging from 0.0005 m^2/s^3 to 1.83 m^2/s^3 and $m\bar{\gamma}$ ranging from 0.29 *mN* to 2.8 *mN*. These PDFs allowed the estimation of the diffusivities from the plot of the variance of the displacement $\sigma^2_{x\tau} = \left(\left\langle x_\tau^2 \right\rangle - \left\langle x_\tau \right\rangle^2 \right)$ versus τ, using the well-known expression: $D = d\left(\sigma^2_{x\tau} \right)/2d\tau$. Here we examine the time evolution of the variance of the displacement distribution corresponding to $m\bar{\gamma} = 0.29$ *mN* and $K = 0.04$ m^2/s^3.
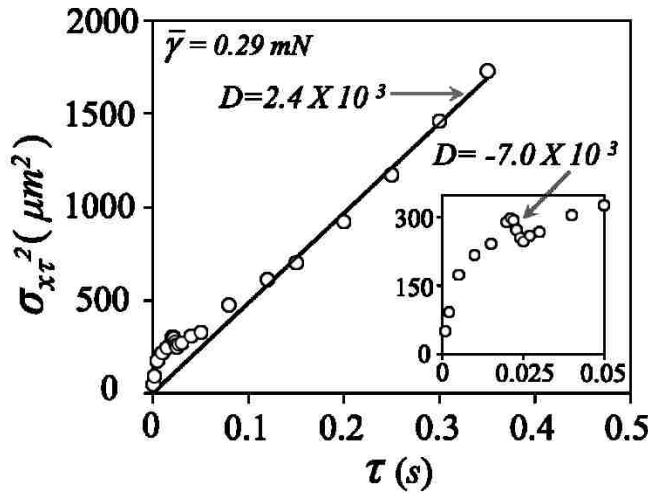
Figure 4.12: Variance of the displacement of the glass prism as a function of time (○). Applied bias is 0.29 *mN* and the power of the Gaussian noise is 0.04 m^2/s^3. Lower inset is the enlarged view of the variance at short time region showing anomalous diffusivity, with even a negative diffusivity ($\sim$ -7000 $\mu m^2/s$) in the range of $\tau \sim 0.021s$ to 0.025s.

The variance of the displacement fluctuation first increases sharply (Figure 4.12) followed by a decrease at $\tau \sim 0.02\ s$; it then increases linearly with time. Clearly, the prism exhibits an anomalous dispersion at short times. This kind of anomalous diffusive behavior at short times is reproducible and has been observed with other biases as well. The diffusivity that we report in this paper is obtained from the slope of the linear portion of the variance of the displacement as a function of τ at a longer time scale.
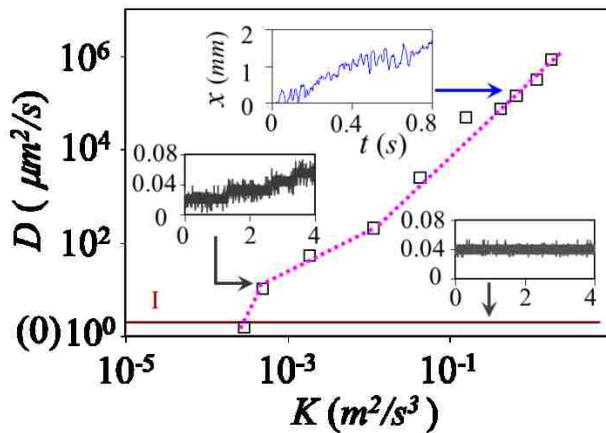
Figure 4.13: Log-log plot of the experimental diffusivity (□) of the glass prism as a function of the power of the noise (*K*) corresponding to the applied bias of 0.29 *mN*. Line I corresponds to the background noise (shown in right inset) and considered as zero diffusivity (marked in bracket). Stick –slip type motion is observed at the powers of 0.0005 m^2/s^3 to about 0.002 m^2/s^3 whereas no stick-slip motion is evident for powers ranging from 0.01 m^2/s^3 to 1.8 m^2/s^3.

The data summarized in Figure 4.13 show that there are three distinct transport behaviors of the prism. The apparent diffusivity at the lowest power (0.0003 m^2/s^3) is already submerged into background noise of the system. Furthermore, at this power of the noise, no net drift of the solid object is observed. This is like a solid phase. A phase

transition like behavior coupled with a stick slip motion of the object is observed (Figure 4.13) as the power is increased from 0.0003 m^2/s^3 to 0.0005 m^2/s^3. The residence time in stick (solid like) phase decreases with the power of the noise. The frequent occurrences of the slip motion eventually merge into the fluid like random motion at higher powers (K > 0.01 m^2/s^3).

The diffusivity of the prism in the fluid-like state varies with K with an exponent of 1.6, which deviates from that (3.0) predicted by de Gennes [33]. This is not surprising at first because de Gennes assumed that only dry friction operates at the interface. However, we suspect that another cause of this difference arises from poor correlations of displacements, which will be discussed below.

4.4.6 Estimation of Diffusivity

The diffusivity governed by purely kinematic friction ($D = K\tau_L^2/2$) is in the range of $10^7 \mu m^2/s$ to $10^9 \mu m^2/s$ for K ranging from 0.01 m^2/s^3 to 1.8 m^2/s^3 which is obviously much larger than the experimental values (~$10^2 \mu m^2/s$ to $10^6 \mu m^2/s$ for same range of K) (Figure 4.13). By ignoring the kinematic friction, de Gennes [33] derived an equation for diffusivity for the dry friction case as follows:

$$D = \frac{4}{\pi} \iint\limits_0^\infty dtdk \frac{pk^2}{(p^2 + k^2)^3} exp[-K(p^2 + k^2)t] \qquad 4.9$$

where, $p=\Delta/2K$.

99

Diffusivities estimated using Eq. 4.9 varies with *K* with an exponent of 3. Furthermore its

values are in the range of 10^3 *μm²/s* to 10^{10} *μm²/s* for the range of *K* as above, which are

still larger than those measured experimentally.

.
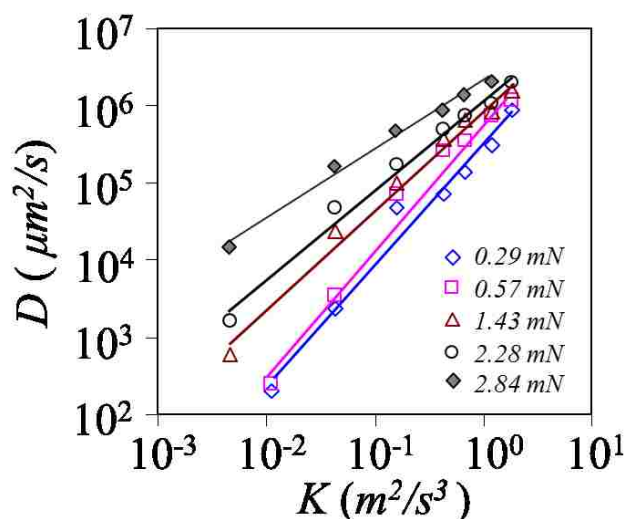
Figure 4.14: Log-log plot of diffusivity *D* estimated for different powers of the noise (*K*) and biases: 0.29 *mN*(◊), 0.57 *mN* (□), 1.43 *mN* (Δ), 2.28 *mN* (○), 2.84 *mN* (♦). Here the data corresponding to the stick slip motion of Fig. 13 for the applied bias 0.29 *mN* are not included.

Experimental diffusivity data are summarized in (Figure 4.14). Clearly, our

experimental data are not totally consistent with the predictions based on the simple

model of de Gennes [33]. Our hypothesis is that the cause for the measured diffusivities

being so much smaller than the predicted values is that the correlation time of the

stochastic velocities is much smaller than either the Langevin or the dry friction times (

τ_L or τ_Δ). Indeed, using the relationship between the diffusivity and the variance of the

velocity estimated from the second moment of Eq. 4.5, at the bias of 0.29 *mN*, the estimated correlation time $\tau*(=\sigma_v^2/2D)$ is in the range of $\sim 37\mu s$ to $56~\mu s$, which is significantly smaller than either the timescale of kinematic friction τ_L (0.06 *s*) or that of the dry friction $\tau_\Delta \sim K/\Delta^2$ (0.5 *ms* to 89 *ms* for *K* ranging from 0.01 m^2/s^3 to 1.8 m^2/s^3). Furthermore we notice that the power spectrum of the fluctuations of the displacements at most powers are rather flat at the time scale of the data recording (0.001 $s << \tau_L$ or τ_Δ). Based on the above scenarios, we envisage an extreme situation where the velocities are delta correlated, i.e. $<V(t_1)V(t_2)>=D\delta(t_1\text{-}t_2)$, and examine how the diffusivities estimated from this approach compare with those found experimentally. Here, the time integral of the above velocity correlation function yields the diffusivity in real space, just as the integral of the correlation function of stochastic acceleration yields the diffusivity in velocity space. Within this model, the velocity vectors (Eq. 4.5or Eq. 4.6) are given by the base state solution of a probability diffusion equation (Eq. 4.3or Eq.4.4), but they are propagated completely randomly producing a stochastic trajectory.

In order to make the estimation of diffusivity, we first define a characteristic displacement (jump length) obtained from the following substitution: $V \approx \bar{x}/\tau_c$, $\bar{x}$ being the jump length and τ_c is a characteristic time scale that we take to be the pulse width of the Gaussian noise. We estimate the diffusivity from the trajectories simulated from this jump length distributions from Eq. 4.10 using the method described below.

$$P(\bar{x}) = P_o exp\left(-\frac{\bar{x}^2}{K\tau_L\tau_c^2} - \frac{2|\bar{x}|\Delta}{K\tau_c} + \frac{2\bar{\gamma}\bar{x}}{K\tau_c} \right)$$

<div align="right">4.10</div>

Equation 4.10 is a modified version of Eq. 4.5, in which the velocity is replaced with $\bar{x}/\tau_c$. We generate a large matrix of jump length vectors ($\bar{x}$) using Eq. 4.10 and randomly select them to construct stochastic paths over a longer time (2 *s*) duration. From these stochastic paths, we calculate the jump lengths for a larger time scale (0.001 *s*) (which also happens to coincide with the resolution time of the camera used in actual experiments).
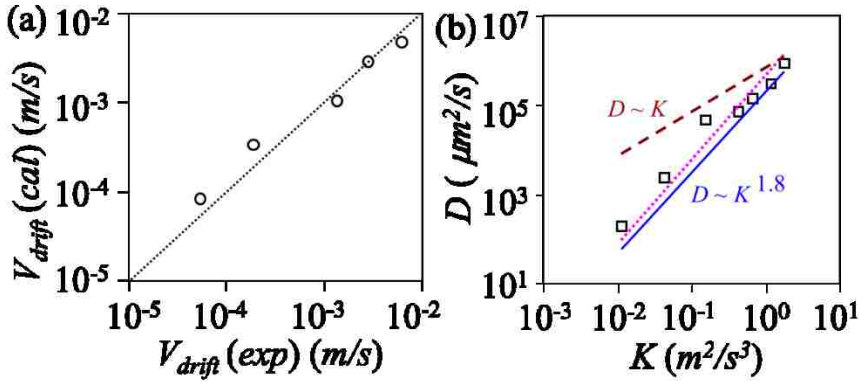
Figure 4.15: (a) Comparison between the experimental and the estimated drift velocities (V_{drift} (exp) and V_{drift} (cal)) as obtained from the trajectories created from the propagation of the steady state jump lengths by stitching them randomly. (b) Log-log plot of the diffusivity as a function of power of the noise. (□) represents the experimental results (ignoring the stick-slip phases of Figure 4.13), whereas the solid line represents the diffusivities estimated from the trajectories created by stitching the randomized jump length as mentioned above. The dashed and dotted lines represent the estimated diffusivities after switching off the dry friction and the kinematic friction terms of Eq. (10) respectively.

The jump lengths corresponding to 0.001 *s* are then randomly selected to construct stochastic trajectories of much longer duration (~ 50 *s*). From these simulated trajectories, the PDF of displacement was constructed for various values of τ and the estimation of diffusivity was carried out in the usual way. Diffusivities were estimated for three different cases: first by setting $\Delta = 0$, second by ignoring the kinematic friction and third by considering both the kinematic and static friction.

These simulations, as summarized in Figure 4.15, show that the diffusivities, in the absence of the dry friction, are higher than the experimental values and it varies almost linearly with *K* as is the case with the correlated kinematic diffusion. The diffusivities for the case of pure dry friction and those for simultaneous actions of both types of frictions have comparable values. They vary with *K* with an exponent ~1.8, which is also close to the experimental result (1.6). We also estimated the drift velocities as well as the energy dissipation from the constructed trajectories when both the kinematic and static frictions operate. These values are also similar to those obtained from the experimental observations (Figure 4.15).

4.4.7 *Stochastic behavior of the PDMS grafted surfaces*

For the PDMS grafted prism on a PDMS grafted silicon wafer, it was somewhat difficult to make measurements at various angles of inclinations as the prism slips easily on its own at angles greater than 1°. Furthermore, here, as the prism has a greater tendency to rotate about its axis than an unmodified prism on the roughened glass, care had to be taken in order to use only those tracks that did not exhibit any rotation for data

analysis. The drift and diffusivity values were estimated at 1° inclination for a given power ($K = 0.1$ m^2/s^3) using 45 tracks, each lasting for 4.5 s to 5 s. The fact that the PDMS grafted prism slides easily at very small angle of the inclination of the supporting plate of a PDMS grafted silicon wafer suggests that the static friction is negligible here. On the other hand, the kinematic friction is non-linear as evidenced from the distributions of displacements (Figure 4.16).
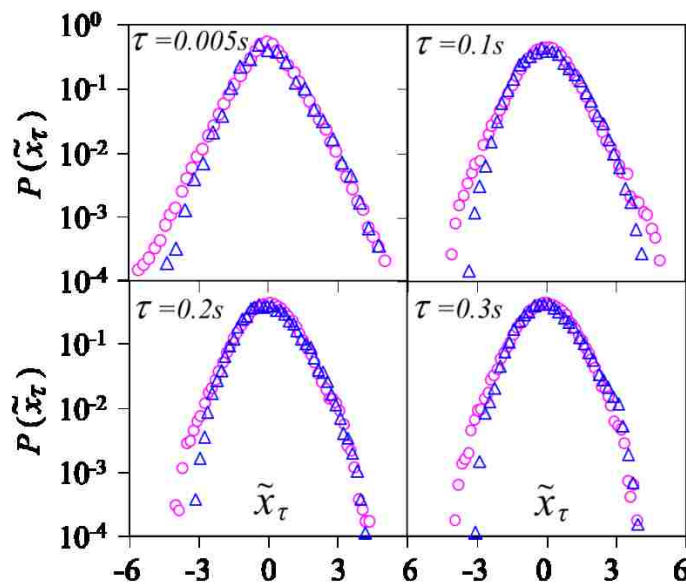
Figure 4.16: Experimental (Δ) and simulated ($\circ$) probability distributions of dimensionless displacements of a PDMS grafted glass prism moving on a PDMS grafted silicon wafer under the influence of a Gaussian noise ($K= 0.1$ m^2/s^3) and a bias of 0.29 mN at different time intervals as indicated inside each figure. The simulation is done using Eq. (2) with $A=0.03$ and $n=0.4$.

The displacement PDF is quite non-Gaussian at $\tau = 0.005$ s, which is supported by the high value of the kurtosis ($\beta = 3.85$). However, at longer time intervals, the value of β decreases to ~ 3.1, indicating that the PDF is more Gaussian. The distributions are somewhat skewed as evident from its values: 0.18, 0.26, 0.31, 0.32 for $\tau = 0.005$ s, 0.1 s, 0.2 s and 0.3 s respectively. From a previous publication [42] we know that the PDMS grafted surfaces exhibit a linear kinematic friction at very low sliding velocity, but progressively become non-linear at high velocity. In the present case, the signature of a non-linear kinematic friction is evident in the non-Gaussian PDF of displacement as discussed above; it is also confirmed in the sub-linear profile of the mobility (Figure 4.17) as a function of the power of noise. Drift velocity of the PDMS grafted glass prism on the PDMS grafted silicon wafer were measured from the displacement of ~ 3 cm as a function of time using a low speed (30 fps) Sony camera (DCR HC-85 NTSC) at eight different powers of Gaussian noise with K ranging from 0.04 m^2/s^3 to 1.2 m^2/s^3 at a bias of 0.29 mN. We attempted to fit the mobilities as a function of K with a velocity weakening form of the friction using an exponent of $n = 0.4$ in (Eq. 4.6). The low K regime are not fitted well with such a non-linear function, while the fit is reasonable at values of $K \geq 0.1$, i.e. starting from the value of K used in our experiment. Using this non-linear from of kinematic friction, we simulated the PDFs at different values of τ using Eq. 4.2. The results summarized in Fig.16 show good agreements between experimental and simulated PDFs. The kurtosis for the simulated PDFs is high at short time, i.e. $\beta = 4.39$ for $\tau = 0.005$ s. However, the value of β decreases to 3.9, 3.4 and 3.3 for $\tau = 0.1$ s, 0.2 s, and 0.3 s respectively. On the other hand, the simulated PDFs are

more symmetric (S= 0.02, 0.11, 0.03 and ~0 for τ = 0.005 s, 0.1 s, 0.2 s and 0.3 s respectively) than the experimental results.
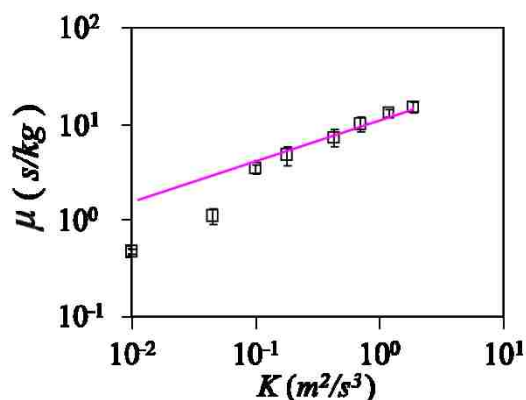
Figure 4.17: The mobility of PDMS grafted glass prism on a PDMS grafted silicon wafer as a function of the power (K) of the Gaussian noises but at a constant bias 0.29 mN. The open squares are the experimental data. The solid line represents the mobilities estimated by dividing the drift velocity (first moment of the PDF given by Eq. 4.6 with A = 0.03 and n = 0.4) with the applied bias force ($m\bar{\gamma}$).

From the gradient of variance of the displacement PDF with time, we estimate the diffusivity of the PDMS grafted prism on the PDMS grafted silicon wafer as 1.7×10^4 $\mu m^2/s$. This value is much lower than expected of a simple diffusion controlled by linear kinematic friction. Here too, as is the case with the prism on a roughened glass, the power spectrum of the displacement at a frequency of 1 kHz is quite flat. We thus estimated the diffusivity using the approach described before (section 4.4.6), assuming that the stochastic velocities are delta correlated. The stochastic trajectories were simulated by stitching randomly selected jump lengths obtained from velocity distribution given in Eq.

4.6 using the substitution $V \approx \bar{x}/\tau_c$ as before. The drift velocity (1.2 *mm/s*) of the simulated trajectories is almost same as the experimental value (1.1 *mm/s*). The diffusivity (10^4 *μm²/s*) obtained from these simulated trajectories is also close to the experimental value (1.7×10^4 *μm²/s*). The fact that the simulated diffusivity value is slightly lower than the experimental value is expected, as in the real situation, the correlation time is finite, although it is smaller than τ_A or τ_L.

4.4.8 An Einstein-like Relation

A driven stochastic system with a thermal noise can be subjected to the analysis of the fluctuations of various types of thermodynamic parameters. As we pointed out previously (section 4.4.2), a work fluctuation like relationship is easily obtained in our system if the work values are non-dimensionalized by dividing it with D/μ. In thermal system, as D/μ is equal to k_BT, it is of interest to find out if a similar equation prevails in our case. We thus explore if an Einstein-like relationship, i.e. $2D\bar{\gamma}/V_{drift}K\tau^* = 1$, can be obtained for this athermal system. However, as the characteristic timescale τ^* is not known *a priori*, we resort to another approach.

107
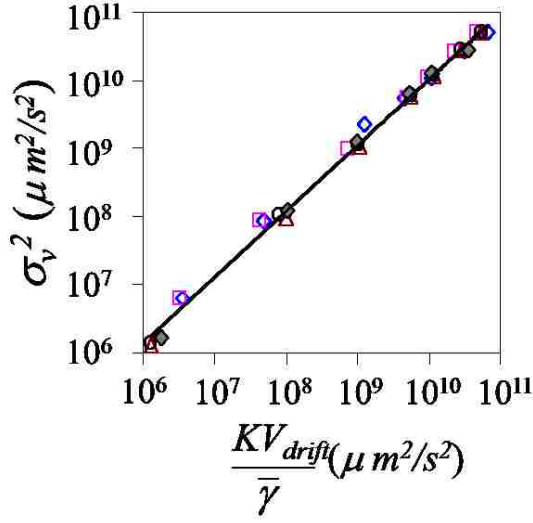
Figure 4.18: A plot of σ_v^2 against $KV_{drift}/\bar{\gamma}$ at different biases: 0.29 *mN* (◊), 0.57 *mN* (□), 1.43 *mN* (Δ), 2.28 *mN* (○), 2.84 *mN* (♦).

While the diffusivity is estimated from the temporal integration of the velocity correlation function (VCF), it scales with the variance of velocity (σ_v^2) as $D \sim \sigma_v^2 \tau^*$ since the VCF usually decays exponentially with time for both the kinematic and static friction [33]. We thus test if $\alpha \sigma_v^2 \bar{\gamma}/KV_{drift} = 1$ with α being a numerical constant. When the variance of the velocity, which is estimated from the second moment of $P(V)$ using Eq. 4.5, is plotted against $KV_{drift}/\bar{\gamma}$ with the data collected at different biases and K (Fig. 18), they cluster nicely around a straight line with its slope approaching unity. This suggests that $\sigma_v^2 \bar{\gamma}/KV_{drift} = 1$, which is a kind of manifestation of the Einstein-like relation for this system.

4.5 Discussions

4.5.1 Diffusive motion of the prism and the phase transition like behavior

The prism exhibits different types of drift and diffusive responses to external vibration. At a very low value of *K*, the prism does not drift. However, as *K* increases, it drifts with velocities increasing with the power of the noise and the imposed bias. Overall linear response of the sliding dynamics confirms our previous observations [27] and is consistent with other studies published in the literature [43–45]. The strong dependence of the drift velocity on the power of the noise is a departure from the standard driven Brownian system, where V_{drift} is simply a product of $\bar{\gamma}$ and τ_L. Previously [27], we presented an approximate expression for the drift velocity of an object on a surface, where both the dry and kinematic frictions operate:

$$V_{drift} = \frac{\bar{\gamma}\tau_L}{1 + \Delta^2\tau_L/K} \qquad\qquad 4.11$$

Equation 4.11 indeed predicts that V_{drift} increases sub-linearly with *K*. In the absence of the dry friction, *i.e.* $\Delta = 0$, the drift velocity is exactly same as that of Einstein's value ($\bar{\gamma}\tau_L$). In the presence of a finite Δ, V_{drift} increases with *K* and approaches the Einstein's value only in the limit of $K \approx \infty$. Equation 4.11 also predicts that V_{drift} should increase linearly with the bias $\bar{\gamma}$. All these predictions are consistent with the experimental observations. The sub linear increase of V_{drift} with respect to *K* is not only observed when dry friction operates, but also with a velocity weakening friction

as is the case with the surfaces grafted with PDMS chains. For the case of a strong dry friction, i.e. when $\Delta^2 \tau_L >> K$, $V_{drift} = K\bar{\gamma} / \Delta^2$. This illustrates an interesting situation, namely that a linear relation prevails between the drift velocity and the driving force in a stochastic situation even when no kinematic friction may be operating at the interface. At the lowest power (0.0003 m^2/s^3), we do not detect any diffusive motion of the prism as any fluctuation exhibited by the prism merges with the background noise. At an intermediate level of the injected power, the glass prism exhibits a net drift but accompanied with intermittent stick-slip modes. Literature is abounding with the observation of stick slip motion in various systems of interests to tribologists and wetting specialists. The subject of tribology is beautifully summarized in a recent paper [46]. Stick-slip motion is evident in the relaxation of the contact line of a liquid drop [23], in the dynamics of granular particles [47], migration of cells [48,49]' on a surface, frictional sliding between lubricated and unlubricated surfaces [50,51] as well as in earthquakes [52]. Many of these instabilities are due to the competition between elastic restoring force and friction coupled with shear weakening of the interface [47,53]. An interesting new picture of stick-slip motion has recently been provided [54], in which Eq. 4.1 is solved without any applied bias within the path integral framework of Onsager and Machlup. The authors found two kinds of solutions referred to as direct and indirect paths. The direct optimal path is characterized by continuous velocity and acceleration of the slider corresponding to the slip phase. The indirect optimal path corresponds to the sticking of the object to the surface for some finite time. These indirect paths have been interpreted by the authors as leading to a stick-slip motion. Our approach to explaining

the stick-slip motion is rather classical. By modifying Eq.4.1 with a periodic perturbation to the background friction, we find that the slider can get trapped to the potential well till a strong acceleration takes it to another potential well, leading to a stick-slip motion. When trapped in a potential well, the slider may still undergo a restricted diffusive motion without a net drift [55], capturing which is beyond our current experimental capability.

At this juncture, we would like to point out that the way the static friction is idealized in Eq. 4.1 may not be quite correct, as there are indications [56,57] that some small scale motion may exist when the external bias is smaller than $m\Delta$. We have seen that a non-linear power law friction may be adequate in describing the drift velocity and the displacement PDFs. However, the situation may also be described by replacing the dry friction term with a different form of non-linear friction as follows:

$$\frac{dV}{dt} + \frac{V}{\tau_L} + \Delta tanh(\alpha V) = \bar{\gamma} + \gamma(t) \qquad 4.12$$

Equation 4.12 with a high value of α indeed reproduces all the drift velocity data as Eq. 4.1. It also reproduces the exponential tails of the displacement PDFs.

4.5.2 *Gaussian and non-Gaussian PDF of displacement fluctuations*

One new, and potentially important, observation in this work is that the displacement PDF is Gaussian at a low power, but it exhibits pronounced exponential tails at higher powers. The Gaussian distribution at a very low power results from the

lack of sufficient high energy pulses, thus leading to poor statistics. As the power of the noise increases, statistics is improved and the displacement PDF starts exhibiting asymmetry with exponential tails. The kurtosis of the PDF is above the value of 3, expected for a non-Gaussian distribution, for *K* ranging from 0.04 m^2/s^3 to 0.43 m^2/s^3, but it becomes Gaussian again at $K = 1.21$ m^2/s^3. This transition from a non-Gaussian to a Gaussian PDF might indicate a transition from a state governed by dry friction to a state governed by a linear kinematic friction, although the displacement correlation remains poor as is evident in the very low diffusivity.

A non-Gaussian PDF of displacement is also evident for the case of a PDMS grafted prism sliding against a PDMS grafted silicon wafer, where a velocity weakening non-linear friction seems to operate. However, in this case, the distribution is strongly non-Gaussian only at a short time scale (i.e. 0.005 *s*), but it becomes more Gaussian at a longer time scale. The general features of the experimental observations are borne out reasonably well with Langevin dynamics simulation with a non-linear kinematic friction.

We anticipate that a non-Gaussian velocity distribution may also be observed for a colloid particle undergoing a Brownian motion in weak adhesive contact with a soft substrate. As the particle moves, it forms new bonds in the advancing edge, but breaks bonds at the trailing edge resulting in hysteresis of adhesion. The Fokker-Planck equation for the motion of the colloidal particle may be of the form:

$$\frac{\partial P}{\partial t} = \omega \tau_L \frac{|\Delta x|}{\Delta x} \frac{\partial P}{\partial x} + D \frac{\partial^2 P}{\partial x^2} \qquad \qquad 4.13$$

Here, ω is a measure of adhesion hysteresis. The stationary solution of the displacement is exponential. The stochastic path of the colloidal particle for a given duration τ is also expected to be exponential with a suppressed diffusivity. These considerations may be relevant to the results reported by Wang *et al.* [6].

4.5.3 Einstein-like Relation

We now turn our discussion to the Einstein-like relation that we observed in our system, which have similarities to some of the previous studies. D'Anna *et al.* [44] conducted an experiment, in which a torsional pendulum was immersed in a granular medium, which was fluidized by strong agitation with a white noise. Meanwhile, a sinusoidal torque was imposed on the pendulum itself. These measurements allowed an estimation of the granular viscosity, which decreased with the strength of the noise with an effective temperature that also scaled linearly with the power of the noise.

A different study [45] focused on the behavior of a single object that is a small ball placed on a smooth screen while exposing it to an upward flow of gas. The turbulence produced due to the flow of the gas about the ball created a random upward and downward motion of the ball, which was consistent with the Langevin dynamics with the random force and a frequency dependent drag satisfying a FDR.

Our study is somewhat comparable to that of Ojha *et al.* [45] in the sense that the system can be characterized by a single "effective temperature". Our studies conducted with drift velocities and diffusivities estimated at different values of K and $\bar{\gamma}$ comply with an Einstein-like relation, where we find $\sigma_v^2 \bar{\gamma} / K V_{drift} = 1$, implying

$D / \mu = m \, K \tau^{*}/2$. Here $\tau*$ is a characteristic velocity correlation timescale. One intriguing observation is that the diffusivity increases with bias at a given value of K implying that fluctuation increases with force. This type of result may be expected in the case of a thermally activated diffusion, where diffusivity could take the form, $D = D_E \exp$ $[(f\lambda - E_a) / k_B T]$. Here D_E is the Einstein's diffusivity ($K\tau_L^2/2$), f is the bias which reduces the activation energy E_a and λ is a length scale separating the potential minima. If we develop a parallel argument to explain our current result, the molecular activation states would plausibly be related to the metastable states on the surface due to defects with the thermal energy replaced by *mKτ*/2*. The prediction of such an equation is qualitatively consistent with our observation in that the diffusivity increases with both *K* and bias. This equation also predicts that all the diffusivity data would converge to D_E at high value of *K* as seen in our experiments. In fact, at a value of *K*~8 *m²/s³*, all the diffusivity data seem to merge, which also gives an estimate of $D_E \sim 2 \times 10^7$ *μm²/s* at this value of *K*. The possibility of the diffusivity being an activated process where the metastable states provide the energy barrier and the mechanical noise provide the excitation is an interesting prospect. However, more studies would be needed to find out if a Kramer like transition may occur in such systems.

We finalize this discussion section by re-iterating the fact that not only the magnitude of the experimental diffusivities are considerably smaller than that predicted by de Gennes [33], the power law exponent (1.6) of the *D-K* relationship also differs from the prediction (3) of de Gennes. Typical methods to construct diffusive trajectory is

to establish the base state of the velocity distribution function, as is given in equations 4.5or 4.6 and then to propagate the base state solution temporally either using an Onsager Machlup or a Fokker-Plank approach. What is striking in the current situation is that no special method is needed to propagate the base state vectors in time since the velocities are almost delta correlated. The method provides estimation of diffusivities that are close to the experimental values not only for the case of a sliding prism on a rough surface, but also for a PDMS grafted prism sliding on a PDMS grafted silicon wafer. The method works because the correlation time of stochastic velocities is very small compared to τ_L and τ_Δ. With the above caveats, it is still intriguing that an Einstein- like relationship is obtained. These considerations may be of importance in other athermal systems, such as granular gas, where the noise correlation time and frictional time scales may be comparable in some cases.

4.6 Conclusions

By studying the drift and the diffusive behavior of a small solid object on a solid substrate as a function of the strengths of the bias and the noise, we arrive at the following conclusions:

1. When a non-linear friction operates at the interface, the displacement distributions are non-Gaussian and asymmetric, with the asymmetry increasing with the bias.

2. Distinct solid-like, a fluid-like and transition regions are identified.

3. An Einstein-like manifestation of fluctuation dissipation relationship is obtained in spite of the evidence that the stochastic velocities may be poorly correlated.

4.7 Appendix

4.7.1 Surface Properties of Roughened Glass Surface:

The roughness of a grit blasted glass surface was estimated using an optical profilometer (STIL micromeasure, CHR 150-N). Because of poor reflectivity of the glass surface, it was coated with a thin layer (~12 *nm*) of Au-Pd (~85%-15% weight percent) using a sputter coater (Polaron SEM coating unit E 5100, Pressure ~0.03 Torr in Argon atmosphere). Seven profilometric measurements were conducted at different spots on the surface with a step size of 2.5 *μm* and scanning area of 500 *μm* x 500 *μm* including one of 1 *mm* x 1 *mm* area. Using "3D Mountains Map", a data post processing software, the root mean square (rms) value of the height (in Z-axis) fluctuation was found to be ~ 16 *μm* with a slight variation (~1 *μm*) of its value from spot to spot. The rms value of the height fluctuation of the control (un-roughened) surface was ~0.4 *μm* which is close to the resolution range of the profilometer. From the power spectrum of the height fluctuation along the X-axis, a correlation length of the roughness was estimated as ~8 *μm*.

From the density of the asperities (~1300 *asperities/mm²*) on the rough surface, we estimate that about 1.6×10^5 asperities are available to make contact with the glass prism during sliding measurements. Although only a fraction of those asperities should

actually be in contact, enough numbers of contacts are probably made and its fluctuation is probably small so that sliding behavior of prism is rather uniform, when observed at a large scale. In Figure 4.19, the position of the glass prism is plotted with time during a sliding experiment, which yielded an excellent straight line over the length of ~35 *mm* with negligible fluctuation of velocity. This suggests that there is no gross variation of surface properties. When measurements are done at different spots on the surface, highly reproducible velocities (1.2 ± 0.04) *mm/s* are also obtained. However, some fluctuation of the contact of asperities at the microscopic level cannot be ignored. This point was also discussed by Buguin *et al* [58].
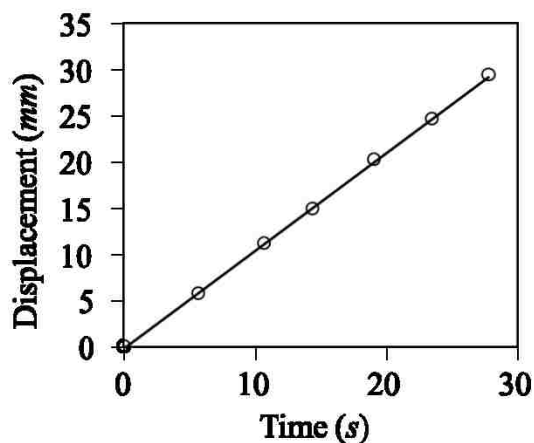
Figure 4.19: Displacement of a glass prism on roughened glass support subjected to a Gaussian noise of 0.1 m^2/s^3 under the applied bias of 0.57 *mN*.

One question that arises is whether there are wears occurring on the smooth glass prism during sliding. Regular optical microscopy did not reveal any such features. Hence, the prism was subjected to Atomic Force Microscopy (Digital Instrument, USA). These studies conducted over a scanning area of 100 μm^2 on different spots show that the prism

is fairly smooth (root mean square roughness ~ 4 *nm*). Very rarely, a scratch line of width $\sim 1\mu m$ and depth ~ 7 *nm* could be observed. However, these seem to be the native features of the surface, and not the wear marks, as they were also observed on a prism that were not subjected to sliding against the rough surface. The area occupied by the scratch marks is however highly negligible in comparison to the total surface area under investigation.

4.7.2 Drift Velocity and Diffusivity of Prism on the Rough Surface: Comments on Equation 1 in the Text

In this section, we discuss as to what extent Eq. 4.1 may be valid in describing the motion of the glass prism on the roughened glass surface.
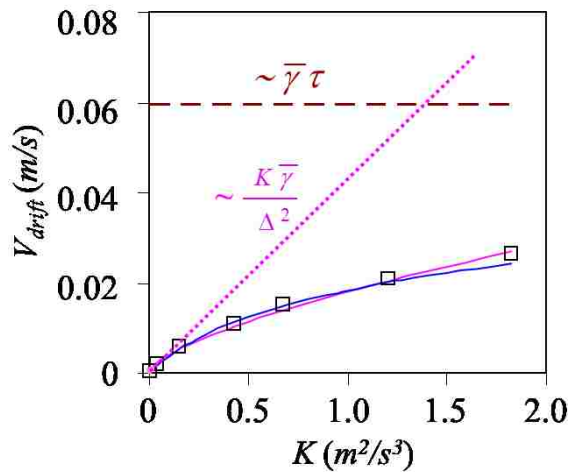
Figure 4.20: Drift velocity as a function of power of the Gaussian noise at an applied bias of 1.43 *mN* is shown. The open squares are experimental data. The blue line represents drift velocity obtained from first moment of PDF given by Eq. 4.5 with $\tau = 0.06$ *s* and $\Delta = 4.5$ *m²/s3* whereas the pink solid line depicts drift velocity estimated using Eq. 4.6 using $A = 0.02$ and $n = 0.2$. The pink dotted line depicts drift velocity estimated using Eq. 4.5 neglecting the kinematic friction term (i.e. $\tau_L = \alpha$) and brown dashed line depicts drift velocity obtained from first moment of PDF given by Eq. 4.5 without the static friction term (i.e. $\Delta = 0$).

At the onset of this discussion, we point out that we have also examined if a highly non-linear friction of the type described in Eq. 4.2 is adequate in describing the observed behavior. We consider the following possibilities: the friction is given only by the kinematic term V/τ_L, by the dry friction $\sigma(V)\Delta$, combination of the above two terms and a non-linear friction $\sim\sigma(V)|V|^n$. Using the appropriate forms of equations 4.5 and 4.6 we first estimate the drift velocities of the prism.

The data summarized in Figure 4.20 show that the drift velocity is independent of the power of the noise if the friction is purely kinematic. On the other hand, if only dry friction operates, the drift velocity increases linearly with power (K). Neither of these predictions is consistent with our experimental observations. When both the dry and kinematic frictions are taken into account, or when a non-linear friction $(\sim\sigma(V)|V|^n$ with $n = 0.2$) is assumed to operates at the interface, the sub-linear velocity profile, as observed in experiments, are reproduced. Now the question is, which of these two forms is the better representative of the situation?

In an effort to discriminate between the two cases, we also solved the full Langevin equations (4.1 and 4.2) to obtain the PDFs of the displacement distribution for a given value of K and τ. The results summarized in Figure 4.21 show that both the models predict non-Gaussian behaviors, which are non-discriminatory. We thus resort to a different strategy. Equation (1) predicts that in the absence of noise, the object would not move till a force of sufficient magnitude is applied. This is consistent with our experimental observation. When the prism is placed on the rough surface and the latter is

gently tilted, the prism does not move till a critical angle of $\sim 17^o$ is reached, beyond which the prism slides on the surface. This is, however, in contrast to the case of the PDMS grafted prism on the PDMS grafted silicon wafer, where the prism start to slide at an angle above 1°.
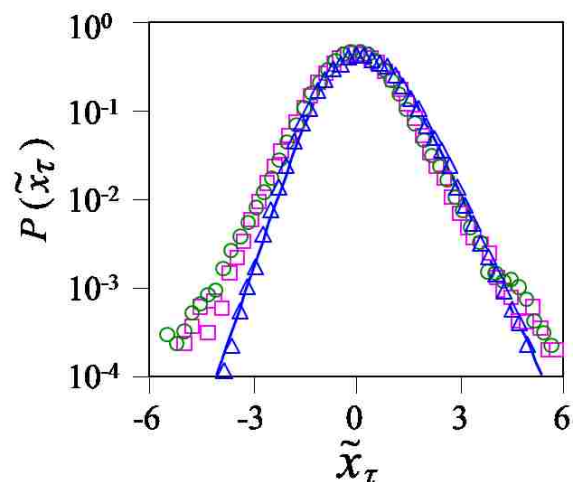
Figure 4.21: The PDF of the dimensionless displacement of a smooth glass prism on a rough glass support with an applied bias of 0.29 *mN* and a Gaussian noise of power 0.04 *m^2/s^3*. The blue triangle (Δ) represents experimental data, whereas the solid line is the fit to that data with an asymmetric double sigmoidal function. Pink squares ($\square$) and green circles ($\circ$) depict the PDFs obtained from Langevin dynamics simulation using Eq. 4.1 and 4.2 respectively.

Existence of this critical angle for the glass on glass suggests that there is a significant static friction, which was also ascertained in a different experiment, in which the prism was placed on a tilted (4°) rough plate, which was subjected to sinusoidal accelerations (100 *Hz*) of various amplitudes. The prism does not move up to an acceleration of $\sim$3 *m/s^2* beyond which the velocity of the prism increased linearly with the imposed acceleration (Fig. S4) . The above experiments suggest that the prism has to overcome a

threshold force before it moves on the surface. Next we investigated if the velocity relaxes exponentially when the prism moves above the threshold force. In order to achieve this goal, we followed a previous suggestion of de Gennes. [33] After placing the prism on a horizontal rough surface, it was knocked at one edge. The prism moved over a distance of about 4 *cm* and then stopped. The decay is exponential with a time constant of about 0.08 *s*. At this juncture, we would also like to mention that the measurements of the drift velocity with the sinusoidal vibrations as carried out with two different surfaces superimpose onto each other. The displacement relaxations were also carried out on different tracks on two different surfaces over a length of 4 *cm*. The data of three such tracks are shown in Figure 4.22 indicate that they are highly reproducible.
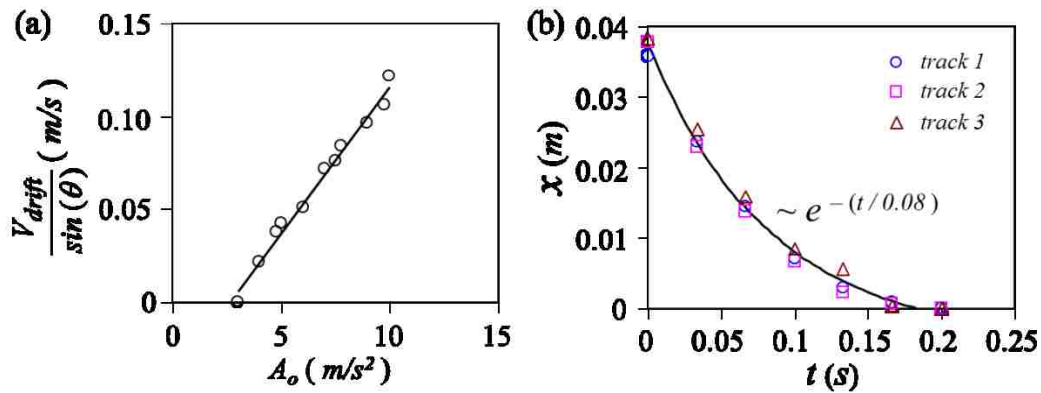
Figure 4.22: (a) Plot of $V_{drift}/sin\,(\theta)$ as a function of amplitude of sine wave of 100 *Hz* for a glass prism on a rough glass support. (b) Plot of displacement (which needs to be traversed before stopping) as a function of time for a glass prism on a horizontal rough glass support when the former is knocked at an edge. Three tracks nicely fall on a single curve having exponential relaxation.

121

The above experimental results are only indicative of the presence of static and kinematic friction. In the real experiment, the prism is sheared against the asperities with high stochastic forces lasting for a very short period of time. To the best of our knowledge, the behavior of friction under these conditions is quite unknown. We take the fitting of the experimental drift velocities at seven different powers and at five different biases using Eq. (5) with only two adjustable parameters as evidence that Eq. 4.1 is a good, although a minimal, model in our system. It also reproduces the exponential tails of certain displacement distributions quite satisfactorily and provides the base state PDF of the velocities. However, there is always the scope in improving this model, which is the subject of ongoing research in our laboratory.

4.7.3 Power Spectrum of the Noise

Traces of a typical noise and its power spectra are shown in figure S5 at two different sampling frequencies. With a total bandwidth ($-f_{max}$ to $+f_{max}$, f_{max} being the maximum frequency) of 10 *kHz*, the spectrum is quite flat (figure S5, left).
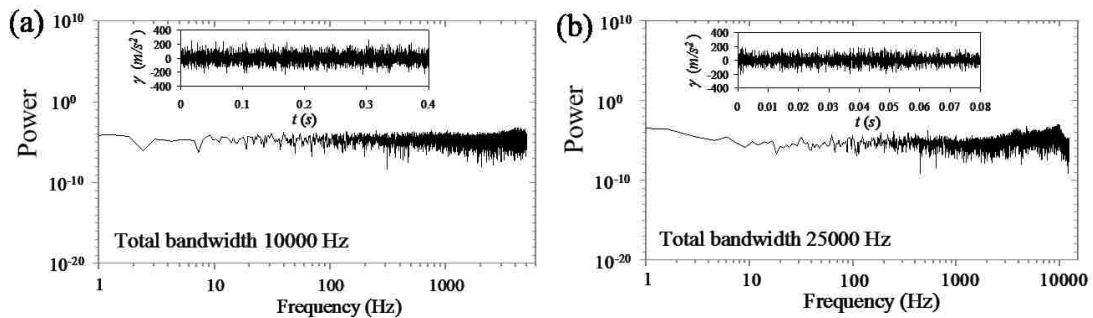
Figure 4.23: Typical traces of the acceleration pulses (inset) and their power spectra taken at two different bandwidths corresponding to $K = 0.16$ m^2/s^3.

Thus the noise can be considered to be a white for an actual bandwidth (0 to f_{max}) of 5 *kHz*, which corresponds to the specification of the oscillator by the manufacturer [59]. We also checked what the spectrum is like when a total bandwidth of 25 *kHz* is used. Here, we see that above about 5 *kHz*, the spectrum tends to drift upward indicating a slight blue shift. After about ~10 *kHz*, a downward drift is observed indicating a Brownian shift. Using 10 *kHz* as the corner frequency (Figure 4.23, right), a time constant τ_c, as estimated from $1/(2\pi f)$, is about 16 μs. However this time scale corresponds to a slightly tainted white noise. More correct time constant should be about 30 μs (Figure 4.23, left) as the spectrum corresponding to this time scale represents an untainted white noise. The important point to convey here is that the above time scale is much smaller than the Langevin (0.06 *s*) or the dry friction time scale $\tau_\Delta \sim K / \Delta^2$ (500 μs to 0.1 *s* for K ranging from 0.01 m^2/s^3 to 2 m^2/s^3). Another issue that deserves comment here is the possible reduction of the bandwidth of the oscillator due to its coupling with the support. We found that a lightweight support (mass = 40 *g*) made of aluminum did not reduce the bandwidth of the oscillator appreciably from its nominal value of 5 *kHz*.

4.7.4 Power Spectrum of Displacement

As mentioned in the text, the displacements of the prism were recorded at a time resolution of 0.001 *s*. The power spectra of these displacements at a sampling frequency of 1 *kHz* are quite flat at low powers (Figure 4.24 and Figure 4.25). At high powers (for a smooth prism on rough support), somewhat correlated signal becomes apparent at the higher frequency range. From the corner frequency of this power

spectrum, a relaxation time of ~ 1 *ms* is estimated, although its actual value is probably

smaller than a 1 *ms*, considering the fact that the slope of the power spectrum is about

1.4. In any case, even this relaxation time is considerably smaller than either the

Langevin time scale (0.06 *s*) or the dry friction time scale $\tau_A \sim K / \Delta^2$ (0.06 *s*).
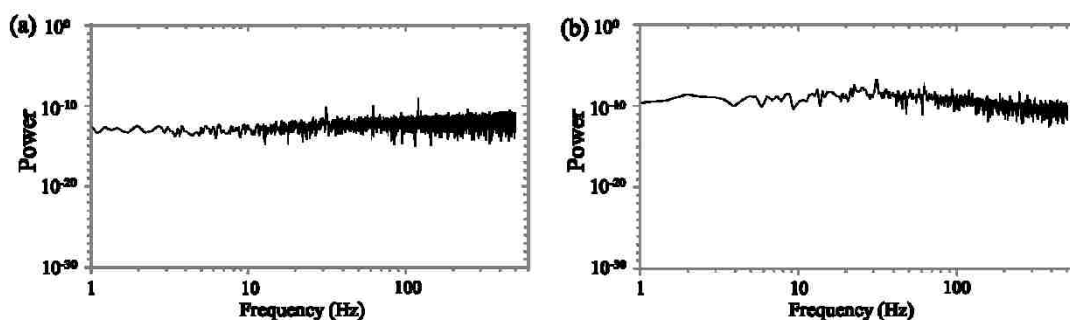
Figure 4.24: Power Spectra of displacements of glass prism on rough glass support at two different values of *K* [0.04 m^2/s^3 (a) and 1.2 m^2/s^3 (b)] taken at the total bandwidth of 1 *kHz*.
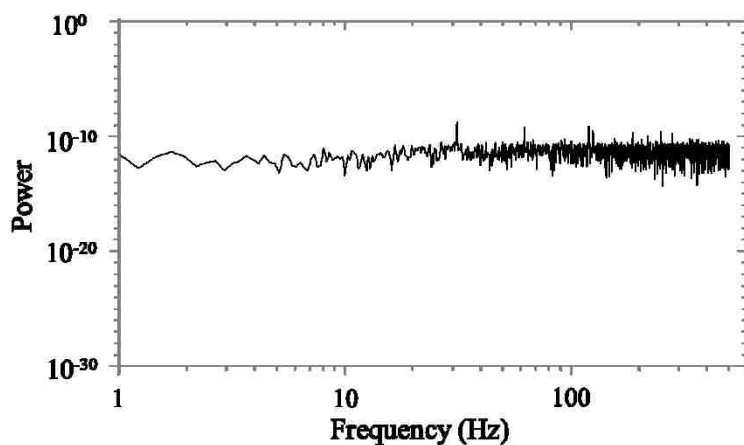
Figure 4.25: Power spectrum of the stochastic displacement of a PDMS grafted prism on a PDMS grafted silicon wafer with *K*=0.1 m^2/s^3. Total bandwidth is 1 *kHz*.

4.7.5 Rate of Work Done by Friction

In order to further validate the method used in section 4.4.6 to estimate diffusivity and drift velocity using the assumption that the velocities are delta correlated, we estimate the energy dissipation using the computed trajectories and compare these with those found from experiments. Neglecting the work done by the external noise, the average rate of work performed on the prism (per unit mass) is composed of the following terms: V_{drift}^2 / τ_L, $\Delta \langle |V| \rangle$ and $\bar{\gamma} V_{drift}$. The term V_{drift}^2 / τ_L is due to kinematic friction, the second term is due to dry friction and the third term is due to external force. As the rates of work done due to kinematic friction and applied bias are negligible in comparison to that due to dry friction, we only compare the values of $\Delta \langle |V| \rangle$ obtained from experimental data and that calculated from simulated trajectories. Figure 4.26 shows that these values do not differ to a significant degree, thus providing further support to the methodology described in section 4.4.6.
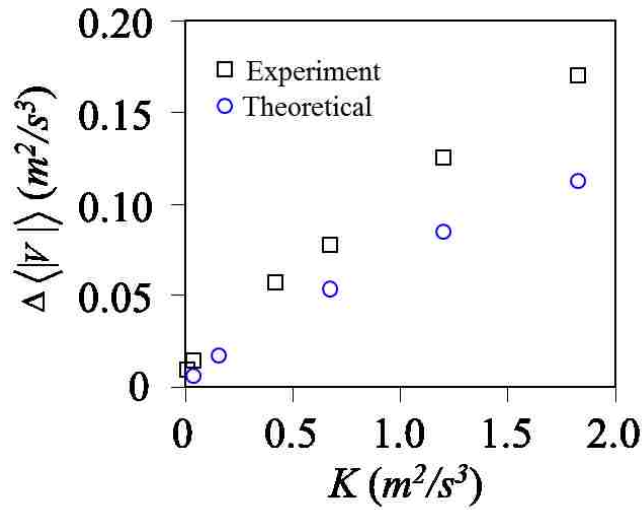
Figure 4.26: Energy dissipation rate due to static friction as a function of power of the noise estimated from experimental observations and from trajectories using Eq. 4.10. The applied bias is 0.29 *mN*. It should be borne in mind that these velocities are approximate values, which are estimated from the displacements over a timescale of 0.001 sec.

4.7.6 Relaxation Time from Work Fluctuation

If the Einstein relation $D/\mu=mK\tau^*/2$ holds for the diffusive drift of the prism, then

Eq. (8) can be written in the following form:

$$\frac{P(+W_\tau)}{P(-W_\tau)} = exp\left[\frac{2W_\tau}{mK\tau^*}\right] \qquad\qquad 4.14$$
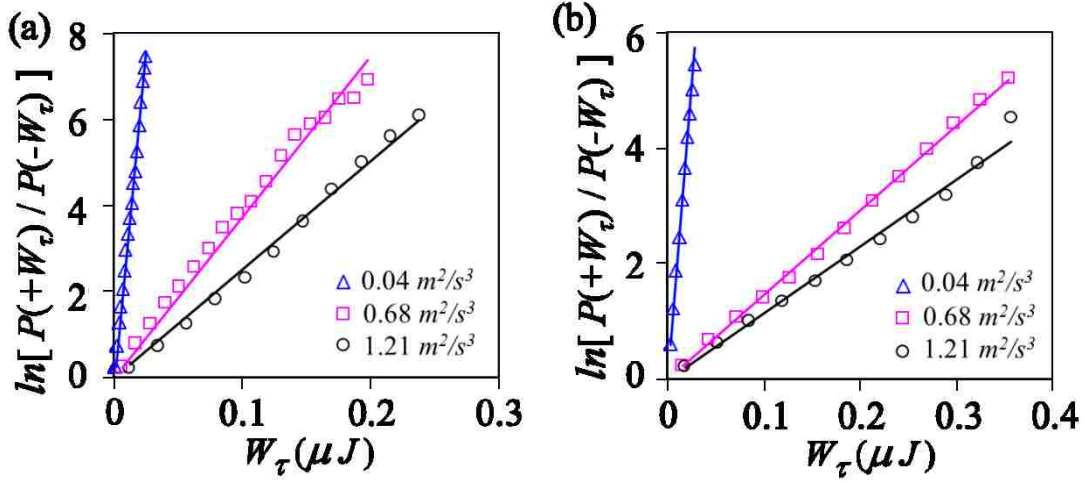
Figure 4.27: Work fluctuation plots for two cases. (a) bias is 0.29 mN (b) bias is 0.58 mN. All the plots are for 0.2 s at three different powers as shown in the inset of the figures. From the slopes of these plots, the values of τ^* are estimated as 93 μs for K=0.04 m^2/s^3; 44 μs for K=68 m^2/s^3 and 33 μs for K=1.21 m^2/s^3 at the bias of 0.29 mN. At a higher bias of 0.58 mN, the values of τ^* are estimated as 150 μs for K=0.04 m^2/s^3; 180 μs for K=68 m^2/s^3 and 99 μs for K=1.21 m^2/s^3.

According to Eq. 4.14, a plot of $\ln\dfrac{P(+W_\tau)}{P(-W_\tau)}$ versus W_τ should be a straight line, the

slope of which provides an estimate of the relaxation time τ^*. This is in the same spirit

as that of a previous publication of Feitosa and Menon [60], although that work was

concerned with the power fluctuation in a granular gas.

Figure 4.27 shows such plots at different values of *K* for two different biases. The

relaxation time τ^* is estimated to be in the range of 33 μs to 93 μs for a bias of 0.29 *mN*,

which are comparable to the values estimated in section 4.4.6. Unfortunately, similar

correlations could not be constructed at higher biases, as the statistics of occurrence of negative fluctuation of displacement becomes very poor.

4.7.7 Diffusive Behavior at Short Time Scale
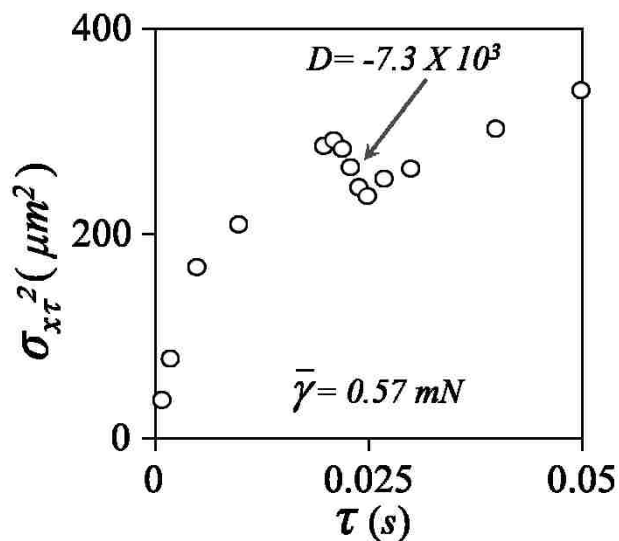
Figure 4.28: At short time scale, the prism exhibit anomalous diffusive behavior at a bias of 0.57 *mN* ($K= 0.04$ *m²/s³*) as is the case with a lower bias reported in FIG 12 in the text.

References

[1]   H. Jaeger, C. Liu, and S. Nagel, Physical Review Letters **62**, 40–43 (1989).

[2]   J. Olafsen and J. Urbach, Physical Review Letters **81**, 4369–4372 (1998).

[3]   I. Sanchez, F. Raynaud, J. Lanuza, B. Andreotti, E. Clement, and I. S. Aranson, Physical Review E **76**, 060301 (2007).

[4]   D. Bi and B. Chakraborty, Philosophical Transactions. Series A, Mathematical, Physical, and Engineering Sciences **367**, 5073–90 (2009).

[5]   S. F. Burlatsky and J. M. Deutch, The Journal of Chemical Physics **103**, 8216 (1995).

[6]   B. Wang, S. M. Anthony, S. C. Bae, and S. Granick, Proceedings of the National Academy of Sciences of the United States of America **106**, 15160–4 (2009).

[7]   D. C. Senft and G. Ehrlich, Physical Review Letters **74**, 0–3 (1995).

[8]   J. A. Mann Jr and W. A. Woyczynski, Physica A **291**, 159–183 (2001).

[9]   T. P. C. Van Noije and M. H. Ernst, Granular Matter **1**, 57–64 (1998).

[10] W. Losert, D. G. W. Cooper, J. Delour, a. Kudrolli, and J. P. Gollub, Chaos (Woodbury, N.Y.) **9**, 682–690 (1999).

[11] X. Nie, E. Ben-Naim, and S. Y. Chen, Europhysics Letters **51**, 679 (2000).

[12] A. Prevost, D. Egolf, and J. Urbach, Physical Review Letters **89**, 1–4 (2002).

[13] K. Feitosa and N. Menon, Phys. Rev. Lett. **92**, 164301 (2004).

[14] A. Puglisi, P. Visco, A. Barrat, E. Trizac, and F. van Wijland, Physical Review Letters **95**, 1–4 (2005).

[15] A. Pumir, Physics of Fluids **8**, 3112 (1996).

[16] X. D. Shang, P. Tong, and K. Q. Xia, Phys. Rev. E **72**, 015301 (2005).

[17] S. Jung, P. J. Morrison, and H. L. Swinney, J. Fluid Mech. **554**, 433–456 (2006).

[18] E. Falcon, S. Aumaitre, C. Falcon, C. Laroche, and S. Fauve, Phys. Rev. Lett. **100**, 064503 (2008).

[19] M. M. Bandi and C. Connaughton, October 1–9 (2008).

[20] L. Mahadevan and J. M. Deutch, Proceedings of the Royal Society A: Mathematical, Physical and Engineering Sciences **466**, 993 (2010).

[21] S. Ratynskaia, G. Regnoli, K. Rypdal, B. Klumov, and G. Morfill, Physical Review E **80**, 1–11 (2009).

[22] M. K. Chaudhury and S. Mettu, Langmuir : the ACS Journal of Surfaces and Colloids **24**, 6128–32 (2008).

[23] S. Mettu and M. K. Chaudhury, Langmuir : the ACS Journal of Surfaces and Colloids **26**, 8131–40 (2010).

[24] S. Daniel, S. Sircar, J. Gliem, and M. K. Chaudhury, Langmuir **20**, 4085 (2004).

[25] S. Daniel and M. K. Chaudhury, Langmuir **18**, 3404 (2002).

[26] S. Daniel, M. K. Chaudhury, and P.-G. de Gennes, Langmuir : the ACS Journal of Surfaces and Colloids **21**, 4240–8 (2005).

[27] P. S. Goohpattader, S. Mettu, and M. K. Chaudhury, Langmuir : the ACS Journal of Surfaces and Colloids **25**, 9969–79 (2009).

[28] C. C. . Craig, The Annals of Mathematical Statistics **7**, 1–15 (1936).

[29] C. Beck, E. G. D. Cohen, and H. L. Swinney, Phys. Rev. E **72**, 056133 (2005).

[30] E. Van der Straeten and C. Beck, Physical Review E **80**, 1–13 (2009).

[31] J. van Zon and F. MacKintosh, Physical Review Letters **93**, 3–6 (2004).

[32] A. Kawarada and H. Hayakawa, Journal of the Physical Society of Japan **73**, 2037 (2004).

[33] P.-G. De Gennes, Journal of Statistical Physics **119**, 953–962 (2005).

[34] a. Mauger, Physica A: Statistical Mechanics and Its Applications **367**, 129–135 (2006).

[35] A. Einstein, *Investigations on the Theory of the Brownian Movement* (Dover Pubns, 1956), p. 122.

[36] T. Baumberger, L. Bureau, M. Busson, E. Falcon, and B. Perrin, Review of Scientific Instruments **69**, 2416–2420 (1998).

[37] H. A. Kramers, Physica VII 284–304 (1940).

[38] H. Risken, *Risken, H., The Fokker-Planck-Equation. Methods of Solution and Applications. ISBN3-540-50498-2 (Springer Series in Synergetics 18)*, Second ed (Springer-Verlag, 1991).

[39]   J. W. Krumpfer and T. J. McCarthy, Faraday Discussions **146**, 13 (2010).

[40]   H. She, D. Malotky, and M. K. Chaudhury, Langmuir **14**, 3090–3100 (1998).

[41]   K. Dahmen, Y. Ben-Zion, and J. Uhl, Physical Review Letters **102**, 1–4 (2009).

[42]   K. Vorvolakos and M. K. Chaudhury, Langmuir **19**, 6778 (2003).

[43]   O. Zik, J. Stavans, and Y. Rabin, Europhysics Letters (EPL) **17**, 315–319 (1992).

[44]   G. D. Anna, P. Mayor, A. Barrat, V. Loreto, and F. Nori, Nature 909–912 (2003).

[45]   R. P. Ojha, P. Lemieux, P. K. Dixon, a J. Liu, and D. J. Durian, Nature **427**, 521–3 (2004).

[46]   T. Baumberger and C. Caroli, Advances in Physics **55**, 279–348 (2006).

[47]   S. Nasuno, a. Kudrolli, and J. Gollub, Physical Review Letters **79**, 949–952 (1997).

[48]   T. Savin and L. Mahadevan., Biophysical Journal **96**, 627a (2009).

[49]   D. Selmeczi, L. Li, L. I. I. Pedersen, S. F. Nrrelykke, P. H. Hagedorn, S. Mosler, N. B. Larsen, E. C. Cox, and H. Flyvbjerg, The European Physical Journal Special Topics **157**, 1–15 (2008).

[50]   B. N. J. Persson, *Sliding Friction: Physical Principles and Applications*, 2nd ed. (Springer, Berlin; New York, 2000).

[51]   M. H. Muser, M. Urbakh, and M. O. Robbins, Advances in Chemical Physics **126**, 187 (2003).

[52]   W. F. Brace and J. D. Byerlee, Science **153**, 990–2 (1966).

[53]   O. Ronsin and K. L. Coeyrehourcq, Proceedings of the Royal Society A: Mathematical, Physical and Engineering Sciences **457**, 1277–1294 (2001).

[54]   A. Baule, E. G. D. Cohen, and H. Touchette, Journal of Physics A: Mathematical and Theoretical **43**, 025003 (2010).

[55]   L. Bureau, C. Caroli, and T. Baumberger, Proceedings of the Royal Society A: Mathematical, Physical and Engineering Sciences **459**, 2787 (2003).

[56]   T. Baumberger, F. Heslot, and B. Perrin, Nature **367**, 544–546 (1994).

[57]   Z. Yang, H. P. Zhang, and M. Marder, Proceedings of the National Academy of Sciences of the United States of America **105**, 13264–8 (2008).

[58]   A. Buguin, F. Brochard, and P.-G. de Gennes, The European Physical Journal. E, Soft Matter **19**, 31–6 (2006).

[59]   *PASCO Mechanical Wave Driver SF-9324* (n.d.).

[60]   K. Feitosa and N. Menon, Phys. Rev. Lett. 1–4 (2004).

5. CHAPTER FIVE: Stochastic Rolling of a Rigid Sphere in Contact with Soft Rubber[3]

5.1 Introduction

We have recently been interested in studying [1–3] the role of non-linear friction in the stochastic motion of a small solid object or a liquid drop on a solid support in the presence of an external noise and a bias. Here, the system size is selected to be large enough to be decoupled from the internal noise, but small enough to respond to an external perturbation in a measurable way. In these cases, the drift velocity increases somewhat sub-linearly, but the diffusivity increases super-linearly [1] with the strength of the noise. The displacement fluctuation exhibits a non-Gaussian behavior at a short time scale, but a Gaussian behavior at a longer time scale. Non-Gaussian systems response has also been reported in the past in the context with granular flow [4–8], hydrodynamic turbulence [9–11], dusty plasma [12], Rayleigh-Bernard convection [13], and self-propelling particles [14]. Explanations for some of these observations have been offered on the basis of a joint probability distribution of the forcing and response functions [11] as in the power input distribution, within the framework of superstatistics [15,16] as in the velocity distribution in turbulence, and inelastic collisions of granular particles [17]. The results of our stochastic sliding experiments [1–3] can be fairly understood within

---

the framework of a Langevin dynamics where the friction has a non-linear component, as was first pointed out by Caughey and Dienes [18]. Being inspired by these previous studies, here we explore how rolling of a sphere is affected by a non-linear friction and a random noise. Additional inspirations for these studies were derived from a recent experiment [19], in which non-Gaussian displacement statistics was observed with a colloidal particle undergoing Brownian motion in contact with a soft substrate.

Specifically, we studied the dynamics of a small sphere rolling on a fibrillated rubber [20] surface in the presence of a random mechanical noise. A fibrillar surface mimics the features of well decorated asperities with which to study the physics of pinning-depinning transition [21] and bioinspired adhesion [20]. The analysis of the stochastic rolling data required us to conjecture a complex non-linear model of friction with the non-linearity decreasing with the strength of the noise. Additional experiments were designed to interrogate this complexity by submitting the ball to a deterministic asymmetric vibration and a stochastic noise.

The dynamics of the motion of a line that is pinned randomly by defects [22] is supercritical in the sense that no motion is observed when the applied force is less than a threshold value, above which the velocity (V) usually grows non-linearly with the applied field. The extended relationship between the force and velocity can, however, be quite complex. For example, in the peeling of a soft rubbery adhesive from a substrate [23] it is known that the adhesion force first increases with velocity. After reaching a peak value, the force decreases only to rise again at even higher velocities. The friction of a

soft rubber [24–27] on a solid substrate also exhibits a complex velocity-force relationship [28,29] that is somewhat similar to that of the peeling of a viscoelastic adhesive from a surface.

Obtaining adequate expressions for velocity dependent friction or crack propagation is not only important for the macro-scale descriptions of these phenomena, they are also critical to the development of appropriate molecular and/or mesoscopic level models of adhesion and friction. During the course of this work, we also explored whether it is possible to obtain an insight into how friction or adhesion depends over a wide range of velocity by subjecting a system to random forces of various magnitudes, and examining its stochastic behaviors. The picture of friction that emerged from such a study could serve as a guideline for future experiments with which to explore the dependence of rolling friction on wide range of state variables.

5.2 Theoretical background

The stochastic motion of an object on a surface in the presence of a Coulombic friction [30] exhibits certain unique characteristics that are different from the dynamics originating from a linear kinematic friction. For example, while the steady state velocity distribution is Gaussian (mesokurtic) with a linear kinematic friction, it can be super Gaussian (leptokurtic) with a Coulombic or a non-linear friction. Furthermore, the self-diffusivity with a Coulombic friction depends more strongly on the strength of the noise than is the case with the linear kinematic friction [1]. The problem of Coulombic friction in a stochastic setting was first tackled by Caughey's group [18,31] at Caltech about fifty

years ago, within the framework of a Fokker-Planck equation. Several other studies followed the lead of Caughey [32–34] in the context of the random motion of sliding buildings in response to earthquake. More recently, the problem of stochastic motion involving Coulombic friction has been enlivened by de Gennes [35] as well as by Kawarada and Hayakawa [36] that also received rigorous treatments of path integral [32,37] and Fokker-Planck [38,39] formalisms in the past and recent times. Major progress has recently been made by Menzel and Goldenfeld [39], who focused on the displacement statistics associated with the random motion governed by Coulombic friction using a Fokker-Planck equation, which was previously addressed using a pulse train excitation approach [40] or a numerical integration of the Langevin equation [1–3]. When both a Coulombic and a viscous friction are at work, Menzel and Goldenfeld [39] demonstrated clearly that the displacement statistics at different time scales are not self-similar – it is exponential at short time scale and Gaussian at a longer time scale, which is consistent with the recent experimental observations [1–3,19]. In spite of the non-Gaussian fluctuation, the variance of the distribution grows linearly [1,2] at the large time limit. Similar observations were also made by Wang *et al* [19] in an unusual Brownian motion of a colloidal particle in contact with a microtubule. When a bias is imposed [1,2], the object drifts with a velocity that increases sub-linearly with the strength of the noise, but linearly with the applied bias. This linear growth of displacement variance with time with a non-Gaussian statistics is not intuitive, but it is observed within the numerical solution of a Langevin [1–3] and/or a Fokker-Planck [39] equation.

In order to focus our discussion, let us consider a modified Langevin equation [1–3,18,41]:

$$\frac{dV}{dt} + \frac{V}{\tau_L} + \sigma(V)\Delta = \bar{\gamma} + \gamma(t) \qquad 5.1$$

Here, V is the velocity of the particle, $\bar{\gamma}$ is the external force divided by the mass of the object, τ_L is the Langevin relaxation time , and $\gamma(t)$ is the time dependent acceleration of the white noise, the power (or the noise strength) associated with which is K. The second term on the left of this equation is due to the linear kinematic friction and the third term is due to the Coulombic friction. Δ is the magnitude of the dry friction expressed in terms of the static friction force divided by the mass of the object. If Δ is smaller than $(\bar{\gamma} + \gamma(t))$, the object moves. On the other hand, if $(\bar{\gamma} + \gamma(t)) < \Delta$, the object remains stuck to the surface, unless its momentum gained from the previous impulse is significantly large [35]. It will set into motion again if another strong acceleration pulse $\gamma(t)$ rescues it from the stuck state. As the non-linear dry (or Coulombic) friction exhibits a jump discontinuity at $V=0$, it is convenient to multiply Δ with a signum function $\sigma(V)$ which is positive when $V > 0$ and negative when $V < 0$ with $\sigma(0)=0$. Within the above formalism, there is no operational difference between dry friction (solid on solid), wetting hysteresis (liquid drop on solid), or adhesion hysteresis [42] as it appears in rolling motion.

Caughey and Dienes [18] considered Eq. 5.1 (without the bias and the kinematic friction terms, i.e. $\bar{\gamma} = 0$ and $\tau_L = \infty$) and its corresponding Fokker Planck equation in

137

order to obtain an expression for the transition probability density in the velocity space. Their results showed that normal diffusive like motion prevails even when the dynamics is governed by the non-linear friction but the diffusivity ($D \sim K^3/\Delta^4$) varies more strongly with the power of the noise than the case with a linear kinematic friction ($D \sim K$). Another important finding of Caughey *et al* [18] is that the transition probability density at the stationary state is exponential with velocity.

Although our recent interests to study the role of non-linear friction in stochastic motion stem from its relevance to the problems of soft matter physics, the early interests in this subject arose from its importance in studying the sliding of the building foundations in response to earthquake. In this arena, following the lead of Caughey and Dienes [18] , Ahmadi [33] and Crandall *et al* [34] presented some approximate, but useful results. Below, we briefly review and extend certain predictions of the above authors, which would be important in interpreting the results of the experiments performed by us.

The non-linear nature of Eq. 5.1 makes it cumbersome to treat it analytically. As far as average values are concerned, one way to tackle the problem is to consider a classical linear version [18,43] of this equation and estimate the equivalent of the Langevin relaxation time. Following Caughey [18,43] and Crandall *et al* [34], we express Eq. 5.1 (without the bias) in the form shown in Eq. 5.2 with the addition of a remainder term φ as in Eq. 5.3.

$$\frac{dV}{dt} + \frac{V}{\tau_L^*} = \gamma(t) \qquad\qquad 5.2$$

$$\varphi = \frac{V}{\tau_L^*} - \frac{V}{\tau_L} - \sigma(V)\Delta \qquad\qquad 5.3$$

The criterion for equivalent linearization is to minimize the average value of φ^2 with respect to τ_L^*, which leads to the following equation:

$$\frac{1}{\tau_L^*} = \frac{1}{\tau_L} + \frac{\Delta\langle\sigma(V)V\rangle}{\langle V^2\rangle} \qquad\qquad 5.4$$

Calculation of the averages shown in Eq. 5.4 requires an expression for the stationary probability density of velocity, which can be obtained by setting the diffusive flux in the velocity space to zero:

$$\frac{K}{2}\frac{\partial P}{\partial V} + \Delta\frac{|V|}{V}P + \frac{VP}{\tau_L} = 0 \qquad\qquad 5.5$$

The stationary velocity distribution ($P(V)$) is

$$P(V) = P_o exp\left(-\frac{V^2}{K\tau_L} - \frac{2|V|\Delta}{K}\right) \qquad\qquad 5.6$$

The averages in Eq. 5.4 can now be carried out with the velocity distribution function given in Eq. 5.6. The analysis can be simplified if the exponential term (due to Coulombic friction) of Eq. 5.6 dominates over the kinematic term, which is often the case. One thus obtains:

$$\frac{1}{\tau_L^*} = \frac{1}{\tau_L} + \frac{\Delta^2}{K} \qquad\qquad 5.7$$

Equation 5.7 defines the equivalent relaxation time in terms of the Coulombic and a linear kinematic friction. When a small external bias is imposed, an expression for the drift velocity [1,2,35,41] can be obtained from the linear response theory, i.e. $V_{drift} = \bar{\gamma}\tau_L^*$. We thus have,

$$V_d = \frac{\bar{\gamma}\tau_L}{1 + \Delta^2\tau_L/K} \qquad\qquad 5.8$$

Equation 5.8 applies with an ideal white noise. However, any noise generated mechanically has a finite bandwidth and has certain amount of correlations. Thus, for a quantitative discussion of the nature of the drift and diffusion caused by an external noise, the value of *K* should be properly calibrated.

In a typical experiment of stochastic rolling or sliding, one can perform two types of measurements. With a random noise and a bias, the ball rocks forward and backward randomly but with a net drift. At a given bias, one can record the motion of the ball over a large distance for a given duration of time and estimate the drift velocity. Alternately, one can record the stochastic motion of the ball with a high speed camera to study the trajectory over certain duration of time. The spatial segments of the trajectories corresponding to a given time segment can then be used to obtain probability distribution function (pdf) of the displacement fluctuation. Such a pdf has a given peak and a dispersion of displacements. By plotting the position of the peak as a function of time

segments, a drift velocity can be estimated. Furthermore, from the slope of the variance

of the displacement versus time, one can obtain the diffusivity. When only a linear

friction operates, the drift velocity should simply be a product of the bias $(\bar{\gamma})$ and the

Langevin relaxation time (τ_L). On the other hand, when only the dry friction operates, the

drift velocity is given by $\bar{\gamma} K / \Delta^2$. With the presence of both the kinematic and a dry

friction, the drift velocity starts [1,2,41] from a very low value and progressively

saturates to $\bar{\gamma} \tau_L$ sub-linearly. These predictions are consistent with our previously

reported sliding experiments [1,2], but not, exactly, with a steel ball rolling on a fibrillar

PDMS substrate. Here the drift velocity increases in a sigmoidal fashion with the strength

of the noise. Understanding this discrepancy is the central objective of this paper.

At this point we should mention that a non-linear evolution of the drift velocity

with *K* can also be observed with a non-linear friction of the type: $(\sim |V|^n)$. Here, the

Langevin equation is:

$$\frac{dV}{dt} + \frac{B|V|^n}{M}\sigma(V) = \gamma(t) \qquad\qquad 5.9$$

The stationary probability distribution function [1,2] for the velocity is given by the

following equation:

$$P(V) = P_o^{''} exp\left(-\frac{2B|V|^{1+n}}{M(1+n)K}\right) \qquad\qquad 5.10$$

Equation 5.10 suggests that the velocity pdf is exponential if the friction is Coulombic (i.e. $n=0$). It is Gaussian for a linear kinematic friction with $n=1$. A super (leptokurtic) or a sub (platykurtic) Gaussian pdf results for $n<1$ and $n>1$ respectively.

Using the method of the equivalent linearization, it is easy to show that the characteristic relaxation time ($\tau*$) scales as $K^{\frac{1-n}{1+n}}$, whereas $\langle V^2 \rangle$ scales as $K^{\frac{2}{1+n}}$ yielding drift velocity and diffusivity [44] growing with K as $\bar{\gamma} K^{\frac{1-n}{1+n}}$ and $K^{\frac{3-n}{1+n}}$ respectively. The exact reproduction of the values of diffusivity that would match the experimental results [1] is not, however, an easy task although the experimentally observed exponent of K is satisfactorily explained. The main difficulty lies in the lack of adequate knowledge of the correlation of the velocity and displacement fluctuations, the origin of which remains somewhat elusive in systems governed by non-linear friction with the possibility of trapped states. With the aid of random trajectories from a given solution of a non-linear Langevin equation, and subsequently destroying the correlation, it is possible to show that different evolution paths of the variance leads to different diffusivities. The values of the drift velocities, however, remain rather robust. The best we can do at present is to make qualitative assessments of the nature of friction that contributes to the shape of a displacement pdf and then use this insight to predict drift velocities. By focusing on the small time behavior of displacement fluctuations we gain insights into the nature of frictional dynamics in the small velocity region, whereas the larger time behavior of displacement fluctuation provides information of such a dynamics contributed by the large velocities underlying an atypical Brownian motion.

5.3 Experimental section

Vibration used sliding motion of objects on a surface has a long history [45] that has been studied systematically by Bohringer *et al* [46]. This method was first used by Baumberger *et al* [47], and later by others [1,2,48], to study the sliding friction of solid/solid interfaces. Here, we use the method to study rolling friction by placing a steel ball on an inclined rubber substrate. When the substrate is only slightly inclined ($< 3^{\circ}$) from the horizontal, no motion of the ball is observed as the force needed to break the adhesive junction is greater than that can be provided by gravity. This is similar to the Coulombic friction preventing the sliding of a solid object, or the wetting hysteresis preventing the rolling of a liquid drop, on a surface. The ball, however, rolls at an inclination less than the threshold value if it is subjected to an external vibration. When the vibration pulses are random, the motion of the ball resembles that of a drifted rotational Brownian motion. We measured both the drift velocity as well as studied the displacement fluctuation of the ball submitted to a random Gaussian noise. Typical experiment is to place a small steel ball (4 mm diameter) on a fibrillated PDMS film that is inclined by only 1° and subject the latter to a random vibration (fig. 1). Although most of our experiments were conducted with a Gaussian random noise, some of the experiments were performed with an asymmetric vibration with or without the noise. The substrate was attached to an aluminum platform connected to the stem of a mechanical oscillator (Pasco Scientific, Model SF-9324). Gaussian white noise was generated with a waveform generator (Agilent, model 33120A) and fed to the oscillator via a power amplifier (Sherwood, Model No: RX-4105). The ball was placed on the plate sufficiently

farther from the oscillator so that there was no interference from the magnetic field of the transducer. Although a glass ball behaved similar to that of the steel ball, the former was more suitable for these experiments because of its roundness and weight. By controlling the amplification of the power amplifier, noises of different powers were generated while keeping the pulse width constant at 40 μs. The acceleration of the supporting aluminum plate was estimated with a calibrated accelerometer (PCB Peizotronics, Model No: 353B17) driven by a Signal Conditioner (PCB Peizotronics, Model No: 482) and connected to an oscilloscope (Tektronix, Model No. TDS 3012B). The pdfs of these accelerations are Gaussian (see section 5.6) and their power spectra are flat [1] up to a total bandwidth of ~10kHz.
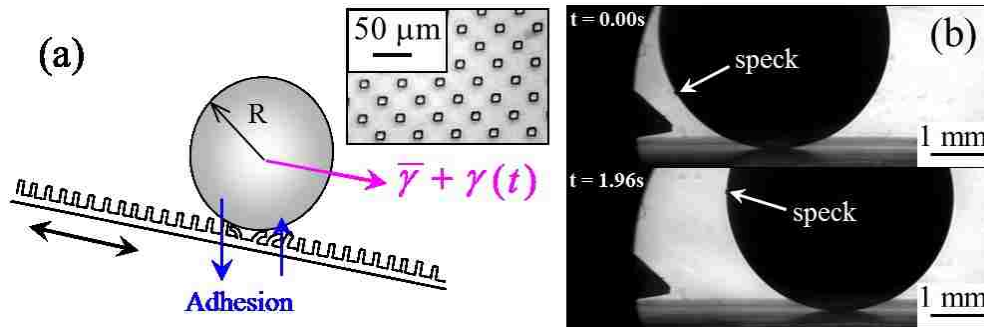
Figure 5.1: (a) A steel ball of diameter 4 mm rolls on a fibrillated rubber surface at an inclination of 1°. When the moment of the gravitational plus the stochastic force about the point of contact is greater than the torque due to adhesion, the ball rolls on the surface. (b) A speck of dust moves along the perimeter of the ball by an amount (1.23 mm), which is almost same as the lateral displacement of the ball indicating that the ball undergoes a net rolling instead of sliding at the macroscopic scale. This experiment was performed at a noise strength of 0.06 m²/s³. Inset of fig. (a) shows microscopic image (top view) of the fibrillated PDMS surface.

The entire setup was placed on a vibration isolation table (Micro-g, TMC) to eliminate the effect of ground vibration. The motion of the ball was recorded with a high speed camera (Redlake, MotionPro, Model 2000) operating at 1000 frames/sec. Motion analysis software MIDAS was used to track the dynamics of the steel ball.

Micro-fibrillated PDMS (Dow Corning Sylgard 184) surfaces were used as a substrate for the rolling experiment. The preparation of such surfaces is reported in detail elsewhere [20]. Briefly, the oligomeric component of the Sylgard 184 kit was thoroughly mixed with the crosslinker in a 10:1 ratio by weight followed by degassing it in vacuum for 2hrs. The degassed mixture was then cast onto lithographically etched silicon master. These master wafers were silanized for easy removal of cured fibrillated PDMS sample. The cast PDMS was then cured at 80°C for 2hrs. The crosslinked PDMS was cooled in dry ice (-78.5^{o}C) for an hour followed by its removal from silicon master wafers manually. The PDMS surface thus prepared has square fibrils of $10\mu m$ size with a center to center distance of the adjacent fibrils of 50 μm. The height of the fibrils was $25\mu m$.

The steel ball used in our experiment was a bearing quality aircraft grade E52100 steel obtained from Mcmaster corporation (http://www.mcmaster.com/#chrome-steel-balls/=cph9ai). The diameter of the ball was 4 mm with a tolerance of $\pm 2.5 \mu m$. The balls were cleaned by sonicating it in acetone and then drying in nitrogen. The root mean square roughness of the surface of the steel ball was ~ 35 nm as obtained from atomic force microscopy (Veeco nanoscopeV, Digital Instruments, Metrology Group) over a scanning area of 400 μm^{2}. The rolling experiments were carried out at 19 different

145

strengths (or powers) of the noise ranging from 0.02 m^2/s^3 to 2.7 m^2/s^3 at a bias of 0.04 mN. The angle of inclination was controlled with a precise goniometer (CVI Melles Griot, Model No: 07 GON 006).

5.4 Results

5.4.1 Stochastic motion of the steel ball

When the substrate is vibrated with a Gaussian noise, the steel ball undergoes backward and forward stochastic rolling motions with a net drift along the inclined plane. In order to ensure that the ball indeed rolls on the surface, we examined few video clips carefully with a small speck of dust on the surface of the ball (Figure 5.1b). At a low intensity of noise (0.06 m^2/s^3), the speck moved on the surface by the same distance as the ball's lateral displacement. At the high intensity of noise (1.7 m^2/s^3), the movement of the speck on the surface of the ball was 3% to 10% lower than its lateral displacement. These measurements ensured that ball undergoes a net rolling motion on the substrate on the average, even though some sliding may occur at a stochastic time scale. The displacement of the ball is linear with time, suggesting that it is controlled by viscous like friction. Prandtl [49,50] pointed out almost 100 years ago that the frictional response of a system changes from Coulombic to kinematic in the presence of a thermal noise. So, we must clarify what we mean by the role of the viscous like friction. These points can be further elucidated by examining the details of how the drift velocity varies with the strength of the noise and how the displacement fluctuation grows with time.

146

5.4.1.1 Drift velocity and the strength of noise

The steel ball rolled on a straight path without exhibiting any significant sidewise drift. Using a low magnification camera, the drift velocities were obtained from the displacement of the ball for a given duration of time using several tracks for each noise strength. The stochastic displacement of the ball was also examined in detail with a high speed camera. At a low power (0.06 m^2/s^3), each track lasted for about 6s. This track was divided into different time segments (0.001s to 1s) using all possible starting and ending
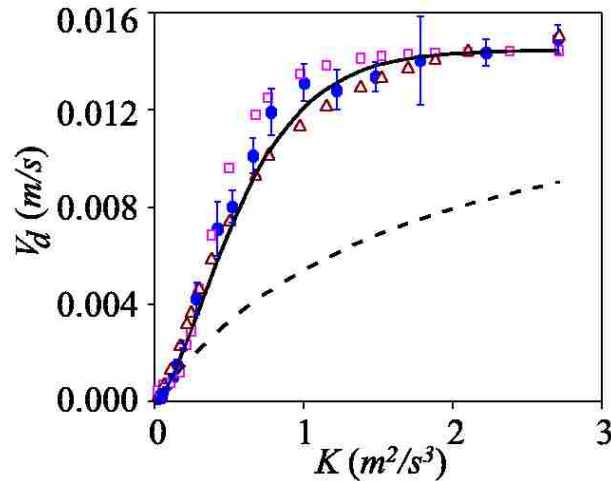
times.

Figure 5.2: Drift velocity increases with the power of the noise. The profile is slightly sigmoidal at low values of *K*. The filled blue circles are the experimental data. The dashed line represents the velocity obtained using Eq. (5.14). In order to construct this plot, particular values of Δ and τ_L had to be used. The value of Δ (0.8 m/s^2) was obtained by fitting the drift velocity with $\bar{\gamma} K / \Delta^2$ at the very low values of *K*, τ_L (0.1 s) was approximated from the saturated value of the drift velocity. Solid line represents the velocity obtained using an empirical equation $V_d = \bar{\gamma}\tau_L \tanh(K/K_1)^{1.4}$. The open squares and triangles represent the data obtained using the three state and two state models of friction (see below).

By combining data obtained from all the tracks, the displacement pdfs were constructed for different durations of time. Each pdf exhibits a certain peak and a variance. The drift velocity obtained from the time dependent shift of the mean is same as what is measured with a low resolution camera. In order to examine the behavior of the displacement pdfs at a high power (1.7 m^2/s^3) a larger number (200) of tracks was used.

The drift velocity of the steel ball increases (Figure 5.2) with the strength of the noise (K) and tends to saturate at high K. This observation is similar to our earlier observations with a noise induced sliding of a small solid object or a small water drop on a surface [1,2]. However, unlike the previous observations, the V_d -K curve here has a knee at low K thus exhibiting a slight sigmoidal behavior. All the data can be fitted fairly with an empirical equation of the type: $V_d = \bar{\gamma}\tau_L \tanh(K/K_1)^{1.4}$ using a value of K_1 as 0.7 m^2/s^3. The unique V_d vs K relationship clearly suggests that a non-linear friction is operative underlying the rolling motion. There is no definite time scale to the problem except at very high K, where the saturation of the velocity implies a Langevin time scale of ~ 0.1s. A fit (Eq. 5.8) of the V_d-K curve by keeping with the fact that that the velocity goes as at very low values of K and it approaches $\bar{\gamma}\tau_L$ at high values of K, exhibit the sublinear evolution of drift velocity as shown in fig. 2. Although this fit does not reproduce the sigmoidal behavior seen experimentally, it is consistent with the fact that the drift velocity is controlled by a non-linear friction at low noise strength but by a linear viscous friction at high noise strength. In order to glean further insights into this complex friction dynamics, let us now examine the evolution of the displacement fluctuation of the steel ball obtained at a low and a high strength of the noise.

5.4.2 The nature of non-linear rolling friction as gleaned from the displacement fluctuations

Figure 3 summarizes the fluctuations of the displacements of the steel ball on the fibrillated PDMS substrate corresponding to a low bias (0.04 *mN*) at two different noise strengths. It should be borne in mind that these displacement pdfs bear the signatures of velocity dependent friction. The displacement pdf for K=0.06 m^2/s^3 at τ=0.001s (Figure 5.3) is much sharper than that would be expected of a Gaussian behavior. This supports the picture that a friction resembling dry friction operates near the zero velocity region. The pdf for τ=0.01s is, superficially, Gaussian thus suggesting that a viscous friction operates at higher velocity. The pdf corresponding to τ=0.05 s also appears to be Gaussian, but it is somewhat asymmetric.

More detailed information regarding the natures of these pdfs can be surmised by considering the velocity distribution as given in Eq. 5.10. As a consequence of a super (n < 1) or a sub (n > 1) Gaussian velocity distribution, the displacement fluctuation at short time limit should also follow a function of the type, $P = P_o \exp\left\{-c\left[(x-x_p)/\sigma\right]^m\right\}$, where σ is the width of the pdf and x_p is the displacement corresponding to the peak of such a distribution.
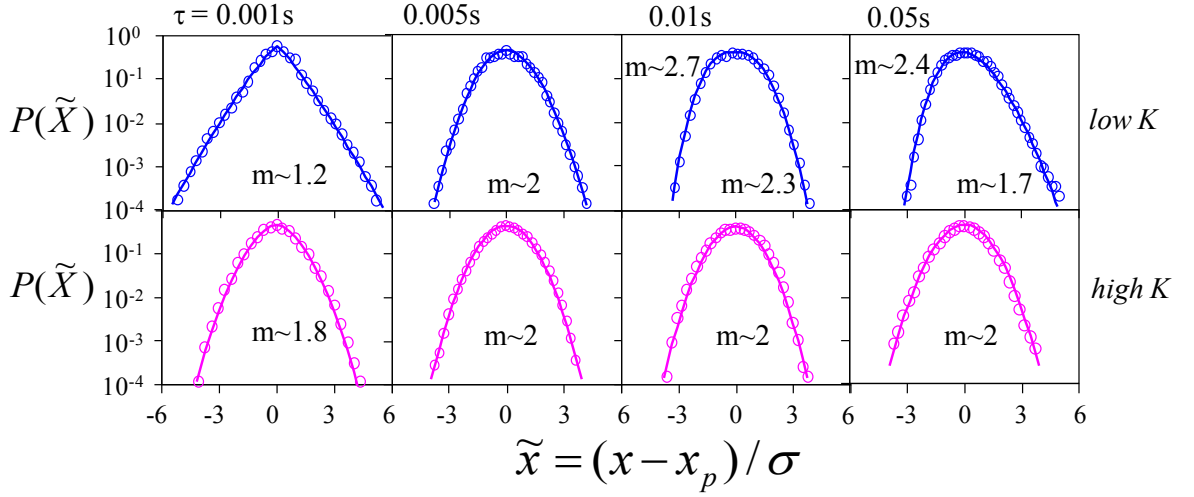
Figure 5.3: Summary of the fluctuations of the displacements of a steel ball rolling on a fibrillated PDMS at a bias of 0.04 mN corresponding to the time segments of 0.001s, 0.005s, 0.01s, and 0.05s respectively. Low K and high K correspond to 0.06 m^2/s^3 (upper panel) and 1.7 m^2/s^3 (lower panel) respectively. The pdfs are fitted as $P \sim \exp(-c|\tilde{x}|^m)$, with the values of m embedded inside the figs. For a symmetric pdf, only one value of m is given. For an asymmetric pdf, two values of m are given, one for the left and the other for the right side of the pdf.

With a power law type friction, it is, however, not easy to define the stationary state as the time to reach that state depends on the strength of the noise. Thus, the stochastic behavior of the displacement needs to be gleaned from a solution of the Langevin equation. Numerical integration of Eq. 5.13a was carried out using a generalized integration method for stochastic differential equations as outlined by Gillespie [50]. Stochastic acceleration of the vibrating plate as measured using an accelerometer were used as the input, $\gamma(t)$, in the same sequence as they were generated experimentally to ensure that the noise correlation is identical in the experiment and the simulation. While the simulated drift velocity as well as the variance of the displacement did not depend on

the integration time step ($20\mu s$–$80\mu s$), all the simulations were carried out with an integration step of $20\mu s$. Eq. 5.9 with a bias of 0.04mN was integrated numerically with the value of n as 0.2, 0.5 and 1.0 respectively for a value of K=0.06m^2/s^3. The value of A was so chosen that the average velocity obtained from simulations consisting of 100 tracks, each being 6s long, matches the experimental value (0.67 mm/s). The pdfs of displacements constructed from such stochastic trajectories are shown in fig. 4 for a time scale of 0.01s. These data were also analyzed by plotting $\ln(-\ln(P/P_o))$ vs $\ln|(x-x_p)/\sigma|$.

The slopes of these plots are about 1.2, 1.5 and 2.0, for n=0.2, 0.5 and 1 respectively suggesting that the exponent (m) of the displacement pdfs is greater than the velocity exponent (n) by unity.
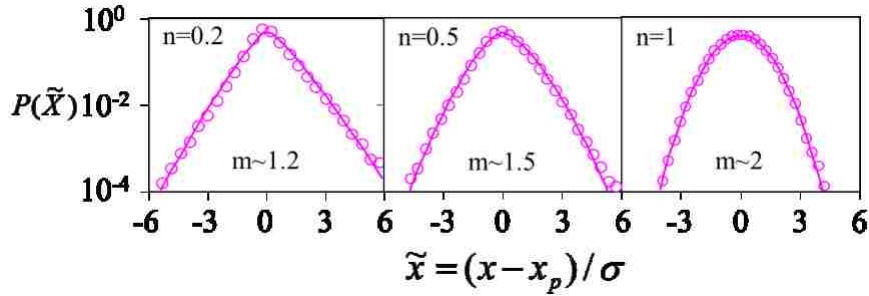
Figure 5.4: Simulated pdfs of displacement for a time segment of 0.01s as obtained from the numerical integration of the Langevin equation using a non-linear friction law: $f(V) \sim |V|^n$. The pdfs are fitted as $P \sim \exp(-c|\tilde{x}|^m)$, with the values of m embedded inside the figs.

In addition to the small time behavior of a displacement pdf, which provides insights into the nature of friction at the low velocity range, we can also examine its longer time

behavior in order to gain insights into its large velocity dynamics. This is so, as a large velocity fluctuation of low probability inserts a large displacement to the trajectory that would be evident at a longer observation timescale. However, a very large timescale should be avoided as all the displacements would ultimately be attracted to a Gaussian distribution. When the data of fig. 3 are analyzed in the same way as that of Figure 5.4, it is found that for small time scale $\tau = 0.001$s, the exponent of the displacement pdf is 1.2. The pdf becomes Gaussian at a time scale of 0.005s, but sub-Gaussian at a larger time scale. Although this pdf is somewhat asymmetric, its average exponent (~2.5) is larger than 2 suggesting that the dynamics is governed by a super-linear friction with a velocity exponent of about 1.5. The average exponent, however, tends to the value of 2 expected of the linear kinematic friction at a large value of τ. In contrast to the behaviors observed with a low strength noise, the displacement pdfs are nearly Gaussian at all timescales for K=1.7 m^2/s^3, thus suggesting that the non-linearity of friction virtually disappears at high noise strengths.

5.4.3 Evidence gathered from the rolling motion with an asymmetric vibration

Another evidence of the complex non-linear nature of rolling friction can be gleaned from an experiment, in which the steel ball is submitted to an asymmetric vibration of the type:

$$\gamma(t) = A_o[|\sin(2\pi\omega t)| - B] \qquad\qquad 5.11$$

This acceleration has a cusp shape on one side, but smoothly varying on the other. The mean value of $\gamma(t)$ is zero. When excited with this waveform, the steel ball moves on the horizontal surface of the fibrillated PDMS. For any type of motion to occur under a periodic forcing, some kind of non-linearity [51–56] is required in order to break the symmetry of the applied force. Here, the observation of the motion of the steel ball by an asymmetric vibration suggests that the friction is non-linear. Next we find out what happens when the asymmetric vibration is used in conjunction with a stochastic noise. Here, the noise defines the effective temperature of the system, whereas the asymmetric vibration interrogates it by subjecting it to a rate. What is observed with a low strength noise is that the rolling speed initially increases slightly from that obtained with K=0. Beyond a value of $K \sim 0.14 \mathrm{m}^2/\mathrm{s}^3$, the drift velocity decreases (Figure 5.5) with K and reaches a very small value of drift velocity ~ 0.1mm/s at high value of $K \sim 1.5 \mathrm{m}^2/\mathrm{s}^3$. This experiment points out as well that the effect of non-linear friction decreases with K, and the system tends towards a nominally fluidized state.
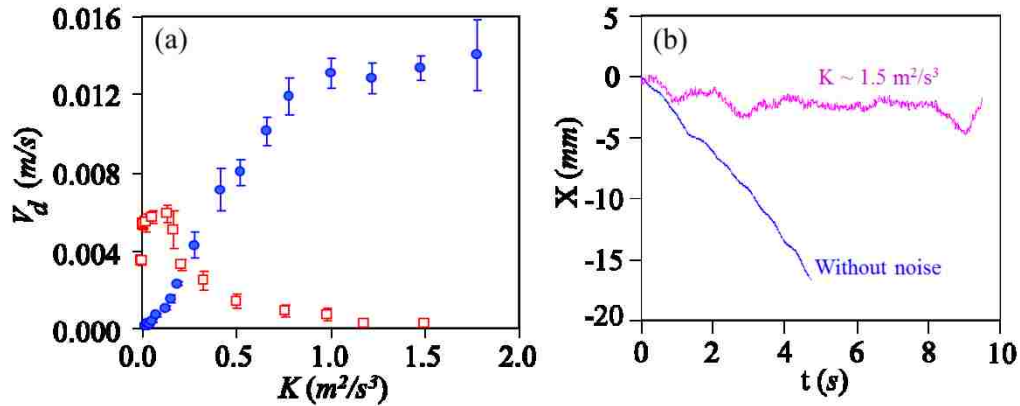
Figure 5.5: (a) The drift velocity as a function of the strength of the noise for an asymmetric periodic bias (open red square) and a fixed bias (filled blue circle). The amplitude of the asymmetric vibration (Eq. 11) is 94 m/s^2 and its frequency is 100 *Hz*. (b) The trajectories of the ball with and without the noise, but with the asymmetric vibration are shown.

These experiments have interesting similarities to some earlier observations [57,58] where a granular medium was fluidized with a strong vibration.

5.4.4 A toy model of non-linear friction

In view of the evidences gathered so far, we arrive at this scenario. A Coulombic type friction operates in the low velocity region followed by a super-linear ($n > 1$) friction at a larger velocity range. Finally, the friction becomes linear kinematic at a much larger velocity region. In going from a superlinear to a linear behavior, the friction has to overcome a hump that mimics the adhesive peeling behavior [23] from solid surfaces.

There is clear evidence of the effect of the noise strength on the overall state[4] of the system, i.e. the system remains in a fluidized state at all velocities when the noise is strong. These are the main findings of this work and any further progress in this research should rest on direct experimentation to obtain the friction force $f(V,K)$ that depends on effective temperature and rate of the system along with a molecular/mesoscopic level understanding of the phenomena. However, a toy model of friction can be constructed that is consistent with the essential features of the displacement pdfs as well as the noise dependent evolution of the drift velocity. In order to illustrate this point, we numerically integrate the Langevin equation (Eq. 5.13a) of the steel ball with a friction law (Eq. 5.12a) as follows:

$$f(|V|, K) = f_1(|V|)exp\left(-\frac{K}{K_1}\right) + \frac{|V|}{\tau_L} \tag{5.12a}$$

$$f_1(|V|) = \Delta exp\left(-\frac{|V|}{V_o}\right) + Aexp\left[-\left(\frac{|V| - V_t}{\sigma_V}\right)^{1.5}\right] \tag{5.12b}$$

$$\frac{7}{5}\frac{dV}{dt} + \tanh(\alpha V)\,f(|V|, K) = \bar{\gamma} + \gamma(t) \tag{5.13a}$$

$$\frac{dx}{dt} = V \tag{5.13b}$$

---

[4] Here, "state" means whether the system is in a solid-like or a liquid-like state. At any given level of noise, friction depends on various variables, leading to the well-known "state and rate" law of friction.

In Eq. 5.12a, $f_1(|V|)$ and $|V|/\tau_L$ are the non-linear and linear components of the friction respectively. The fact that the pdf for $\tau=0.001$s at the lower power is sharp, but is nearly Gaussian at the higher power suggests that the non-linear part of friction progressively dies out with increasing K, which is captured by the term $\exp(-K/K_1)$. The value of K_1 is taken to be 0.7 m^2/s^3, which is same as that used to fit the drift velocity data using the empirical equation: $V_d = \bar{\gamma}\tau_L \tanh(K/K_1)^{1.4}$. The non-linear friction itself has an exponential term coupled to the dry friction Δ indicating that its effect decreases with velocity, as we have seen in the pdf at the low noise strength. We should point out that an exponential form of the velocity weakening Coulombic friction is within the scope of the current treatment of solid friction [59]. The value of Δ (0.8 *m/s^2*) is close to that obtained from fitting the drift velocity to $0.03\bar{\gamma}K/\Delta^2$ in the very low K limit. The second term of the right hand side of Eq. (5.12b) is a super Gaussian with an exponent of 1.5 (Figure 5.6) that reflects the broadening of the displacement pdf at the intermediate time scale (Figure 5.3). The distribution is centered around $V_t \sim 0.012$ m/s, which is similar to our previous observations [27] of sliding friction of PDMS that exhibits a maximum at a similar velocity region.
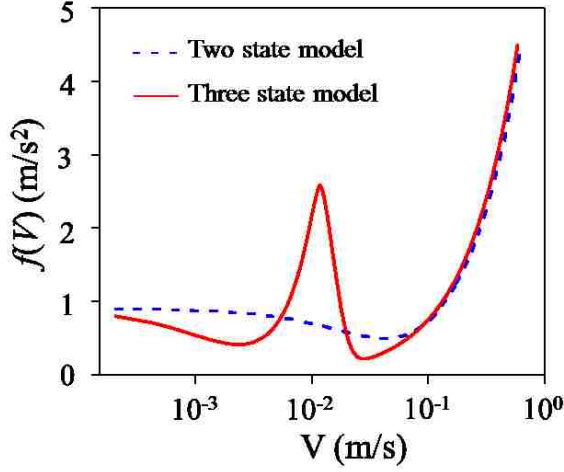
Figure 5.6: A toy model of rolling friction versus velocity.

The third term of Eq. 5.12a represents a simple viscous friction with a Langevin relaxation time τ_L, which is obtained from the drift velocity ($\bar{\gamma}\tau_L$) in the limit of high K. The parameters V_o, A and σ_V were obtained by a numerical fitting procedure, i.e. matching the drift velocities at few values of K. Eq. 5.13a is similar to Eq.5.1 with the difference that the acceleration term dV/dt is multiplied by 7/5 which appears as a pre-factor to the acceleration when the equation of motion is derived from the balance of rotational torque and the derivative of angular momentum. $f(|V|)$ is the generalized friction force per unit mass, which is multiplied by $tanh(\alpha V)$. This hyperbolic function with a high value of α (~ 10000 s/m) is a good replacement for the signum function. Here, $\bar{\gamma}$ is 0.04 mN corresponding to the angle of inclination of 1°. Numerical solution of Eq. 5.13a was carried out using a generalized integration method of Gillespie [50], as outlined before.

Before describing the friction model of Eq. 5.12a, we first study a model in which a dry friction decreases exponentially with the velocity, i.e. $\Delta = \Delta_o \exp(-V/V_o)$, in conjunction with a viscous friction. Although such a model can reproduce the experimental drift velocity at different values of K fairly well (Figure 5.2), the spatial displacement statistics (Figure 5.7) simulated with this model, however, are visibly sharp, with the sharpness persisting for a longer τ than that is observed experimentally.
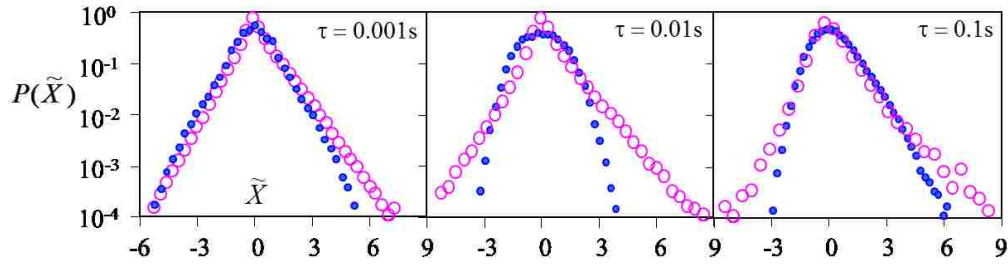
Figure 5.7: The pdfs of the displacement fluctuation at different values of τ as obtained from experiments (filled blue circle) and from simulations (open pink circle) using the two state model of friction, in which the friction is described as $f(V) = \Delta_o \exp(-V/V_o) + V/\tau_L$. The values of Δ_o, V_o and τ_L are set as 0.9m/s^2, 0.028m/s and 0.13s respectively.

The simulated pdfs of displacement fluctuation obtained using the three state model of friction (Eq. 5.12a) are shown in Figure 5.8. The essential features of the pdfs are, in general, consistent with the experimental observations. However, there are discrepancies. For example, the simulated pdf at $0.001s$ for the low power noise is not as fat tailed as that of the experiment. The exponent of the super Gaussian pdf is about 1 near the peak region, but it progressively increases to 1.7 near the tail region in comparison to overall exponent of ~ 1.2 obtained experimentally.
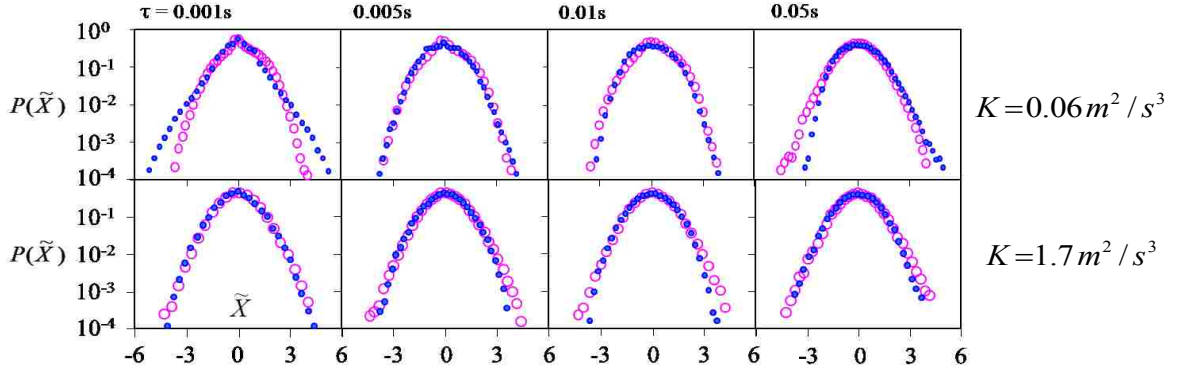
Figure 5.8: The pdfs of the displacement fluctuation at different values of τ as obtained from experiments (filled blue circle) and from simulations (open pink circle) using the three state friction model (Eq. (5.12)).

Nevertheless, the sharpness of the pdf disappears faster with τ, and the transition to a smoother pdf occurs at a much shorter time scale than that predicted by the two state model of friction (Figure 5.7). The simulated pdfs at the higher power of the noise are in better agreement with those obtained experimentally. Using the same friction model (Eq. 5.12), we also estimated the drift velocities by integrating Eq. (5.13) at various values of K, the values of which are in satisfactory agreement with the experimental observations (Figure 5.2).

5.5 Concluding remarks

This exploratory research revealed several interesting phenomenology of non-linear rolling friction under a stochastic setting. We summarize below the main points of the work and discuss what remains as open questions. The first point is about the Brownian

159

like drift of the steel ball, which is linear in time in spite of the fact that the underlying frictional dynamics is non-linear. In the Einsteinian Brownian motion with a linear kinematic friction, it is an established fact that the object drifts linearly with time that being independent of the strength of the noise. However, in the current case of a non-Einsteinian Brownian motion, the drift velocity depends strongly on the strength of the noise. The rolling motion is controlled by a Coulomb like friction at low *K,* but by a viscous like friction at high *K* suggesting, furthermore, a possible fluidization of the interface with noise. The pattern of the displacement pdfs suggests that a higher order non-linearity operates at an intermediate velocity, while a linear friction operates at even a higher velocity with the non-linearity weakening with *K.*

An evidence of a complex friction law comes from the observation of the drifted motion of the ball when it is subjected to an asymmetric vibration. What is pertinent to the point regarding the state dependent friction is that the drift velocity due to asymmetric vibration decreases significantly with the strength of the noise, which is contrary to what happens with a fixed bias. Taken together, the above evidences suggest that friction depends not only on the rate (*V*), but also on the state (*K*) as well.

In terms of developing a microscopic model of friction, we need to consider several factors. The first one being the rates at which interfacial bonds are formed and broken. It is also important to consider the roles of certain characteristic time scales of the fibrils, one of which comes from the ratio of the fibrillar spacing [26,60] to the rolling speed and the other relates to the resonant frequency (~100 kHz) of the fibrils. The

advantage of the current model system is that these parameters can be rigorously studied by careful design of the fibrillar geometry with which to develop a state and rate [61,62] dependent model of friction at any given value of *K*. Although a *K* and *V* dependent toy model of friction reproduces the essential features of the drift velocity and the evolution of the displacement pdf, some of the disagreements of the displacement statistics of the simulation and experiment clearly show that our understanding of the rolling friction dynamics is incomplete. A direct measurement of the rolling friction, clearly decoupling it from microscopic sliding, spanning several decades of velocity and acceleration is very much needed in order to make further progress in this research. Modification of a recently proposed [25] apparatus may be adequate for such a study. The value of the current work, however, is that it could guide the designs of such experiments and set the stage for studying friction using the tools of statistical mechanics. If methods are developed to measure the statistics of the velocity fluctuations, then these data, in conjunction with the displacement statistics, could be used for analyzing frictional dynamics more directly than that can be achieved with displacement statistics.

In the Langevin model, we tacitly assumed that the friction term has no memory. However, with the simultaneous presence of the elastic (due to fibrils) and viscous response of the system, friction may be viscoelastic. The elastic response of the fibrils, along with the non-linear friction dynamics may also exhibit spatio-temporal oscillations [23,63,64] in the rolling motion.

The experiments presented in this paper complement the previous reports where a non-classical Brownian motion was anticipated [18,35,36] and observed [1–3] with a small object undergoing a Coulombic slip on a surface under a stochastic forcing. It is clear that an adhesion hysteresis arising from a pinning-depinning dynamics at the interface can also give rise to a threshold force that is akin to the Coulombic dry friction. Wang *et al* [19] recently observed a non-Gaussian displacement fluctuation with a colloidal particle undergoing a Brownian motion in weak adhesive contact with a soft microtubule. As the particle moves, it is possible that new bonds are formed at the advancing edge, whereas older bonds are broken at the trailing edge resulting in a hysteresis of adhesion. Based on what we report here, it is not implausible that such type of adhesion hysteresis could give rise to a non-Gaussian displacement statistics of the colloidal particle as was observed by Wang *et al* [19]. A possibility of this type has also been pointed out recently by Menzel and Goldenfeld [39]. What is also interesting in the displacement statistics observed by Wang *et al* [19] is that a transition from a non-Gaussian to a Gaussian pdf occurs rather abruptly, as is also observed in our current experiments. Similar issues may also be important in understanding the hindered diffusion of a soft colloid near a surface [65].

5.6 Appendix

5.6.1 Rolling of the steel ball on the fibrillated rubber without noise

The ball starts rolling on the fibrillated rubber at an angle of about 3°. A video microscopic image of the motion of the ball shows that it accelerates as it rolls down. The fact that the data can be fitted with a simple equation of accelerating motion of the type $S = V_i t + 0.5\ at^2$ (V_i being the initial velocity and a is the falling acceleration) suggests that there is virtually no kinematic friction acting on the ball. Only resistance here is a Coulombic type dry friction. If this is the case, the acceleration should simply be $mgsin\theta - \Delta$. Experiments carried out at different angle of inclination show that beyond a threshold angle (θ_c), the acceleration increases (Figure 5.9) with the angle of inclination as, $a \sim (sin\theta - sin\theta_c)^{2/3}$. This sub linear
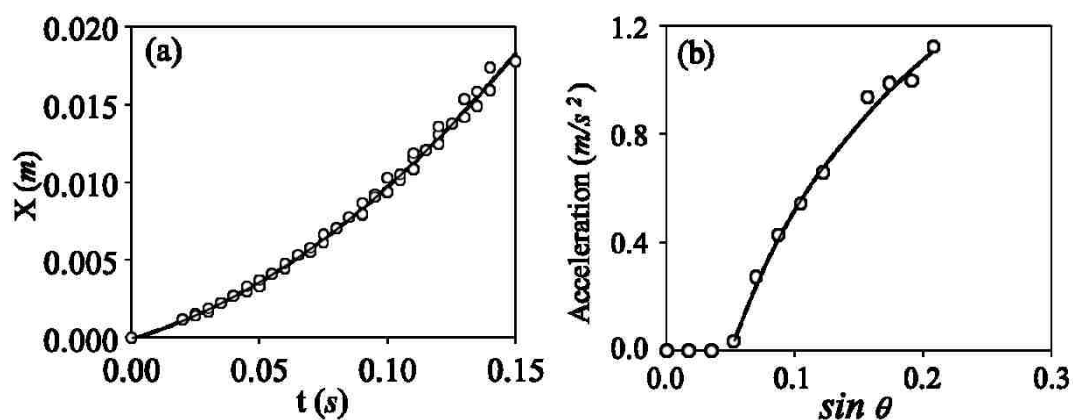
Figure 5.9: (a) Figure shows a parabolic growth of the distance travelled by a ball on an inclined (10°) surface with time. The falling accelerations are summarized in fig. (b).

163

growth of acceleration with the angle of inclination suggests that the dry friction resistance (Δ) increases with the applied force as well. In the past, it has been proposed [1, 2] that the dynamics of the motion of a line that is pinned randomly by defects exhibits a supercritical behavior in the sense that no motion is observed when the applied force (F) is less than a threshold value (F_c), above which the velocity (V) grows as $V \sim (F - F_c)^\theta$. θ is the velocity exponent, the value of which lies in the range of 0.6 to 0.8. We are not aware of any analysis suggesting the strengthening of dry friction with force.

5.6.2 Characteristics of the noise

The approximate Eq. 5.8 was derived on the condition that the noise is strictly white and Gaussian.
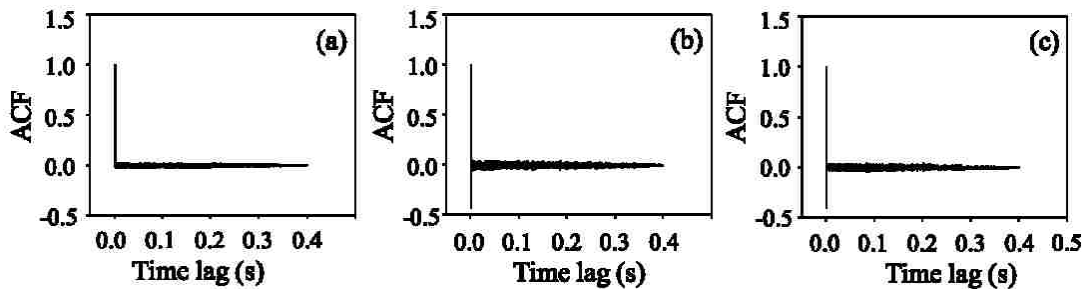
Figure 5.10: The autocorrelation of the noise file (a) as generated from the computer and that (b) obtained from the output of the oscillator as measured with an accelerometer. The Gaussian noise as generated from the waveform editor, $\gamma(t)$, was used to solve the Langevin equation of the oscillator: $\ddot{x} = -\dot{x}/\tau - \omega_o^2 x + \gamma(t)$. Here, x is the displacement of the oscillator, τ (250 μs) is its relaxation time and ω_o (~1.5x10^4 s^{-1}) is its fundamental frequency of vibration. The autocorrelation of the simulated noise of the acceleration is shown in fig.

This is not exactly the case for the type of noise that we generate experimentally. In our case, the Gaussian white noise is generated with a waveform generator that feeds pulses of random heights, but of a finite width (40 μs) to an oscillator. The output of these pulses is used to vibrate the stage on which the rolling experiment is performed. Since a mechanical oscillator has a tendency to spring back after each excitation, the autocorrelation of the output noise exhibits a negative peak (Figure 5.10b), which is also consistent with the Autocorrelation Function (ACF) of the noise generated numerically using the properties of the oscillator (Figure 5.10c). The noise pulses, however, are Gaussian with a probability density of $P = P_o \exp\left[-0.5(\gamma/\sigma_\gamma)^2\right]$, as evidenced from the slope (~2) of the plot of ln(-ln(P/P_0)) versus $\ln|\gamma/\sigma_\gamma|$ (Figure 5.11). Because the noise is somewhat correlated, Eq. (8), which is derived on the basis of the classical Fokker Planck equation, needs to be corrected. This correction is carried out as follows. By numerically integrating the Langevin equation (Eq. 5.1) with the omission of the kinematic friction term and using the sequence of the noise pulses obtained directly from the accelerometer, several trajectories are generated. The strength of the noise as used in these experiments is nominally defined as the product of the mean square acceleration and the pulse width (τ_c), i.e. $K = \left\langle \gamma^2(t) \right\rangle \tau_c$.
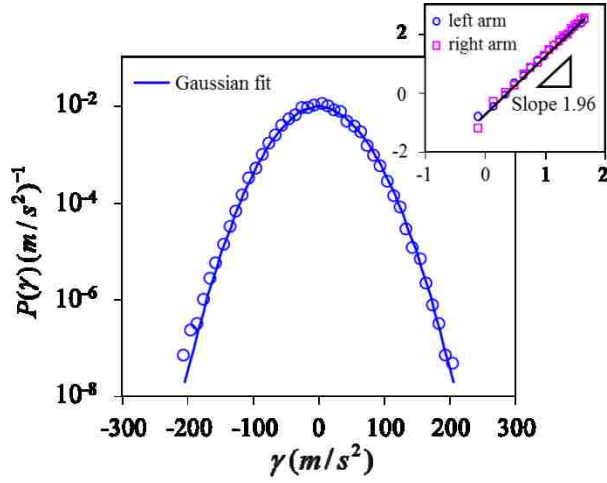
Figure 5.11: Probability distribution function of the noise obtained from accelerometer at a given value of K (0.06 m^2/s^3). The pdf is also fitted with a Gaussian function as indicated by the solid line. The inset shows the plot of $\ln(-\ln(P/P_o))$ versus $\ln|\gamma/\sigma_\gamma|$, the slope of which is ~2.

However, the value of this K is re-normalized in order to use it in Eq. 5.8. For a given set of Δ and K, 100 trajectories, each lasting for 6 seconds, were used to estimate the drift velocity. Although this drift velocity varies (Figure 5.12) linearly as $\bar{\gamma}K/\Delta^2$, its slope is found to be 0.03. Thus, Eq.5.8 is modified as:

$$V_d = \frac{\bar{\gamma}\tau_L}{1 + 33\Delta^2\tau_L/K} \qquad 5.14$$
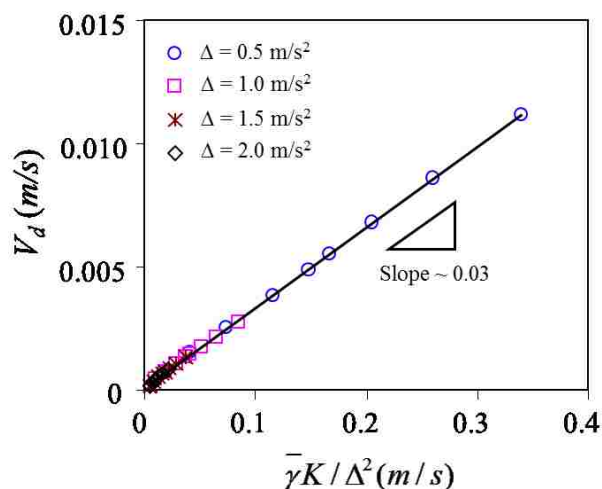
Figure 5.12: The drift velocity is calculated using Eq. 5.1 without the kinematic term using the noise output file of an accelerometer attached to an oscillator. Various values of Δ are used. A master plot is obtained by plotting all the drift velocity data against $\bar{\gamma} K / \Delta^2$.

References

[1]   P. S. Goohpattader and M. K. Chaudhury, The Journal of Chemical Physics **133**, 024702 (2010).

[2]   P. S. Goohpattader, S. Mettu, and M. K. Chaudhury, Langmuir : the ACS Journal of Surfaces and Colloids **25**, 9969–79 (2009).

[3]   S. Mettu and M. K. Chaudhury, Langmuir : the ACS Journal of Surfaces and Colloids **26**, 8131–40 (2010).

[4]   T. P. C. Van Noije and M. H. Ernst, Granular Matter **1**, 57–64 (1998).

[5]   W. Losert, D. G. W. Cooper, J. Delour, a. Kudrolli, and J. P. Gollub, Chaos (Woodbury, N.Y.) **9**, 682–690 (1999).

[6]   X. Nie, E. Ben-Naim, and S. Y. Chen, Europhysics Letters **51**, 679 (2000).

[7]   A. Prevost, D. Egolf, and J. Urbach, Physical Review Letters **89**, 1–4 (2002).

[8]   K. Feitosa and N. Menon, Phys. Rev. Lett. **92**, 164301 (2004).

[9]   S. Jung, P. J. Morrison, and H. L. Swinney, J. Fluid Mech. **554**, 433–456 (2006).

[10]   A. La Porta, G. A. Voth, A. M. Crawford, J. Alexander, and E. Bodenschatz, Nature **970**, 1017–1019 (2001).

[11]   M. M. Bandi and C. Connaughton, October 1–9 (2008).

[12]   S. Ratynskaia, G. Regnoli, K. Rypdal, B. Klumov, and G. Morfill, Physical Review E **80**, 1–11 (2009).

[13]   S. Ciliberto and C. Laroche, Le Journal De Physique IV **8**, Pr6–215–Pr6–219 (1998).

[14]   N. Kumar, S. Ramaswamy, and a. Sood, Physical Review Letters **106**, 18–21 (2011).

[15]   C. Beck, E. G. D. Cohen, and H. L. Swinney, Phys. Rev. E **72**, 056133 (2005).

[16]   E. Van der Straeten and C. Beck, Physical Review E **80**, 1–13 (2009).

[17]   J. van Zon and F. MacKintosh, Physical Review Letters **93**, 3–6 (2004).

[18]   T. K. Caughey and J. K. Dienes, Journal of Applied Physics **32**, 2476–2479 (1961).

[19]   B. Wang, S. M. Anthony, S. C. Bae, and S. Granick, Proceedings of the National Academy of Sciences of the United States of America **106**, 15160–4 (2009).

[20]   N. J. Glassmaker, A. Jagota, C. Hui, W. L. Noderer, and M. K. Chaudhury, Proceedings of the National Academy of Sciences **104**, 10786 (2007).

[21]   K. Dahmen, Y. Ben-Zion, and J. Uhl, Physical Review Letters **102**, 1–4 (2009).

[22]   D. S. Fisher, Physics Reports **301**, 113–150 (1998).

[23]   D. Maugis and M. Barquins, *Maugis Barquins Adhesion 12 Edited by K W Allen 1988.pdf* (London, Elsevier, 1988).

[24]   M. Barquins and A. D. Roberts, J Phys. D: Appl. Phys. **19**, 547 (1986).

[25] B. N. J. Persson, The European Physical Journal. E, Soft Matter **33**, 327–333 (2010).

[26] K. a. Grosch, Proceedings of the Royal Society A: Mathematical, Physical and Engineering Sciences **274**, 21–39 (1963).

[27] K. Vorvolakos and M. K. Chaudhury, Langmuir **19**, 6778 (2003).

[28] a Leonov, Wear **141**, 137–145 (1990).

[29] a. Filippov, J. Klafter, and M. Urbakh, Physical Review Letters **92**, 2–5 (2004).

[30] B. N. J. Persson, *Sliding Friction: Physical Principles and Applications*, 2nd ed. (Springer, Berlin; New York, 2000).

[31] T. K. Caughy, Journal of Acoustical Society of America **35**, 1683 (1963).

[32] J. M. Johnsen and A. Naess, *Structural Dynamics-Eurodyn'93*, Balkema, R (1993), p. 735.

[33] G. Ahmadi, Int. J. Engng. Sci. **21**, 93 (1983).

[34] S. H. Crandall, S. S. Lee, and J. H. Williams, Journal of Applied Mechanics 1094–1098 (1974).

[35] P.-G. De Gennes, Journal of Statistical Physics **119**, 953–962 (2005).

[36] A. Kawarada and H. Hayakawa, Journal of the Physical Society of Japan **73**, 2037 (2004).

[37] a Baule, H. Touchette, and E. G. D. Cohen, Nonlinearity **24**, 351–372 (2011).

[38] H. Touchette, E. Van der Straeten, and W. Just, Journal of Physics A: Mathematical and Theoretical **43**, 445002 (2010).

[39] A. Menzel and N. Goldenfeld, Physical Review E **84**, 1–9 (2011).

[40] M. A. Moser and W. D. Iwan, 223–235 (1991).

[41] M. K. Chaudhury and S. Mettu, Langmuir : the ACS Journal of Surfaces and Colloids **24**, 6128–32 (2008).

[42] J. a Greenwood, K. L. Johnson, S.-H. Choi, and M. K. Chaudhury, Journal of Physics D: Applied Physics **42**, 035301 (2009).

[43] T. K. Caughey, The Journal of the Acoustical Society of America **35**, 1706 (1963).

[44] B. Lindner, New Journal of Physics **9**, 136–136 (2007).

[45] G. Boothroyd, *Assembly Automation and Product Design* (MarcelDekker,Inc., New York, 1991).

[46] K.-F. Bohringer, V. Bhatt, and K. Y. Goldberg, in *IEEE iIternational Conference on Robotics and Automation* (Nagoya, Japan, 1995), pp. 1989–1996.

[47] T. Baumberger, L. Bureau, M. Busson, E. Falcon, and B. Perrin, Review of Scientific Instruments **69**, 2416–2420 (1998).

[48] I. Sanchez, F. Raynaud, J. Lanuza, B. Andreotti, E. Clement, and I. S. Aranson, Physical Review E **76**, 060301 (2007).

[49] M. H. Muser, Proceedings of the National Academy of Sciences of the United States of America **107**, 1257–8 (2010).

[50] L. Z. Prandtl, Angew Math. Mech. **8**, 85 (1928).

[51] S. Daniel, M. K. Chaudhury, and P.-G. de Gennes, Langmuir : the ACS Journal of Surfaces and Colloids **21**, 4240–8 (2005).

[52] D. Fleishman, Y. Asscher, and M. Urbakh, Journal of Physics: Condensed Matter **19**, 096004 (2007).

[53] P. Brunet, J. Eggers, and R. Deegan, Physical Review Letters **99**, 3–6 (2007).

[54] M. Eglin, M. a. Eriksson, and R. W. Carpick, Applied Physics Letters **88**, 091913 (2006).

[55]   a Buguin, F. Brochard, and P.-G. de Gennes, The European Physical Journal. E, Soft Matter **19**, 31–6 (2006).

[56] S. Mettu and M. K. Chaudhury, Langmuir : the ACS Journal of Surfaces and Colloids **27**, 10327–10333 (2011).

[57] O. Zik, J. Stavans, and Y. Rabin, Europhysics Letters (EPL) **17**, 315–319 (1992).

[58] G. D. Anna, P. Mayor, A. Barrat, V. Loreto, and F. Nori, Nature 909–912 (2003).

[59] S. Andersson, A. Söderberg, and S. Björklund, Tribology International **40**, 580–587 (2007).

[60] E. Wandersman, R. Candelier, and A. Prevost, arXiv:cond-mat 8–11 (2011).

[61] J. R. Rice and A. L. Ruina, Journal of Applied Mechanics **50**, 343 (1983).

[62] J. R. Rice, N. Lapusta, and K. Ranjith, Journal of the Mechanics and Physics of Solids **49**, 1865–1898 (2001).

[63] M. Morishita, M. Kobayashi, T. Yamaguchi, and M. Doi, Journal of Physics. Condensed Matter : an Institute of Physics Journal **22**, 365104 (2010).

[64] R. De, A. Maybhate, and G. Ananthakrishna, Physical Review E **70**, 1–12 (2004).

[65] P. Sharma, S. Ghosh, and S. Bhattacharya, Nature Physics **4**, 960–966 (2008).

6. CHAPTER SIX: Athermal Activation[5]

6.1 Introduction

This paper is about a form of a Brownian motion that is induced by a mechanical noise to a system where the friction arises from the irreversible adhesive contact of two surfaces. The specific experiment involves the motion of a small rigid sphere on a soft fibrillated rubber substrate with which it can undergo a noise assisted pinning-depinning transition. With such a system, we address the question of an effective temperature using the Einstein's ratio of diffusivity and mobility in a driven diffusive condition that agrees with what is obtained from a work fluctuation relation. Next we attempt to validate this effective temperature by designing a barrier crossing experiment, the dynamics of which is controlled by a non-linear friction. The essential conclusion of these studies is that a system with a non-linear friction may not have a unique effective temperature.

A random motion with an *interfacial resistance* was first discussed about fifty years ago by Caughey and Dienes [1] in the context of sliding structures responding to earthquake. Similar kinds of motion with a weak *adhesive contact* have been reported recently with a colloidal particle on a soft microtubule [2], and with a small object on a solid surface [3–5]. Frictional dynamics in many of these systems are hysteretic or non-linear [6–13], in that they are driven by instabilities [8,9] . As Muser [8] eloquently pointed out, the viscous drag friction results from the distribution of collision energy

---

from the central degree of freedom of a Brownian particle to other degrees of freedom of the solvent particles. However, even at a vanishingly small velocity of sliding of one solid past another, fast motions of certain degrees of freedom result in "stick slip" instability that lead to non-linear friction. These instabilities are observed not only with a spring/mass system, but with random noise excitations [5] as well. They are also observed with the relaxation of the contact line [4] of a liquid drop on a solid surface. It was proposed [14] long ago that a similar Coulomb friction like instability accompanies the collapse of the Bloch wall structures and the Barkhausen noise in magnetism as well.

Recent experiments carried out in our laboratory [3–5] showed that the sliding of a small block and the motion of a liquid drop on a solid support exhibit certain comparable characteristics in a stochastic setting. For example, when a small external force is applied, no motion occurs. However, in conjunction with an external noise, a kinematic friction like property emerges out of the static friction so that a ball moves through a granular medium [14], a slider slides [3,5] or a drop glides [5] with an uniform drift velocity that increases linearly with the applied force. The signature of the non-linear friction, nonetheless, is evident in that the drift velocity increases non-linearly with the strength of the noise $[K\ (m^2/s^3) = \Gamma^{2}\tau_c$, where Γ is the root mean square acceleration (m/s^2) of the object, and $\tau_c\ (s)$ is the time duration of the pulse], but saturating at large values of K [3–5]. Furthermore, the microscopic displacement distributions are super Gaussian [3–5] at short time limit but, they all evolve towards a skewed Gaussian distribution in the long time limit. While the variance of the displacement is linear with time, the diffusivity grows super linearly with the strength of

the noise. Displacement spikes [3] (stick-slip type instability) are observed as well. All these features contrast the behavior of a linear kinematic friction, where the motion is always smooth and the diffusivity grows linearly with K. In the current paper, we are interested to find out as to what extent such a non-linear stochastic dynamics is amenable to a standard definition of an effective temperature, e.g. the Einstein's ratio of diffusivity and mobility [15–17] or that extracted from a typical fluctuation relation [18]?

A temperature like intensive property has been long sought after [19–25] in systems driven by active as well as quenched fluctuations. In dynamic systems, ranging from vibrated granular media [18–23] to earthquake [24], various definitions of a non-equilibrium temperature have been proposed. Several path breaking experiments [21–23] were conducted as well, including a torsional pendulum immersed in a vibrated granular medium [21], fluctuation of a ball in a turbulent flow [22], and the diffusion of particles in a shear flow [23] to name a few. These experiments provided estimates of the effective temperature using the familiar concepts of statistical mechanics, such as the kinetic energy, the Einstein's ratio of diffusivity and mobility as well as the density of states [22]. Notably, Abate and Durian [22] published a paper, in which they reported reasonable agreements of the estimates of the "effective temperature" of a granular medium obtained using different metrics, mentioned as above.

Motivated by the encouraging results of the previous studies, we ask how does an "effective temperature" obtained from a driven diffusion experiment compare with an energy exchange process that we are familiar with. A sub-critical instability, such as a

174

barrier crossing phenomenon, is an example of the latter. This subject of activated dynamics in an athermal system has also been discussed recently in the context of the deformation and flow behaviors of glassy systems [17–25], the relaxation of a sand pile [26], the shear rate dependent stiffening of granular materials [27] and in slow granular flows [28]. While driven diffusive experiments [3–5,29] can be performed with various systems exhibiting non-linear friction, the systems with which to conduct both this as well as a barrier crossing experiment involve the motion of a small rigid sphere [29] on a soft fibrillated rubber substrate. The fibrillar surface mimics the features of well-decorated asperities with which a sphere undergoes a pinning-depinning [30,31] transition (fig. (2)). This leads to a threshold force somewhat like the Coulombic sliding or wetting hysteresis, which has to be overcome before rolling occurs. We show below how this experiment could also be adapted to study the barrier crossing rate with the aid of an undulated support. While the bulk of our research concerns the rolling motion of a rigid sphere, we also report results of some barrier crossing experiments involving a deformable sphere, i.e. a liquid drop.

6.2 Non-linear rolling friction

When a rigid sphere is brought into contact and separated from a fibrillated rubber surface [30,31], a significant difference of the adhesion energy is observed signifying that the interaction of the contactor with the substrate is hysteretic. Rolling of a sphere on a surface accompanies the propagation of two cracks [32–37], one closing at the advancing edge and the other opening at the receding edge. Because of the difference in the energies of the opening and closing the cracks, a threshold force or torque is needed to

roll a sphere on a substrate. Using an energy argument (see also section 6.8.1), one can show that a torque [32–37] of the following magnitude must be supplied about the point of contact for the incipient rolling:

$$Q \approx (W_r - W_a)r^2 \qquad\qquad 6.1$$

where, W_r and W_a are the receding and advancing works of adhesion or, more accurately, the strain energy release rates associated with the opening and closing the cracks and r is the width of contact. In the presence of a very low strength noise, the de-pinning events exhibit activated dynamics. In this region, the drift velocity exhibits a logarithmic variation with respect to the strength of the bias (see section 6.6.1 for details). However, as the noise strength increases, the slip (here, microscopic rolling) events start to occur along and opposite to the net drift, leading to a drifted diffusive motion of the object. In order to capture this diffusive process, we make use of an *ansatz* proposed independently by Caughey and Dienes [1] as well as de Gennes [38], that is the friction has a jump discontinuity at zero velocity, but is linear kinematic beyond it. The object moves following the standard equation of motion, as long as the strength of a noise pulse is greater than the threshold friction. However, the object does not move when the net force (noise plus bias) acting on it is less than the threshold, unless its previously gained momentum is large enough to carry it through (see references [1] and [38] for more details). The random motion of the sphere on the fibrillated surface is then expressed by the following equation of motion that describes by the balance of all the inertial, frictional and external torques:

$$I\frac{d\omega}{dt} + \Lambda\omega + (W_r - W_a)r^2\frac{|\omega|}{\omega} = (\bar{F} - F(t))R \qquad\qquad 6.2$$

where, I is the moment of inertia of the sphere about the point of contact, ω is the angular velocity, R is the radius of the sphere and Λ is a kinematic friction factor, whereas $\bar{F}$ and $F(t)$ are the fixed and time dependent forces respectively. This equation belongs to the same class of equations proposed earlier for the sliding of a solid object references [1,38], for the motion of a liquid droplet [39] or for the friction between granular particles [40], for which several elegant solutions [41–44] are now available. Such a model of Coulombic dry friction has also been useful [45] to study the kinetics of a granular asymmetric piston within the framework of a Boltzmann-Lorentz equation. In the context of sliding, it is the Coulombic dry friction while for the drop motion it is the wetting hysteresis, which are analogous to the adhesion hysteresis as outlined above
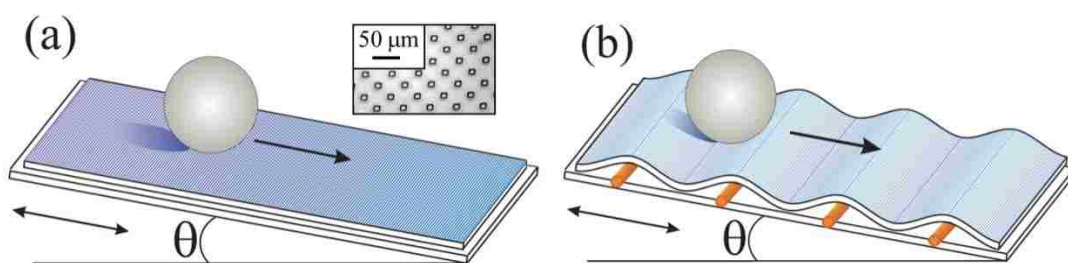
Figure 6.1: (a) Illustration of the driven diffusive experiment with a steel ball on a fibrillated rubber surface, microscopic image of which is shown in the inset. (b) Illustration of a barrier crossing experiment. In either case, the ball remains stationary if the angle of inclination (θ) is less than some critical angle (θ_c). However, with an external vibration imposed parallel to the support, the ball rolls down as in fig. (a) or crosses over the barrier as in fig. (b).

. The situation of the stochastic rolling of the sphere also belongs to a class of a rotational Brownian motion [46–49] that was studied earlier with a mirror hanging from a

pendulum [46,47], a floating micro-needle [50] and a colloidal sphere [48,49]. However,

in those instances, only linear friction was considered.
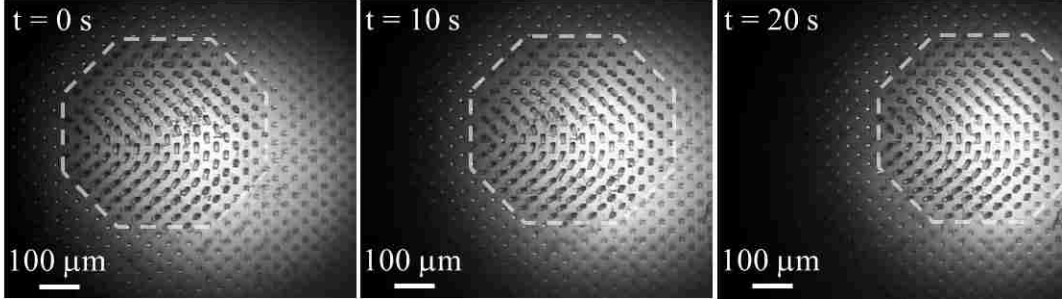
Figure 6.2: Video microscopic images of the contact area of a steel ball rolling on a fibrillated rubber surface in the absence of noise. Here the support is slowly inclined till the sphere just begins to roll. The fibrillar (dark spots) contacts are inside the dashed octagon. As the sphere rolls, the fibrils ahead of the contact make new contact with it, while those in the rear are detached. The dissipation of energy due to the relaxation of the fibrils gives rise to an adhesive hysteresis.

A translational version [29] of Eq. 6.2 can be written down as follows:

$$\frac{7}{5}\frac{dV}{dt} + \frac{V}{\tau_L} + \sigma(V)\Delta = \bar{\gamma} + \gamma(t)$$

$$\frac{dx}{dt} = V$$

6.3

here, $\Delta = (W_r - W_a)r^2/mR$, τ_L is the Langevin relaxation time, $\bar{\gamma} = \bar{F}/m$ and

$\gamma(t) = F(t)/m$.

As has been discussed in the past [1,29], a useful simplification of Eq. 6.3 is to

consider an equivalent linear version of this equation with a remainder term φ shown in

Eq. 6.5. For the purpose of this discussion, we ignore the factor 7/5 of Eq. 6.3, which is not important for the scaling argument to follow.

$$\frac{dV}{dt} + \frac{V}{\tau_L^*} = \gamma(t) \qquad\qquad 6.4$$

$$\varphi = \frac{V}{\tau_L^*} - \frac{V}{\tau_L} - \sigma(V)\Delta \qquad\qquad 6.5$$

The criterion for equivalent linearization is to minimize the expected value of φ^2 with respect to τ_L^*, which leads to the following equation:

$$\frac{1}{\tau_L^*} = \frac{1}{\tau_L} + \frac{\Delta\langle\sigma(V)V\rangle}{\langle V^2\rangle} \qquad\qquad 6.6$$

The quantities in the angular brackets of Eq. 6.6 can be estimated with the help of a probability distribution function of the velocity, i.e. from the Fokker-Plank solution of the probability density in the velocity space. Following the procedures outlined in references [1] and [29], one obtains:

$$\frac{1}{\tau_L^*} = \frac{1}{\tau_L} + \frac{\Delta^2}{K} \qquad\qquad 6.7$$

Equation 6.7 defines the equivalent relaxation time in terms of the Coulombic and a linear kinematic friction. When a small external bias is imposed, an expression for the drift velocity can be obtained from the linear response approximation, i.e. $V_{drift} = \bar{\gamma}\tau_L^*$. One thus has,

$$V_d = \frac{\bar{\gamma}\tau_L}{1 + \Delta^2\tau_L/K} \qquad 6.8$$

The concurrence of a randomized non-linear system to a linear response behavior as above has already been demonstrated experimentally by us in the past [3,5]. Using the above expression for the effective relaxation time τ_L^*, we can express the diffusivity as $D = K\tau_L^{*2}/2$, and an effective temperature (T_{eff})as the ratio of the diffusivity and mobility as

$$T_{eff} = \frac{mK\tau_L}{2(1 + \Delta^2\tau_L/K)} \qquad 6.9$$

With a non-linear friction of the type: $(\sim |V|^n)$, it can be shown [29] that the characteristic relaxation time (τ_L^*) scales as $K^{\frac{1-n}{1+n}}$, so that the drift velocity, diffusivity and the effective temperature scale with the noise strength as $K^{\frac{1-n}{1+n}}$, $K^{\frac{3-n}{1+n}}$ and $K^{\frac{2}{1+n}}$ respectively. In all these cases, the effective temperature approaches a zero value more rapidly with K than is the usual case with a linear kinematic friction.

6.3 Brief summary of previous studies

Recently, we reported [29] the behavior of a rigid sphere on a solid support intervened by an external force and a random Gaussian noise. One main observation was that the drift

velocity (V_d) increases linearly at small K , but it saturates to a constant value at a high noise strength. These results are shown in fig. (3) by dividing the measured V_d with the bias ($\bar{\gamma}$) that yields a response time. The evolution of $V_d/\bar{\gamma}$ as a function of the noise strength (K) is consistent with two characteristic time scales to the problem (Eq. 6.7and 6.8), one being the noise independent Langevin relaxation time τ_L and the other is the noise dependent response time K/Δ^2 as discussed above. In the short observation time scale, and with a weak noise, K/Δ^2 dominates the drift velocity, which increases linearly with K. However, at large values of K, the dynamics is dominated by the Langevin relaxation time. This transition from a non-linear (at low K) to a linear control (at high K) of motion was further interrogated [29] by subjecting the ball to a stochastic noise and an asymmetric vibration simultaneously. At low K, the non-linear friction rectifies the asymmetric vibration [51], thereby giving rise to a ratchet like motion. However, with the preponderance of the linear-friction at high K, the drift velocity nearly vanishes. A more complex scenario of the rolling friction in the intermediate velocity range was also considered in the previous paper [29]. In particular, a super-linear velocity dependent friction plays a role in the complex evolution of the pdf of the displacement fluctuation resulting in a sigmoidal variation of the drift velocity with K. Specifically, a noise strength dependent state and a velocity dependent rate law was needed to explain the overall behavior of friction.
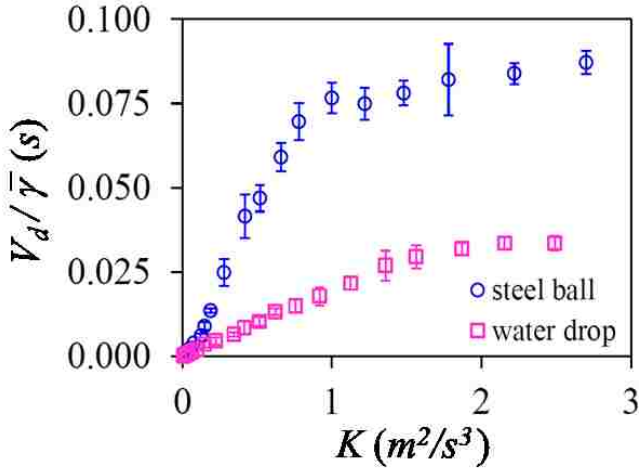
Figure 6.3: The measured drift velocity (V_d) is divided by the bias $(\bar{\gamma})$ that yields the response time $(V_d / \bar{\gamma})$. The response time is plotted as a function of the strength (K) of a Gaussian vibration for a steel ball (4 mm diameter) and a water drop (8 □l) rolling on the surface of a fibrillated silicone rubber. The data for the steel ball are from reference [29], whereas those for the water drop are from the current study.

Extending the theoretical discussions of a Brownian motion to account for the sliding or rolling dynamics has certain limitations. For example, most of the theoretical frameworks of driven diffusion and barrier crossing are developed for an ideal white noise in a Markovian setting. In our experiments, all noises have finite band widths. Furthermore, the idea of extracting a temperature from the Einstein's ratio of diffusivity and mobility is sensible for systems controlled by linear friction, which are at or very close to the equilibrium. *A priori*, there is not guarantee that such a notion would apply to an athermal dynamics controlled by a non-linear friction. The issue needs to be settled experimentally. Our strategy here is to extract a temperature like intensive property from a driven diffusive motion of a rigid ball rolling on a surface. The novel aspect of this work is the introduction of a barrier crossing experiment from which an effective temperature can be extracted using the analogy of the theory of thermal activation. The

rest of the paper is organized as follows. The first part of the paper describes the method of extracting the effective temperature from the standard method of diffusivity and mobility, or, equivalently a work fluctuation relation. Next, we venture into estimating the noise strength dependent effective temperature from the experiments of mechanical activation in the light of the Van't Hoff-Arrhenius-Eyring equation. Some discrepancy is observed in the values of the T_{eff} obtained from the two methods. After discussing the possible origin of the discrepancy, we make additional conjectures.

6.4 Experimental method

6.4.1 Drift and diffusivity

Rolling experiments were carried out with a small steel ball (4 mm diameter, 0.26 gm mass, rms roughness of 35nm) on a fibrillated PDMS support (0.6 mm thick underlayer, modulus of 2.2 MPa [32]) that was inclined by about 1° from the horizontal and subjecting it to a random vibration (fig. 1(a)). The PDMS surface had square fibrils of 10μm size that were vertical to the underlayer with a center to center distance of the adjacent fibrils of 50 μm on a rhombic (or diagonal square) lattice. The height of the fibrils was 25μm. When a sphere rolls on a smooth rubber, the resistance to rolling [32] is amplified by the viscoelastic dissipation in the rubber. This force can be so large that very strong vibration is needed to dislodge the ball from the surface. The viscoelastic dissipation is considerably minimized on the fibrillated rubber surface owing to the diminished area of contact. The energy dissipation here is primarily due to the elastic distortion and the subsequent relaxation of the fibrils. While the adhesion/detachment

processes are still hysteretic [30,31], its magnitude is still low such that the ball can be easily dislodged from the surface with a small amount of vibration. In the absence of vibration, the steel ball rolls on the fibrillated rubber (Eq. 6.2) when the latter is inclined by $\theta > 2.5^o$ from the horizontal plane. This amounts to a threshold rolling torque ($mgRsin\theta$) of 0.22 μJ. Balancing this torque with that due to adhesion (Eq. 6.1), the hysteresis of adhesion (W_r -W_a) is estimated to be about 0.8 J/m^2. This value is considerably larger than the free energy of adhesion (40 mJ/m^2) between steel and a smooth surface of PDMS obtained using the method of contact mechanics, thus suggesting that the elastic hysteresis resulting from the deformation and relaxation between the PDMS fibril contributes to the threshold force of rolling [30,31].

The following paragraph is quoted from reference [29] so that the reader can follow the experimental details of this work without being compelled to read the previous paper. "The solid support was attached to an aluminum platform connected to the stem of a mechanical oscillator (Pasco Scientific, Model SF-9324). Gaussian white noise was generated with a waveform generator (Agilent, model 33120A) and fed to the oscillator via a power amplifier (Sherwood, Model No: RX-4105). In all experiments described here, vibration was applied parallel to the support. By controlling the amplification of the power amplifier, noises of different powers were generated while keeping the pulse width constant at 40μs. The acceleration of the supporting aluminum plate was estimated with a calibrated accelerometer (PCB Peizotronics, Model No: 353B17) driven by a Signal Conditioner (PCB Peizotronics, Model No: 482) and connected to an oscilloscope (Tektronix, Model No. TDS 3012B). The pdfs of these accelerations are Gaussian with

flat power spectra up to a total bandwidth of ~10kHz. The entire setup was placed on a vibration isolation table (Micro-g, TMC) to eliminate the effect of ground vibration. The motion of the ball was recorded with a high speed camera (Redlake, MotionPro, Model 2000) operating at 1000 frames/sec. Motion analysis software MIDAS 2.0 was used to track the dynamics of the steel ball". The strength of noise at a given setting is nominally given as $K = \Gamma^2 \tau_c$, where Γ is the root mean square value of the accelerations of the vibrating stage that were recorded with an accelerometer (see above), and τ_c is the time duration (40 μs) of the pulse. Even though the pdf of the acceleration pulses is Gaussian [29], there is a certain correlation of the noise pulses generated by a mechanical transducer. In a previous publication [29], we discussed this issue and showed that that the above estimate of K needs to be normalized by a constant numerical factor in order for the data to be amenable to quantitative analysis. Here we do not invoke this numerical factor, as the main parameters of interest are D, μ and T_{eff}, which are all obtained directly from the driven diffusive and the barrier crossing experiments.

We perform two types of measurements. With a Gaussian noise and a bias, both acting parallel to the support, the object moves forward and backward randomly (except at very low noise strengths, when the sphere exhibits a stick-slip behavior with only a forward drift) but with a net downward drift [29]. At a given bias $(m\bar{\gamma} = 0.044\,mN)$ and noise range of $K > 0.01$ m^2/s^3, we record the stochastic motion of the object with a high speed camera at 1000 fps to study the trajectory over certain duration of time. A total of 1.8×10^5 elementary displacements obtained from 60 (3s duration) trajectories were

collected. From these data, the spatial segments corresponding to a certain observation time window are used to obtain the distribution function (*pdf*) of the displacement fluctuation (fig. 6). Such a *pdf* has a given mean and a dispersion of displacements. By plotting the mean value as a function of time segment, a drift velocity is estimated. Furthermore, from the slope of the variance of the displacement versus time, we obtain the diffusivity. The ratio of this diffusivity to mobility is the first measure of the effective temperature. Estimation of the effective temperature from the displacement fluctuation is described later in the text.

6.4.2 Barrier crossing

The barrier crossing experiment (fig.1(b)) was performed with a periodically undulated surface that was prepared by simply placing a thin (0.6 mm thick) fibrillar rubber sheet over a flat surface decorated with parallel gold wires. By varying the diameter (25 μm to 75 μm) of the wires, barrier height was controlled. The topography of the surface produced this way is not exactly sinusoidal as the part of rubber in between the two wires makes a flat contact with the underneath surface. The overall shape is more like Gaussian humps with its height adjusted by the diameter of the wire, which are separated periodically from each other. Numerical simulation, however, shows that this difference of the undulation, be it sinusoidal or periodically separated Gaussian humps, has no effect in the estimation of the effective temperature. The ball was placed in one of the valleys and then the substrate was subjected to a random noise of a given strength. The time

needed for the ball to cross one of the barriers was noted with a stopwatch, or using a video camera. 35 such measurements were made at each power, from which the average escape frequency was estimated. With the substrate inclined at a given angle, average escape time was estimated at several different noise strengths with which the Van't Hoff-Arrhenius-Eyring (VHAE) plot was constructed. The number of jumps used in these experiments was optimized on the basis of simulation results so that no significant error is introduced in the averaging process.

6.5 Simulations

In order to estimate the drift velocity and the diffusivity at a given external bias and a noise strength, numerical solution of Eq.6.3 was carried out using a generalized integration method for stochastic differential equations [52] (see also reference [29] for additional details). Stochastic accelerations of the vibrating plate as measured using an accelerometer were used as the input, $\gamma(t)$, in the same sequence as they were generated experimentally to ensure that the noise correlation is identical in the experiment and the simulation. While the simulated drift velocity as well as the variance of the displacement did not depend on the integration time step ($20\mu s$–$80\mu s$), all the simulations were carried out with an integration step of $20\mu s$.

Another set of simulations was carried out to estimate the barrier crossing probability. When the height of the barrier is much smaller than the spacing of the wires,

as is the current case, the Langevin dynamics for the motion of the ball can be described by Eq. 6.10.

$$\frac{7}{5}\frac{dV}{dt} + \frac{V}{\tau_L} + \sigma(V)\Delta + \frac{\pi gh}{\lambda}\cos\frac{2\pi x}{\lambda} = \bar{\gamma} + \gamma(t)$$

$$\frac{dx}{dt} = V$$

6.10

Equation 6.10 was integrated by varying the strength of the noise. The trajectories thus obtained had certain numbers of discrete jumps of the ball from one potential minimum to the next. By dividing the total time of simulation with the numbers of jumps, the average escape frequency was estimated.

As discussed in the previous section, the topography of the experimental surface is not sinusoidal; it rather resembles Gaussian humps separated by regular intervals. We simulated this situation as well using a Langevin dynamics by assuming the energy potential around each hump to be $gh\exp\left[-(x/\sigma)^2\right]$ and replacing the fourth term of Eq. 6.10 with a periodic modulation of $(2ghx/\sigma^2)\exp\left[-(x/\sigma)^2\right]$.

6.6 Results and discussion

6.6.1 Stick-slip behavior at low noise strengths

The stochastic rolling of the steel sphere on a slightly inclined fibrillated rubber exhibits two types of behaviors. At a noise strengths $K > 0.01$ m^2/s^3, the balls rolls forward as well as backward, but with a net downward drift. At a very low noise strengths ($K < 0.01$m^2/s^3), on the other hand, the trajectories bear the signatures of stick-slip (more accurately, stick-roll) motion with a drift occurring only along the direction of the bias.
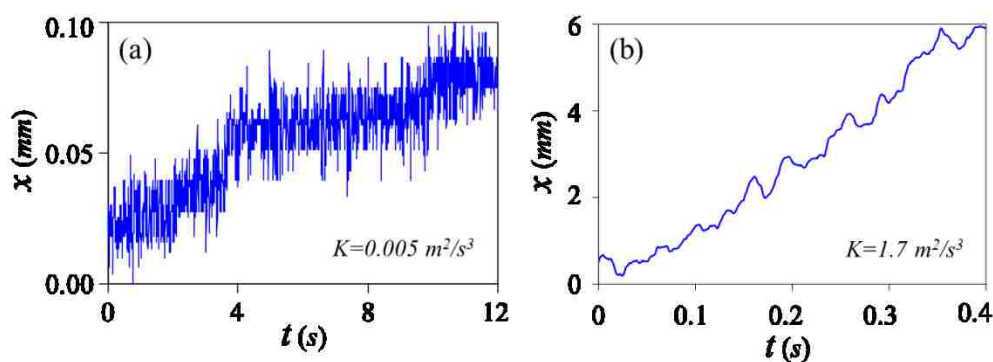
Figure 6.4: Examples of the trajectories of a steel sphere rolling on a flat fibrillar PDMS substrate tilted at an angle of 1° from the horizontal plane under the influence of Gaussian white noise at a very low (a) and a very high (b) noise strength.
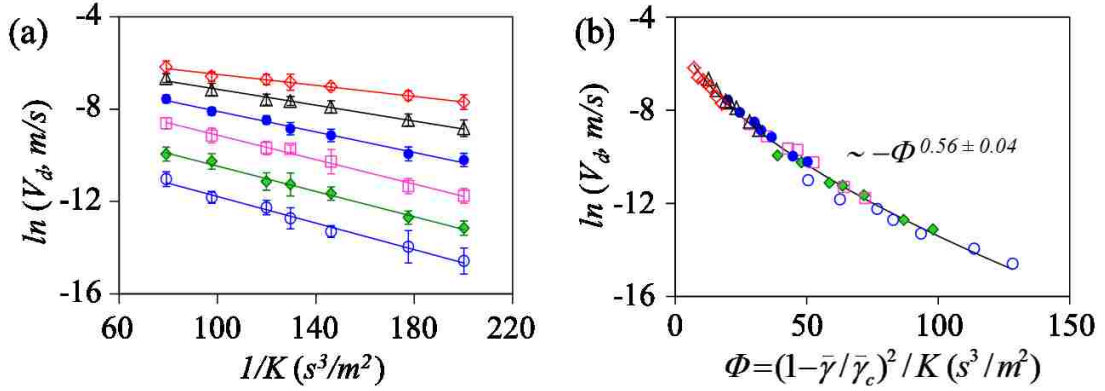
Figure 6.5: (a) Drift velocity (V_d) of a steel sphere on a fibrillar PDMS substrate shows logarithmic dependency on $1/K$ at low power regime at different applied biases (red open diamond (◊, 0.078mN), black open triangle (Δ, 0.067mN), filled blue circle (●, 0.056mN), open pink square (□, 0.044mN), filled green diamond (♦, 0.033mN), open blue circle (○, 0.022 mN). Each velocity is measured from the average of 10 to 20 tracks, each lasting for 180s duration. (b) Master curve showing nice collapse of the data of fig.(a) when $1/K$ is normalized by multiplying it with a factor of $(1-\bar{\gamma}/\bar{\gamma}_c)^2$.

Postponing the detailed analysis of such type of stick-slip data (i.e. the distributions of the stick time and the avalanche size) for the future, here we adopt a conservative approach, in which we measure the average drift velocity obtained from the displacement of the steel ball over a certain duration of time by varying the noise strength and the bias. Based on the observation that the drift velocity varies rather rapidly than either with the variation of K or $\bar{\gamma}$, we examined whether these data would be amenable to the analysis of an activated rate theory. It is apparent in fig. (5) that the drift velocities do, indeed, conform to a Van't Hoff-Arrhenius-Eyring form in the sense that the $ln(V_d)$ varies fairly linearly with $1/K$. This observation and the fact that the slope of the $ln(V_d)$ - $1/K$ plot decreases with the applied bias suggests that the de-pinning process of the sphere from

190

the fibrillated rubber is noise and force activated, along the lines of reasoning provided by several authors [6,53,54] in the past in other related contexts. In particular, it has certain semblance to the noise induced de-pinning of interfacial asperities during the sliding of a solid on another near the threshold, for which Caroli and Nozieres [54] proposed a logarithmic relationship between the sliding velocity and the friction coefficient, which can be written in terms of the variables defined in this paper as: $\ln(V_o/V) \sim (1 - \bar{\gamma}/\bar{\gamma}_c)^{3/2}/K$. Here, V is the sliding velocity and V_o is the velocity at which the applied bias reaches the threshold value $(\bar{\gamma}_c)$. Being inspired by this work, we explored what a comparable scaling would be for the current situation of rolling, which too is a depinning process (*albeit* the action here is concentrated near the contact perimeter). The data collected at different biases cluster satisfactorily around a master curve, provided that the horizontal axis (1/K) is multiplied with $(1 - \bar{\gamma}/\bar{\gamma}_c)^2$. The curvature of the collapsed plot, however, indicates that the underlying kinetics departs from a simple Arrhenius behavior.

6.6.2 Diffusive behavior at high noise strengths: effective temperature from drift and diffusivity

At higher noise strengths ($K > 0.01$ m^2/s^3) the sphere rolls both along and opposite to the bias, leading to a driven diffusive motion. The resulting displacement pdfs (probability distribution function) could be fitted with a stretched Gaussian function [29], i.e.

$$P = P_o \exp\left\{-\left[(x - x_p)/\sigma\right]^m\right\}$$ with different values of *m* for the left and right wings of the

distribution that account for the asymmetry.
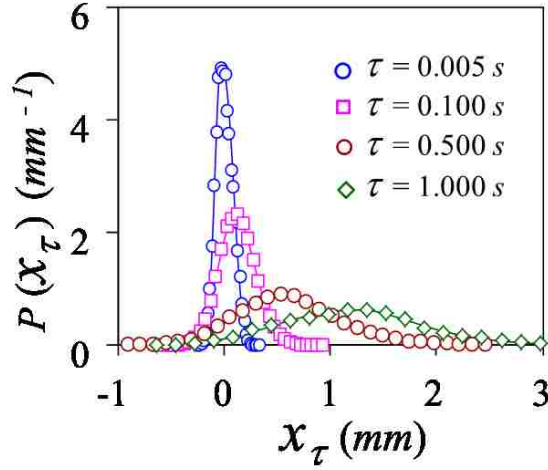
Figure 6.6: Probability distribution functions (*pdfs*) of displacements corresponding to four different observation windows illustrate that the mean value of the pdf drifts with time, while its width broadens. These data correspond to steel ball on a flat fibrillar PDMS substrate tilted by an angle of 1° and a noise strength of 0.1 m^2/s^3. Data of this kind are used to construct fig. (7).

Here x_p is the position of the peak, σ is the width of the distribution and P_o is a constant.

Although these values of *m* change with the observation time, the mean and the variance

of the distribution increase almost linearly with time at each noise strength (fig. (7)).
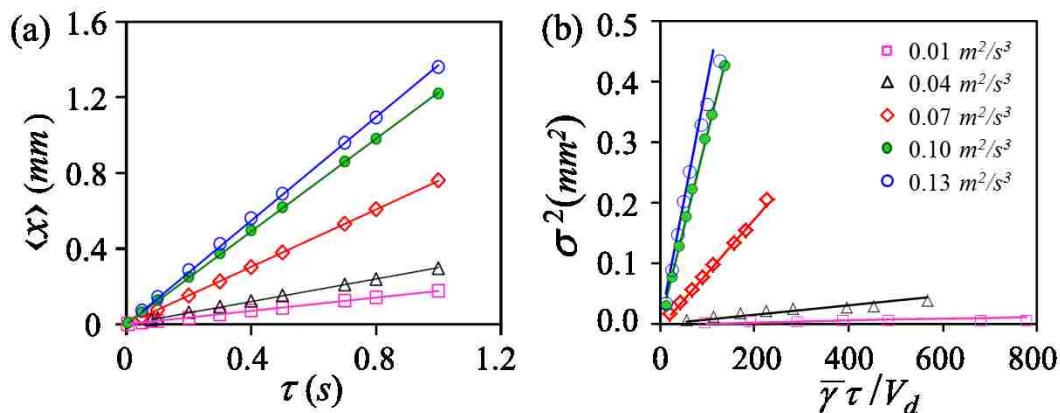
Figure 6.7: The drift of the steel ball on a flat fibrillar PDMS substrate tilted by 1° from horizontal plane is estimated from the evolution of the mean value (a) of the displacement pdf, whereas the diffusivity is obtained from the evolution of the variance (b) of the displacement fluctuation. The different symbols indicate the values of K at which the data were taken. Note that the variance is plotted as a function of $\bar{\gamma}\tau/V_d$ which is the ratio of the observation time (τ) to response time ($V_d/\bar{\gamma}$). The horizontal scale shows that the range of the observation time far exceeds the response time. Both the mean and root mean square of the displacements exceed the spacing (50 μm) of the fibrils as well. Similar symbols in figures (a) and (b) correspond to the same K.

The first moment of the displacement *pdf* yields the mean position $\langle x \rangle$ of the ball (fig.

7(a)), the evolution of which gives the drift velocity (V_d), whereas the growth of its

variance (fig. 7(b)) yields the diffusivity. It is well-known that the determination of

diffusivity from the evolution of variance suffers from poor statistics in the long time

limit. Our experience with the types of system studied here and those reported in

references [3] and [5] is that the variance versus time data can be fitted with a second

order polynomial, the quadratic component of which is minor and, usually, decreases

with improved statistics. We thus estimate the values of the diffusivity from the linear fit

193

of the variance vs time plots. Figure 8(a) shows that the diffusivity D increases super-linearly with K even within a small range of the noise strength ($0.01 \text{m}^2/\text{s}^3 < \text{K} < 0.13$ m^2/s^3) that is distinctly different from the classical behavior of $D \sim K$. We limited our investigation to this small range where the ratio of the diffusivity to mobility increases nearly linearly with K (Fig. 8(b)).
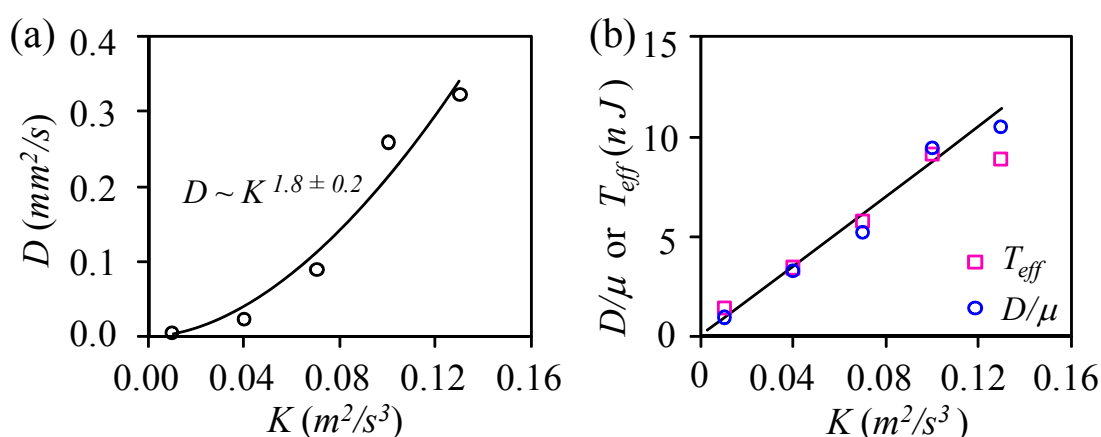
Figure 6.8: (a) The diffusivity of the sphere increases non-linearly with the strength of the noise ($D \sim K^{1.8 \pm 0.2}$, correlation coefficient ~ 0.97) (b) D/μ increases almost linearly with K. The pink squares correspond to the effective temperatures obtained from the integration of the data shown in fig. 9(a). The data are not well-behaved at $K > 0.1 \text{ m}^2/\text{s}^3$. All the barrier crossing experiments at the low K regime were carried out for $K < 0.1$ m^2/s^3. As the error bars of diffusivities are of the same size or smaller than the circles, they are not shown on the graphs.

This range was also used for the barrier crossing experiment (see below) where a large change in barrier crossing frequency is observed with a small change in K, similar to that of chemical kinetics. At this point, it should be pointed out that the net displacements of the ball in the above measurements of drift and diffusivity are much larger than fibrillar

spacing (50 μm), thus ensuring that they are above the elementary activation steps. They are also larger than the dynamic length scale ($V_d^{\ 2}/\bar{\gamma}$), thus ensuring that the transients are not accounted for in these analysis. The ratio of diffusivity to mobility is an estimate of the effective temperature, which was validated against another measurement that we accomplished with the help of a work fluctuations relation as discussed in the next section.

6.6.3 Persistence of negative fluctuation and effective temperature

The probability distribution of the displacements at a low noise strength exhibits substantial amount of negative fluctuations [29] that persists over certain observation time window. It is, therefore, tempting to analyze the data in the light of a conventional fluctuation theorem and extract an effective temperature [18] from such a plot. Unfortunately, an attempt to construct such a plot suffers from the malady that the pdfs are significantly asymmetric. Since the analysis of the displacement data in a typical fluctuation relation is carried out with the left wing of the distribution, the information contained in the right wing of any asymmetric distribution is ignored. It, perhaps, makes more sense to analyze the data using the integrated probabilities [55] of the positive and negative displacements (P_+ and P_-).

$$P_- = P(w_\tau < 0) = \int_{-\infty}^{0} P(w_\tau)dw_\tau \quad and \qquad 6.11$$

$$P_+ = P(w_\tau > 0) = \int_0^\infty P(w_\tau)dw_\tau$$

here, $w_\tau = m\bar{\gamma}\, x_\tau$ is the fluctuating work corresponding to a random displacement x_τ.

With the drift velocity measured at a given strength of the noise, the mean work

performed on the sphere over time τ is $W_\tau = m\bar{\gamma}\, V_d\tau$. Figure (9(a)) shows that the

ratio P_-/P_+ decreases monotonically with W_τ. Since, there are no other variables in such

a plot, the integral value of P_-/P_+ should be an intensive property of this driven diffusive
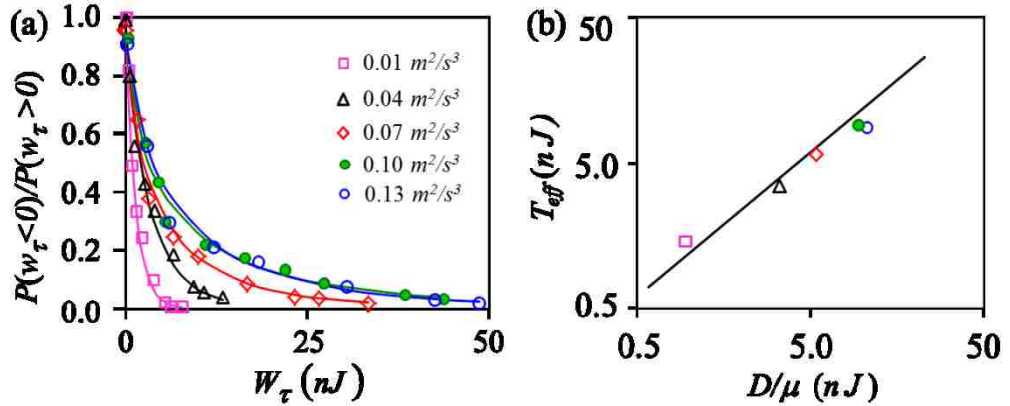
system.

Figure 6.9: (a) An integrated work fluctuation plot for a sphere rolling on a fibrillated PDMS surface. (P-/P+) decreases monotonically with the mean work Wτ at each noise strength, K. All the data could be fitted with an exponential or a slightly stretched function and integrated. (b) The effective temperatures obtained from the integration of the data shown in fig. 9(a) are compared with the ratio D/μ obtained from fig.(8).

When the displacement distribution is Gaussian and symmetric, the value of P_-/P_+ can be

easily computed [56], and it can be shown that this value is only 10% higher than the

ratio D/μ. Figure (9(b)) shows that the temperature like intensive parameters (shown as T_{eff}) obtained from the integrated fluctuations and those obtained from the Einstein's ratio of diffusivity and mobility cluster very closely around the theoretical line expected for the linear friction. While such a result would be quite generic for the case with a linear friction and with a Gaussian noise, it was not anticipated *a priori* for a non-linear system (see also Appendix section 6.8.2). It is also gratifying to note that an estimate of the time of persistence of negative displacement fluctuation in a driven diffusive system can be obtained from this integration as: $\tau_p = T_{eff}/(m\bar{\gamma}V_d)$.

6.6.4 *Effective temperature of the rolling ball*

Figure (8(b)) shows that T_{eff}, as estimated either from the integration of P_-/P_+ or from the ratio of the diffusivity and mobility, increases almost linearly, even though the diffusivity increases non-linearly with K. This analysis yield the value of D/μ to be (84 ± 3) K, where the former is given in terms of nJ and the latter in terms of m^2/s^3. As the total kinetic energy of the rolling ball with a drift is about 40% higher than that of the linear kinetic energy, the effective temperature of the ball undergoing stochastic rotation should be about (118 ± 4) $K\ nJ$.

At this juncture, we bring up an important issue regarding the temperature (T) of a non-equilibrium system as was pointed out by Speck and Seifert [57]. These authors showed that the diffusivity (D) of the particle in a non-equilibrium driven diffusive state is always larger than $T\mu$ by a certain amount. The subject has recently been re-iterated by Chaudhuri and Chaudhuri [58], who calculated the values of D and $T\mu$ using a flashing

ratchet model and reported that the ratio $D/T\mu$ departs from the equilibrium value of unity as a function of the asymmetry of the ratchet. Although it is premature to adapt these analyses to our system governed by a non-linear friction, we are led to suspect that D/μ could be an over-estimated value of the temperature in the absence of the bias. This parameter should now be treated as an apparent temperature that must be compared with a value obtained from a more direct measurement (see below).

6.6.5 *Barrier crossing and Van't Hoff-Arrhenius-Eyring equation*

As described in the experimental section, the barrier crossing experiment (fig. 1(b)) was performed with a steel ball on a periodically undulated rubber substrate, in which the amplitude of the undulation was varied from 25 μm to 75 μm.
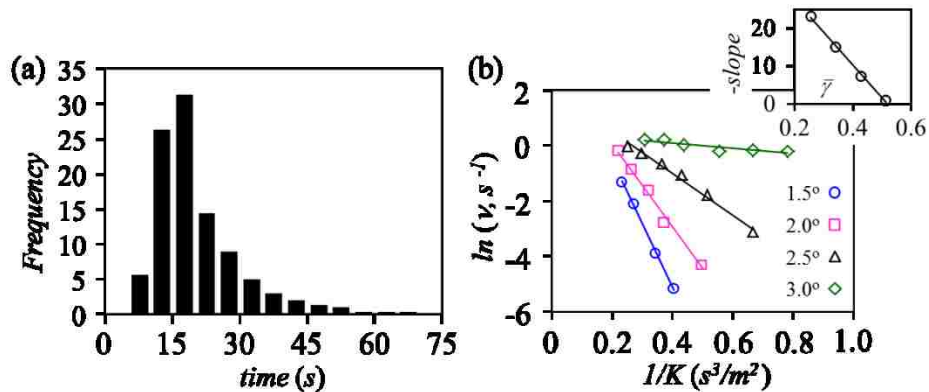
Figure 6.10: (a) A typical distribution of waiting times of the ball before it crosses from one potential valley to the next. Mean waiting time (t_w), as estimated from such a distribution, is used to calculate the barrier crossing frequency ($\nu \sim 1/t_w$). (b) VHAE type plots obtained with a barrier height of 75 μm at different angles of inclination. As the angle of inclination increases, the barrier height decreases leading to a diminished slope of the VHAE line. The inset shows that the slopes (m^2/s^3) of these lines as a function of the bias ($\bar{\gamma}$, m/s^2) .

At relatively larger barrier heights (i.e. 50 μm and 75 μm), high noise strengths (1 m^2/s^3 to 4 m^2/s^3) were required to initiate barrier crossing as compared to the low noise strengths (0.01 m^2/s^3 to 0.1 m^2/s^3) required for a barrier height of 25 μm. We have already noted that the friction becomes linear for $K > 1$ m^2/s^3, where the frequency of barrier crossing increases with the noise strength as well as the tilt angle of the substrate that reduces the energy barrier.

At any given noise strength, the ball persisted in a potential well for certain amount of time before transiting to the next. The corresponding waiting time has a certain probability distribution (fig. (10)), the first moment of which yields the mean waiting time (t_w). The transit time to cross the barrier is very much shorter than t_w. The frequency of the barrier crossing (ν) is thus given as the reciprocal value of this mean waiting time. The escape rate follows the rudimentary form of a force activated [59–62] Eyring's equation (Van't Hoff-Arrhenius-Eyring or VHAE form) as follows:

$$\nu = \nu_o e^{-\frac{(gh - \bar{\gamma}\lambda)}{K\tau^*}}$$

6.12

here, ν is the rate of escape, λ is an activation length and τ^* is a time scale that converts the noise strength to an effective temperature as $mK\tau^*$. The experimentally measured escape frequencies conform well to Eq. 6.12, i.e. the plots of $\ln(\nu)$ vs $1/K$ are linear. Furthermore, the slopes of these lines vary linearly with $\bar{\gamma}$ (fig. 10(b)) from which $mK\tau^*$ is estimated to be (4.3±0.1) K nJ , which is remarkably same with the experiments performed with the 50 μm and 75 μm height barriers. An estimation of the effective

temperature using the method of displacement fluctuation, however, could not be conveniently performed at high *K*, where the ball exhibits rather fast dynamics. These analyses could, however, be performed comfortably at a low noise strength.

6.6.6 Barrier crossing with non-linear friction
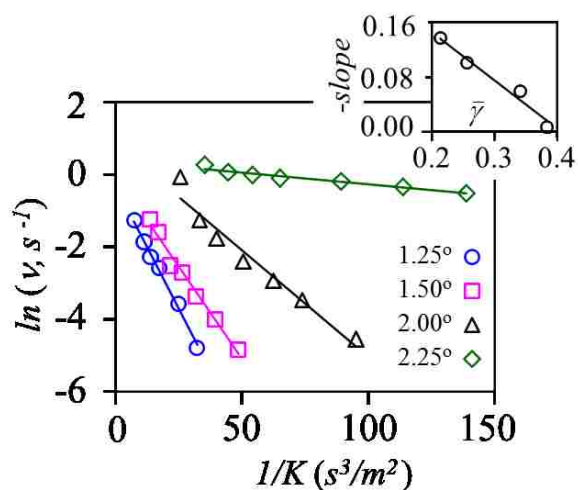
Figure 6.11: VHAE type plots obtained with a barrier height of 25 μm at different angles of inclination. The inset shows the slopes (m^2/s^3) of these lines as a function of the bias ($\bar{\gamma}$, (m/s^2)).

The results of the barrier crossing experiment at a barrier height of 25 μm are summarized in fig. (11). The logarithm of the barrier crossing rate is still linear with 1/*K*, even though these low- *K* dynamics are controlled by a non-linear friction. We already got the hint that this could be so, as the ratio *D*/μ varies almost linearly with *K*. From the slopes of the ln(ν) - 1/*K* plots (fig. (11)) an effective temperature is estimated to be T_{eff}

=(210±6) *K nJ*. This value is nearly 78% higher than that obtained from the driven

diffusive experiments. In order to shed more light on this discrepancy, we simulated

barrier crossing experiments by integrating Eq. 6.10 first with a linear friction model and

then with a non-linear friction model assuming certain values of Δ and τ_L [29].
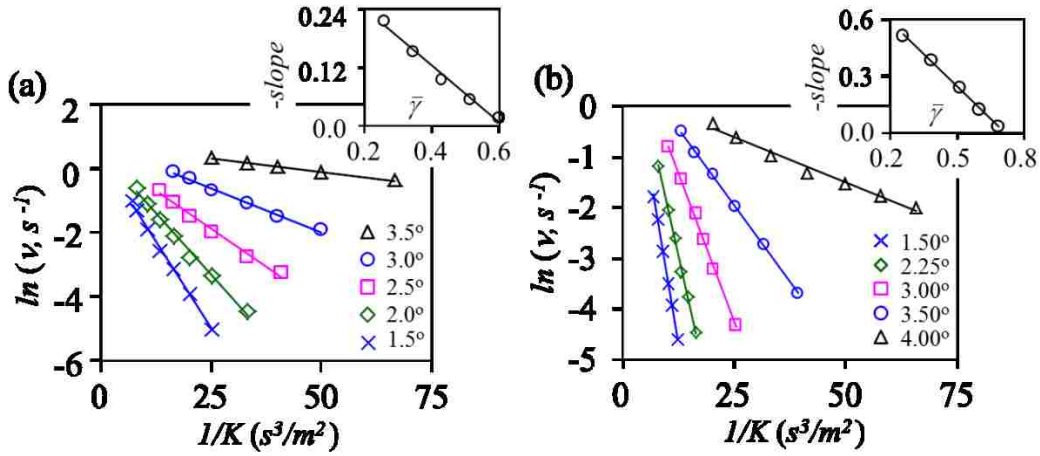
Figure 6.12: (a) VHAE plots simulated with a linear friction model i.e. Eq. (10) with Δ=0 m/s^2 and τ_L=0.01s. Barrier height of 25 μm and periodicity λ of 1 mm is used for simulation at different angles of inclination shown inside the figure. The slopes (m^2/s^3) of these lines are plotted as a function of $\bar{\gamma}$ (m/s^2) in the inset of the fig. 12(a). (b) Similar plot as in (a) except that a non-linear friction model was used, i.e. Eq. (10) with Δ=0.8 m/s^2 and τ_L=0.1s. While all the data were obtained with a surface having a sinusoidal profile, identical values of T_{eff} were also obtained (not shown here) with a surface having Gaussian humps separated at same periodic intervals as λ.

The barrier crossing simulations performed with a linear friction model (i.e. Δ=0) is

consistent with Eq. 6.12 in that the plots of ln(v) vs 1/K are linear at all angles of

inclinations. Simulations of diffusivity and mobility yielded the value of D/μ to be

(96.0±0.2) *K* nJ. By correcting for the rotational motion, the effective temperature is

estimated to be about (134.4±0.3) K nJ, which is slightly smaller than that (173±4 K nJ) obtained from the barrier crossing simulation. Simulations with the combination of a linear and a non-linear friction show that the drift velocity increases linearly, but the diffusivity increases super-linearly with K leading to $D/\mu \sim K^{1.50\pm0.01}$. Barrier crossing frequencies (fig. 12(b)) obey Eq. 6.12 in that the plots of $\ln(\nu)$ vs $1/K$ are linear at all angles of inclination. Consequently, the corresponding effective temperature is linear with K, i.e. $T_{eff} = (77\pm1)$ K nJ , which differs from what is observed with the ratio of diffusivity and mobility (i.e. $T_{eff} \sim K^{1.50\pm0.01}$) (fig. (13)). We thus conclude that the two methods do not yield the same effective temperature.
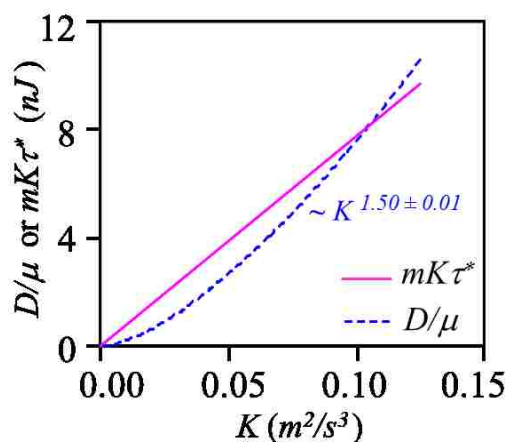
Figure 6.13: Comparison of the D/μ and the mKτ* values as obtained from the barrier crossing simulations with a non-linear friction model.

While the simulation reproduces the general experimental features that the diffusivity is super-linear and the drift velocity is linear with the noise strength, it has not

been able to reproduce the fact that D/μ is linear with K. Clearly, a much more detailed state and rate dependent model of rolling friction would be needed in order to make better comparison between the simulation and the experiment. Nevertheless, both the experiment and the simulation thus far suggest that the effective temperature of a non-linear system does not have a unique value. As already pointed out, there are two response times (τ_L and K/Δ^2) to a non-linear dynamics. The effective temperature may then be determined by any of those values or by their average (Eq. 6.9) depending upon the experiment used to interrogate it. It is plausible that the diffusivity is biased by the slower part of the dynamics, the response time of which is dominated by K/Δ^2, whereas the barrier crossing is dominated by the higher end of the velocity distribution that is dominated by τ_L. In other words, the ball could be hotter at the transition time scale than the overall diffusive time scale.

Another interesting part of the story is that the effective temperature (21.0±0.6 nJ) at $K \sim 0.1$ m^2/s^3 is found to be considerably higher than that (4.3±0.1 nJ) at a value of $K \sim$ 1 m^2/s^3. This surprising result suggests that only a small part of the externally supplied energy is transmitted to the ball at high noise strength. This would be possible if the ball spends a considerable time in a levitated state, i.e. detached from the rubber support. This picture is, in fact, supported by the video microscopic observations. No detachment of the ball, however, occurs with a low strength of the vibration. The ability of the ball to cross a larger barrier at a higher K with a reasonable rate, in spite of a reduced T_{eff}, can be ascribed to a reduced friction, thus to the enhancement of the pre-exponential factor of

the VHAE equation. This transition from an attached to a partially levitated (i.e. detached) state also appears to be a reason of the solid-like to a fluid-like transition of the drift velocity (fig. (3)) that is observed in going from a low to a high strength of the vibration.

6.6.7 Barrier crossing experiment with water drops

We conclude this section by reporting a barrier crossing experiment with a soft deformable sphere, such as a drop of water, which, in the same spirit of the above section, exhibits a slowing down of barrier crossing rate due to a difference in v_o.
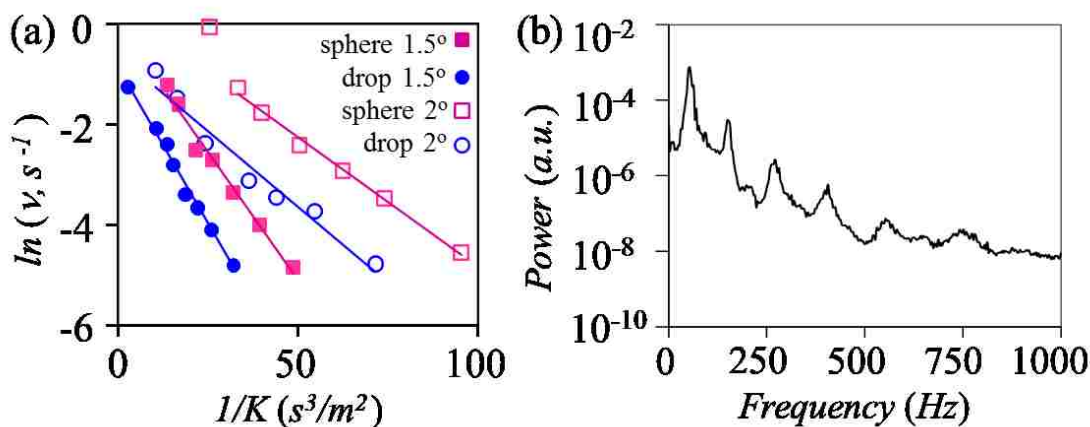
Figure 6.14: (a) Comparison of the VHAE plots obtained for a sphere and a drop of water with a barrier height of 25 μm. The data for the sphere are same as those summarized in fig.(11). (b) An 8μl sessile drop exhibits shape fluctuation when it is excited with a Gaussian noise. Various harmonics of the shape fluctuation are shown in this power spectrum that was obtained by averaging several power spectra and de-noising it with a wavelet transform in order to reduce the background noise.

The origin of the non-linear friction here is the wetting hysteresis [5] that gives rise to a sub-linear growth of the mobility of the drop as a function of the strength of the noise (fig. (3)). The results of the experiments performed with small droplets (8 μl) of water on an undulated rubber surface (barrier height of 25 μm) are summarized in fig. (14). While the slopes of the VHAE plots with a water drop are nearly parallel to those of a rigid sphere - meaning that the effective temperatures normalized by the masses of the respective objects are the same in both cases, the pre-exponential factor (ν_0) for the water drop is nearly half of that of the steel sphere.

As the pre-exponential factor is inversely proportional to the frictional relaxation frequency [63] in the Smoluchowski limit, one may say that the velocity relaxation rate of a water drop is greater than that of the steel ball. This trend is consistent with the fact that the slope of the mobility versus K of the water drop (fig. (3)) on a flat surface is nearly half of that of the steel sphere. By the same token, one would expect that the effective temperature of the water drop to be smaller than the rolling steel ball, which is, however, not the case. The dynamics of a liquid drop is richer than that of a steel ball in that it undergoes a noise induced excitations of numerous spherical harmonics [64] (fig.14(b)). Further experiments with liquids drops of different surface tension and viscosity could shed more light on whether the internal dynamics related to these noise induced oscillations could contribute to the effective temperature of the drop in the barrier crossing experiments.

6.7 Concluding remarks

We presented here a report on the rotational coupled with a translational behavior of a small sphere on a surface that is driven by external fields and randomized by external noises. The results are encouraging in that an intensive temperature like parameter could be estimated from the Einstein's ratio of diffusivity and mobility, which is consistent with that obtained from the decay of the negative displacement fluctuation. With such a model system, it was also possible to design a novel barrier crossing experiment, thus allowing measurements of the escape frequency of the sphere in terms of the tilt angle of the substrate and the barrier height. The overall behavior is consistent with the Van't Hoff-Arrhenius-Eyring form of the escape rate in its rudimentary form. The results with a small barrier height could be analyzed in detail as the dynamics was slow enough to be followed carefully. This region is also interesting owing to the fact that the dynamics is controlled by a non-linear friction. The dynamics of the ball on the flat PDMS at K $<0.01\text{m}^2/\text{s}^3$ is a sub-critical barrier crossing process. At higher noise strengths (i.e. $K >$ $0.01 \text{ m}^2/\text{s}^3$), the slip (more accurately, the microscopic rolling) events occur both along as well as opposite to the bias that results in a driven diffusive motion. The drift velocity here grows almost linearly with K (i.e. $V_d \sim \bar{\gamma} K / \Delta^2$, see also ref. 29) which is in surprisingly good agreement with the predictions based on a simple model of threshold friction by Caughey and Dienes [1] as well as de Gennes [38]. While an effective temperature could be estimated from the barrier crossing experiments (an activated process at the scale of undulation), a discrepancy, nonetheless, has been observed between this estimate and that obtained from D/μ in the low K region. It is plausible that

these two experiments may be probing different regions of the velocity statistics of a non-linear system that exhibits two different response times. What essentially transpires is that we are dealing with a two level activation process, in which each requires a specific temperature to describe it. We expect that much more can be learned on this issue by performing barrier crossing experiments with a fat tailed (e.g. a stretched exponential) noise that could accentuate any difference of the type mentioned as above. With additional efforts, it should be possible to visualize the de-pinning process itself and to follow the avalanches resulting from the co-operative detachments of the fibrils from the surface. It would also be desirable to improve the experimental technique so that the distribution of the stick phases as well as the sizes of the avalanches at the low noise and high strengths can be carried out in detail, as these features could shed more light on the origin of the non-linear friction itself.

6.8 Appendix

6.8.1 (Adapted from Greenwood et al. [32])

The origin of the non-linear friction in Eq. 6.1 can be understood rigorously in a 2d system, with a cylinder rolling on a rubber slab in which the contact is smooth and rectangular. According to the theory of contact mechanics [32–34] the stress distribution underneath the cylinder is:

$$\sigma(x) = (b^2 - x^2)^{-1/2} \left(-\frac{P}{\pi} + \frac{E^*}{2R}(x^2 + xd - 0.5b^2) \right) \qquad 6.13$$

Here, b is the half-width of contact band, R is the radius of the roller, P is the applied load, d is the shift of the midpoint of the contact band from the point beneath the roller center, and E^* is the contact modulus. According to the Griffith-Irwin theory of fracture mechanics, the stress has a square root singularity near the contact edges. The corresponding stress intensity factors are ($x \rightarrow \pm b$):

$$N|_{\pm b} = \frac{1}{\sqrt{2b}} \left(-\frac{P}{\pi} + \frac{E^*}{2R}(0.5b^* \pm bd) \right)$$

$$\frac{4RN}{E^*}\bigg|_{\pm b} = \frac{1}{\sqrt{2b}} \left(-b_h^2 + b(b \pm 2d) \right)$$

$$\qquad 6.14$$

Using the relationship between the strain energy release rate, the stress intensity factor and the contact modulus $G = \pi N^2 / E^*$, we have

$$\frac{32}{\pi} \frac{R^2 G}{E^*}\bigg|_{\pm b} = \frac{1}{b}(b^2 - b_h^2 \pm 2bd)^2 \qquad 6.15$$

Subtraction of the values of G at the receding and advancing edges gives

$$[G|_{+b} - G|_{-b}] = \frac{\pi}{4} \frac{E^*}{R^2} d(b^2 - b_h^2) \qquad 6.16$$

The rolling torque Q is obtained from the integration of the stress distribution as:

$$Q = dL\left(\frac{\pi E^* b^2}{(4R)} - P\right) = L\left(\frac{\pi E^*}{(4R)}\right) d(b^2 - b_h^2) \qquad 6.17$$

Combining Eq. 6.16 and 6.17, we have the essential result:

$$Q = RL[G|_{+b} - G|_{-b}] \qquad 6.18$$

Although Eq. 6.18 is derived here using the method of contact mechanics for a smooth contact, it can also be derived entirely using an energy argument [32–37]. This energy argument is also applicable for the sphere on the fibrillated surface either for a circular or for a symmetric polygonal contact. If we equate the strain energy release rate with the work of adhesion in making and breaking the contact, we can write down an equivalent expression for the rolling torque of a sphere on a flat surface as:

$$Q \approx [W_r - W_a]r^2 \qquad 6.19$$

where r is the width of contact.

6.8.2 *Effective temperature for different non-linear systems*

The effective temperature obtained from the integral of P_-/P_+ with W_τ has also been tested against the ratio of the diffusivity and mobility for several other non-linear systems. One of those involves the sliding of a small glass cube on a slightly inclined (2°) glass plate in the presence of a Gaussian [3] or a non-Gaussian noise [5]. The second and the third cases involve the motion of a small water drop on a smooth silicon wafer

induced either by a chemical [5] or a thermal gradient [65] of surface energy in the presence of a Gaussian noise. With the measured diffusivity and the drift velocity as discussed in the text, we define a non-dimensional observation time for each system as $V_d^2\tau/D$. The first observation we make is that the kurtosis of the distribution is not constant with respect to the time of observation (fig. (15a)). Although a Leptokurtic distribution is observed at short observation time, the excess Kurtosis plateaus out to a constant value in all cases.
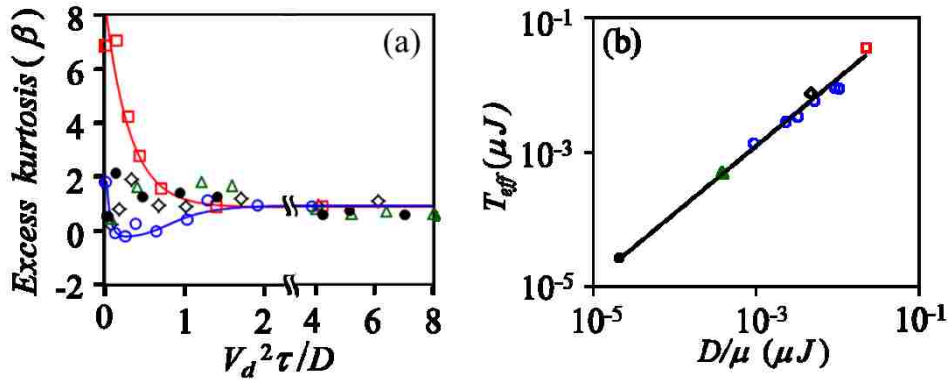
Figure 6.15: (a) Excess kurtosis (β) is plotted against dimensionless time ($V_d^2\tau/D$) for some representative cases. (b)T_{eff} as a function of D/μ for different systems. Black diamond ($\blacklozenge$) represents the sliding (2° inclination) of a glass cube on glass surface excited by Gaussian noise, red square ($\square$) depicts same system excited by stretched exponential noise, blue open circle ($\circ$) corresponds to rolling sphere on fibrillated PDMS surface subjected to Gaussian noise (all the data are from the current work, except one from a previously published work [29]), green triangle (Δ) represents water drop on wettability gradient surface and filled black circle ($\bullet$) depicts water drop on thermal gradient surface.

While different evolutions are observed with different systems, the effective temperature obtained from the integrated fluctuation is in good agreement (fig. (15b)) with the Einstein's ratio of diffusivity and mobility in all these cases that include (rather surprisingly) the sliding induced by a highly stretched exponential noise [$P = P_o \exp\left\{-(\gamma/\sigma)^{0.3}\right\}$]. These results provide additional support to that discussed in the text, namely that the integration of the *P-/P+* with respect to W_τ is a temperature like intrinsic property, i.e. it is equal to *D/μ.*

References

[1]   T. K. Caughey and J. K. Dienes, Journal of Applied Physics **32**, 2476–2479 (1961).

[2]   B. Wang, S. M. Anthony, S. C. Bae, and S. Granick, Proceedings of the National Academy of Sciences of the United States of America **106**, 15160–4 (2009).

[3]   P. S. Goohpattader and M. K. Chaudhury, The Journal of Chemical Physics **133**, 024702 (2010).

[4]   S. Mettu and M. K. Chaudhury, Langmuir : the ACS Journal of Surfaces and Colloids **26**, 8131–40 (2010).

[5]   P. S. Goohpattader, S. Mettu, and M. K. Chaudhury, Langmuir : the ACS Journal of Surfaces and Colloids **25**, 9969–79 (2009).

[6]   L. Z. Prandtl, Angew Math. Mech. **8**, 85 (1928).

[7]   M. H. Muser, Proceedings of the National Academy of Sciences of the United States of America **107**, 1257–8 (2010).

[8]   M. Müser, Physical Review B **84**, (2011).

[9]   B. N. J. Persson, *Sliding Friction: Physical Principles and Applications*, 2nd ed. (Springer, Berlin; New York, 2000).

[10]   M. H. Muser, M. Urbakh, and M. O. Robbins, Advances in Chemical Physics **126**, 187 (2003).

[11]   S. Nasuno, a. Kudrolli, and J. Gollub, Physical Review Letters **79**, 949–952 (1997).

[12]   W. Losert, D. G. W. Cooper, J. Delour, a. Kudrolli, and J. P. Gollub, Chaos (Woodbury, N.Y.) **9**, 682–690 (1999).

[13]   T. Baumberger and C. Caroli, Advances in Physics **55**, 279–348 (2006).

[14]   O. Zik, J. Stavans, and Y. Rabin, Europhysics Letters (EPL) **17**, 315–319 (1992).

[15]   K. Hayashi and M. Takano, Physical Review E **76**, 4–7 (2007).

[16]   P. Ilg and J.-L. Barrat, Europhysics Letters (EPL) **79**, 26001 (2007).

[17]   L. Joly, S. Merabia, and J.-L. Barrat, EPL (Europhysics Letters) **94**, 50007 (2011).

[18]   K. Feitosa and N. Menon, Phys. Rev. Lett. **92**, 164301 (2004).

[19]   L. F. Cugliandolo, Journal of Physics A: Mathematical and Theoretical **44**, 483001 (2011).

[20]   D. Bi and B. Chakraborty, Philosophical Transactions. Series A, Mathematical, Physical, and Engineering Sciences **367**, 5073–90 (2009).

[21]   G. D. Anna, P. Mayor, A. Barrat, V. Loreto, and F. Nori, Nature 909–912 (2003).

[22]   a. Abate and D. Durian, Physical Review Letters **101**, (2008).

[23]   C. Song, P. Wang, and H. A. Makse, Proceedings of the National Academy of Sciences **102**, 2299 (2005).

[24]   E. G. Daub and J. M. Carlson, Ann. Rev. Cond. Matt. Phys. **1**, 397 (2010).

[25]   T. Haxton and A. Liu, Physical Review Letters **99**, 7–10 (2007).

[26]   H. Jaeger, C. Liu, and S. Nagel, Physical Review Letters **62**, 40–43 (1989).

[27] R. Behringer, D. Bi, B. Chakraborty, S. Henkes, and R. Hartley, Physical Review Letters **101**, 1–4 (2008).

[28] K. Reddy, Y. Forterre, and O. Pouliquen, Physical Review Letters **106**, 1–4 (2011).

[29] P. S. Goohpattader, S. Mettu, and M. K. Chaudhury, The European Physical Journal. E, Soft Matter **34**, 120 (2011).

[30] N. J. Glassmaker, A. Jagota, C. Hui, W. L. Noderer, and M. K. Chaudhury, Proceedings of the National Academy of Sciences **104**, 10786 (2007).

[31] W. L. Noderer, L. Shen, S. Vajpayee, N. J. Glassmaker, A. Jagota, and C.-Y. Hui, Proceedings of the Royal Society A: Mathematical, Physical and Engineering Sciences **463**, 2631 (2007).

[32] J. a Greenwood, K. L. Johnson, S.-H. Choi, and M. K. Chaudhury, Journal of Physics D: Applied Physics **42**, 035301 (2009).

[33] H. She, D. Malotky, and M. K. Chaudhury, Langmuir **14**, 3090–3100 (1998).

[34] H. She and M. K. Chaudhury, Langmuir **16**, 622–625 (2000).

[35] A. D. Roberts, Rubber Chemistry and Technology **52**, 23 (1979).

[36] K. Kendall, Wear **33**, 351 (1975).

[37] M. Barquins, J Adhesion **26**, 1 (1988).

[38] P.-G. De Gennes, Journal of Statistical Physics **119**, 953–962 (2005).

[39] S. Daniel, S. Sircar, J. Gliem, and M. K. Chaudhury, Langmuir **20**, 4085 (2004).

[40] A. Kawarada and H. Hayakawa, Journal of the Physical Society of Japan **73**, 2037 (2004).

[41] J. M. Johnsen and A. Naess, *Structural Dynamics-Eurodyn'93*, Balkema, R (1993), p. 735.

[42] A. Baule, H. Touchette, and E. G. D. Cohen, Nonlinearity **24**, 351–372 (2011).

[43] H. Touchette, E. Van der Straeten, and W. Just, Journal of Physics A: Mathematical and Theoretical **43**, 445002 (2010).

[44]   A. Menzel and N. Goldenfeld, Physical Review E **84**, 1–9 (2011).

[45]   J. Talbot and P. Viot, Phys. Rev. E **85**, 021310 (2012).

[46]   W. Gerlach and E. Lehrer, Naturewiss **15**, 15 (1927).

[47]   G. E. Uhlenbeck and S. Goudsmit, Physical Review **34**, 145 (1929).

[48]   Z. Cheng and T. Mason, Physical Review Letters **90**, 1–4 (2003).

[49]   B. H. McNaughton, P. Kinnunen, M. Shlomi, C. Cionca, S. N. Pei, R. Clarke, P. Argyrakis, and R. Kopelman, The Journal of Physical Chemistry. B **115**, 5212–8 (2011).

[50]   K. Altintas, H. Boehringer, and H. Fujita, IEIC Tech. Rep. **105**, 51 (2005).

[51]   S. Mettu and M. K. Chaudhury, Langmuir : the ACS Journal of Surfaces and Colloids **27**, 10327–10333 (2011).

[52]   D. T. Gillespie, Am J Phys **64**, 225 (1996).

[53]   M. Brillouin, *Notice Sur Les Travaux Scientifiques* (Gauthier-Villars, Paris, 1904).

[54]   C. Caroli and P. Nozieres, in *Proceedings of the NATO Advanced Research Workshop and Adriatico Research Conference*, edited by B. N. J. Persson and E. Tosatti (Nato Science Series E: (closed), Vol. 311, Miramare, Trieste, Italy, June 20-23, 1995), p. 7923.

[55]   G. M. Wang, E. M. Sevick, E. Mittag, D. J. Searles, and D. J. Evans, Rev. Lett. **89**, 050601 (2002).

[56]   R. Van Zon and E. G. D. Cohen, Physical Review E (2003).

[57]   T. Speck and U. Seifert, Europhysics Letters **74**, 391–396 (2006).

[58]   D. Chaudhuri and A. Chaudhuri, Phys. Rev. Lett. **85**, 021102 (2012).

[59]   H. Eyring, The Journal of Chemical Physics **4**, 283 (1936).

[60]   T. D. Blake and J. M. Haynes, Journal of Colloid and Interface Science **30**, 421 (1969).

[61]   A. Schallamach, Proc. Phys. Soc. B **66**, 386 (1953).

[62] A. Ghatak, K. Vorvolakos, H. She, D. L. Malotky, and M. K. Chaudhury, The Journal of Physical Chemistry B **104**, 4018–4030 (2000).

[63] H. A. Kramers, Physica VII 284–304 (1940).

[64] H. Lamb, *Lamb.pdf* (Cambridge University Press, UK, 1932).

[65] S. Mettu and M. K. Chaudhury, Langmuir : the ACS Journal of Surfaces and Colloids **24**, 10833–7 (2008).

7. CHAPTER SEVEN: Noise Activated Dissociation of Soft Elastic Contacts[6]

7.1 Introduction

Morphological and/or elastic heterogeneities can play important roles in improving the toughness of an adhesive interface [1–3] . Built upon the path breaking ideas of Thomson *et al* [4,5] and Kendall [6], it is now well appreciated that such heterogeneities are capable of trapping a crack locally and intermittently. Every time a crack is de-pinned from such a trapped state, some energy is dissipated; thus the overall fracture toughness is enhanced. Examples of defect enhanced fracture toughness are plenty in natural and laboratory settings, which have been reviewed [1,3] recently. The main emphasis of the conventional treatments has, however, been on the ballistic separation of surfaces from a pinned state. What has not been much appreciated is that these joints, like all systems in nature, are subjected to various types of noises originating from thermal, environmental, and mechanical processes. It is therefore imperative to develop an understanding of how two surfaces separate from a pinned state in the presence of a noise. The subject of this paper is to illustrate this situation with a specific example of the rolling of a rigid sphere on a surface, where it is initially pinned by deformable elastic fibrils but is de-pinned when it is subjected to a low strength mechanical noise. We discuss the kinetics of such a

---

phenomenon after providing the required backgrounds on how a pinning potential develops from the completion of elastic and surface forces in a soft elastic system.

Beginning with the pioneering works of Johnson, Kendall and Roberts and others [7–18] it is now well-established that the interfacial forces can deform a soft elastic object when it comes into contact with another rigid material. Several studies [15–18] have also pointed out that the adhesive forces can be so significant that a soft object jumps into contact with another material when they are in close proximity following which one or both of them may deform elastically.
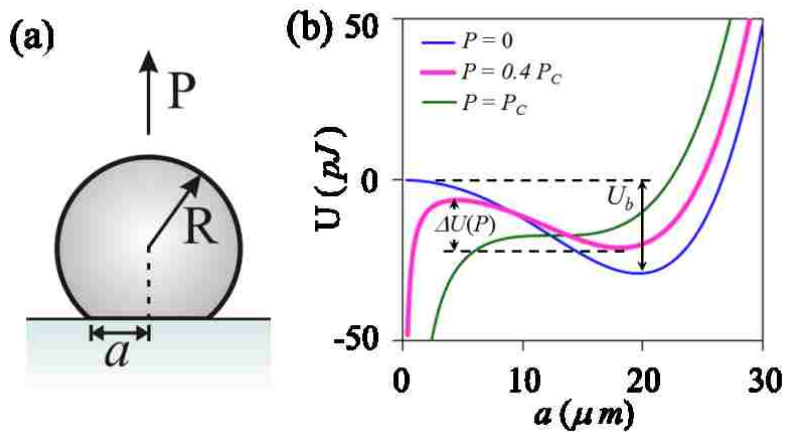
Figure 7.1: (a) Schematic of a sphere in contact with a flat substrate. A negative load (P) is applied on the sphere of radius R and contact modulus of E*. (b) Total energy of the system at fixed loads but at different values of the contact radius calculated with the following parameters. R= 100 μm, E*= 1MPa, W=0.04 J/m2. For this combination of material parameters, the critical load Pc is -19 μN. In the absence of the load, the system has one minimum. However, as the load is increased, a maximum and a minimum appear in the energy potential. At a critical negative load, the energy barrier disappears.

The simplest illustrative case [7,8,10] is the deformation of a sphere is shown schematically in Figure 7.1. For the purpose of illustration, we consider that a negative load ($P < 0$) is applied onto the sphere. The total energy of the system [7,8,10] is the summation of the potential, elastic and adhesion energies:

$$U(a, P) = \frac{E^* a^5}{15R^2} - \frac{P^2}{3E^* a} - \frac{Pa^2}{3R} - \pi W a^2 \qquad 7.1$$

Here, E^* is the contact modulus, P is the applied load, R is the radius of the sphere, W is the work of adhesion and a is the radius of the contact area. When $P = 0$, the energy U (a, P) exhibits a minimum with a depth of $U_b = \frac{(6\pi W)^{5/3} R^{4/3}}{10 E^{*2/3}}$ that can be easily deduced by setting the first derivative of the total energy of the system (Eq. 7.1) to zero. The system is unconditionally stable at this stage. However, with a negative load, the energy landscape changes substantially as shown in Figure 7.1. A local minimum still exists as long as the load is smaller than a critical value, but now an unstable equilibrium state appears in the energy landscape. There is a difference of energy between the unstable and the stable equilibrium states that disappears only at a critical load thus leading to a ballistic separation of the sphere from the substrate. What we emphasize in this paper is that the sphere can explore various states of the energy landscape (Figure 7.1) diffusively in the presence of a noise. When the unstable equilibrium state is crossed, the contact falls apart. Like any chemical kinetics, the frequency of this rupture should follow a Van't Hoff-Arrhenius-Eyring [19] type rate law, which is generic to the force induced

dissociation of molecular bonds as witnessed in various types of thermally activated processes such as plastic flow [19,20], friction [20–29], wetting dynamics [30], sub-critical fracture [31] and the dissociation kinetics of single molecules [32,33], to name a few.

We approach the current problem within the framework of a Smoluchowski-Kramers equation [34,35], in which two physical parameters are important. The first is the barrier height and second is the frequency at which attempts are made to cross the barrier. Several studies [19–33] have pointed out that an external force reduces the height of any pre-existing energy barrier. To the best of our knowledge, Garg [36] was the first to point out that it is not only the barrier height, but also the pre-exponential frequency factor that changes with the applied load. Afterwards several studies [37–41] used the force modulated frequency and the barrier energy terms in the Kramers equation to simulate the dissociation kinetics of polymer chains with a linear loading rate in the style of Evans and Ritchie [33], as well as Schallamach [23]. The findings of the later studies [38–41] agree with Garg [36] in that the applied force (f) modifies the energy barrier as $\sim (1\text{-}f/f_c)^{1.5}$, where f_c is the critical force of detachment. Recently, such a scaling has been verified in molecular dynamics simulations as well [28,42]. The finding of Lacks *et al* [42] is particularly interesting in that they showed that it is not only the energy barrier, but also the free energy barrier that follows the scaling of $\sim(1\text{-}f/f_c)^{1.5}$. In the light of these previous studies, we write the overall frequency of rupture of a soft sphere from a solid substrate (assuming a linear friction) as follows:

$$\nu = \left[\frac{\tau_L}{2\pi}\omega_1(P)\omega_2(P)\right] exp\left[-\frac{2\Delta U(P)}{mK\tau_L}\right] \qquad\qquad 7.2$$

Equation 7.2 is the celebrated Kramers' equation in the strong friction limit, where τ_L is the Langevin relaxation time, $\omega_1(P)$ and $\omega_2(P)$ are the frequencies corresponding to the curvature of the energy potential near its maximum and minimum values, $\Delta U(P)$ is the barrier height, m is the mass of the sphere. K (m^2/s^3) is the strength of a Gaussian white noise, which is defined as $\Gamma^2\tau_c$, Γ (m/s^2) being the root mean square acceleration of the noise, and τ_c (s) is its pulse width. The term $mK\tau_L/2$ of Eq. 7.2 is the surrogate for the kinetic energy (k_BT) of a thermal system. The random noise can be thermal in micron scale systems or it can be environmental in macroscopic systems. In a controlled experiment at the laboratory setting, the noise can also be generated with a waveform generator and fed to an oscillator. An accelerometer can be used to estimate the acceleration pulses from which Γ can be estimated. Details of these procedures can be found in our previous publications [43,44].

7.2 Noise induced detachment of the JKR like contact

7.2.1 Spherical contact

The energy barrier and the spring constant needed to estimate the frequency of transition can be obtained from a Taylor series expansion of Eq. 7.1 about a critical point a_i as follows:

$$U - U_o = a \left(\frac{E^* a^3}{3R^2} + \frac{P^2}{3E^* a^3} - \frac{2P}{3R} - 2\pi W \right)\bigg|_P (a - a_i)$$

$$+ \frac{1}{2} \left(\frac{E^* a^3}{R^2} - \frac{P^2}{E^* a^3} \right)\bigg|_P (a - a_i)^2 + \cdots$$

7.3

Setting the first term of the right hand side of equation 7.3 to zero, one obtains the classical JKR [3] equation (Eq. 7.4) that gives two critical values of the contact radius (a_i) - one at the unstable (a_1) and the other at the stable (a_2) position of the energy landscape.

$$W = \frac{\left(\frac{E^* a_i^3}{R} - P \right)^2}{6\pi E^* a_i^3}$$

7.4

Or, equivalently:

$$a_i^3 = \frac{R}{E^*} \left[P + 3\pi W R P \pm \sqrt{6\pi W R P + (3\pi W R)^2} \right]$$

7.5

The curvatures of the potential (second term of Eq. 7.3) around these two (stable and unstable) equilibrium points yield the spring constants that can be expressed as:

$$m\omega_i^2(P) = \left|\left(\frac{E^*a_i^3}{R^2} - \frac{P^2}{E^*a_i^3}\right)\right|$$

7.6

Now collecting all the terms, the frequency of separation of the sphere from the surface in the presence of a negative load P and a noise of strength K can be expressed in terms of the following form of the Kramers equation:

$$\nu(P)$$

$$= \left[\frac{\tau_L}{2\pi m}\sqrt{\left(\frac{P^2}{E^*a_1^3} - \frac{E^*a_1^3}{R^2}\right)\left(\frac{E^*a_2^3}{R^2} - \frac{P^2}{E^*a_2^3}\right)}\right] exp\left[-\frac{2}{mK\tau_L}\left(\frac{E^*(a_2^5 - a_1^5)}{10R^2}\right.\right.$$

7.7

$$\left.\left. + \frac{P^2}{2E^*}\left(\frac{1}{a_2} - \frac{1}{a_1}\right)\right)\right]$$

Note that the term work of adhesion (W) is implicit in equation 7.7, which has been eliminated by combining equations 7.1 and 7.4 in order to obtain a compact form of the exponent.
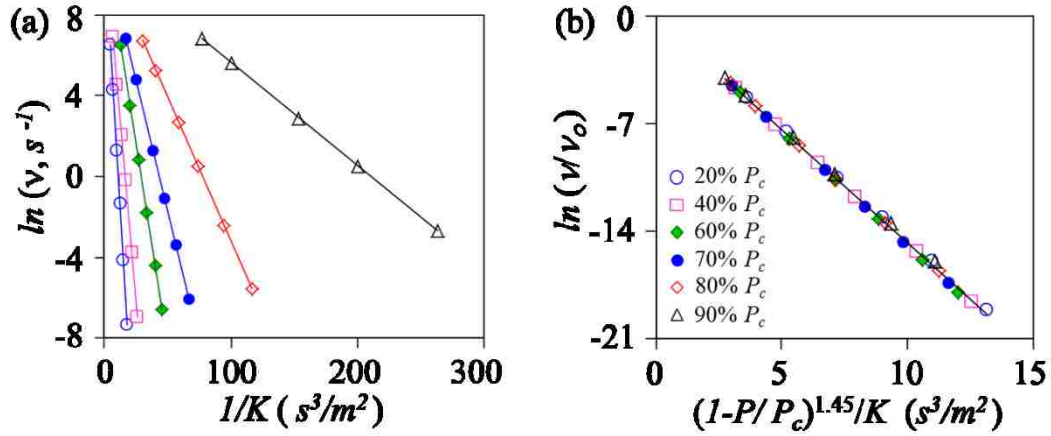
Figure 7.2: (a) Logarithm of the frequency of rupture of a sphere from a flat surface varies linearly with *1/K* at a given load. These calculations were performed with the following parameters: *R*= 100 μm, *E**= 1MPa, *W*=0.04 J/m^2, *m*=4.2 μg and τ_L=0.01 s. (b) collapse of the rupture kinetic data results when ln(v/v_o) is plotted against ($1-P/P_c$)$^{1.45}$/*K*. Similar symbols in figures (a) and (b) correspond to the same load.

With the reasonable values of the material and geometric properties of a soft elastic contact, Eq.7.7 was solved numerically. The results, as summarized in Figure 7.2, show that the logarithm of the rupture frequency is linear with the reciprocal of the noise strength at a fixed value of the applied load that is typical of a Van't Hoff-Arrhenius-Eyring type kinetics. The data obtained at various values of the applied load can also be summarized (Figure 7.2b) using Eq. 7.8:

$$v \approx v_o exp\left[-\frac{2U_b(1-P/P_c)^{1.45}}{mK\tau_L}\right]$$

7.8

Where $U_b = \frac{(6\pi W)^{5/3} R^{4/3}}{10 E^{*2/3}}$ is the depth of the potential well in the absence of the load,

which we identified earlier in the text. The exponent (1.45) of the reduced bias ($1\text{-}P/P_c$)

is close to that (1.5) of Garg's expression [36] and can be verified (approximately) as

well by integrating the following form of the rupture dynamics (see Appendix) with a

noise term γ (t) as follows:

$$\left(\frac{2a}{3R} - \frac{2P}{3E^*a^2}\right)^2 \ddot{a} + \left(\frac{2a}{3R} - \frac{2P}{3E^*a^2}\right)\left(\frac{2}{3R} + \frac{4P}{3E^*a^3}\right)\dot{a}^2 + \frac{E^*a^4}{3mR^2}$$

$$+ \frac{P^2}{3mE^*a^2} - \frac{2Pa}{3mR} - \frac{2\pi Wa}{m} + \frac{4\pi aT\sigma_o^2}{mE^*}\dot{a} = \gamma(t)$$

7.9

While the above analysis has been carried out with a circular contact of a spherical

object, similar analysis can also be performed with other types of contacts as well. For

example, with a flat circular contact [8,45] with a deformable substrate, the total energy

is of the following form:

$$U \approx -\frac{P^2}{3E^*a} - \pi Wa^2$$

7.10

Where a is the radius of contact. For this particular geometry, the barrier energy is:

$$\Delta U(P) \approx Wa^2 \left[0.89 \left(\frac{P}{P_c}\right)^2 \left(1 - \left(\frac{P_c}{P}\right)^{2/3}\right) + 0.44 \left(1 - \left(\frac{P}{P_c}\right)^{4/3}\right)\right]$$

7.11

Numerical evaluation of Eq. 7.11 leads to a barrier height as $\Delta U(P) \sim Wa^2(1 - P/P_c)^2$.

On the other hand, the energy of the contact of a cone [46,47] of semi angle $\pi/2 - \beta$ is:

224

$$U(a,P) = \frac{\pi^2(sec\beta tan^2\beta)E^*a^3}{48} - \frac{P^2 sec\beta}{4E^*a} - \frac{\pi(sec\beta tan\beta)Pa}{4}$$
$$- \pi W a^2 sec\beta$$

7.12

Here, the depth of the potential scales as W^3/E^{*2}. Numerical analysis of Eq. 7.12 shows that the force dependent barrier height is of the form: $\Delta U(P) \sim (W^3/E^{*2})(1-P/P_c)^{1.4}$.

From the above discussions, it is clear that the energy barriers are strong functions of the geometry of the contacting object. While for the sphere and the flat, the energy barrier scales as $W^{5/3}R^{4/3}/E^{*2/3}$ and Wa^2 respectively, it scales as W^3/E^{*2} for the conical contact that lacks a clear geometric length scale. By contrast, the exponent of the reduced bias is close to 2 for the flat contact, whereas it is close to 1.5 for both the spherical and conical contacts. We now explore how the insights gained from these discussions could be useful to understand certain features of the noise induced micro-fibrillar detachments as we witnessed in our previous studies [43,44].

7.3 Rolling of a rigid sphere on a fibrillated rubber

Recently, we studied the behavior of the rolling of a small rigid sphere on a low modulus flat rubber that was decorated with the microfibrils of the same material using a lithographic method [48,49]. A rigid sphere is pinned on such a surface via adhesion to

the   fibrils.
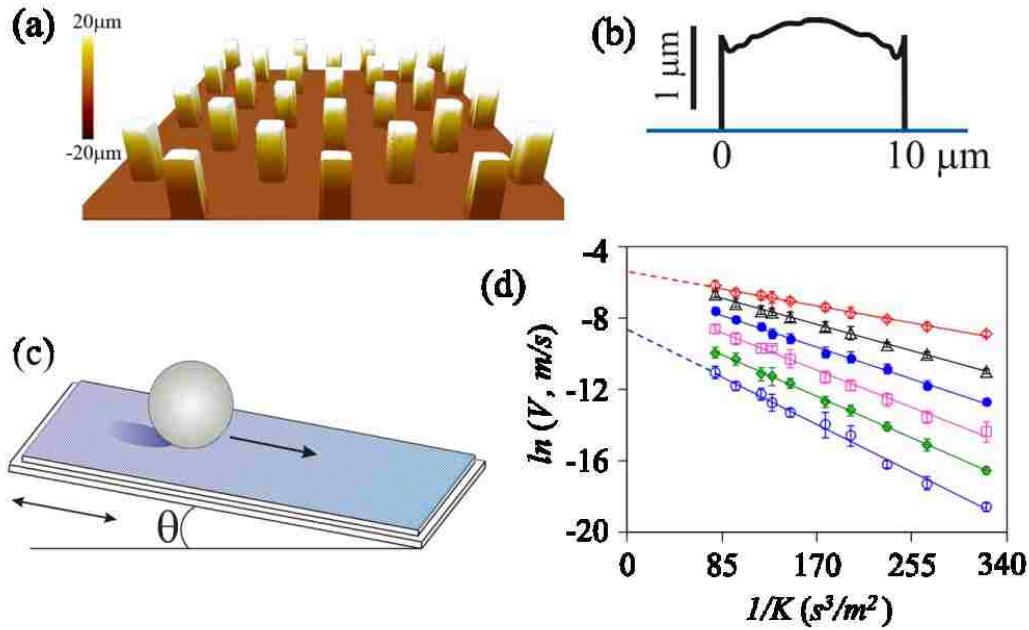
Figure 7.3: (a) 3D Profile of the fibrillar rubber substrate measured with a noncontact optical 3D profilometer (ZeGage with ZeMaps V.1.11, from Zemetrics, Inc.). (b) The profile of the end of a fibril showing that it is slightly curved. The spikes are artifacts arising from the fact that the profilometer failed to follow the edges of the fibrils (c) Schematic of a rigid sphere (a small steel ball of 4 mm diameter and 0.26 gm mass) on an inclined substrate of a silicone rubber (0.6 mm thick with a modulus of 2.2 MPa), from which square fibrils of the same material are projected outwards on a diagonal square lattice at a spacing of 50 μm. In the absence of any noise, the sphere rolls at an angle of about 2.5$^{\mathrm{o}}$. However, with an angle less than 2.5$^{\mathrm{o}}$, the sphere rolls with a velocity that increases with both the noise strength and the bias. (d) At each bias, ln(V) varies linearly with $1/K$. The symbols are as follows. red open diamond ($\Diamond$, 0.078mN), black open triangle (Δ, 0.067mN), filled blue circle ($\bullet$, 0.056mN), open pink square ($\square$, 0.044mN), filled green diamond ($\blacklozenge$, 0.033mN), open blue circle ($\circ$, 0.022 mN). Some of these data were originally reported in reference [45]. However, in this study, we extended the dynamic range of the noise strength by going to even smaller values of K.

When the substrate is inclined above a critical angle ($\theta_c \sim 2.5^{\mathrm{o}}$), the sphere rolls by de-

pinning from the fibrils in the receding edge, but making fresh contact with them at the

advancing edge.

226
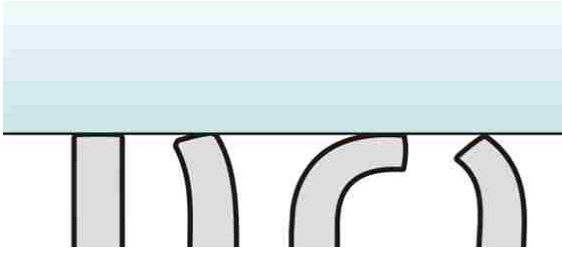
Figure 7.4: Schematic illustrations of the pining and de-pinning events of the fibrils in contact with a rigid sphere.

The ball can also roll sub-critically, i.e. at an angle of inclination $\theta < \theta_c$, provided that it is subjected to an external vibration. In previous publications [43,44], we reported this type of stochastic rolling behavior of a steel ball on a fibrillated rubber substrate, when the later was vibrated parallel to its base with a Gaussian noise. As discussed in references [44] and [50], the torque applied on the ball by the external force about its point of contact with the surface is balanced by the torque due to adhesion. The contact mechanical force due to adhesion is compressive at the advancing edge of contact, but is tensile at its receding edge. From a balance of the two torques, it can be shown that the collective tension caused by all the fibrils, each experiencing a force of magnitude P, is proportional to the applied bias $F\,(= mgsin\theta)$.

The basic observation [44] was that the ball exhibits a stick-roll motion at very low noise strength with the net drift always occurring along the direction of the bias. The rolling velocity of the sphere on the fibrillated rubber could indeed be described by an Arrhenius equation in the sense that $\ln(V)$ is fairly linear with $1/K$ over a substantial dynamic range of the velocity (Figure 7.3d).

In order to analyze this type of rolling dynamics data in the light of the discussion of section 2, we first need to multiply the fibrillar detachment frequency with a length scale in order to obtain the scale of a velocity. This is, however, not a simple proposition as this length scale itself would depend on how effectively the detached sphere is damped. If the damping is weak, the sphere would roll over several fibrillar spacings before being arrested by another set of fibrils.
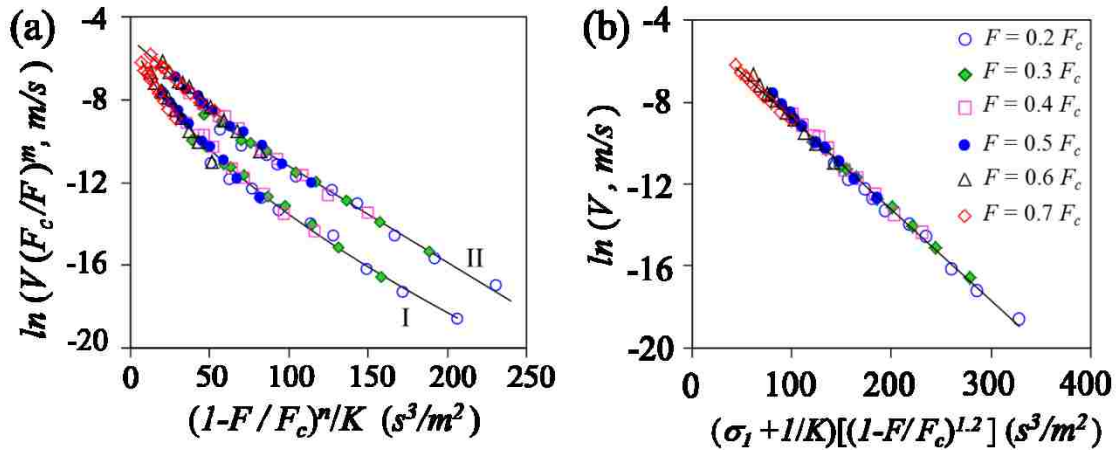
Figure 7.5: (a) Collapse of the rolling velocity data of Figure 7.3. Curve I plots $\ln(V)$ against $(1-F/F_c)^2/K$ and curve II plots $\ln(VF_c/F)$ against $(1-F/F_c)^{1.5}/K$. (b) Collapse of the same data when $\ln(V)$ is plotted against $(\sigma_1 + 1/K)[(1-F/F_c)^{1.2}]$ with σ_1 = 108 s^3/m^2 and F_c= 0.1mN. Similar symbols in figures (a) and (b) correspond to the same load.

With an overdamped system, the sphere could move by only one spacing length (λ) before it is pinned again. If we employ the latter scenario, the rolling velocity ($V=\lambda v$) would depend on F and K in the same way as does the rupture frequency. Thus, V is given by:

$$V/V_o \approx exp\left(-2U_b\left(1-\frac{F}{F_c}\right)^n /mK\tau_L\right) \qquad 7.13$$

Where F is the applied bias. At this juncture, it would be prudent to point out that this form with n=1.5 is also consistent with the ball rolling (see Appendix) on a sinusoidal potential that is, perhaps, the simplest functional (or coarse grained) generalization of the rolling behavior accompanied by the pinning/depinning kinetics, excepting that the fibrillar detachments could lead to an avalanche (discussed in section 4) whereas rolling on a sinusoidal potential does not. Various types of detachment modes are plausible as shown schematically in Figure 7.4. If the termini of the fibrils are truly flat ended, we expect that ln(V) to be proportional to $(1-F/F_c)^2/K$. When treated this way, the data do indeed cluster around a single curve, as was observed by us in a previous publication [44]. The bothersome feature here is that the overall rupture kinetics is non-Arrhenius, which is inconsistent with the observation that the rupture data exhibit an Arrhenius behavior over a significant range of the noise strength (K) at each applied bias. The direct observation of the fibril terminus using an optical profilometer (Figure 7.3b) shows that it is, in fact, rounded with a radius of curvature ~ 40 μm. Thus it is more reasonable to try to collapse the data by plotting ln(V) against $(1-F/F_c)^{1.5}/K$. When attempted this way, good collapse of data (plot II of Figure 7.5a) is obtained only when the drift velocity is divided by the bias. Although the curvature of the collapsed plot now is reduced from that of plot I, the overall rupture kinetics is still non-Arrhenius.

There is however another angle from which to look at these data. Figure 7.3 reveals that all the ln$V$ vs $1/K$ lines needed to fit the experimental data at all the biases, when extrapolated, tend to meet at a point farther to the left quadrant of the plot. A simple way to collapse the data would, therefore, be to first shift the $1/K$ axis to the right by a certain amount and then use this shifted values of $1/K$ to fit the data with an Arrhenius equation. Figure 7.5b shows that this method works remarkably well. The idea of shifting the $1/K$ axis is equivalent to a generalized rupture kinetics of the form

$$V/V_o \sim \exp\left(-\frac{2(U_b + K\sigma)(1 - F/F_c)^{1.2}}{mK\tau_L}\right).$$ There are two issues related to this fit. The

first of which is that the observed exponent (1.2) of $(1 - F/F_c)$ is somewhat smaller than that (1.4 to 1.5) obtained from the simulations and secondly, the barrier energy needs to be modified by an additional entropy like term: $K\sigma$. In the context of a particle escaping from a potential well, Lin *et al* [41] suggested that an exponent of ~ 1 ensues when the applied force is much smaller than a critical force, which is clearly not the case in our current experiments. We believe that our results are influenced by other modes of separation of the fibrils, including peeling (Figure 7.4) that being in a state of undifferentiated equilibrium [8] requires no activation. Postponing a detailed statistical analysis of this kind of mixed mode micro-rupture dynamics for future, we focus here on the other important issue related to the shift of the *1/K* axis that was required to collapse the experimental data.

7.4 Sequential rupture of fibrils

The basic premise here is that the fibrils do not detach all at once. When one fibril detaches from the surface, the load gets distributed to the remaining undetached fibrils thus enhancing the rupture rates of any of the remaining fibrils. The process continues till the load on the remaining fibrils are such that all of them detach ballistically, thus causing an avalanche. Within this scenario, the rupture kinetics may be described by the following equation:

$$\frac{d\phi}{dt} = -\phi v(\phi, P) \qquad\qquad 7.14$$

Where $\phi = \phi(t)$ is the fraction of the total numbers of fibrils that is in contact with the rigid sphere at any time t.   For a spherical contact, $v(\phi, P)$ can be expressed as (see Eq. 7.8):

$$v(\phi, P) \approx v_o(\phi, P) exp\left[-\frac{13.3(W^5 R^4/E^{*2})^{1/3}(1 - P/\phi P_c)^{3/2}}{mK\tau_L/2}\right] \qquad 7.15$$

The total time to rupture can be estimated by integrating equation 7.14 as follows:

$$T = \int_{P/P_c}^{1} \frac{d\phi}{\phi v(\phi, P)} \qquad\qquad 7.16$$
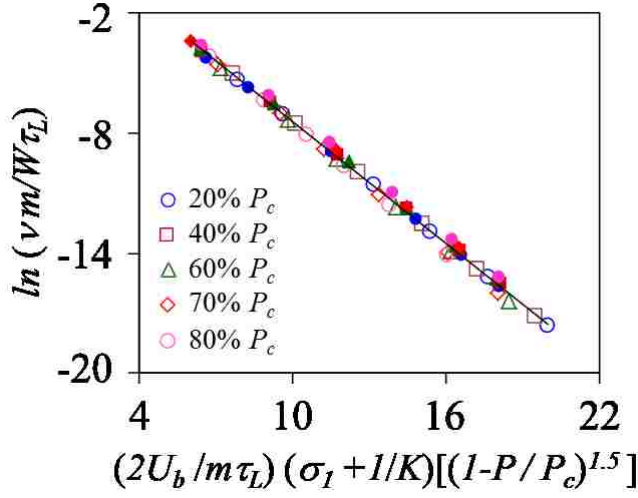
Figure 7.6: Arrhenius plots of the frequency of detachment of multiple fibrils from a surface with a JKR contact. The parameters of these calculations are same as those of Figure 7.2, except that two different values of W (0.04 J/m^2: open symbols; 0.01 J/m^2 filled symbols) were used. The data collapse in one master line when the normalized frequency ln ($\nu m/W\tau_L$) is plotted against $(2U_b/m\tau_L)(\sigma_1 + 1/K)[(1 - P/P_c)^{1.5}]$ where $\sigma_1 = \sigma/U_b$ with the value of σ as 48 pJ s^3/m^2.

By calculating the rupture frequencies (*1/T*) using Eq. 7.14 to 7.16 for two different values of W, we attempted to collapse all the data as follows. First, the rupture frequency was normalized as $m\nu/W\tau_L$, where $W\tau_L/m$ is the characteristic escape frequency of mass *m* fluctuating in the JKR potential (compare equations 7.2, 7.6and 7.8). Next, we modulated $(1 - P/P_c)^{1.5}/K$ with $2U_b/mK\tau_L$ so that the data obtained with different values of W can be collapsed on to a single curve. With these normalizations, Figure 7.6 shows that $\ln(m\nu/W\tau_L)$ is indeed linear with $2U_b(1 - P/P_c)^{1.5}/mK\tau_L$ provided that the horizontal axis is shifted by a constant amount. This analysis thus leads to an equation of

the type shown below that provides partial justification for the shift of the *1/K* axis of the experimental data as was done in Figure 7.5b.

$$\frac{mv}{W\tau_L} \approx exp\left[-\frac{2(U_b + K\sigma)(1 - \frac{P}{P_c})^{1.5}}{mK\tau_L}\right] \qquad 7.17$$

7.5 Discussions and final remarks

The main point of this paper is that the contact formed by the adhesive interaction of a soft deformable object with a rigid substrate can be broken sub-critically in the presence of a noise. This idea of the noise induced dissociation of a soft elastic contact has been useful in understanding some recently reported experimental results [44] of the pinning-de-pinning induced rolling of a rigid sphere on a soft fibrillar substrate. Although, there is a slight discrepancy in the exponent (1.2) of the reduced bias needed to fit the experimental data and that (1.4 − 1.5) expected of the detachment of a spherical contact, the discrepancy is not large. The kinetic analysis provided a new insight in that an "entropy" like term contributes to the energy barrier. Further studies are, however, required in analyzing the mixed mode ruptures of multi-fibrillar contacts in which load is shared by certain modes that are activated and others (i.e. peeling) that are not. Careful experiments with single fibrillar contacts with various other geometries are expected to provide further insights in these types of contact separation problems. The studies presented here could also be useful in understanding the pinning-depinning dynamics in various other types of bio-inspired adhesives and composites as well as understanding the

(thermal) noise induced detachments of cells, macromolecules and soft colloids [51] from surfaces. Study of a noise induced separation of contact of soft materials may also be useful in obtaining the depth of the energy potential which may contrast and complement the conventional fracture mechanics methods of obtaining the strain energy release rates. We believe that noise induced detachments of soft adhesive contact may also find interesting applications in recently emerging transfer printing technologies [47].

7.6 Appendix

7.6.1 Langevin dynamics simulations of the splitting of soft contact

The purpose of this section is to try to recover the result that the energy barrier to rupture a sphere from a rigid flat plate scales with the reduced bias as $(1-P/P_c)^{1.5}$ using a Langevin dynamics simulation. In order to accomplish this objective, our first step is to write down the Lagrangian (L), in terms of the mass (m), elastic displacement (δ) and the energy of the system as

$$L = \frac{1}{2}m\dot{\delta}^2 - U(a)$$

7.18

$$\delta = \frac{a^2}{3R}\left(1 + \frac{2PR}{E^*a^3}\right)$$

7.19

$U(a)$ is the thermodynamic potential energy, which is given by Eq.7.1. Now, solving the Lagrangian equation (Eq. 7.18), we obtain the crack growth equation with a frictional dissipation as in Eq. 7.20.

$$\frac{\partial}{\partial t}\left(\frac{\partial L}{\partial \dot{a}}\right) = \frac{\partial L}{\partial a} - \frac{\partial \varepsilon}{\partial \dot{a}}$$

7.20

Where ε is the energy dissipation function $G\frac{dA}{dt}$, where $G\left(\sim \sigma_0^2 T\dot{a}/E^*\right)$ is the energy release rate in the linear friction regime [52] and $A=\pi a^2$. Here, T is the relaxation time of the adhering polymer chains, σ_o is the cohesive stress , and E^* is the contact modulus. Now solving Eq. 7.20 and adding a noise term $\gamma(t)$, we have the Eq. 7.9 of the text:

$$\left(\frac{2a}{3R} - \frac{2P}{3E^*a^2}\right)^2 \ddot{a} + \left(\frac{2a}{3R} - \frac{2P}{3E^*a^2}\right)\left(\frac{2}{3R} + \frac{4P}{3E^*a^3}\right)\dot{a}^2 + \frac{E^*a^4}{3mR^2}$$
$$+ \frac{P^2}{3mE^*a^2} - \frac{2Pa}{3mR} - \frac{2\pi Wa}{m} + \frac{4\pi aT\sigma_o^2}{mE^*}\dot{a} = \gamma(t)$$

7.21

Although a more exact form of the friction is non-linear with the crack velocity [52], the linear friction model as used above is useful for capturing essential physics of the rupture dynamics that can be compared with a Kramers' model. In the current simulation, we treat the term $4\pi T\sigma_o^2/E^*$ of equation 7.21 as an empirical parameter. A computer generated [43] Gaussian random noise was used to integrate Eq. 7.21 using a fixed load

condition. Logarithm of the rupture rate at each load was linear with $1/K$. All the rupture data can be collapsed (Figure 7.7) by plotting $\ln(v/v_o)$ against the reduced bias as $(1-P/P_c)^{1.38}/K$. Note that that the exponent of the reduced bias is slightly smaller than 1.5.
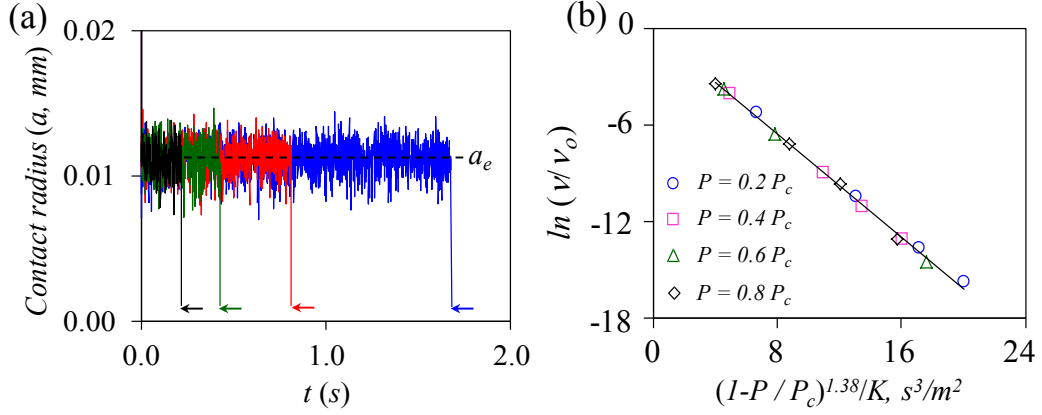
Figure 7.7: (a) The fluctuation of the radius (a) of contact about a mean value (a_e) is obtained from the simulations based on Eq. 7.21. The contact falls apart eventually (indicated by the arrows). From the mean value of the watiting times, a rupture frequency was estimated. (b) Summary of the rupture kinetics data using Langevin dynamics simulations (Eq. 7.21). These calculations were made using the following parameters: R= 100 μm, E*= 1MPa, W=0.04 J/m2, m=4.2 μg with a friction term of Eq. (7.21) i.e. $(mE*/4\pi\sigma_o^2T)$ set as 12 ns.m.

7.6.2 Motion over a periodic potential

Motion of a particle over a periodic potential was used by Prandtl [20] to study the nature of friction. This model is also generic to study the motion of particle in a tilted potential [53]. Here, we consider a translational form of the stochastic rolling equation of motion of the sphere on a periodic potential of wavelength λ :

$$\frac{7}{5}\frac{dV}{dt} + \frac{V}{\tau_L} + \frac{\pi U_b}{m\lambda}cos\frac{2\pi x}{\lambda} = \frac{F}{m} + \gamma(t) \qquad\qquad 7.22$$

$$\frac{dx}{dt} = V \qquad\qquad 7.23$$

Here, F (=$mgsin\theta$) is the force acting through the center of gravity of the sphere parallel to the substrate. The force P acting on each fibril is proportional to F through a geometric factor.
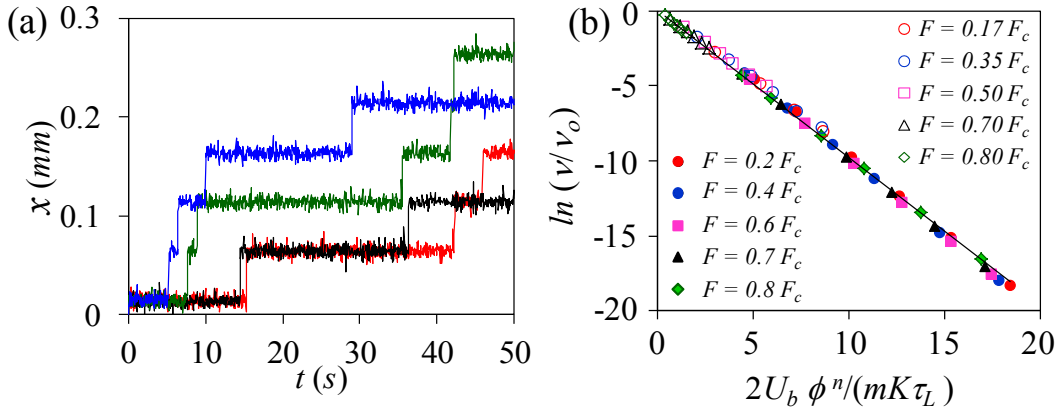
Figure 7.8: (a) Typical trajectories of a sphere moving over a sinusoidal potential in the presence of a bias and an external noise. From the mean value of the waiting times, a barrier crossing frequency was estimated. (b) Comparison of rolling kinetics data as obtained from Langevin simulation (Eq. 7.22) (open symbols) and Kramers' formalism (Eq. 7.7) (filled symbols). ϕ is the reduced bias. The value of n is 1.4 for the Kramers' calculations and 1.5 for the rolling using Langevin dynamics. For the Kramers' calculations, the parameters are same as those of Figure 7.2, while for the Langevin dynamics simulations, the following parameters were used: λ= 50 µm, τ_L=0.001 s, h= 1.6 µm, U_b = 0.06 pJ.

Using a computer generated Gaussian random noise, Eq. 7.22 and 7.23 were integrated with a fixed value of the reduced bias: $\phi = 1 - F/F_c$. From the trajectories generated at each noise strength, the drift velocity was estimated directly. Logarithm of this drift velocity is linear with $1/K$ at each value of ϕ. Now, the data collected at different values of K and ϕ were normalized by plotting $\ln(V/V_o)$ against the reduced bias as $2U_b\phi^{1.5}/K$. This result was compared with the prediction of the fibril detachment model using Kramers theory in which $\ln(V/V_o)$ was plotted against $2U_b\phi^{1.4}/K$ with the value of U_b as $13.3\dfrac{W^{5/3}R^{4/3}}{E^{*2/3}}$.

Figure 7.8 shows that the both set of data collapse on to a single curve thus demonstrating the rolling on a potential well is functionally equivalent to that accompanied with the detachment of fibrils.

References:

[1]   K. Kendall, *Molecular Adhesion and Its Applications* (Kluwer Academic/ Plenum Publishers, New York, 2001).

[2]   J. E. Gordon, *The New Science of Strong Materials* (Princeton University Press, Princeton, 1976, 1976).

[3]   A. Jagota and C.-Y. Hui, Materials Science and Engineering: R: Reports **72**, 253–292 (2011).

[4]   R. Thomson, C. Hsieh, and V. Rana, Journal of Applied Physics **42**, 3154 (1971).

[5]   R. Thomson and E. R. Fuller, Bull. Am. Phys. Soc. **22**, 443 (1977).

[6]   K. Kendall, Proceedings of the Royal Society A: Mathematical, Physical and Engineering Sciences **341**, 409 (1975).

[7]   K. L. Johnson, *Contact Mechanics* (Cambridge University Press, UK, 1985).

[8]   D. Maugis, *Contact, Adhesion and Rupture of Elastic Solids,* (Springer-Verlag, Solid- State Sciences, Berlin, 2000).

[9]   V. L. Popov, *Contact Mechanics and Friction* (Springer-Verlag Berlin Heidelberg, 2010).

[10]   K. L. Johnson, K. Kendall, and A. D. Roberts, Proc. R. Soc. Lond. A. **324**, 301–313 (1971).

[11]   V. M. Muller, V. S. Yushchenko, and B. V. Derjaguin, J Colloid Interface Science **92**, 92 (1983).

[12]   M. E. R. Shanahan, J Adhesion **79**, 881 (2003).

[13]   D. Maugis and M. Barquins, J Phys D: Appl. Phys. **16**, 1843 (1983).

[14]   J. Shi, S. Müftü, and K. Wan, Journal of Applied Mechanics **79**, 041015 (2012).

[15]   J. B. Pethica and A. P. Sutton, Journal of Vacuum Science & Technology A: Vacuum, Surfaces, and Films **6**, 2490 (1988).

[16]   J. R. Smith, G. Bozzolo, A. Banerjea, and J. Ferrante, Physical Review Letters **63**, 1269 (1989).

[17]   P. Attard and J. Parker, Physical Review. A, Statistical Physics, Plasmas, Fluids, and Related Interdisciplinary Topics **50**, 5145 (1994).

[18]   J. N. Israelachvili, *Intermolecular and Surface Forces*, Third edit (Academic press,, 2011).

[19]   H. Eyring, The Journal of Chemical Physics **4**, 283 (1936).

[20]   L. Z. Prandtl, Angew Math. Mech. **8**, 85 (1928).

[21]   M. Brillouin, *Notice Sur Les Travaux Scientifiques* (Gauthier-Villars, Paris, 1904).

[22]   G. A. Tomlinson, Philosophical Magazine **7**, 905 (1929).

[23]   A. Schallamach, Wear **6**, 375 (1963).

[24]   C. Caroli and P. Nozieres, in *Proceedings of the NATO Advanced Research Workshop and Adriatico Research Conference*, edited by B. N. J. Persson and E.

Tosatti (Nato Science Series E: (closed), Vol. 311, Miramare, Trieste, Italy, June 20-23, 1995), p. 7923.

[25] B. N. J. Persson, Phys. Rev. B **51**, 1995 (1995).

[26] B. N. J. Persson, *Sliding Friction: Physical Principles and Applications*, 2nd ed. (Springer, Berlin; New York, 2000).

[27] M. Srinivasan and S. Walcott, Physical Review E **80**, 046124 (2009).

[28] M. Müser, Physical Review B **84**, (2011).

[29] A. K. Singh and V. A. Juvekar, Soft Matter **7**, 10601 (2011).

[30] T. D. Blake and J. M. Haynes, Journal of Colloid and Interface Science **30**, 421 (1969).

[31] B. Lawn, *Fracture of Brittle Solids - Second Edition* (Cambridge University Press, 1993).

[32] G. Bell, Science **200**, 618–627 (1978).

[33] E. Evans and K. Ritchie, Biophysical Journal **72**, 1541 (1997).

[34] H. A. Kramers, Physica VII 284–304 (1940).

[35] R. Zwanzig, *Nonequilibrium Statistical Mechanics* (Oxford University Press, New York, 2001).

[36] A. Garg, Phys. Rev. B **51**, 15592 (1995).

[37] A. Ghatak, K. Vorvolakos, H. She, D. L. Malotky, and M. K. Chaudhury, The Journal of Physical Chemistry B **104**, 4018–4030 (2000).

[38] O. K. Dudko, G. Hummer, and A. Szabo, Proceedings of the National Academy of Sciences of the United States of America **105**, 15755–60 (2008).

[39] O. K. Dudko, a E. Filippov, J. Klafter, and M. Urbakh, Proceedings of the National Academy of Sciences of the United States of America **100**, 11378–81 (2003).

[40] L. B. Freund, Proceedings of the National Academy of Sciences of the United States of America **106**, 8818–23 (2009).

[41] H.-J. Lin, H.-Y. Chen, Y.-J. Sheng, and H.-K. Tsao, Physical Review Letters **98**, 088304 (2007).

[42] D. J. Lacks, J. Willis, and M.-P. Robinson, The Journal of Physical Chemistry. B **114**, 10821–5 (2010).

[43] P. S. Goohpattader, S. Mettu, and M. K. Chaudhury, The European Physical Journal. E, Soft Matter **34**, 120 (2011).

[44] P. S. Goohpattader and M. K. Chaudhury, The European Physical Journal. E, Soft Matter **35**, 67 (2012).

[45] K. Kendall, J Phys. D: Appl. Phys. **4**, 1186 (1971).

[46] D. Maugis and M. Barquins, J. PHys. Lett **42**, 95 (1981).

[47] S. Kim, J. Wu, A. Carlson, S. H. Jin, A. Kovalsky, P. Glass, Z. Liu, N. Ahmed, S. L. Elgan, W. Chen, P. M. Ferreira, M. Sitti, Y. Huang, and J. a Rogers, Proceedings of the National Academy of Sciences of the United States of America **107**, 17095 (2010).

[48] N. J. Glassmaker, A. Jagota, C. Hui, W. L. Noderer, and M. K. Chaudhury, Proceedings of the National Academy of Sciences **104**, 10786 (2007).

[49] W. L. Noderer, L. Shen, S. Vajpayee, N. J. Glassmaker, A. Jagota, and C.-Y. Hui, Proceedings of the Royal Society A: Mathematical, Physical and Engineering Sciences **463**, 2631 (2007).

[50] J. a Greenwood, K. L. Johnson, S.-H. Choi, and M. K. Chaudhury, Journal of Physics D: Applied Physics **42**, 035301 (2009).

[51] P. Sharma, S. Ghosh, and S. Bhattacharya, Nature Physics **4**, 960–966 (2008).

[52] J. a Greenwood, Journal of Physics D: Applied Physics **40**, 1769–1777 (2007).

[53] H. Sakaguchi, Journal of the Physical Society of Japan **75**, 124006 (2006).

8. CHAPTER EIGHT: Activated Drops[7]

8.1 Introduction

While many macroscopic transport processes are described satisfactorily within the scope of continuum hydrodynamics, there are a broad range of phenomena that call for an intermediate level description of continuum mechanics and activated rate theories. Such is the case with the dynamics of wetting [1–5] or the broader classes of stick-slip instabilities and avalanches [6–10] as found in disturbed granular packing and plastic flow of amorphous solids. An intriguing recent finding in this field of research is what is known as self-generated noise that can affect the flow behavior of disordered systems [11,12]. In wetting dynamics, we have already reported [13] how the coalescence of condensing droplets leads to a self-generated noise, in which the coalescing droplets undergo a random motion on a surface due to the internal gradient of Laplace pressure. If there is an external field, such as a gradient of wettability or temperature, the condensed drops drift towards a prescribed direction with its rate controlled by the difference between the temperatures of the steam and the substrate. Such types of self-generated noise field can supply so much energy to the drops that they completely overcome the surface pinning forces, which can be used for efficient removal of drops in various engineered systems such as micro-heat transfer and heat pipe technologies [13,14]. The purpose of this paper is to report a new type of self-generated

---

[7] This work has been published as: M. K. Chaudhury and P. S. Goohpattader; *Activated drops: self-excited oscillation, critical speeding and noisy transport.* Submitted to Eur. Phys. J. E, *36*,15 (2013).

noise that is brought about by the depinning of a liquid drop from a fibrillar superhydrophobic surface in the presence of a small external force. The noise generated from such events can even give rise to a self-excited structural oscillation of the drop. This is an intriguing observation that deserves detailed study with respect to understanding the relaxation behavior of the three phase contact line as well as for further exposition of various models [1–5,15] that underpin the view that the motion of contact line on a surface is facilitated by thermal fluctuation.

Beginning with the original idea of Dettre and Johnson [16] that the air between the asperities of a rough surface cannot be displaced by water when its roughness exceeds a critical value, there has been an explosion of research [17–27] surrounding a class of surface that are categorically called as "superhydrophobic". A timely review of the subject can be found in [28]. The term "fakir state" is coined by Mahadevan [29] to indicate the state of a liquid drop that is virtually suspended on the posts or pillars of a structured substrate, as would a legendary "fakir" support himself on a bed of nail. There always is a globally minimum free energy state for such a drop to assume. However, the metastable energy barriers [16,30,31] due to defects arrest a drop farther from such a state. Dettre and Johnson [32] suggested that the angle that a drop can display on such a surface depends on the depth of the metastable states as well as the vibrational state of a drop. While certain equations [33,34] can be used to predict the contact angle corresponding to a globally minimum state on a non-ideal surface, Good [35,36] pointed out that an additional term representing the energy barrier of the metastable state (that is related to the contortional energy of the contact line) must be taken into account to

predict the maximum advancing and receding angles of a drop. Joanny and de Gennes [37] as well as Pomeau and Vannimenus [38] showed that the elastic property of the contact line in conjunction with its non-linear interaction with a defect give rise to a bistable state that is the root cause of hysteresis. Later, these methodologies have been further extended [39,40] to study the critical wetting dynamics slightly above a threshold force in terms of the quenched disorder, fluctuation of local spreading coefficient and the stiffness of the contact line. In many ways, the state of the affair of a drop interacting with the morphological or energetic heterogeneities is similar to that of molecules interacting with a substrate through a corrugated molecular potential. Just as the thermal fluctuation can activate the motion of the molecules near the contact line on a smooth surface [1], a random external vibration [5] can activate the motion of the pinned contact line on a non-ideal surface.

The subject of our story begins with a curious observation that a small (5-20 μl) droplet of water, glycerin or their mixture displays an unusually complex dynamics on a micro-pillared surface. Very small (~ 5 μl) droplets do not move, whereas a slightly larger (10 μl) droplet exhibits the interesting critical dynamics in that it does not move for quite some time, but then suddenly, it runs away from the pinned location with a substantial speed. As can be expected, the larger drops sprint away rather freely on such a surface without much ado. Understanding the behaviors of the small droplets constitute the central theme of this research. It became rather clear from the outset of this investigation that the conventional hydrodynamics, in itself, may be incapable of providing adequate

description of such a complex dynamics and that it calls for an intervention of statistical mechanics, especially within the scope of an activated rate theory. Once this line of reasoning developed further, it became natural to inquire how such a dynamics would depend on the viscosity of the liquid as well as the temperature. Since it is impractical to vary the thermodynamic temperature of a liquid drop without affecting its physical properties, we resorted to using a mechanical noise. The energy scale of a mechanical noise is such that the activated depinning dynamics of the contact line could be studied by varying its intensity in a systematic way. What was revealed to us is that the dynamics of a drop of water, or up to a 50% solution of water and glycerol, falls within the scope of the low friction limit of the Kramers' [41,42] barrier crossing rate, in which Ω_o increases with solvent friction. This scenario gained additional support from a barrier crossing experiment in which the drops were forced to cross a barrier at different noise intensities.

8.2 Experimental section

8.2.1 Materials

The liquid used for the experiments was either deionized water or various solutions of water and glycerin (Fisher Chemical, CAS 56-81-5, 100%). The viscosities of these liquids, measured with Ubbelohde viscometer (Cannon Instrument company) under ambient condition (25^0C and 48% relative humidity) were 1, 1.6, 3.4, 5.3, 9.4, 18.6, 47, 168, 468 and 1040 mPa-s $(\pm 1\%)$, for pure water and 20, 40, 50, 60, 70, 80, 90, 95 and 100 weight percent of glycerin in water respectively. The viscosities of these liquids

245

agreed with the literature values [43], except for the nominally pure glycerin, for which the measured viscosity was slight less than the literature value (1260mPa-s) suggesting that it absorbed a small amount of water soon after the highly hygroscopic glycerin was exposed to the atmosphere. The surface tensions of these liquids that were used for the drop dynamics studies were 71.9, 70.8, 69.7, 68.6, 68.0 and 64.4 mN/m $(\pm 0.1\%)$ for pure water and 20, 40, 50, 60 and the nominally 100 weight percent of glycerin respectively as obtained from a Wilhelmy plate method. All these values are also in good agreement with those reported in literature.

The principal test surfaces were micro-fibrillated PDMS rubber (Sylgard 184, Dow Corning), which were prepared using the methods described in several recent publications [44–46]. Two types of silicone rubbers with a base thickness of 0.6mm had square fibrils (10μm width and 25 μm height) on a square diagonal lattice, which were separated by 50 μm and 95 μm respectively (fig. 2) respectively. Another surface was hydrophobized silicon wafer (Silicon Quest International), which were silanized by reacting them with the vapor decyltrichlorosilane (CH_3-$(CH_2)_9$-$SiCl_3$, Gelest Inc.) following the methods described previously [5]. The silanized silicon wafers were hydrophobic with advancing and receding contact angles of 107^0 and 97^0 respectively.

8.2.2 Methods

Fibrillated PDMS rubber surface was placed on a clean glass slide, which was then fixed to an aluminum stage as described previously [47]. The stage itself was attached to the stem of a mechanical oscillator (Pasco Scientific, model no. SF-9324) having the

provision of tilt and three dimensional translation with the help of a precise goniometer (CVI Melles Griot, Model No: 07 GON 006) and a XYZ translator (CVI Melles Griot, Model No: 07TXS224, 07TEZ204). Water drops of volumes ranging from 5µl to 20µl were placed on the test substrates and their motions were recorded with either a low speed (30 fps) Sony camera (DCR HC-85 NTSC) to obtain the displacement versus time trajectories (fig. 1) or with a high speed (500-2000fps) camera (Redlake motion Pro) for detailed examination of motion with the help of a 'Midas 2.0 XCITEX' motion tracking software. In some experiments, 10µl liquid drops of different viscosities were placed on a slightly inclined (2^0) fibrillar PDMS surface. While these drops did not move spontaneously at such an inclination, they crept steadily when they were excited with low intensity random mechanical noises applied parallel to the substrate. In another experiment, a small physical defect was induced in the rubber, by placing a thin wire underneath the substrate. A liquid drop usually does not move over such a defect, unless it is excited by an external noise. The details of the apparatus and the measurement methods can be found in the recent publications [44–46,48,49]. However, certain essential details of these measurements will be given when appropriate in the text to follow.

8.3 Results and Discussion:

8.3.1 Critical dynamics of liquid drops on a fibrillar surface:

When a small water drop (10 μl) is placed on a fibrillated PDMS surface, it does not move till the surface is tilted to or above 10°. At this critical inclination, the drop exhibits very slow motion for a substantial period of time, following which, it suddenly accelerates and subsequently reaches a steady velocity (Figure 8.1a).
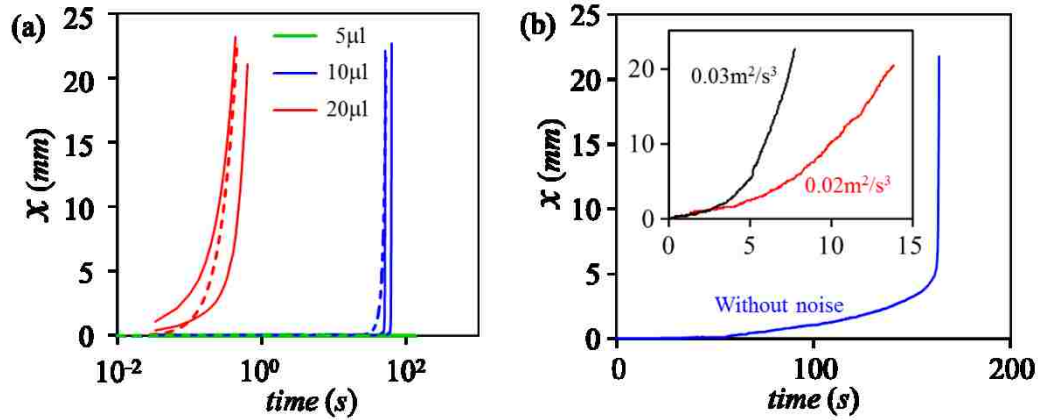
Figure 8.1: (a) Trajectories of water drops on a 100 inclined fibrillar PDMS substrate. A 5 μl drop does not move on such a surface even after several minutes. A 10 μl drop moves very slowly for about 100s, above which it accelerates and sprints off the substrate. For even a larger drop size (i.e. 20 μl), the drop starts accelerating with negligible pause time. These types of dynamics can be predicted by equations 8.1 and 8.2 with the following sets of parameters (n=0.24 and Vc=0.02m/s for all the drops and, τ_L=0.5,0.8 and 1.3s, Δ_1=2.5, 1.6 and 1.0m/s², Δ_2=0.16, 0.1 and 0.07m/s², for 5, 10 and 20 μl drops respectively). The solid and dotted line represent experimental and simulated (using Eq. 8.1 and 8.2) trajectories respectively. (b) These plots show that a 10 μl drop sprint off a 10^0 inclined surface, when it is excited with a random mechanical vibration. The speed increases with the intensity of the noise. The results for two different noise strengths (0.02 m²/s³ and 0.03 m²/s³) are shown.

In a recent manuscript, Pomeau and Le Berre [50] discussed the possibility of a critical speeding-up dynamics in the sliding motion of a solid block on a solid support by invoking a state and rate dependent law of friction. A functionally equivalent model in our system is to consider two types of pinning forces acting on the liquid drop. One of these forces (Δ_1) is independent of velocity, while the other (Δ_2) depends on a contact time dependent interaction between the liquid and the substrate. The latter force may arise from surface reconstructions in which some hydrophilic groups diffuse to the surface after it senses a nearby polar environment [51]. Once bloomed to the surface, these groups can interact with the drop via by specific hydrogen bonding forces that via spatial disorder can pin the drop. As the drop starts rolling, the specific bonds are broken at the trailing edge (depinning), while new bonds are formed at the advancing edge. The residence time (τ_r) of the drop, which is the ratio of the width (w) of the drop to its velocity ($V(t)$), determines how many bonds are formed and thus the strength of the interaction. As long as the time of contact is larger than a critical time scale τ_c (= w/V_c, V_c being a critical velocity), there is enough time for interfacial reconstruction to occur and thus the drop experiences the pinning resistance. However when the residence time is smaller than τ_c, the functional groups do not have enough time to diffuse to the surface and the drop is not obligated to submit itself to a pinning force. These ideas may be captured in two semi-empirical equations of motion (equations 8.1and 8.2) of the drop -- one applies when $V(t)<V_c$ (pinning by chemical interaction) whereas the other applies when $V(t) >V_c$ (no pinning by chemical interaction).

$$\frac{dV(t)}{dt} + \frac{V(t)}{\tau_L} + \Delta_1 + \Delta_2 \left(1 - \frac{V(t)}{V_C}\right)^n = \bar{\gamma}, \qquad V(t) < V_C \qquad\qquad 8.1$$

$$\frac{dV(t)}{dt} + \frac{V(t)}{\tau_L} + \Delta_1 = \bar{\gamma}, \qquad V(t) > V_C \qquad\qquad 8.2$$

Where n is an exponent that determines how quickly the chemical interaction term vanishes as the critical velocity is approached, τ_L is the Langevin relaxation time and $\bar{\gamma} = g \sin \theta$ is the gravitational bias acting on the drop.

Numerical solution of Eq. 8.1and 8.2 with certain adjustable values of V_c, Δ_1, Δ_2, τ_L and n reproduces the critical dynamic behavior of the drop observed experimentally; it also predicts correctly the fact that the sticking period of the drop is reduced as the size of the drop (thus its inertia) is increased (Figure 8.1a). This is so as both Δ_1 and Δ_2 increase linearly with the width of the contact, but decrease with the volume (V), i.e. $\Delta_1, \Delta_2 \sim V^{-2/3}$ whereas the Langevin relaxation time (the ratio of the mass to kinematic friction coefficient) increases with the volume (V) of the drop as $\tau_L \sim V^{2/3}$. Even though this trend is predicted correctly, there is a significant variation in the time required for the critical speed up to occur for any drop. This stochastic nature of the transition of the drop from a slow to a fast regime suggests that it is governed by noise of some sort. What is the source of this noise? We show below that this noise is self-generated and it comes from the co-operative de-pinning of the contact line from the tips of the fibrils.
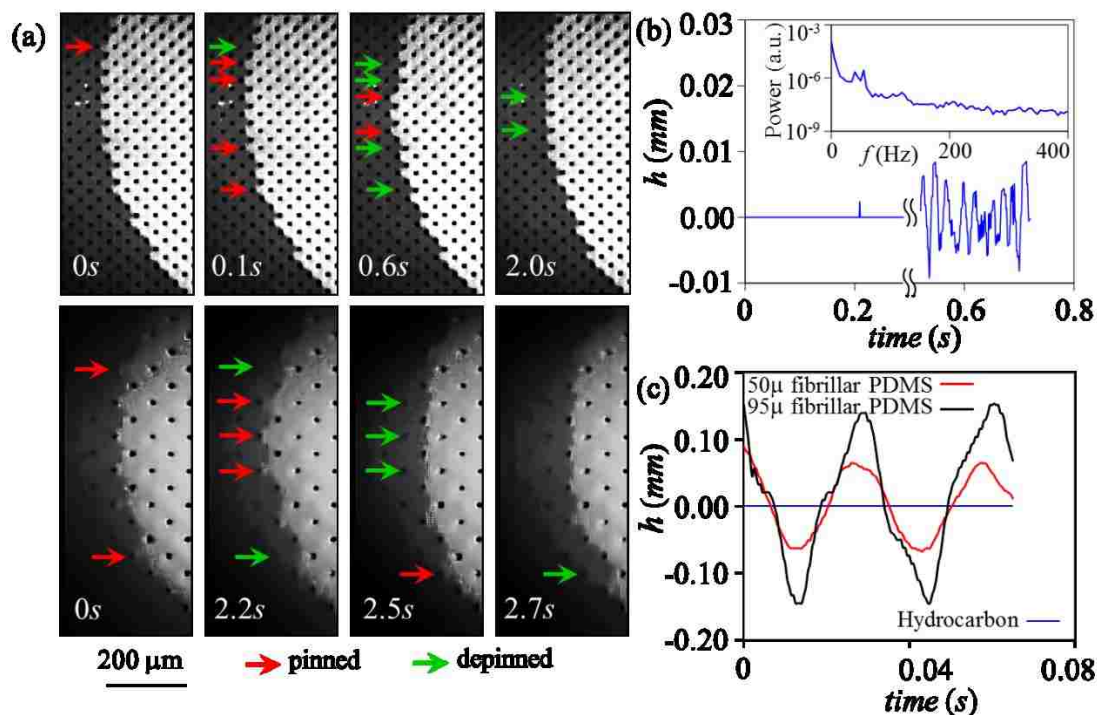
Figure 8.2: (a) Microscopic images showing the de-pinning sequences of the contact line of a drop from a fibrillar surface. The upper and lower panels correspond to fibrillar spacings of 50μm and 95μm respectively. The contact line is significantly rougher on the surface with larger spacing between the fibrils. (b) Typical trace of the height fluctuation of a 10 μl drop of water on a surface with 50 μm spacing (referenced to the height in the quiescent state). This trace depicts that there is no fluctuation of the drop when it is in the quiescent state; however, considerable fluctuations are generated as the drop sprints off the surface. The power spectrum (inset) shows the resonance modes of the drop. (c) Height fluctuation of a 20μl water droplet on a 10^0 inclined PDMS with two different fibrillar spacings. The drop moving on a surface with larger fibrillar spacing shows larger fluctuation. By contrast, no fluctuation is observed when the drop moves on a featureless surface (a silicon wafer that was hydrophobed by silanization).

Indeed, detailed microscopic observations reveal that the contact line undergoes a series of depinning, roughening and avalanche events even when the drop appears to be quiescent to the naked eye (Figure 8.2a). The disturbances generated in the drop by these

events are dissipated when its frequency of occurrence is small. However, when the de-pinning events occur at a rapid rate, the resulting noise coalesces and leads to a structural oscillation of the drop (Figure 8.2b). Various resonance modes of the drops are evident in the power spectra of their height fluctuations, the background of which displays a $1/f^{1.6}$ noise. Large structural oscillations are observed with larger size drops (20 µl), the intensity of which depends on the spacing between the fibrils. Even though there is some of vibration introduced to such a drop as it is released from the needle used to deliver it to the substrate (appendix: Figure 8.10), this oscillation is magnified when the drop sprints on the surface with larger fibrillar spacing. On the other hand it is, at least, sustained on the surface with the smaller spacing. None of this oscillation is evident on a featureless hydrophobic surface within the limitation of our experimental technique (Figure 8.2c). An obligatory control study shows that the resonance peaks that are observed with a liquid drop are absent with a rigid glass sphere rolling on such a fibrillar surface (appendix: Figure 8.11). The above results are, therefore, novel examples of a self-generated noise that leads to a structural oscillation of the drop. Since a shape fluctuation itself can mitigate the pinning effects, it may be a significant contributing factor to the critical speeding dynamics as discussed above. There are many dynamically complex systems [52] that exhibit abrupt transition from one state to another. One topic of current research is how can a catastrophe be forewarned [52] by studying the fluctuations and the correlations of certain system level properties. In what we presented here, the growth of the flickering noise due to depinning could be such an indicator, with which the subject of the critical dynamics can be studied in detail. That the noise could play a role

in such type of dynamics is further revealed in a simple experiment where a drop was exposed to a small intensity external vibration. Here, the stick phase disappears completely and the drop accelerates no sooner than the noise is applied (Figure 8.1b). When the same type of noise is applied to the drop on a sub-critically inclined substrate, it moves steadily without any acceleration. We report below the results of an investigation on how such a sub-critically inclined drop responds to external noise, and how its motion is promoted or retarded by the liquid viscosity.

8.3.2 Effect of viscosity on critical drift velocity:

The critical speeding dynamics with water drops as discussed above was also observed with various solutions of water and glycerol. These solutions were selected because their surface tensions do not differ to a great extent from each other and that they all exhibit similar type of wettability on the fibrillar surface. The facile parts of the dynamics of these liquids (Figure 8.3) displays the unusual feature that the velocity of a drop first increases with viscosity, reaches a maximum and then it decreases. One may attempt to capture the physics of this unusual phenomenon by assuming that these drops undergo a sliding to rolling type transition with viscosity by borrowing a concept proposed by Mahadevan and Pomeau [53]. Although, such an insight may be valuable in partial understanding of results of our experiments, we note that the drop velocity neither increases, nor decreases, monotonically with viscosity, i.e. the observed maximum is not easily explained within the scenario of a sliding to rolling transition alone. Furthermore, microscopic examination reveals that all these drops undergo very similar pinning-depinning behaviors, roughening and sudden relaxations of the contact line as they move

on. Stepwise relaxation of a contact line has also been reported recently on structured

hydrophobic surfaces [54].
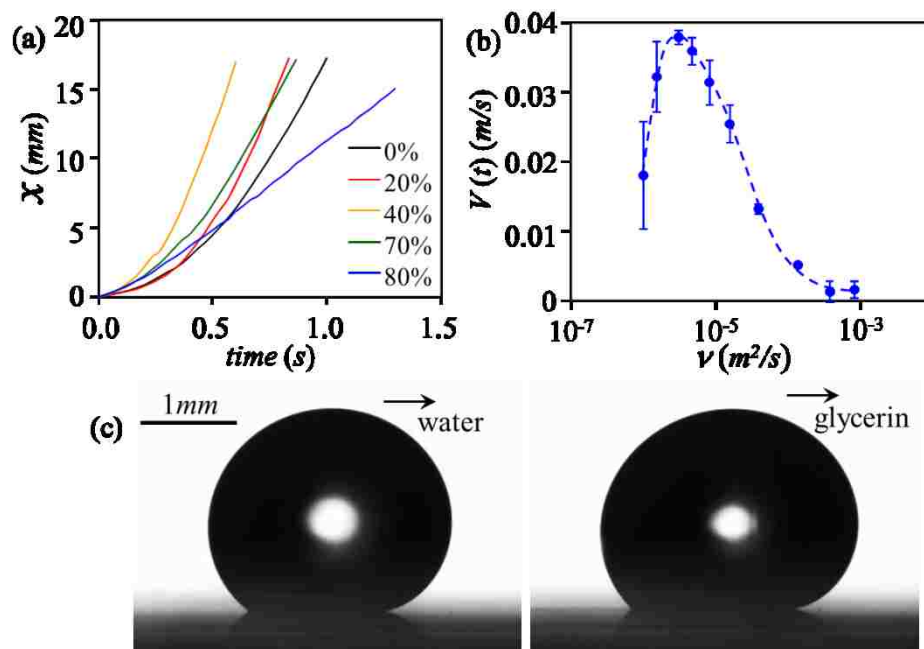
Figure 8.3: (a) Sample trajectories of liquid drops of water and the solutions of glycerin and water on a 10^0 inclined PDMS substrate that had the fibrillar spacing of 50 μm. In these trajectories, the initial pause periods are not shown. The compositions of the solutions in terms of the percentage of glycerin in water are stamped inside the figure (b) Drift velocities as measured from the displacement-time trajectories at long time limit are shown in terms of the kinematic viscosity of the glycerin water solutions. (c) Video micrographs of a 10 μl drop of water and glycerol slowly moving on a fibrillar PDMS surface of 50 μm spacing, inclined by an angle of 10^0. Advancing and receding contact angles are 160^0 and 139^0 for water and 162^0 and 139^0 for glycerin respectively.

A recent study [55], in fact, showed that the dynamics of the droplet motion can be

satisfactorily explained using a molecular kinetic model of thermal activation in the light

of what was proposed four decades ago by Blake and Haynes [1] and Cherry and

Holmes [2]. If indeed such type of drop dynamics could be viewed as an activated

process, then we are poised to ask how it fits the well-known theory of barrier crossing that was expounded by Kramers [41].

In a typical barrier crossing problem, Kramers [41,42] considered two limits. The first limit corresponds to that of strong friction, in which the dynamics is controlled by spatial diffusion. The other limit is that of weak friction, in which diffusion occurs in the action coordinate. The analysis led to the prediction that the rate of a kinetic process first increases with friction; after reaching a maximum value, the rate decreases with friction. Various physico-chemical processes, such as isomerization kinetics of *trans*-stilbene [56], protein folding [57], and positron annihilation [58] rate have now provided strong support in favor of what is known as Kramers Turnover rate. In view of the significant similarity between the solvent viscosity dependent drop velocity and the above described turnover kinetics, it is tempting to consider the implications of Kramers formalism in the context of what we observed with the drops.

8.3.3 Sub critical drifted motion of liquid drop as an activated process:

Kramers' reaction rate (r) is given as follows:

$$r \approx r_o exp(-E_b/k_BT) \qquad\qquad 8.3$$

Here, r is the rate of reaction, E_b is the activation energy and $k_B T$ is the energy of the thermal fluctuation. In the high friction limit, the pre-exponential factor (r_o) is independent of temperature, but it is inversely proportional to the friction coefficient (ζ). On the other hand, in the low friction limit, the pre-exponential factor increases with friction but decreases with temperature, i.e. $r_o \sim \zeta / k_B T$.

Equation 8.3 applies strictly to a thermodynamically closed system ruled by a fluctuation dissipation theorem (FDR), where its thermal state is uniquely defined by temperature. For a complete realization of the scope of Kramers framework to our problem, it would be preferable to study how wetting dynamics depends on temperature over a substantial range. The difficulty associated with this approach is that the temperature of a liquid drop cannot be the altered without affecting its surface tension and viscosity. One way to bypass this difficulty would be to design an experiment in which the excitation is performed by an external noise of a given intensity that does not affect the physical properties of the drops. However, as the system is now thermodynamically open, there can be an interplay between the internal and the external noises. A recent paper [59] analyzed a type of a barrier crossing problem in a thermodynamically open system, in which one of the noises is provided externally. These authors showed that the reaction rate can still follow the typical Kramers behavior in that it increases with friction in the low friction limit, but it decreases in the high friction limit. The authors, however, did not report how the reaction rate would vary as a function of the intensity of the external noise by keeping the thermodynamic temperature constant, which is, essentially, the situation that we are interested in.

Our previous studies demonstrated [10,48] that the noise temperature of a random mechanical fluctuation affects the transport and the barrier crossing properties much like that of a thermodynamic temperature. However, as there is no fluctuation-dissipation relation with an external noise, the thermal energy term ($k_B T$) of equation 8.3 should be replaced with $mK\tau_L/2$ where K is the noise strength and the relaxation time (τ_L) of the drop of radius R is taken to be proportional to the ratio of mass and friction co-efficient i.e. $\tau_L \sim m/\eta R$. The pre-exponential factor $r_o \sim E_b/(\tau_L k_B T)$ in the low friction limit [41] should also be re-written in terms of the above form of $k_B T$. Using appropriate transformations, a *heuristic* low friction version of the Kramers transition rate with an external noise becomes:

$$r \sim \left[\frac{v^2 E_b}{\rho K V^{7/3}}\right] exp\left[-\frac{cv E_b}{\rho K V^{5/3}}\right] \qquad 8.4$$

Here c is a numerical constant. Our *hypothesis* is that the dynamics of a drop on a fibrillar surface may be described by the above form of Kramers equation in the low viscosity limit. Once the frequency r is estimated, the drift velocity is given as the product of r and a length scale (i.e. the fibrillar spacing). Below, we test this hypothesis by designing a barrier crossing experiment.

8.3.4 Barrier crossing of a liquid drop

We designed an experiment, in which an artificial mechanical barrier (Figure 8.4) was created in the form of a slight undulation by simply inserting fine wires beneath the fibrillated PDMS sheet. A drop crossed over such a barrier with the assistance of an external mechanical noise when the substrate was slightly inclined (2^0) from the horizontal plane. Previously, such an experiment was performed with a rigid sphere, in which the barrier crossing frequency systematically followed the Van't Hoff-Arrhenius-Eyring (VHAE) type equation [48] consistent with an activation energy arising from the difference of the gravitational energy between the trough and the valley of a non-linear potential profile. The basic experiment with a water drop was same as that with a rigid sphere, in that it was placed in one of the valleys of the potential and then the support was vibrated with a random mechanical noise till the drop crossed over to the next valley.

From the typical barrier crossing trajectories of a drop of either water or of glycerin, it is evident (Figure 8.4) that the drop waits in valley near the top part of the barrier for certain amount of time and then it crosses over to the next valley and the process continues. From 40 such observations, the mean waiting time, t_w, was estimated which gave the barrier crossing frequency as $r = 1/t_w$. We have discussed in a previous publication [48] that the number of measurements to be carried out for such barrier crossing studies is in the neighborhood of 30 without significantly compromising the errors of measurements.
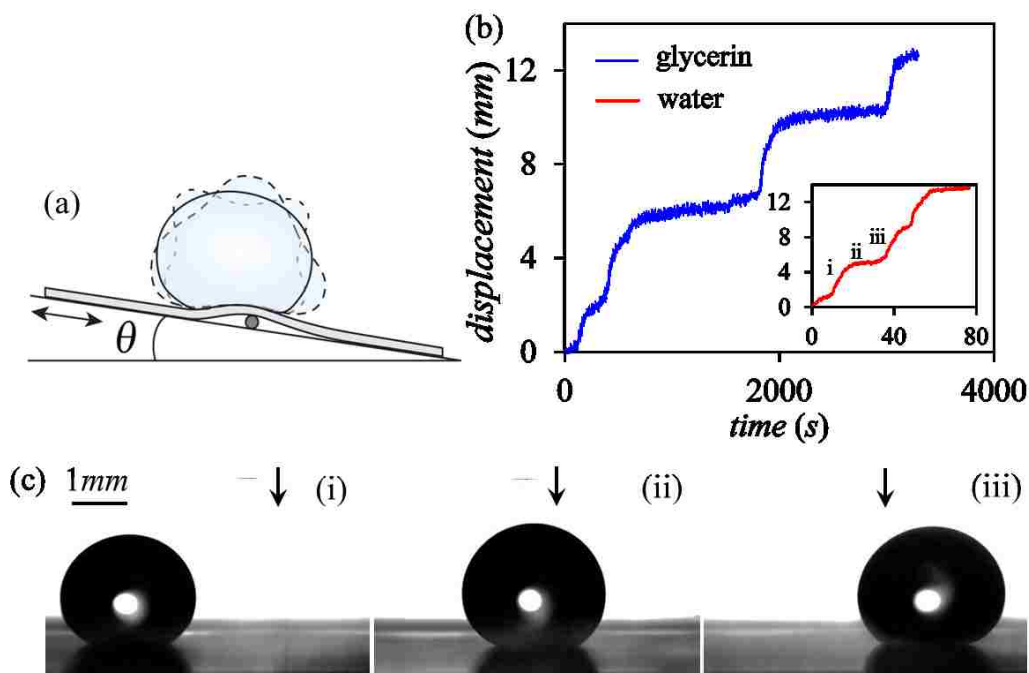
Figure 8.4: (a) Schematic of the experiment used to study barrier crossing dynamics with drops of various compostions of water and glycerin. (b) Sample trajectories of 10µl drops of water and glycerin crossing over several barriers are shown (c) Video-microscopic images of a water drop at different stages of barrier crossing (the barrier top is indicated by the arrow): a) before crossing, b) at the top of the barrier and c) after crossing the barrier. These stages are also indicated in the sample trajectory.

A plot of ln (*r*) versus 1/*K* is found to be linear only for a drop of glycerin that reminisces the behavior observed previously with a rigid sphere (Figure 8.5). By contrast, the experiments carried out with water and water/glycerin solutions exhibit a sub-Arrhenius behavior in similar plots. These barrier crossing data cluster around a single curve (Figure 8.5) when the barrier crossing frequencies are re-plotted as $\ln(r\rho KV^{7/3}/v^2)$ versus ($v/\rho KV^{5/3}$). Although the resulting plot is sub-Arrhenius i.e. $r\rho KV^{7/3}/v^2 \sim \exp[-$

$(v/\rho K V^{5/3})^{0.2}]$, it is gratifying to note that an excellent collapse is obtained when the low

friction limit of a Kramers-like equation is used (see also Appendix: Figure 8.12).
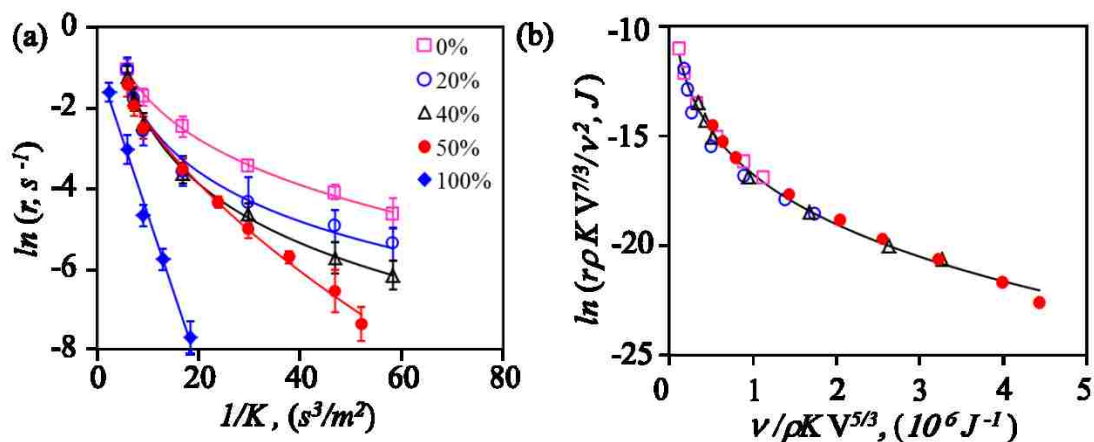
Figure 8.5: (a) Arrhenius plot summarizing the results of the barrier crossing experiments, in which the logarithm of the barrier crossing frequency a 10 μl drop is plotted against the reciprocal noise strength for various compositions of glycerin-water solutions (0% corresponds to water and 100 % corresponds to glycerin). (b) collapse plots of the barrier crossing experiments, in which $\ln(\Omega \rho K Q^{7/3}/v^2)$ versus $(v/\rho K Q^{5/3})$.

8.3.5 Shape fluctuation:

There are only limited amount of literature [60,61] that discusses the origin of a sub-Arrhenius type kinetics. The root cause of such an anomalous behavior has been suspected to be the non-extensivity of a system, i.e. a system where the distribution functions do not follow the usual Gaussian statistics.
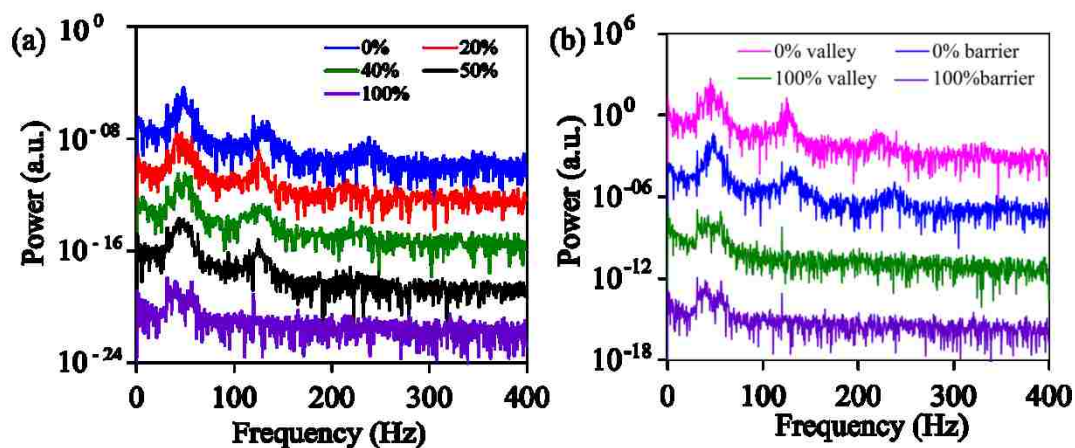
Figure 8.6: (a) Power spectra of height fluctuation of a 10 μl liquid drop at Gaussian noise strength of 0.17m^2/s^3 at the top of the barrier. The weight percent of the glycerin is indicated inside the figures. (b) Comparisons of the power spectra of height fluctuation of a drop of water and glycerin at the trough and the valley of the potential wells. The Y-axis is shifted arbitrarily for the clarity of representation.
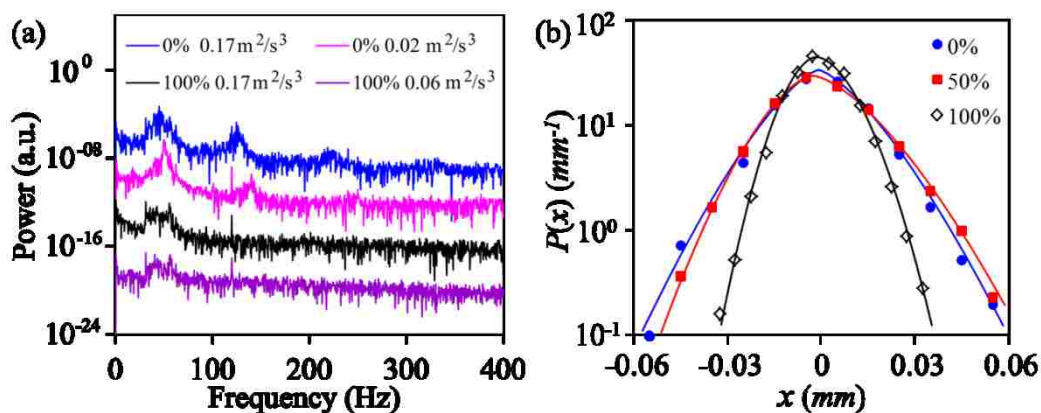
Figure 8.7: (a) Effect of the noise strength on the resonance fluctuation of the drops of water and glycerin. (b) The probability distribution functions of the contact diameter fluctuations for a water, glycerin and its solution. The pdf is Gaussian for glycerin, but non-Gaussian for water and the solution of water and glycerin.

Jiulin [61] has explicitly considered a power law probability distribution function (i.e. a κ-distribution or a Tsallis distribution in non-extensive thermodynamics) to show that the solution of a Klein–Kramers equation leads to a non-Arrhenius barrier crossing kinetics.

There are certain signatures in the barrier crossing dynamics in our experiments that are worth noting. The power spectral density of the fluctuations of the air-liquid interface of the drops as recorded with a high speed camera [62] reveal their various resonance modes (Figure 8.6). A drop of water that exhibits a strong sub-Arrhenius kinetics also exhibits the most pronounced shape fluctuation in that several of its higher modes are excited along with the lower ones. The higher modes are increasingly suppressed in high viscosity liquids. For glycerin, only the first mode is apparent. Although a slight blue shift (Figure 8.6) of the resonance peak is also observed for the water drop when it is at the top of the barrier as compared to that in the valley, the effect is not very pronounced. Most importantly, however, the higher modes of all the drops are progressively weakened with the noise strength (Figure 8.7). This observation, coupled with the fact that the displacement fluctuations of the contact lines of all the liquid drops (except glycerin) are non-Gaussian (Figure 8.7) provide enough anecdotal evidence that there is a complex interplay between the energy states of the drops, fluctuation of the contact line and the noise strength that may be behind the observed non-Arrhenius barrier crossing statistics at lower viscosities. We now examine the behavior of a drop on an inclined fibrillar surface without any additional barrier that too, presumably, is an activated process.

8.3.6 *Noise Assisted Drift on an Inclined Substrate*

Thermal noise is incapable of de-pinning a 10 µl size liquid drop on a fibrillar surface when it is inclined subcritically (i.e. $\theta < 10^0$); however, it glides over the surface with a constant drift velocity (v_d) (Figure 8.8) if enough energy is injected to the system through an external noise. With such an arrangement, we measured the drift velocities of 10µl liquid drops on a fibrillated PDMS substrate tilted to a 2^0 inclination from the horizontal plane with systematic variation of noise intensity.
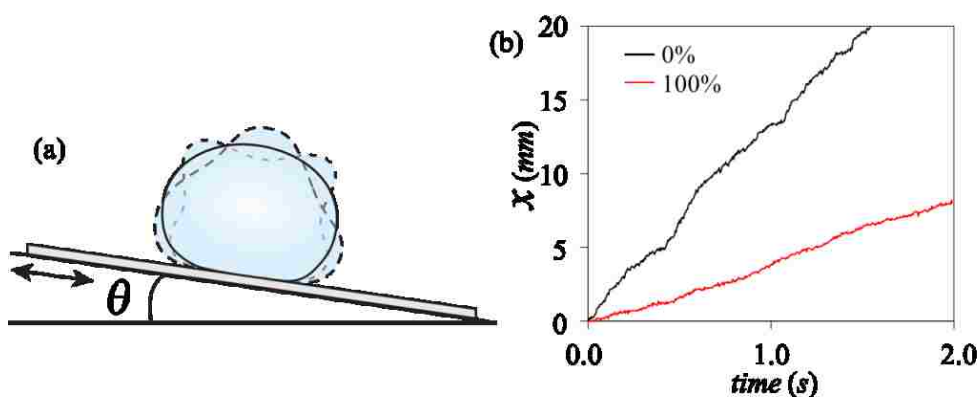
Figure 8.8: Schematic of a drop moving on a surface at a subcritical angle (2^0) in the presence of an exernal noise. (b) Sample trajectories of 10µl size drops of water (0%) and glycerin (100%) in the presence of the Gaussian noise of strength $0.17 m^2/s^3$ at 2^0 inclination.

The plots of the logarithm of the drift velocity ($\ln v_d$) of a drop of water, glycerin or their solution against $1/K$ remarkably parallel the behavior observed with the barrier crossing statistics (Figure 8.9). Glycerin again exhibits an Arrhenius behavior, whereas sub-Arrhenius behaviors are observed with water and the low viscosity solutions of water and glycerin. When the drift velocity data of water and up to 50 % solutions of water and

glycerin are re-plotted in terms of $\ln(v_d \rho K V^{7/3}/v^2)$ versus $(v/\rho K V^{5/3})$, they nicely cluster around a single master curve (upper curve of Figure 8.9b) as is the case with the barrier crossing data. In fact, if the barrier crossing frequencies are converted to velocity by multiplying it with a characteristic a length scale, i.e. the distance between two valleys of a potential well, then the both types of plots exhibit very similar patterns (Figure 8.9b).
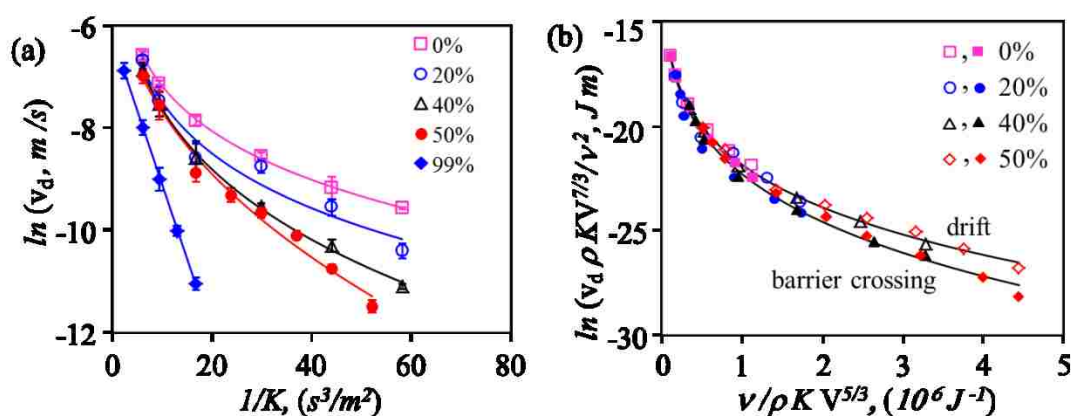
Figure 8.9: (a) Arrhenius plot summarizing the results of the subcritical dynamics with noise, in which the logarithm of the drift velocity of a 10 μl drop is plotted against the reciprocal noise strength for various compostions of glycerin-water solutions (0% corresponds to water and 100 % corresponds to glycerin). (b) The results of the subcritical drift dynamics (upper curve) are compared with those of the barrier crossing experiments (lower curve) by plotting $ln(v_d \rho K V^{7/3}/v^2)$ versus $(v/\rho K V^{5/3})$ in both cases.

8.4 Summary and Conclusion

A drop of water or a solution of glycerin and water displays fascinating behaviors when it moves on superhydrophobic surface in a "fakir" state. First of all, such a drop undergoes the prototypical pinning/depinning transition on a fibrillar surface in that the segments of the contact line that are initially pinned on the fibrils are de-pinned randomly - most

264

likely, being activated by the force and the thermal fluctuation. The role of the partial evaporation of the drop in initiating such types of depinning cannot be overruled in view of some recent reports that a contact line of an evaporative drop recedes on a structured surface in a stepwise manner [54,63]. A beautifully performed recent experiment [63] took advantage of the evaporation induced de-pinning and a gradient of pillar density to induce a directional motion of a drop. In our experiments, the contact line continues to roughen till a critical point is reached when it detaches from all the fibrils like an avalanche. Part of the energy released from such an avalanche is transmitted to the drop in the form of a noise that builds up to the point that it undergoes a structural oscillation. Notably, the power spectral density (*psd*) of the background noise is neither $1/f$ nor $1/f^2$; but, it is intermediate of the two i.e. $psd \sim 1/f^{1.6}$.

Certain previous elegant studies [64–66] have already demonstrated the roughening behavior of contact line on a disordered substrate. However, what is new in the current study is that it pinpoints some additional effects resulting from the contact line depinning, namely the self-excited noise in the drop. This noise and the overall oscillation of the drop may also contribute to drop dynamics, by virtue of which the critical speeding exhibits a stochastic behavior. All the features expected of a moving rough contact line, i.e. quenched disorder, a threshold force, contact line roughening and a noise, are present in this problem. However, the role of dissipation and its relationship to viscosity is found to be non-trivial. Specifically, the terminal velocity of the drop increasing with viscosity for low concentrations of glycerin/water solutions was not expected *a priori*. While it is tempting to address this behavior in the light of a sliding to rolling transition by

extending a proposal of Mahadevan and Pomeau [53], the direct observations [67,68] of the velocity field, however, have yet to establish a very clear picture of how a drop moves on a structured substrate and how it is affected by viscosity. Our own studies revealed a complex picture of the contact line de-pinning, which is amenable to a molecular kinetic theory. The low friction limit of Kramers' turnover rate appears to be consistent with both the barrier crossing and the drifted motion of a drop on an inclined support. The close similarity of these two different experiments, however, suggests that they are governed by similar activation energies. We surmise at this point that this agreement may be fortuitous.

Even though a good collapse of data was obtained in the barrier crossing as well as the drift experiments, both of the results are remarkably sub-Arrhenius. A departure from the conventional exponential kinetics signifies that various distribution functions characterizing the dynamics are non-Gaussian which is, partially, evident in the fluctuation of the contact diameter of the low viscosity drops. This non-Gaussian distribution function coupled with the fact that the higher modes of the shape fluctuation of the drops undergoes significant noise strength dependent attenuation could be responsible for the observed anomalous kinetics. It is noteworthy that a drop of Glycerin is most well behaved in the sense that it displays a Gaussian distribution of contact line fluctuation and its higher modes are all attenuated at any noise intensity. This is also the drop for which an Arrhenius behavior is observed in both the barrier crossing and the drift velocity studies. In the high viscosity limit, we expect the drop dynamics to follow the strong friction limit of Kramers equation, i.e. $r \sim (V^{2/3} \omega_1 \omega_2 / v) \exp[-c v E_b / (\rho K V^{5/3})]$,

where ω_1 and ω_2 correspond to the frequencies of the valley and the tough of the potential well. While the low viscosity regime of the activated dynamics of a drop has been studied in this work with the solutions of water and glycerin, similar studies in the high viscosity limit could not be performed at present with such a solution as slight evaporation of water changes the viscosity of the solution rather drastically. In future, we hope to study the high viscosity regime systematically using the solutions of glycerin and ethylene glycol as well as by quenching the resonant modes by increasing its extensional viscosity with polymeric additives. These studies are important in order to understand the nature of the drop dynamics that is under the influence of thermal as well as the self-generated noise of the type reported in Figure 8.3b.

267

8.5 Appendix:

Figure 8.10: Fluctuation of the air-water interface of a 20μl water drop when it was deposited on a horizontal flat PDMS surface of 95μm fibrillar spacing (upper panel), 50μm fibrillar spacing (middle panel) and smooth hydrocarbon treated Si wafer respectively. As soon as a drop of water is released on a surface via retraction of a needle, it starts to oscillate, the amplitude of which decays with time. The amplitude of this oscillation after 1s of disposal of the drop on a PDMS surface (50μm fibrillar spacing) is comparable to that observed with the drop undergoing critical speeding (Figure 8.2c, main text) on a similar surface (1s after the release of the drop). However, under a comparable condition, the amplitude of this oscillation on a PDMS surface with larger fibrillar spacing (95 μm) is significantly smaller than that observed with a drop undergoing a critical dynamics on a similar surface. As the measurements of the interface fluctuation shown in Figure 8.2c were performed after 1s of the drop disposal, we can safely say that the oscillation due to syringe retraction did not contribute significantly on a surface with a 95 μm fibrillar spacing. Although the argument is weaker for a 50 μm spaced fibrillar surface, we note that the amplitude of oscillation did not decay as the drop sprinted over such a surface, i.e. the initial oscillation is, at least, sustained. The amplitude of the interface oscillation decays much faster (within 1.5s) for a drop released on a smooth hydrophobic Si wafer. The air-water interface fluctuation of a water drop moving steadily on such a surface (Figure 8.2c) was recorded long time (~ 40s) after the deposition of the drop as it moved rather slowly (~ 0.06 cm/sec).

Figure 8.11: Power spectra of the interface fluctuation of a water drop and a solid glass sphere on a fibrillar surface. The upper blue curve depicts the power spectrum of a 10 μl drop of water trapped before a barrier (see Figure 8.4a) by subjecting it to an external noise of strength $0.17\text{m}^2/\text{s}^3$. This spectrum is similar to that of Figure 8.6a except that the background noise of the spectrum was reduced by adding and averaging the spectra obtained from ten different experiments. The red curve represents the power spectrum of the self-excited noise a 10 μl water drop undergoing a critical speeding dynamics on an inclined (10°) fibrillar surface (see Figure 8.2b). The lower black curve represents the power spectrum of a rigid glass sphere (2.4mm diameter) as it drifted on a fibrillar surface that was inclined by 5^0 without any external noise. These control experiments were performed to show that the resonance modes of a drop excited by a self-generated noise is similar to that obtained with an external noise, whereas no such resonance modes are observed with a rigid sphere that cannot undergo a shape fluctuation.

Figure 8.12: The barrier crossing data of Figure 8.5a are rescaled according to the high friction limit of Kramers' theory, according to which the barrier crossing frequency is: $r \sim (V^{2/3}\omega_1\omega_2/v)\exp[-cvE_b/(\rho K V^{5/3})]$, instead of that given in Eq. 8.4 of the text. However this plot of $\ln(rv/V^{2/3})$ versus $(v/\rho K V^{5/3})$ fails to collapse the barrier crossing data on a single master curve, unlike the low friction limit of Kramers theory (Figure 8.5b).

References

[1]   T. D. Blake and J. M. Haynes, Journal of Colloid and Interface Science **30**, 421 (1969).

[2]   B. W. CHerry and C. M. Holmes, Journal of Colloid and Interface Science **29**, 174 (1969).

[3]   T. D. Blake, Advances in Colloid and Interface Science **179-182**, 22–8 (2012).

[4]   M. Voué, R. Rioboo, C. Bauthier, J. Conti, M. Charlot, and J. De Coninck, Journal of the European Ceramic Society **23**, 2769–2775 (2003).

[5]   S. Mettu and M. K. Chaudhury, Langmuir : the ACS Journal of Surfaces and Colloids **26**, 8131–40 (2010).

[6]   H. Jaeger, C. Liu, and S. Nagel, Physical Review Letters **62**, 40–43 (1989).

[7]   J. M. Carlson, J. S. Langer, and B. E. Shaw, Reviews of Modern Physics **66**, 657 (1994).

[8]   V. V. Bulatov and A. S. Argon, Modelling and Simulation in Materials Science and Engineering **2**, 167 (1994).

[9]   K. Dahmen, Y. Ben-Zion, and J. Uhl, Physical Review Letters **102**, 1–4 (2009).

[10]   M. K. Chaudhury and P. S. Goohpattader, The European Physical Journal. E, Soft Matter **35**, 131 (2012).

[11]   K. Reddy, Y. Forterre, and O. Pouliquen, Physical Review Letters **106**, 1–4 (2011).

[12]   A. Lemaître and C. Caroli, Physical Review Letters **103**, 065501 (2009).

[13]   S. Daniel, M. K. Chaudhury, and J. C. Chen, Science (New York, N.Y.) **291**, 633–6 (2001).

[14]   R. Bonner, III, in *The International Heat Transfer Conference* (IHCT 14, Washington, D.C., 2011).

[15]   Y. Pomeau, J. De Physique Lett. **44**, L585 (1983).

[16]   R. E. Johnson and R. H. Dettre, Advances in Chemistry Series **43**, 113 (1964).

[17]   T. Onda, S. Shibuichi, N. Satoh, and K. Tsujii, Langmuir **12**, 2125–2127 (1996).

[18]   D. Öner and T. J. McCarthy, Langmuir **16**, 7777–7782 (2000).

[19]   M. Miwa, A. Nakajima, A. Fujishima, and K. Hashimoto, **1998**, 5754–5760 (2000).

[20]   C. W. Extrand, **1**, 7991–7999 (2002).

[21]   A. Marmur, Langmuir **19**, 8343–8348 (2003).

[22]   X. Gao, X. Yan, X. Yao, L. Xu, K. Zhang, J. Zhang, B. Yang, and L. Jiang, Advanced Materials **19**, 2213–2217 (2007).

[23] M. Reyssat, D. Richard, C. Clanet, and D. Quere, Faraday Discussions **146**, 19 (2010).

[24] L. Feng, S. Li, Y. Li, H. Li, L. Zhang, J. Zhai, Y. Song, B. Liu, L. Jiang, and D. Zhu, Advanced Materials **14**, 1857–1860 (2002).

[25] E. Bormashenko, R. Pogreb, G. Whyman, and M. Erlich, Langmuir : the ACS Journal of Surfaces and Colloids **23**, 6501–3 (2007).

[26] N. a Patankar, Langmuir : the ACS Journal of Surfaces and Colloids **20**, 7097–102 (2004).

[27] B. m. Mognetti, H. Kusumaatmaja, and J. M. Yeomans, Faraday Discussions **146**, 153 (2010).

[28] J. Genzer and K. Efimenko, Biofouling **22**, 339–60 (2006).

[29] L. Mahadevan, Nature **411**, 895–6 (2001).

[30] J. . Eick, R. . Good, and A. . Neumann, Journal of Colloid and Interface Science **53**, 235–238 (1975).

[31] A. Marmur, Advances in Colloid and Interface Science **50**, 121–141 (1994).

[32] R. E. Johnson and R. H. Dettre, J Phys Chem **68**, 1744–1750 (1964).

[33] R. N. Wenzel, Industrial and Engineering Chemistry **28**, 988–994 (1936).

[34] A. B. D. Cassie and S. Baxter, Trans. Faraday Soc. **40**, 546 (1944).

[35] R. . Good, J Am. Chem Soc. **74**, 5041 (1952).

[36] R. . Good and M. K. Chaudhury, in *First International Congress on Adhesion Science and Technology*, edited by W. J. Van Ooji and H. R. Anderson (Netherlands, 1998), pp. 181–197.

[37] J. F. Joanny and P. G. de Gennes, The Journal of Chemical Physics **81**, 552 (1984).

[38] Y. Pomeau and J. Vannimenus, Journal of Colloid and Interface Science **104**, 477–488 (1985).

[39] M. O. Robbins and J. F. Joanny, Europhysics Letters (EPL) **3**, 729–735 (1987).

[40] D. Ertas and M. Kardar, Phys. Rev. E **49**, R2532–2535 (1994).

[41] H. A. Kramers, Physica VII 284–304 (1940).

[42] R. Zwanzig, *Nonequilibrium Statistical Mechanics* (Oxford University Press, New York, 2001).

[43] . Glycerin producers Association, *Physical Properties of Glycerine and Its Solutions* (Glycerin producers' association, 1963), pp. 1–27.

[44] N. J. Glassmaker, A. Jagota, C. Hui, W. L. Noderer, and M. K. Chaudhury, Proceedings of the National Academy of Sciences **104**, 10786 (2007).

[45] W. L. Noderer, L. Shen, S. Vajpayee, N. J. Glassmaker, A. Jagota, and C.-Y. Hui, Proceedings of the Royal Society A: Mathematical, Physical and Engineering Sciences **463**, 2631 (2007).

[46] P. S. Goohpattader, S. Mettu, and M. K. Chaudhury, The European Physical Journal. E, Soft Matter **34**, 120 (2011).

[47] P. S. Goohpattader and M. K. Chaudhury, The Journal of Chemical Physics **133**, 024702 (2010).

[48] P. S. Goohpattader and M. K. Chaudhury, The European Physical Journal. E, Soft Matter **35**, 67 (2012).

[49] P. S. Goohpattader and M. K. Chaudhury, The Journal of Chemical Physics **133**, 024702 (2010).

[50] Y. Pomeau and M. Le Berre, arXiv:1107.3331 [physics.geo-ph] 1–8 (2011).

[51] A. Vaidya and M. K. Chaudhury, Journal of Colloid and Interface Science **249**, 235–45 (2002).

[52] M. Scheffer, J. Bascompte, W. a Brock, V. Brovkin, S. R. Carpenter, V. Dakos, H. Held, E. H. van Nes, M. Rietkerk, and G. Sugihara, Nature **461**, 53–9 (2009).

[53] L. Mahadevan and Y. Pomeau, Physics of Fluids **11**, 2449 (1999).

[54] D. Orejon, K. Sefiane, and M. E. R. Shanahan, Langmuir : the ACS Journal of Surfaces and Colloids **27**, 12834–43 (2011).

[55] D. W. Pilat, P. Papadopoulos, D. Schäffel, D. Vollmer, R. Berger, and H.-J. Butt, Langmuir : the ACS Journal of Surfaces and Colloids (2012).

[56] G. R. Fleming, S. H. Courtney, and M. W. Balk, **42**, 83–104 (1986).

[57] R. Best and G. Hummer, Physical Review Letters **96**, 228104 (2006).

[58] B. N. Ganguly, Radiation Physics and Chemistry **58**, 675–680 (2000).

[59] A. Shit, S. Chattopadhyay, S. K. Banik, and J. R. Chaudhuri, arXiv:1206.2450 [cond-mat.stat-mech] (2012).

[60] V. Aquilanti, K. C. Mundim, M. Elango, S. Kleijn, and T. Kasai, Chemical Physics Letters **498**, 209–213 (2010).

[61] D. Jiulin, Physica A: Statistical Mechanics and Its Applications **391**, 1718–1728 (2012).

[62] S. Mettu and M. K. Chaudhury, Langmuir : the ACS Journal of Surfaces and Colloids **28**, 14100–6 (2012).

[63] L. Xu, Z. Li, and S. Yao, Applied Physics Letters **101**, 064101 (2012).

[64]   a. Prevost, E. Rolley, and C. Guthmann, Physical Review Letters **83**, 348–351 (1999).

[65] S. Moulinet, C. Guthmann, and E. Rolley, The European Physical Journal B - Condensed Matter **37**, 127–136 (2004).

[66] S. Moulinet, C. Guthmann, and E. Rolley, The European Physical Journal. E, Soft Matter **8**, 437 (2002).

[67] S. Suzuki, A. Nakajima, M. Sakai, Y. Sakurada, N. Yoshida, A. Hashimoto, Y. Kameshima, and K. Okada, Chemistry Letters **37**, 58 (2008).

[68] P. Hao, C. Lv, Z. Yao, and F. He, EPL (Europhysics Letters) **90**, 66003 (2010).

9. CHAPTER NINE: Sliding Dynamics as an Activated Process

9.1 Introduction

In chapter six we discussed about the rolling friction at the interface of a rigid steel sphere and a structured rubber surface [1] and the rolling motion of the sphere was identified as an activated rate process. Study with liquid, confers that gliding of the droplets on a fibrillar PDMS surface is also an activated process having rich dynamics [2]. These studies kindle enough curiosity to know whether sliding dynamics of a solid object can also be analyzed in the light of Arrhenius rate equation.

When a solid object is placed on another solid substrate, the asperities of the two bodies come into intimate contact at the interface, which make the real contact area very small compare to the apparently large contacting surface [3–5]. These asperities are randomly distributed on the surfaces. When a force is applied on the object, these asperity-asperity contacts resist the motion and create a potential energy barrier. This energy barrier needs to be overcome to set the object in motion. Whether the rate of this barrier crossing is an activated process when an external weak noise is operative is the main theme of this chapter. We experimentally demonstrated that sliding object is indeed a noise induced activated process which follows Arrhenius rate equation.

9.2 Experimental section

we study the motion of a small glass prism (~ 1.7g) having dimension of ~ 11mm X 11mm X 6mm on a partially inclined glass substrate in the presence of a Gaussian white noise. For very smooth surfaces, the glass prism adheres to the glass support so strongly that a very high level of vibration is needed to dislodge it. We deliberately avoided this situation by roughening the glass support as we study the motion of the prism at very low noise strength ranging from 0.0009 m^2/s^3 to 0.0018m^2/s^3.
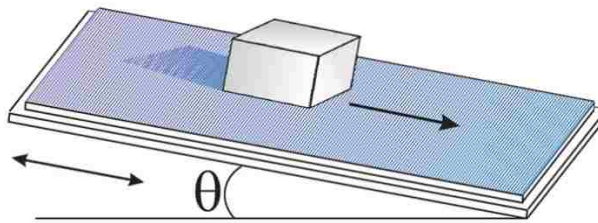
Figure 9.1 Schematic of the experimental set-up.

The experimental details are as follows. The glass substrate was firmly attached to an aluminum platform which was fixed at the stem of a mechanical oscillator (Pasco Scientific, Model No: SF-9324). Gaussian white noise that was generated using a function generator (Agilent, model 33120A), was fed to the oscillator via a power amplifier (Sherwood, Model No: RX-4105). The whole set-up was placed on a vibration isolation table (Micro-g, TMC) to eliminate the effect of ground vibration. The acceleration of the supporting aluminum plate was estimated with a calibrated accelerometer (PCB Peizotronics, Model No: 353B17) driven by Signal Conditioner

(PCB Peizotronics, Model No: 482) and connected to an oscilloscope (Tektronix, Model No. TDS 3012B). The drift velocities of the prism were measured on the inclined plate with the help of a high resolution (Redlake motion-pro) camera at different powers of noise by measuring the displacement of the prism at a given time. Few trials of the prism motion, recorded with Sony camera (DCR-HC85 NTSC) and subsequently analyzed with an object tracking software (MIDAS 2.0 Xcitex Inc.) enabled us to construct displacement versus time plot. The strength of the noise at a given setting is defined as $K=\Gamma^2\tau_c$, where Γ is the root mean square acceleration (m/s^2) and τ_c is the acceleration pulse width. The component of gravitational force along the inclined support ($\bar{\gamma} = mg\sin\theta$) was used as the constant biased force which is varied for different experiments by controlling the inclination angle (θ) with a precise goniometer (CVI Melles Griot, Model No: 07 GON 006). The range of the applied bias (F) used in this study was 0.15mN to 1.7mN. The critical biased force, F_c (2mN) was estimated from the critical angle (7^0) of inclination, at which the prism just started to move on the surface without any external perturbation.

9.3 Results

9.3.1 Drifted motion of the prism

A sample trajectory of the prism on 1^0 inclined support vibrated with Gaussian white noise of strength 0.0012m^2/s^3 is shown in Figure 9.2. From the figure it appears that there is stick slip type of motion of the prism with stick phases of different duration. However
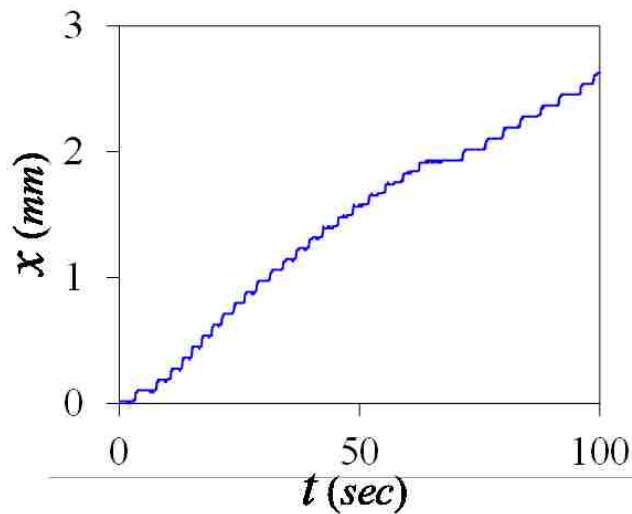
Figure 9.2 Sample trajectory of the prism drifted on 1^0 inclined glass support under the influence of Gaussian white noise of strength 0.0012m^2/s^3.

the slip displacement, which is of constant magnitude and is close to the image resolution (~0.1mm) impels us to being skeptical about the Figure 9.2 as true representation of the stick-slip motion. Nevertheless, monotonically increasing trajectory in Figure 9.2 assures that there is no perceivable negative fluctuation of the prism motion.

9.3.2 Drift velocity as an activated rate

We estimated the drift velocity from the displacement traversed by the glass prism at a given time interval ranging from 45min (at the lowest velocity) to 15s (at the highest velocity). The experiment was done at five different powers of the noise and seven different applied biases. For each set of data 10trial experiments were performed. As the prism slides on the surface it has to overcome the potential energy barrier. The drift

velocity is the average rate at which the prism overcomes the energy barrier multiplied with an average length scale pertinent to the system.
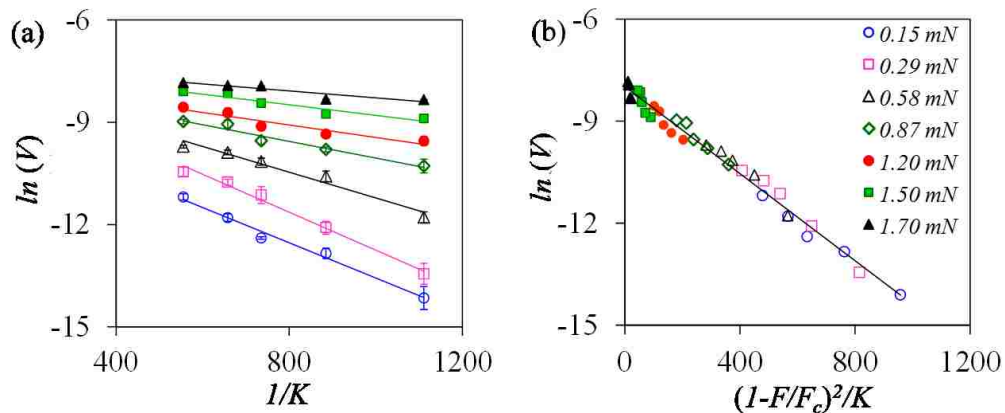
Figure 9.3 (a) ln (*V*) as a function of 1/*K* . (b) The collapse of Arrhenius plot (figure a) when normalized using reduced power by multiplying 1/K with (1-*F/F$_c$*)^2. The applied bias forces *F* are indicated inside the figure.

The face that the ln(*V*) linearly dependent on the inverse of the noise strength (1/K) (Figure 9.3 a), immediately suggested that the sliding motion is a noise activated process and follows Arrhenius rate equation of the form:

$$V \sim \exp(-1/K) \qquad\qquad 9.1$$

These data cluster around a single straight line when the drift velocities were replotted as ln(*V*) versus (1-*F/F$_c$*)^2/K (Figure 9.3b).

9.4 Discussion and Concluding remark

An important picture emerges from this study is that the slow dynamics of a solid object can be viewed as an activated process. The drift velocity, which is representative of the average rate at which the object overcomes energy barriers, is exponentially dependent on the inverse of noise strength. An extensive study of sliding friction at very low strength of noise is yet to be done. The bias dependency of the effective barrier energy was reported earlier by several authors [6–13] using molecular dynamic simulations as well as with experimental support. Most of these authors suggested the energy barrier $\Delta E \sim (1 - \frac{F}{F_c})^{1.5}$ whereas we have found slightly different exponent, i.e. $\Delta E \sim (1 - \frac{F}{F_c})^2$. Similar dependency of the energy barrier on biased force was observed in the rupture kinetics of a rigid sphere from a structured rubber surface, although the overall kinetics was non Arrhenius [1,14]. The studies presented here could be useful in micromanipulation of solid particles in weakly perturbed settings. Careful experiments with highly sensitive displacement transducer may allow one to observe the stick slip events associated with the activated sliding, which will be a subject of our future study.

Reference

[1]   P. S. Goohpattader and M. K. Chaudhury, The European Physical Journal. E, Soft Matter **35**, 67 (2012).

[2]   M. K. Chaudhury and P. S. Goohpattader, The European Physical Journal. E, Soft Matter **36**, 15 (2013).

[3]   F. P. Bowden and D. Tabor, *The Friction and Lubrication of Solids* (Oxford Univ. Press, Oxford, 1958, 1958).

[4]   P. Berthoud and T. Baumberger, Proc. R. Soc. Lond. A. **454**, 1615–1634 (1998).

[5]   J. H. Dieterich and B. D. Kilgore, Tectonophysics **256**, 219–239 (1996).

[6]   E. Riedo, E. Gnecco, R. Bennewitz, E. Meyer, and H. Brune, Physical Review Letters **91**, 084502 (2003).

[7]   A. Garg, Phys. Rev. B **51**, 15592 (1995).

[8]   O. K. Dudko, a E. Filippov, J. Klafter, and M. Urbakh, Proceedings of the National Academy of Sciences of the United States of America **100**, 11378–81 (2003).

[9]   O. K. Dudko, G. Hummer, and A. Szabo, Proceedings of the National Academy of Sciences of the United States of America **105**, 15755–60 (2008).

[10]   H.-J. Lin, H.-Y. Chen, Y.-J. Sheng, and H.-K. Tsao, Physical Review Letters **98**, 088304 (2007).

[11]   L. B. Freund, Proceedings of the National Academy of Sciences of the United States of America **106**, 8818–23 (2009).

[12]   D. J. Lacks, J. Willis, and M.-P. Robinson, The Journal of Physical Chemistry. B **114**, 10821–5 (2010).

[13]   B. N. J. Persson, O. Albohr, F. Mancosu, V. Peveri, V. N. Samoilov, and I. M. Sivebaek, Wear **254**, 835–851 (2003).

[14]   M. K. Chaudhury and P. S. Goohpattader, The European Physical Journal. E, Soft Matter **35**, 131 (2012).

10. CHAPTER TEN: Splitting of Noise and Bias in Orthogonal Direction

10.1 Introduction

A small water droplet on a glass surface may not move even when the glass surface is kept perfectly vertical. This happens due to presence of contact angle hysteresis and the drop is stuck in one of the metastable states in the energy landscape of surface [1]. This scenario changes when the glass surface is vibrated and the liquid drop gets enough energy to overcome the energy barriers and move on.

A rain drop is in the similar situation but exhibits a rich dynamics when it drifts down on a windowpane. In its journey, the rain drops also fuses with other drops, hence grows in size and at the same time its center of mass follows a stochastic path while drifted down. Apart from the external noise due to wind, an internal self-excited noise is generated due to fusion of these rain drops. This internal noise builds up within the drop with time [2] and coupled with the increasing gravitational bias force, due to increase in the fused mass, the drop speeds up and eventually leads to an avalanche.

In a recent work [3] motion of condensing droplets on an energy gradient surface is investigated with the intention of an industrial application- to increase the heat transfer coefficient of a heat exchanger. In a conventional heat exchanger, on the hydrophilic surface, a thin water film is formed from the condensation of steam. This reduces the heat

flux across the heat transfer surface. Daniel *et al* made use of gradient of wettability to drive the condensed droplets toward the more hydrophilic region of the surface and inhibit the formation of the water film. During condensation of steam, numerous small droplets deposit on the surface. At a low steam flow rate, these droplets move very slowly, whereas at high steam flow rate the droplets move very fast. While moving the droplets coalesce with each other and random zigzag path is taken by center of mass. Here also self-excited noise, generated due to coalescence of droplets, can supply enough energy to the drops to overcome the surface pinning forces.

The basic notion behind all these examples is the direction of the drifted motion which is dictated by applied bias is decoupled from the direction of the random noise impulses. We introduced a simple model experiment where we orthogonally split the noise direction and the applied subcritical bias. Such an experiment performed with a steel ball on a fibrillated rubber shows the difference between the spatial fluctuations in the orthogonal directions that are parallel and perpendicular to the bias. Thus the stochastic dynamics have been split into two orthogonal directions – one reversible and the other irreversible. This study shows that application of external noise in any direction is sufficient to set free a stuck object in other directions.

10.2 Experiment

The experimental set up is similar to that described in our previous work [4] except the inclination angle is in the direction perpendicular to the vibrating stem of the oscillator. We placed a steel sphere (4mm diameter, Mcmaster corporation, steel grade

E52100) on a fibrillated PDMS surface that is inclined at an angle of 1^0 with the horizontal plane and perpendicular to the direction of applied external noise.

Micro-fibrillated PDMS (Dow Corning Sylgard 184) surfaces were used as a substrate for the rolling experiment. The preparation of such surfaces is reported in detail elsewhere [5]. Briefly, the oligomeric component of the Sylgard 184 kit was thoroughly mixed with the crosslinker in a 10:1 ratio by weight followed by degassing it in vacuum for 2hrs. The degassed mixture was then cast onto lithographically etched silicon master. These master wafers were silanized for easy removal of cured fibrillated PDMS sample. The cast PDMS was then cured at 80^oC for 2hrs. The crosslinked PDMS was cooled in dry ice (-78.5^oC) for an hour followed by its removal from silicon master wafers manually. The PDMS surface thus prepared has square fibrils of $10\mu m$ size with a center to center distance of the adjacent fibrils of $50 \mu m$. The height of the fibrils was $25\mu m$.

The substrate was attached to an aluminum platform connected to the stem of a mechanical oscillator (Pasco Scientific, Model SF-9324). Gaussian white noise was generated with a waveform generator (Agilent, model 33120A) and fed to the oscillator via a power amplifier (Sherwood, Model No: RX-4105). By controlling the amplification of the power amplifier, noises of different powers were generated while keeping the pulse width constant at $40 \mu s$. The acceleration of the supporting aluminum plate was estimated with a calibrated accelerometer (PCB Peizotronics, Model No: 353B17) driven by a Signal Conditioner (PCB Peizotronics, Model No: 482) and connected to an oscilloscope (Tektronix, Model No. TDS 3012B). The entire setup was placed on a vibration isolation

table (Micro-g, TMC) to eliminate the effect of ground vibration. The motion of the ball was recorded with a high speed camera (Redlake, MotionPro, Model 2000) operating at 1000 frames/sec. Motion analysis software Xcitex Midas 2.0 was used to track the dynamics of the steel ball.
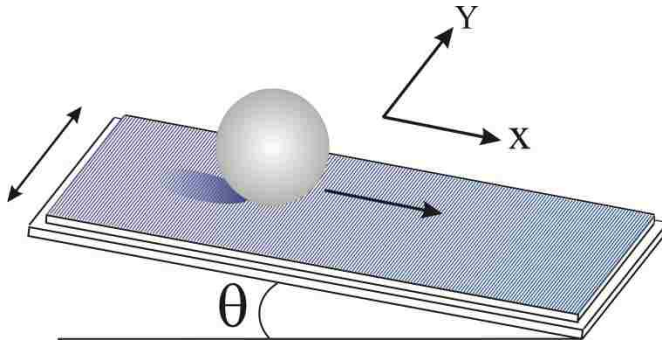
Figure 10.1: Schematic of the experimental set up. The substrate is inclined in x-direction and subjected to Gaussian noise vibration in y-direction.

10.3 Results

The situation can be explained by splitting the dynamics into two Langevin equations orthogonal to each other: Along the direction of bias:

$$\frac{dV_x}{dt} + \frac{V_x}{\tau} + \sigma(V_x)\Delta cos\alpha(t) = \bar{\gamma} \qquad \text{10.1}$$

Along the direction of vibration:

$$\frac{dV_y}{dt} + \frac{V_y}{\tau} + \sigma(V_y)\Delta sin\alpha(t) = \gamma(t) \qquad \text{10.2}$$

Here V_x and V_y are the velocity components in the direction of bias and applied noise respectively. $\sigma(V)$ is the unary signum function of the argument V with $\sigma(0)=0$. Δ is the Coulombic friction force per unit mass. $\alpha(t)$ is the instantaneous angle between the direction of velocity V and the bias direction. $\bar{\gamma}$ is the applied bias force per unit mass, measured as (g sin θ). $\gamma(t)$ is the instantaneous acceleration applied to the system as an external Gaussian white noise.
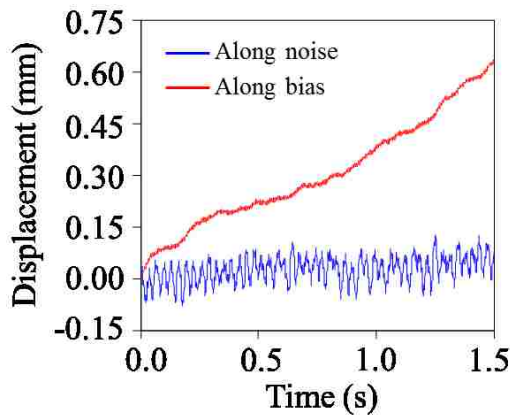
Figure 10.2: Displacement trajectories of a rolling sphere on a 1° inclined fibrillated PDMS rubber subjected to Gaussian noise excitation when noise is applied to the orthogonal direction to the inclination.

Figure 10.2 reveals that the net drift of the object is in the direction of the bias only, although there is no acceleration pulse in the direction of the bias. It may be possible that the once the object is dislodged from a stuck state by the acceleration pulse in the Y-direction, all the contacts with the underlying surface are broken and hence the object is free to move. In this situation subcritical bias force in the X direction along with

the component of inertial instantaneous velocity in the biased direction is sufficient to drive the object. Careful examination of the displacement pdfs (Figure 10.3), however, reveals the presence of some very small amount of negative displacements along the bias, which we ascribe to the rare defect induced deflection of the ball on the surface.
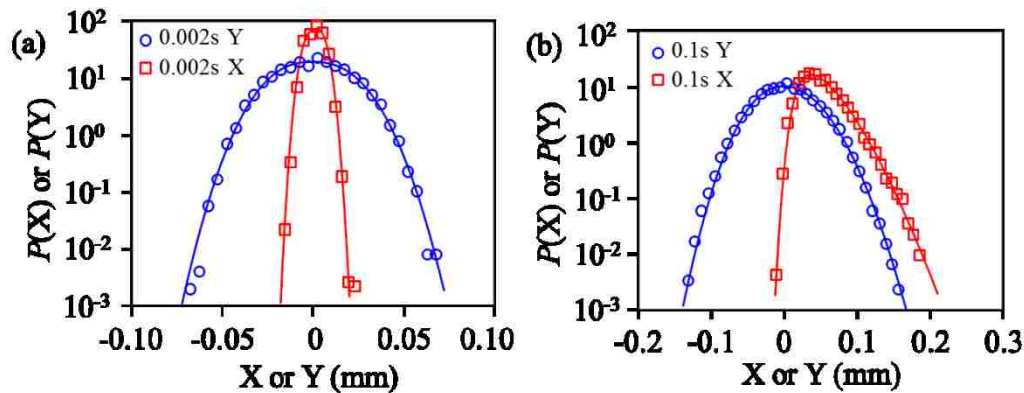
Figure 10.3: Displacement PDFs at (a) 0.002s and (b) 0.1s time interval for a rolling sphere on a 1° inclined fibrillated PDMS rubber subjected to Gaussian noise excitation when noise is applied to the orthogonal direction of the inclination. Y-displacement (blue) represents in the direction of the noise and X-displacement (red) corresponds to the direction of applied bias.

The asymmetry of the displacement distribution is observed for the bias direction (X-direction) as expected, which increases with the size of the time window. On the other hand no asymmetry is noticed in the PDFs of the displacement in noise direction (Figure 10.3).
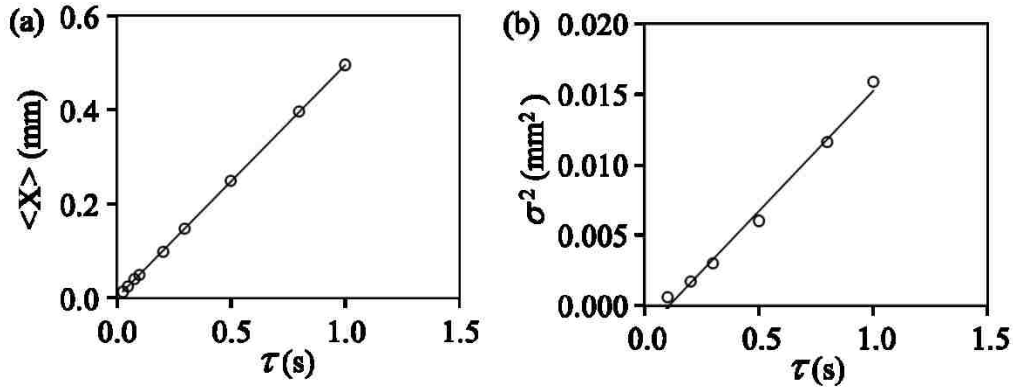
Figure 10.4: (a) Mean and (b) variance of the displacement distribution with time.

The mean of the displacement distribution in the direction of the bias increases linearly with the width of observation time window τ (Figure 10.4), from which the drift velocity is estimated as 0.5mm/s. Diffusivity along this direction is 0.0085mm^2/s as estimated using the equation: $2D \sim d\sigma^2/d\tau$, where σ^2 being the variance of the distribution.

10.4 Discussions and concluding remark

The main point of this letter is that an external noise in one direction can imparts sufficient energy to a stuck object that it can become mobile and can be steered in any preferred direction by application of a subcritical biased force. Our recent work [6] on noise activated dissociation of an adhered object from a surface suggests that in presence of external vibration two adhered surface can be detached at much lower pulling force

288

than that required for a vibration free system. The current study reveals that this applied noise could be of any other direction than that of the pulling force.

It may be possible that the object may choose the minimum energy path in the energy landscape when vibration is applied orthogonal to that of the bias direction. Instead of overcoming the apex of the barrier directly it may explore the lowest barrier height in the neighborhood and take the minimum energy path to bypass the energy loss associated with the apex-crossing.

Motion of a colloidal charged particle or DNA through polymer gel matrix in response to an applied electric field has been investigated recently [7,8]. It is well known that the motion of the particle is hindered due to solid friction, engendered from the interaction between particle and the gel matrix. From our previous and present works we learned that one can reduce the effect of friction by introducing vibration in the system. Thus one can expect enhanced mobility of charged particle or DNA molecule through gel matrix when fluctuating voltage is applied in the direction orthogonal to the applied electric field and hence the separation process might be very fast. This model study gives useful insight which can be applicable to many practical situations. Other than DNA separation or mobility of charged particle through gel, this may be used in chromatographic separation as well. Vibration effectively increases the "athermal" temperature of the system and makes it fluidized in some sense. Hence separation by gel electrophoresis should be faster and at low biased voltage if an orthogonal fluctuating voltage of zero mean is used.

References

[1]   S. Mettu and M. K. Chaudhury, Langmuir : the ACS Journal of Surfaces and Colloids **26**, 8131–40 (2010).

[2]   M. K. Chaudhury and P. S. Goohpattader, The European Physical Journal. E, Soft Matter **36**, 15 (2013).

[3]   S. Daniel, M. K. Chaudhury, and J. C. Chen, Science (New York, N.Y.) **291**, 633–6 (2001).

[4]   P. S. Goohpattader, S. Mettu, and M. K. Chaudhury, The European Physical Journal. E, Soft Matter **34**, 120 (2011).

[5]   W. L. Noderer, L. Shen, S. Vajpayee, N. J. Glassmaker, A. Jagota, and C.-Y. Hui, Proceedings of the Royal Society A: Mathematical, Physical and Engineering Sciences **463**, 2631 (2007).

[6]   M. K. Chaudhury and P. S. Goohpattader, The European Physical Journal. E, Soft Matter **35**, 131 (2012).

[7]   S. F. Burlatsky and J. M. Deutch, The Journal of Chemical Physics **103**, 8216 (1995).

[8]   J.-L. Viovy, Reviews of Modern Physics **72**, 813–872 (2000).

11. CHAPTER ELEVEN: Conclusion and Future Work

11.1 Summary

Steady state non-equilibrium phenomena have been investigated using a simple model system –dynamics of solid or liquid object on solid surface in presence of a bias and external noise. We extensively studied the energy dissipative mechanism (i.e. friction) at solid-solid interface using statistical tools. The nonlinear nature of the friction was identified by interrogating the system with random white noise, without engaging any sophisticated apparatus to measure the friction force directly. The main findings of this research are discussed in the following.

Unlike a Brownian particle in fluid, the solid object requires a threshold force known as Coulombic friction force (=$m\Delta$, where m=mass and Δ = acceleration) to initiate the motion on a solid surface [1,2]. However when a solid object, placed on a vibrating solid support, exhibits one dimensional drifted Brownian like motion under the influence of an applied bias force much less than that required when the underlying support is stationary. This external vibration is one dimensional and applied parallel to the solid support. Mobility of a colloid particle in fluid is independent of the thermal noise, whereas due to presence of Coulombic friction the mobility of a solid object strongly depends on the strength of the noise. The diffusivity of such an object also reduced in order of magnitude due to presence of Coulombic friction.

Table 11.1:Summary of scaling laws and experimental results for drift and diffusivity.

	V_{drift}	Diffusivity
$\Delta=0$	$\bar{\gamma}\tau_L$	$K\tau_L^2/2$
$\Delta\neq0$	$K\bar{\gamma}/\Delta^2$	K^3/Δ^4
Experiment	$K^{0.8}$	$K^{1.6}$

The above table summarizes the scaling law for drift velocity and diffusivity with power of the noise in the absence and presence of Coulombic dry friction along with experimental results.

We also investigated the displacement fluctuation of the solid, using a high speed camera, and found that the distribution of the time segmented displacements (jumps) is non-Gaussian with a prominent exponential tail in presence of Coulombic dry friction. Whereas, the displacement distribution is Gaussian if kinematic linear friction force is operative. Another important observation is that the jump length distribution is asymmetric with asymmetry increases with bias force when dry Coulombic friction is operating, but is symmetric when only linear kinematic friction dictates the motion [3].

Diffusivity, as estimated from the gradient of the variance of the jump distribution with respect to the time segment, is very small when the noise strength is very weak and the object is practically in sticking phase. With increment of the noise strength the diffusivity is increased and the net motion of the solid object comprises of intermittent stick and slip phases. The free flowing motion is achieved at very high noise strength with undetectable stick phase. This phase transition like behavior of the solid dynamics is experimentally demonstrated [3].

A similar experiment with solid object on a solid surface, in which both the contacting surfaces were grafted with a polymer brush exhibits negligible critical force [3]. In this case also displacement distribution was significantly non-Gaussian at small time limits. This situation was modeled with a non-linear kinematic friction that successfully explained the sublinear behavior of the mobility as a function of strength of the noise.

To study the rolling friction between a soft and a rigid surface we used a steel sphere on an inclined fibrillated rubber surface in presence of white noise [4]. The steel sphere exhibits stochastic forward and backward motion with net drift in forward direction along gravitational bias force. We interrogated the system with noise of different strength to estimate drift velocity as well as distribution of displacement fluctuation. This investigation sets a new approach to determine frictional behavior using simple statistical analysis of response function without engaging any sophisticated friction force measurement apparatus. The friction law between rubber and steel surface suggests that friction depends on both rate (i.e. velocity) and state (i.e. strength of noise) of the system. At very high strength of noise the system is governed by linear kinematic friction but at low noise strength the system exhibits friction behavior similar to that observed in case of peeling of a soft adhesive [5,6].

Integrating the displacement distribution in positive and negative regime we measured the positive and negative work. The ratio of the probability of negative to positive work decreases monotonically with the mean work. Using integrated work

fluctuation theorem we measured the effective temperature of the system. This measure of effective temperature was found comparable to $D \: / \: \mu$. We introduced another experiment to measure effective temperature of a system when an object has to overcome an energy barrier [7]. The barrier crossing frequency was found to agree with the Arrhenius rate equation, as power of the noise being the athermal analogue of the temperature. The effective temperature estimated from these barrier crossing experiments is higher than that derived from work fluctuation theorem or from fluctuation dissipation theorem. This indicates that the effective temperature is not unique for system governed by nonlinear energy dissipation. The drift velocity of the steel sphere on inclined but flat fibrillated PDMS rubber also follows Arrhenius rate equation which suggests that the pinning depinning transition during motion of the sphere is also an activated process. To understand this system analytical expression was derived based on JKR type adhesion between soft spherical contact and a rigid surface in presence of noise. Numerical simulation of dynamic Langevin equation strengthened this analysis [8].

We studied the critical and subcritical dynamics of small liquid droplets of different viscosities on a superhydrophobic fibrillated rubber surface [9]. At a critical inclination the droplets initially move slowly and after a critical velocity is reached the drops speed up. Some of the natural vibration modes of the droplets are excited due to pinning-depinning transition at the solid liquid contact line which is supported by the fact that these excitation is not observed when droplets move on a smooth surface. The terminal velocity of the droplets first increases - reaches a maxima and then decreases with the increasing viscosity of the liquid. The initial slow dynamic phase vanishes and a

picture of steady velocity emerges during subcritical motion of the droplets when the support is subjected to an external vibration. The behavior of this subcritical dynamics is similar to that of a designed experiment where the drops are impelled to cross over a physical barrier in presence of external noise. The barrier crossing frequency as well as the drift velocity of the liquid drops is amenable to the low friction regime of the Kramers' formalism within the viscosity range (1 *mPa-s* to 5.3 *mPa-s*) of the liquid drops studied.

11.2 Future work

Experiments on various different substrates to understand material dependent friction laws were just the beginning of the research in this field. We have studied solid-solid friction using glass on glass and polymer grafted glass on polymer grafted Si wafer. What we found that polymer grafted surface reduced the Coulombic static friction but the kinematic friction itself was nonlinear. We already studied the rolling friction between soft polymer and rigid steel surface. Overall friction behavior was nonlinear with respect to the velocity except at very high strength of the external noise. All these characteristics suggest that the friction cannot be fully described by simple phenomenological models.

We have studied the noise induced detachment of a steel sphere from a fibrillar PDMS rubber. The study revealed that the subcritical detachment is a noise activated process. The experimental settings involved multi-contact detachment. The single contact

detachment experiment with various geometries of the contact will give new insight to the problem.

In chapter 9 we discussed about the sliding friction as an activated process. In that experiment we could not verify the stick slip behavior of the slow dynamics of a slider at weak external perturbation due to experimental limitation. Use of highly sensitive displacement transducer will eliminate this limitation.

References

[1]   P. S. Goohpattader, S. Mettu, and M. K. Chaudhury, Langmuir **25**, 9969–79 (2009).

[2]   L. Mahadevan, S. Daniel, and M. K. Chaudhury, Proceedings of the National Academy of Sciences **101**, 23 (2004).

[3]   P. S. Goohpattader and M. K. Chaudhury, The Journal of Chemical Physics **133**, 024702 (2010).

[4]   P. S. Goohpattader, S. Mettu, and M. K. Chaudhury, The European Physical Journal. E, Soft Matter **34**, 120 (2011).

[5]   D. Maugis and M. Barquins, *Maugis Barquins Adhesion 12 Edited by K W Allen* (London, Elsevier, 1988).

[6]   M. Barquins and M. Ciccotti, Int. J. Adhesion and Adhesives **17**, 65 (1997).

[7]   P. S. Goohpattader and M. K. Chaudhury, The European Physical Journal. E, Soft Matter **35**, 67 (2012).

[8]   M. K. Chaudhury and P. S. Goohpattader, The European Physical Journal. E, Soft Matter **35**, 131 (2012).

[9]   M. K. Chaudhury and P. S. Goohpattader, The European Physical Journal. E, Soft Matter **36**, 15 (2013).

VITAE

Partho Sarathi Gooh Pattader

Date of Birth: 5th October, 1980

Place of Birth: Kolkata, WB, India

Parents: Late Amarendra Nath Gooh Pattader and Dipali Gooh Pattader

Education

Ph.D. Candidate	2007-2013
Advisor	Professor Manoj K. Chaudhury
Institute	Lehigh University, Bethlehem, PA
Thesis	*Effect of nonlinear friction on the motion of an object on solid surface induced by external vibration*
M. Tech Chemical Engineering	2005-2007
Supervisor	Professor Ashutosh Sharma
Institute	Indian Institute of Technology Kanpur (IITK), Kanpur, India
Project	*Patterning of thin visco-elastic polymer films using different techniques*
B.Tech. Chemical Engineering	2001-2004
Institute	University College of Science and Technology, Kolkata, WB, India
B. Sc Chemistry	2005-2007
Institute	Presidency College, Kolkata, WB, India

Professional experience

Research associate	08/2004-07/2005
Company	Hindustan Unilever Research Center (HLRC), Bangalore, India
Vocational trainee	07/2003
Company	Indian Farmers Fertiliser Cooperative Limited, (IFFCO, Phulpur)
Internship	10/2002
Company	Unilever Research Center (HLRC), Bangalore, India

Publications

[1] M. K. Chaudhury and **P. S. Goohpattader**; *Activated drops: self-excited oscillation, critical speeding and noisy   transport.* **Eur. Phys. J. E,** *36*, 15 **(2013)**.

[2] M. K. Chaudhury and **P. S. Goohpattader**; *Noise activated dissociation of soft elastic contacts*. **Eur. Phys. J. E,** *35*, 131 **(2012)**.

[3] **P. S. Goohpattader** and M. K. Chaudhury; *Random motion with interfacial contact: driven diffusion vis-a-vis mechanical activation.* **Eur. Phys. J. E,** *35*, 67 **(2012)**.

[4] **P S Goohpattader**, S Mettu and M K Chaudhury; *Stochastic rolling of a rigid sphere in weak adhesive contact with a soft substrate.* **Eur. Phys. J. E,** *34***,** 120 **(2011)**.

[5] **Partho Sarathi Gooh Pattader**, Indrani Banerjee, Ashutosh Sharma and Dipankar Bandyopadhyay; *Multiscale pattern generation in viscoelastic polymer films by spatio-temporal modulation of electric field and control of rheology.* **Adv. Func. Mat.** *21*, 324 **(2011)**.

[6] **P. S. Goohpattader** and M. K. Chaudhury; *Diffusive motion with nonlinear friction: apparently Brownian*. **J. Chem. Phys.** *133*, 024702 **(2010)**.

[7] **P S Goohpattader**, S Mettu and M K Chaudhury; *Experimental investigation of the drift and diffusion of small objects on a surface subjected to a bias and an external white noise: roles of coulombic friction and hysteresis.* **Langmuir** *25*, 9969 **(2009)**.

[8] N. Arun, Ashutosh Sharma, **Partho S. G. Pattader**, Indrani Banerjee, Hemant M. Dixit, and K. S. Narayan; *Electric-field-induced patterns in soft viscoelastic films: from long waves of viscous liquids to short waves of elastic solids*, **Phys. Rev. Lett.** *102*, 254502 **(2009)**.

[9] Rabibrata Mukherjee, Ashutosh Sharma, Ganesh Patil, Danish Faruqui and **Partho Sarathi Gooh Pattader**; *Soft lithography meets self-organization: some new developments in meso-patterning*. **Bull. Mater. Sci**.*31*, 249 **(2008)**.

Invited talks (06/2012)	Graduate student seminar on "Experimental study of non-equilibrium athermal systems", Lehigh university.
Poster Presentation (07/2009)	**P. S. Goohpattader**, Srinivas Mettu, M. K. Chaudhury, "Drift and Diffusion of Small Objects on a Surface Subjected to a Bias and an External White Noise", **Gordon Research Conference on Science of Adhesion**.
Teaching Experience (2008-2011)	Teaching Assistant in Lehigh University: Mass transfer and Separation process Introduction to Heat transfer
(2005-2007)	Teaching Assistant in IIT Kanpur: Unit Operation Laboratory Responsibility- teach and supervise undergraduate students, conduct experiments, grade examinations and projects.

Skills

Technical	Physical and chemical modification of surfaces
	UV spectroscopy, FTIR, Dynamic Light Scattering, Reflectometry
	Experience in clean room protocols
	Microfabrication using photolithography, micro contact printing, soft lithography
	Polymer micropatterning using thermal and solvent vapor dewetting, E-field patterning
	Surface characterization using optical profilometry, contact profilometry
Computer	C, C++, Fortran, Matlab, MS-Office (Word, Excel, PowerPoint), Adobe Illustrator, Adobe Photoshop, CorelDraw, Origin, Autocad, Mathematica, Windows
Language	English (fluent -written/oral), Bengali (native), Hindi (basis).

Fellowship and Honors

2008	Leonard A. Wenzel award for best presentation in Qualifying examination, Department of Chemical Engineering, Lehigh University
2007	Graduate Student Fellowship, Lehigh University
2004	Ranked 1st in B.Tech. (Chemical Engineering) from Calcutta University
2001	Ranked 99th in B.Sc. (Chemistry Honors) from Calcutta University out of ~5,000 students
1996-1998	National Scholarship holder in Higher Secondary
1996	Ranked 51st in 10th Standard out of ~30,000 students